Fully Distributed Optimal Power Flow

Diwangkoro Muhammad Dolaputra

Technische Universiteit Delft

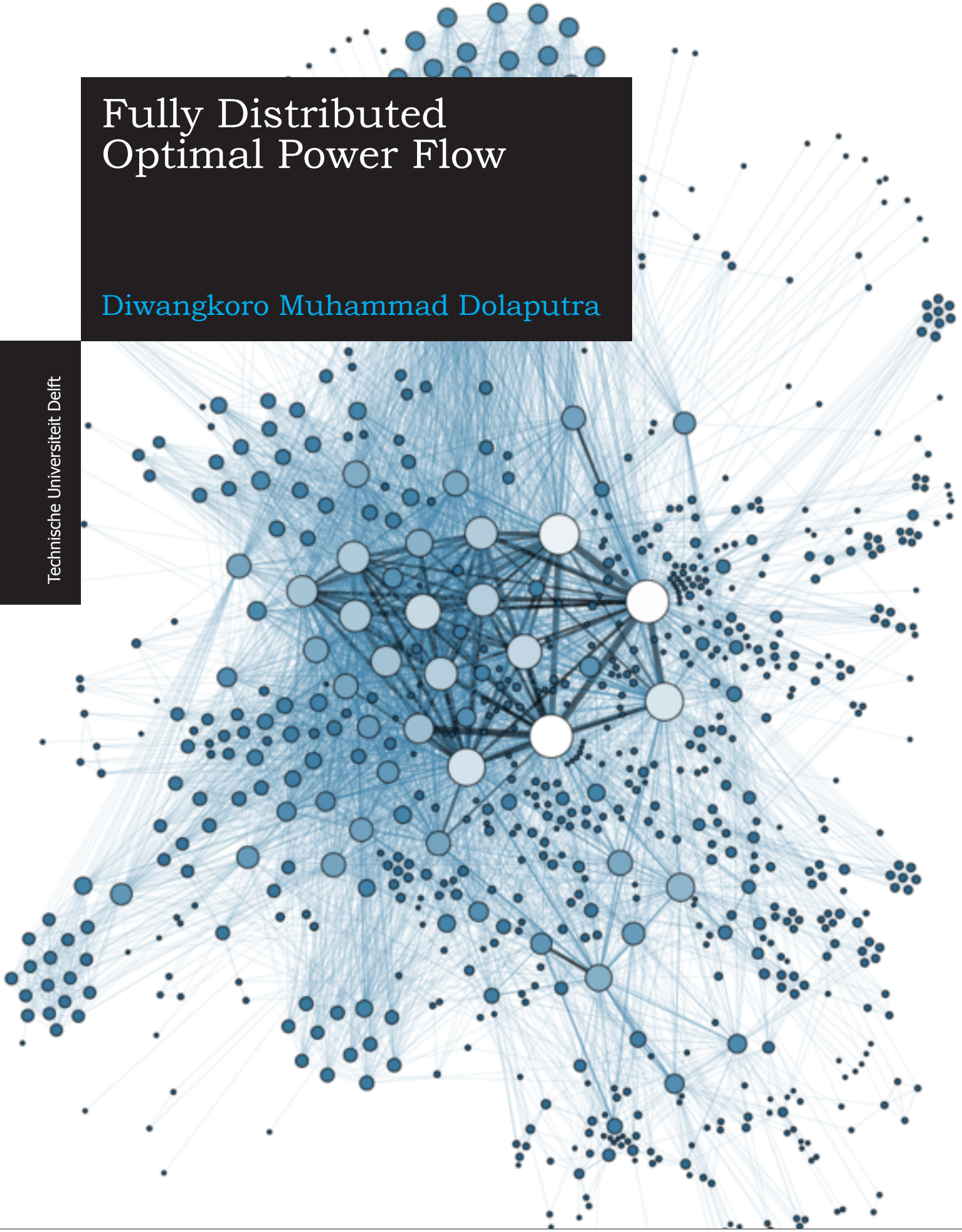

TU Delft Delft University of Technology

Challenge the future

Fully Distributed Optimal Power Flow

by

Diwangkoro Muhammad Dolaputra

in partial fulfillment of the requirements for the degree of

Master of Science
in Electrical Sustainable Energy

at the Delft University of Technology,
to be defended publicly on Wednesday August 29, 2018 at 09:00 AM.

Supervisor:	Dr. Ir. Milos Cvetkovic,	TU Delft
Advisors:	Dr. Ir. Laurens Mackay,	DC Opportunities R&D BV
	Ir. Shantanu Chakraborty,	TU Delft
Thesis committee:	Prof. Dr. Peter Palensky,	TU Delft
	Dr. Ir. Milos Cvetkovic,	TU Delft
	Dr. Ir. Mathijs de Weerdt,	TU Delft

TU Delft Delft University of Technology

DC pportunities

Acknowledgement

To:

1. Allah swt
2. Papa, Mama, Dyas, Dhanes
3. Laurens, Shantanu, and Milos as supervisors
4. Prof. Peter Palensky and Mathijs de Weerdt as thesis committees
5. Hana
6. All Indonesian and ESE colleagues
7. LPDP (Indonesia Endowment Fund for Education), the one that funds this past 2 years

THANK YOU

I'm lost for words.

Diwangkoro Muhammad Dolaputra
Delft, August 2018

Abstract

There are many methods for solving an optimal power flow (OPF) problem. Most of them employ one central unit to solve the problem (centralized) while in others, every node/area computes for its coverage and send information to its neighbor(s) every time. The mentioned method is called Distributed OPF. In this thesis, the Distributed OPF aims for a fast and resilient algorithm to solve a DC-OPF problem based on Consensus + Innovation (C+I) method.

The research focuses on developing a faster algorithm in solving an OPF problem for a DC distribution grid. The current C+I method has tuning parameters, all of which are determined by trial and error for every case. They are sensitive parameters that determine the speed of the iteration to converge to the solution. This thesis attempts to form adaptive tuning parameters by understanding their function in every equation for a variable update. By understanding the purpose of each tuning parameter and the physical interpretation, some parameters can be formulated while the other is still determined by estimating the value. The losses and congestion are also taken into account. In the results, by formulating these parameters, they are shown that the iteration number has dropped significantly compared to the previous research.

Regarding the resilience of the algorithm, the distributed approach relies on the information exchange between the nodes and delay on the information exchange will stall the whole iteration process. Therefore, an asynchronous algorithm is implemented to resolve the problem by setting a timeout duration. The timeout duration enables the algorithm to wait for the new information only for the desired duration, and therefore the calculation converges in faster.

keywords: DC Optimal Power Flow, Consensus + Innovation, Tuning Parameters Formulation, Asynchronous Algorithm

Contents

Nomenclature

m	Index for the observed node
n	Index for the neighbor of the observed node
l	Iteration number
$\mathcal{N}$	Total number of nodes
Ω_m	List of nodes which are connected to node m
A_m	Quadratic cost coefficient
B_m	Linear cost coefficient
p_m^S	Power generation or load consumption in node m
$G_{m,n}$	Conductance of line m,n
u_m	Voltage at node m
$p_{m,n}$	Power flow in line m,n
$i_{m,n}$	Current flow in line m,n
$\overline{P}_{m,n}$	Power flow limit in line m,n
$\overline{I}_{m,n}$	Current flow limit in line m,n
$\overline{P}_m^S$	Maximum power generation at node m
$\underline{P}_m^S$	Minimum power generation at node m
$\overline{U}_m$	Maximum voltage at node m
$\underline{U}_m$	Minimum voltage at node m
$\mathcal{L}$	Lagrange function
λ_m	Locational marginal price (LMP) at node m
$\mu_{m,n}$	Dual variable for the line limit at line m,n
$\mu_m^{\overline{P}}$	Dual variable for the maximum power generation limit at node m
$\mu_m^{\underline{P}}$	Dual variable for the minimum power generation limit at node m
$\mu_m^{\overline{U}}$	Dual variable for the maximum voltage limit at node m
$\mu_m^{\underline{U}}$	Dual variable for the minimum voltage limit at node m
DC	Direct current
AC	Alternating current
OPF	Optimal power flow

1

Introduction

1.1. Microgrids and Distributed Energy Generation

The power system is built to fulfill the energy needs nowadays. Conventionally, it is by having bulk generators in a remote area and transmit the power to the industrial and residential load through a long high voltage (HV) transmission line. However, this model is not necessarily suitable for every kind of load. For instance, in a rural area, sometimes it is not economically feasible to access the power from the main grid due to the cost of the infrastructure. Therefore, having distributed units of lower capacity located nearby the consumption points without connection to a main grid becomes an option. The distributed units are usually renewable energy sources such as solar, micro-hydro, and fuel cells. This concept is called microgrids which is defined as a discrete energy system consisting of renewable energy sources and loads which can work parallel with, or independent from the main grid [1]. Another research [2] assumes that a microgrid is a cluster of load and source operating as a single system that provides both power and heat to a local area. According to the Departement of Energy (United States) [3], a microgrid is a set of interconnected load and distributed energy resources with clear boundaries that act as a single entity regarding the grid.

Rise of the DC System

The power system now mostly operates in AC voltage due to its easiness of transforming ac electrical energy to a different voltage level which leads to more efficient transportation over a long distance [4]. However, the DC starts to take over in high and low voltage level. In the high voltage, it is applied for HVDC transmission which has the advantage of low cost and decreased losses [5]. At the low voltage level, currently, DC systems are mostly used for specific industrial applications such as telecommunication and data centers. However, it is possible to have an increase in the number of applications such as LED street lighting, motors with speed control, and shipboard power system [6]. It seems promising to help in providing more connections of distributed renewable energy units. DC microgrids have a simple structure, cost lower price, and need fewer converters as the renewable energy units and the storage are already in DC [7].

1.2. Centralized vs. Distributed Optimal Power Flow

Optimal power flow (OPF) is a method to optimize the power generation in generators or the load consumption in loads to minimize the total cost while taking into account the operational limit [8]. Centralized computation has been the original way for running the optimization algorithm, conducted by independent system operators (ISO) to find the minimum cost [9]. However, with the presence of a central computer, this conventional method has some important disadvantages. Based on [10], during more penetration of distributed generation (DG), the disadvantages are:

1. The central has to collect information from all DGs and controllable loads. It leads to high requirements of a communication network when the number of DGs and loads becomes larger.

2. The central is a single point of failure.

3. Privacy of a DG's information will be an issue as all the data have to be collected to the ISO.

Rather than doing a centralized computation, a distributed/decentralized method is introduced. Related work [11] differentiates distributed and decentralized that distributed still needs a central coordinator while decentralized does not. To avoid confusion, this thesis only considers the one without the central coordinator and address it as a distributed (or a fully distributed) method. In principle, the algorithm for solving the OPF problem is run in each agent in parallel and only allows communication between neighboring agents. The agent is defined as a node consisting of a component (a DG or a load). However, for some algorithms presented in [11], an agent is an area, and the communications occur between areas.

1.3. Introduction to Consensus and Innovation Algorithm

Consensus and Innovation (C+I) is chosen in [12] as an algorithm to solve an optimal power flow problem. The algorithm is one of the distributed algorithm methods with an advantage that it can be deconstructed into nodal or component level [12] so that it works in a fully distributed fashion. This algorithm is based on Karesh Kuhn Tucker optimality condition and uses its derivative term to update parameters through iteration [9]. The results in [13–15] proved that the algorithm could converge to the solution by implementing it in a fully distributed way. However, they have tuning parameters that are determined by trial and error. The parameters are extremely sensitive and have to change when the problem changes. An extensive explanation about the C+I algorithm will be presented in Section 2.4.

1.4. Research Motivation

The problem formulation presented in [14, 15] are lossless DC approximation for AC optimal power flow. On the other hand, a work regarding the optimal power flow for the DC grid by taking into account the losses in the system is done in [13]. This algorithm is later called Exact OPF. It results in a converged solution, but it took up to 200000 iterations to converge due to the tuning parameters. Therefore, this thesis emphasizes in finding a proper tuning parameter formulation to speed up the convergence rate and also to avoid performing trial and error in discovering the right tuning parameters. Moreover, a straight-forward update did not guarantee the convergence and modification of the update had to be made.

Within the update, when a limit in the line is determined, the generators cannot casually produce power. This will affect the update for the voltage, and a special treatment should be applied for converging to the right solution. Moreover, when congestion occurs in a meshed network, it results in a different way as the radial network.

Additionally, losses are always present in the power system due to the current flow. To minimize the losses that will lead to the minimized cost, the voltage should be determined as high as possible. Therefore, modification in the voltage update should be applied to have the algorithm converging at the maximum voltage.

During the implementation, information exchanges take significant time and cost the whole duration due to the delays. Therefore, an asynchronous update has to be implemented to avoid delay and accelerate the convergence time.

1.5. Objective and Research Questions

The research has a primary objective which is:

To improve the speed and resilience of the C+I based distributed optimal power flow algorithm by formulating the tuning parameters and asynchronous update.

The objective is then broken down into four research question:

1. How can the physical interpretation be used to improve the convergence rate?
2. How can the line congestion be taken into account for the voltage and the dual variable updates, especially for a meshed grid?
3. How can the losses and the voltage limit be accounted for in the distributed OPF?
4. How can the algorithm be modified in order to run asynchronously for reducing delays?

1.6. Thesis Structure

This section will discuss the outline of the thesis and its content.

Chapter 2 presents the literature review supporting this thesis. The basic of energy economics, methods for distributed OPF, and also existing approaches for asynchronous updates are the content of the chapter.

The next two chapters, Chapter 3 and Chapter 4 is the main work of the thesis. Chapter 3 discusses the optimization problem to be solved using a Lossless OPF algorithm. It contains the concluded formulation for every variable update and its supporting tuning parameters for answering research questions 1-2. The answer for research question 1 is present in the end of section 3.6 while the next section, section 3.7 answers research question 2. For simplicity and more understandable equations, the formulation is explained in Chapter 3 which uses the Lossless OPF.

Chapter 4 includes the losses for the calculation and some modifications for the parameter updates are applied. Some of the equation stays due to a similar characteristic with the Lossless OPF. Section 4.5 about voltage update shows the answer for research question 3.

Chapter 5 provides the explanation about the simulation utilized for running the algorithm and study cases to show how the Exact OPF algorithm results for various cases. Moreover, a comparison to the previous study is shown to answer the research question 1 regarding the convergence rate.

Chapter 6 shows the method on how to modify the algorithm to run asynchronously. It also exhibits the results of the asynchronous update in the microcomputer implementation to answer research question 4.

Chapter 7 concludes the whole thesis followed by critical reflections of this thesis and opportunities for future work.

2

Literature Review

2.1. Energy Economics in Power System

Since electrical energy is produced massively and has a role as a worldwide necessity, it is treated as a commodity. Every producer sets its price so that through the market operator, the consumers can buy it. Trade in electrical energy refers to the price of a certain amount of megawatt-hours of electricity over a specified period of time [16]. However, a failure in producers or the electrical energy transmission can influence quickly in price change and disturb the market significantly.

Based on [16], there are two techniques for hedging limitation in the network which are Decentralized Trading and Centralized Trading. In the centralized trading, all producers and consumers submit their bid to an entity called the market operator. This system operator will then determine the market clearing price. On the other hand, in the decentralized trading, a set of generators and loads have an exclusive contract regarding the power transfer and the price for their own. Due to the relevance, this chapter will cover more about the centralized trading. The following subsections will discuss about the fundamentals of the Locational Marginal Pricing (LMP), as one of the energy economics model. They will cover an example of an electricity trade between two imaginary countries called Borduria and Syldavia, provided by reference [16]. This thesis will mainly discuss about DC distribution grids but only for an example and explanation, a transmission system will be used as a sample case.

2.1.1. Unconstrained Transmission

Borduria and Syldavia are countries with 500 MW and 1500 MW demand respectively. Both countries have their generator with the supply function or later called as marginal pricing as follows:

$$\pi_B = 10 + 0.01P_B \tag{2.1}$$

$$\pi_S = 13 + 0.02P_S \tag{2.2}$$

In the absence of a transmission line, both countries have a different price to satisfy their demand. Substituting $P_B = 500$ and $P_S = 1500$ into (2.1) and (2.2) , the price are 15 \$/MWh and 43 \$/MWh respectively. If a transmission line is built between both countries, there will be power flowing in the transmission. It is assumed that there is no power losses, unlimited generator capacity, and unlimited power transfer in the line. Referred to Figure 2.1, Borduria will generate 1433 MW (P_B), Syldavia will generate 567 MW (P_S), and there will be 933 MW transfer from Borduria and Syldavia (P_{BS}). The equilibrium point in Figure 2.2 shows the market clearing price of 24.3 \$/MWh.

Extensively, this Borduria and Syldavia case can be modeled as an optimization problem with the objective of minimizing the cost of power production in both countries.

The cost of production in both countries, denoted as C_B and C_S are:

$$C_B(P_B) = \int_0^{P_B} \pi_B(P)dP = 10P_B + \frac{1}{2} \cdot 0.01P_B^2 \tag{2.3}$$

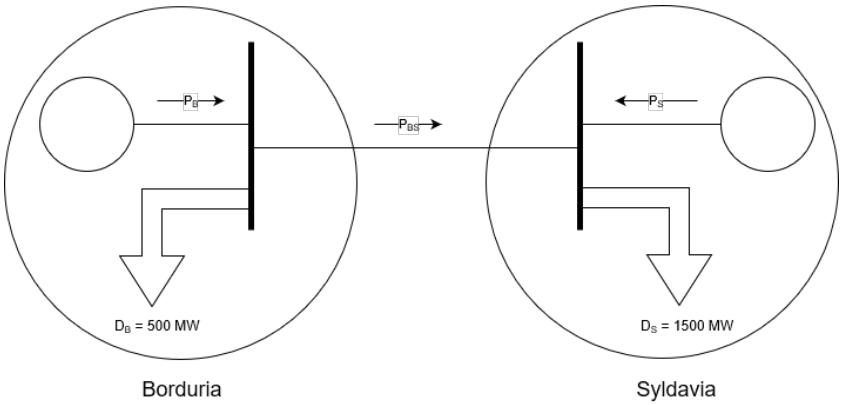

Figure 2.1: A sample case for imaginary two countries, Borduria and Syldavia. The presence of the transmission line allows the power P_{BS} flowing from Borduria to Syldavia, resulting in the same marginal cost for both countries.

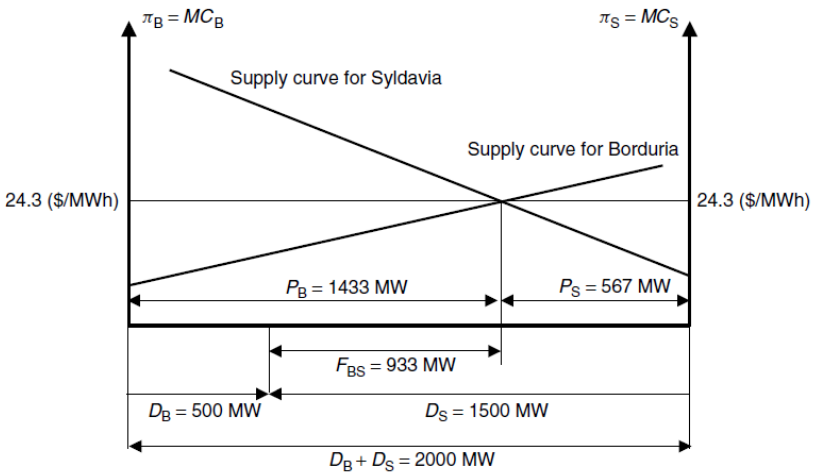

Figure 2.2: Equilibrium point of the marginal price when Borduria and Syldavia electricity market is combined into one market. [16]

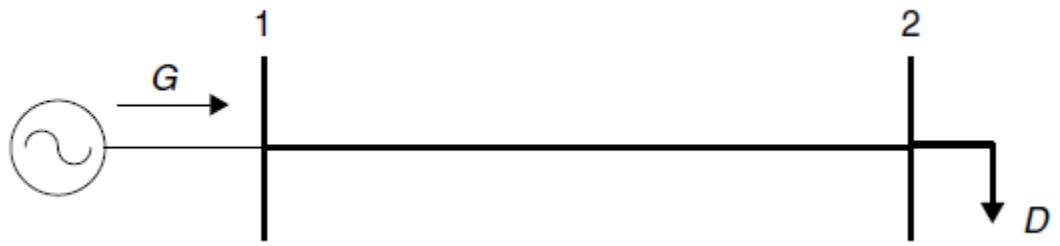

Figure 2.3: A simple model of a generator connected to a load through a transmission line. Losses occur in the transmission line, leading to a higher power production in the generator. The figure is cited from [16].

$$C_B(P_S) = \int_0^{P_S} \pi_B(P)dP = 13P_B + \frac{1}{2} \cdot 0.02P_S^2 \tag{2.4}$$

Therefore, the objective function is:

$$\min(C_B + C_S) = \min(10P_B + \frac{1}{2} \cdot 0.01P_B^2 + 13P_B + \frac{1}{2} \cdot 0.02P_S^2) \tag{2.5}$$

The objective has a constraint of the power balance. The power balance equation is as simple as $P_B + P_S = D_B + D_S$. Therefore, the optimum solution is when Borduria produces 1433 MW and Syldavia does 567 MW with the marginal price is $\pi = 24.3\$/MWh$.

2.1.2. Constrained Transmission

Due to their physical limitation, no transmission line can transfer infinite amount of power. In this Borduria and Syldavia case, it is assumed there is 400 MW maximum transfer. Therefore, 933 MW transfer is not possible. Borduria reduces its generation to 900 MW (500 MW self-consumption and 400 MW transfer) while production in Syldavia rises to 1100 MW. The price of each area is now:

$$\pi_B = 10 + 0.01(900) = 19\$/\text{MWh} \tag{2.6}$$

$$\pi_S = 13 + 0.02(1100) = 35\$/\text{MWh} \tag{2.7}$$

Equation (2.6) and (2.7) show the locational marginal pricing (LMP) since its location determines the marginal cost. When there is a transmission constraint, the LMP will vary throughout the network. [17]

2.1.3. Losses in the Transmission Line

Naturally, the current flowing will dissipate heat and lead to power losses in the line. The power sent from the sending end will not be the same as the one at the receiving end. In reference [16], this losses is denoted as variable losses.

$$L^{\text{variable}} = I^2 \cdot R \approx \left(\frac{P}{V}\right)^2 R = \frac{R}{V^2} \cdot P^2 = K \cdot P^2 \tag{2.8}$$

In a simplified mathematical model for Figure 2.3, it is assumed that the load is purely active and no voltage drop along the line, resulting the following equation for the losses:

$$L = K \cdot D^2 \tag{2.9}$$

The generation at bus 1 is

$$G(D) = D + L = D + K \cdot D^2 \tag{2.10}$$

with an increase in the load by ΔD, the generator must increase by

$$\Delta G = G(D + \Delta D) - G(D) = \Delta D + 2\Delta D \cdot K + \Delta D^2 K \approx (1 + 2D \cdot K)\Delta D \tag{2.11}$$

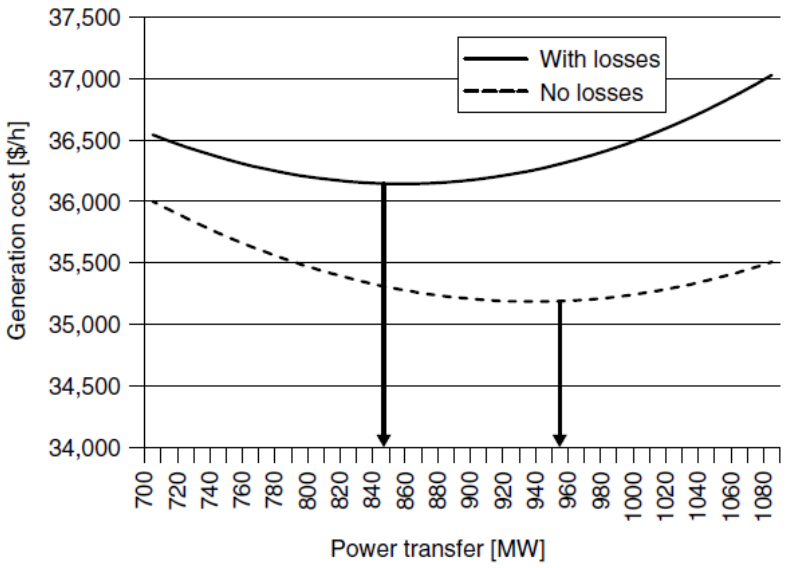

Figure 2.4: Total generation cost in Borduria-Syldavia transmission line as a function of the power transfer when the the losses is taken into account and not taken into account. When the losses taken into account, the optimim solution lies when the transmission transfers less power. [17]

and due to the extra D in bus 2, and π_1 is defined as the marginal cost at bus 1, the cost of the generation rises to:

$$\Delta C = \pi_1(1 + 2D \cdot K)\Delta D \tag{2.12}$$

Equation (2.12) implies that the cost goes up due to ΔD in bus 2. Therefore, the marginal cost in bus 2 becomes

$$\pi_2 = \frac{\Delta C}{\Delta D} = \pi_1(1 + 2D \cdot K) \tag{2.13}$$

It is concluded that there will be a difference in the marginal price with the presence of the power losses even though there is no congestion in the transmission line. The receiving end has a higher marginal price than the sending end.

Borduria and Syldavia Case

The losses is now taken into account, and the power balance in (2.1.1) should be modified into this equation:

$$P_B + P_S = D_B + D_S + K \cdot F_{BS}^2 \tag{2.14}$$

It is assumed that $K = 0.00005MW^{-1}$, and (2.14) can be split into:

$$P_S = D_S - F_{BS} \tag{2.15}$$

$$P_B = D_B + F_{BS} + K \cdot F_{BS}^2 \tag{2.16}$$

Substituting (2.16) and (2.15) into (2.5), it will resulted in the cost equation as a function of F_{BS}. Figure 2.4 shows the plot between total cost (y-axis) and power (x-axis) and it can be concluded that the minimum cost is achieved when the power transfer equals to 853 $/MWh.

2.2. Overview of Methods for Distributed Optimal Power Flow

Algorithms to solve the OPF problem in a distributed way have been developed in many research. Moreover, extensive comparison analysis between algorithms have been studied in [9, 11, 12]. The foundation of distributed DC OPF is classified into Augmented Lagrangian Relaxation and Karesh Kuhn Tucker (KKT) Conditions. Each classification has several algorithms as presented in [11, 12].

The comparative analysis in [11] concluded that Consensus and Innovation (C+I) from KKT Conditions can be employed to solve opf problem in a nodal level and also regional level. Moreover, this thesis is an advanced work from the previous thesis [12] which went deeply into C+I algorithm. Therefore, C+I is chosen to be the basic of the algorithm in this thesis and will be extensively explained in the following sections. This section will briefly show the basic of Alternating Direction Multiplier Method (ADMM) and Dual Decomposition as representations from the Lagrangian Relaxation classification, and Optimality Condition Decomposition and Interior Point Method as a representation from KKT Conditions.

2.2.1. ADMM with Proximal Message Passing (PMP)

The alternating direction method of multipliers (ADMM) is a famous method for optimization problem in a distributed manner, especially for a large-scale problem and Unit Commitment in power system [18]. In principle, the objective has several decision variables and it is broken down into sub-problems. These subproblems are solved sequentially over sequential Gauss-Seidel iterations by having a central coordinator. Using ADMM solely is not a fully distributed optimization as desired since a central coordinator is still required. Hence, proximal message passing (PMP) [19] is needed to be included in the algorithm.

Consider an optimization problem:

Objective Function

$$\min_{x,y} \quad f(x) + g(y) \tag{2.17}$$

subject to

$$Ax + By = c \tag{2.18}$$

where x and z are the decision variables, A and B are coefficients in the equality constraint, and c is a constant vector regarding the constraint. The problems are then formulated into an augmented Lagrangian below:

$$\mathcal{L}(x, y, \lambda) = f(x) + g(y) + \lambda(Ax + By - c) + \frac{\rho}{2}\|Ax + By - c\|_2^2 \tag{2.19}$$

where $\rho > 0$ is a specified penalty parameter and $\|.\|_2$ is the two norm for absolute value. The ADMM algorithm conducts decomposing the problem in sub-problems of minimizing each decision variables and the dual variable.

$$x(l+1) = \arg\min_{x} \quad \mathcal{L}(x(l), y(l), \lambda(l)) \tag{2.20}$$

$$y(l+1) = \arg\min_{y} \quad \mathcal{L}(x(l+1), y(l), \lambda(l)) \tag{2.21}$$

$$\lambda(l+1) = \lambda(l) + \rho(Ax(l+1) + By(l+1) - c) \tag{2.22}$$

note that x, y, and λ are updated after one another. All the updating variables use new values from the other. For example, in the y update, new value of $x(x(l+1))$ is used instead of $x(l)$. The algorithm is repeated until they are converged.

Equation (2.22) shows the necessity of central coordinator. To use ADMM as a distributed algorithm, a modification called PMP has to be used [9]. By using PMP, each agent (node) evaluates a prox function:

$$\text{prox}_{f,\rho}(v) = \arg\min_{x}(f(x) + \rho/2\|x - v\|_2^2) \tag{2.23}$$

The vector x contains the primal (x, y) and dual (λ) variables while v is a vector containing the average values of the variable in x from the neighboring nodes. In the OPF problem, the shared variable is the voltage angle and the node price [11]. The function $f(x)$ is the local objective and ρ is scalar for tuning parameter. Hence, the prox function optimizes the node's local objective and pass the prox value to the neighbors to continue the iterations. The iterations stop after the agents agree on a common value x (convergence).

2.2.2. Dual Decomposition

Dual Decomposition separates the problem into subproblems to be solved by each agent independently. Consider an optimization problem as below:

$$\min_{x} \sum_{m \in \mathcal{N}} f_m(x_m) \tag{2.24}$$

subject to

$$\sum_{m \in \mathcal{N}} A_m x_m = b \tag{2.25}$$

where m is the observed node as a set of $\mathcal{N}$ number of nodes. The Lagrangian equation for the problem is:

$$\mathcal{L}(x, y) = \sum_{m \in \mathcal{N}} [f_m(x_m) + \lambda(A_m + x_m - b)] \tag{2.26}$$

the dual decomposition method uses an iterative method called "dual ascent" [9]:

$$x_m(l+1) = \arg\min_{x_m} \ \mathcal{L}(x_m, \lambda(l+1)) \tag{2.27}$$

$$\lambda(l+1) = \lambda(l) + \alpha(l)\left[\sum_{m \in \mathcal{N}} A_m x_m(l+1) - b\right] \tag{2.28}$$

where $\alpha(l)$ is a tuning parameter and y is the dual variable that states the nodal price. It can be seen from (2.27) that the subproblems can be solved separately. However, (2.28) shows that a central coordinator remains necessary. Another drawback of this algorithm is the tuning parameter plays a massive role in determining the convergence.

2.2.3. Optimality Condition Decomposition

Optimality Condition Decomposition (OCD) is a KKT based optimization algorithm. This method in an iterative solution wherein each iteration the OPF problem is solved independently for every agent (node) [11]. OCD is suitable for solving an optimization problem with a unique characteristic of constraints. The constraint should include a variable from another node.

The OPF problem is decomposed into subproblem which is then solved by deriving its KKT condition and applying Newton Raphson Method [11]. The update for the primal and dual variables employ the Jacobian matrix of the KKT condition. After the update, the new information is shared with its neighbor for the next iteration until the KKT condition is reached.

2.2.4. Distributed Interior Point Method

The algorithm is based on the interior point method [20] and modified into a distributed interior point method. The algorithm still can not run in a fully distributed way, hence in [21], a unidirectional ring communication graph and message passing are utilized.

As the other optimization methods, The basic of interior point method starts with problem formulation and also forming the Lagrangian function:

$$\min \ f(x) \tag{2.29}$$

$$\text{s.t.} \ \ h(x) = 0 \tag{2.30}$$

$$\underline{G} \leq g(x) \overline{G} \tag{2.31}$$

$$\mathcal{L} = f(x) - \lambda^T h(x) - (\mu^{\overline{G}})^T [g(x) + u - \overline{G}] - (\mu^{\underline{G}})^T [g(x) - k - \underline{G}] - z\left(\sum_{i=1}^{r} \ln u_i + \sum_{i=1}^{r} \ln k_i\right) \tag{2.32}$$

where $\overline{G}$ and $\underline{G}$ are the upper and lower limit of the inequality constraint, x is a primal variable, u and k are slack variables, and λ, $\mu^{\overline{G}}$, and $\mu^{\overline{G}}$ are the Lagrange multipliers (dual variables). Additionally, z is the the barrier parameter and r is the number of equality constraints [21].

The Newton-Raphson method is then applied to the KKT optimality condition in (2.32), Δ for all variables (primal, dual, and slack) can be acquired. The variables are then updated such as:

$$x(l+1) = x(l) + \alpha_p(l+1)\Delta x \tag{2.33}$$
$$\lambda(l+1) = \lambda(l) + \alpha_d(l+1)\Delta\lambda \tag{2.34}$$

Note that there are α_p and α_d which state the tuning parameters for primal and dual variables respectively. The tuning parameters change throughout the iterations. The iteration stops when a defined complementary gap is lower than a threshold. Extensive details about the algorithm is studied in [21].

To conduct the algorithm in a fully distributed way, (2.33) are written for each area (agent). Since the primal variable x also includes boundary variable such as voltage and price, the updates are done one by one per area. After one area finishes the updates for all the variables, it sends the boundary variables to the next area. The last area updating sends to the first area, and it makes a full cycle of a one way ring communication.

2.3. Fundamentals of Karesh Kuhn Tucker

Consensus + Innovation will be the chosen algorithm to investigate further, and it is based on Karesh-Kuhn-Tucker (KKT) necessary condition.

Consider a simple problem for optimization.

$$\text{minimize } f(x) \tag{2.35}$$

subject to

$$h_i(x) = 0 \qquad \forall i \in \mathcal{N} \tag{2.36}$$
$$g_j \leq \overline{G}_j \qquad \forall j \in \mathcal{M} \tag{2.37}$$
$$g_j \geq \underline{G}_j \qquad \forall j \in \mathcal{M} \tag{2.38}$$

where i and j is the number of the equality constraints and the inequality constraints respectively. The problem is simply to minimize a function $f(x)$ that is variable dependant on x. The solution x must follow the equality constraints $h_i(x)$ and must not violate maximum and minimum boundaries, $\overline{G}$ and $\underline{G}$ respectively. Due to the presence of the inequality constraints, and no information about which constraints is active, KKT has to be used instead of the standard Lagrangian function [22].

A Lagrangian function is first formulated:

$$\mathcal{L}(x) = f(x) + \lambda_i h_i(x) + \mu_j^{\overline{G}}(g_j(x) - \overline{G}_j) + \mu_j^{\underline{G}}(-g_j(x) + \underline{G}_j) \tag{2.39}$$

Some necessary conditions needs to be followed which are:

1. Optimality condition

$$\frac{\partial \mathcal{L}}{\partial x} = 0 \tag{2.40}$$
$$\frac{\partial \mathcal{L}}{\partial \lambda_i} = 0 \tag{2.41}$$

2. Feasibility condition (Equation (2.36)-(2.38))

3. Complementary slackness condition

$$\mu^{\overline{G}_j}(g_j(x) - \overline{G}_j) = 0 \tag{2.42}$$
$$\mu^{\underline{G}}(-g_j(x) + \underline{G}) = 0 \tag{2.43}$$

4. Positivity condition

$$\mu_j^{\overline{G}}, \mu_j^{\underline{G}} \geq 0 \tag{2.44}$$

All the λ and μ is the KKT multipliers [22] or also called the dual variable. In the optimal power flow case, λ is the locational marginal price (LMP) which has been explained in the previous section.

2.4. Consensus and Innovation (C+I)

This method [14] is going to be emphasized more and becomes the fundamental for the algorithm developed in this thesis. It is based on a decentralized solution of the Karesh-Kuhn-Tucker (KKT) necessary condition for local optimality and uses iterative algorithm so that the variables vary throughout the iterations [9].

Consensus and Innovation (C+I) has been utilized in some researches [14, 15] due to its ability to be fully distributed without any central communication entity. Every point can only communicate with its neighbor without any global parameters required. The approach is composed based on DC approximation for an AC power system. It is assumed that the voltage in all buses are 1 pu and the resistance is negligible. Hence, The power flowing in the line is a result of voltage angle difference divided by the line reactance. It is equivalent with DC network that has the current flow as a result of the voltage difference divided by the resistance.

The following explanation will use the DC Approximated AC OPF from [14]. Therefore, it is going to be represented by AC OPF terms such as voltage angle (θ_m) instead of voltage (u_m) and admittance ($Y_{m,n}$) instead of conductance ($G_{m,n}$). This method is initiated by stating the objective of minimizing the cost of power production.

$$min \sum_{m \in \mathcal{N}} A_m (p_m^{\mathrm{S}})^2 + B_m p_m^{\mathrm{S}} \tag{2.45}$$

subject to

$$p_m^{\mathrm{S}} = \sum_{n \in \Omega_m} Y_{m,n}(\theta_m - \theta_n) \qquad \forall (m) \in \mathcal{N} \tag{2.46}$$

$$\underline{P}_{m,n} \leq Y_{m,n}(\theta_m - \theta_n) \leq \overline{P}_{m,n} \qquad \forall (m,n) \in \mathcal{N} \tag{2.47}$$

$$\underline{P}_m^{\mathrm{S}} \leq p_m^{\mathrm{S}} \leq \overline{P}_m^{\mathrm{S}} \qquad \forall (m) \in \mathcal{N} \tag{2.48}$$

In the objective, the cost of power production is obtained by multiplying the power produced by each generator with its corresponding cost parameters. The subscript m indicates the observed node and $\mathcal{N}$ is the whole set of generators. There are three critical constraints in this problem.

1. Power Flow Equation (2.46)
   The power injected in a node is the sum of all power going in to or out from the observed node m. In case of a load node, the term p_m^{S} will have a negative value. As explained, (2.46) is a DC approximation from the AC power flow. The power flow is calculated by dividing the voltage angle difference with the reactance. The term θ_m is the voltage angle of the observed node while θ_n belongs to Ω_m which means the set of neighboring nodes. Meanwhile, the reactance is expressed as the inverse of the admittance $Y_{m,n}$

2. Line Limit (2.47)
   The power flowing in the line is bounded by line limit $\overline{P}_{m,n}$ during outgoing flow and $\underline{P}_{m,n}$ during in-going flow. This term will determine further if the line is congested or non-congested.

3. Generator limit (2.48)

The term $\underline{P}^{S}_{m}$ and $\overline{P}^{S}_{m}$ represent lower and upper limit of the generator respectively.

The objectives and constraints are then constructed as a Lagarange function below:

$$\begin{aligned}\mathcal{L} = & \sum_{m\in\mathcal{N}} A_m (p^{S}_{m})^2 + B_m p^{S}_{m}) \\ & + \sum_{m\in\mathcal{N}} \lambda_m \Bigg(\sum_{n\in\Omega_m} Y_{m,n}(\theta_m - \theta_n) - p^{S}_{m} \Bigg) \\ & + \sum_{n\in\Omega_m} \mu_{m,n} \Big(Y_{m,n}(\theta_m - \theta_n) - \overline{P}_{m,n} \Big) + \sum_{n\in\Omega_m} \mu_{n,m} \Big(- Y_{m,n}(\theta_m - \theta_n) - \overline{P}_{m,n} \Big) \\ & + \sum_{m\in\mathcal{N}} \mu^{\overline{P}}_{m} \Big(p^{S}_{m} - \overline{P}^{S}_{m} \Big) + \sum_{m\in\mathcal{N}} \mu^{\underline{P}}_{m} \Big(- p^{S}_{m} + \underline{P}^{S}_{m} \Big)\end{aligned} \tag{2.49}$$

In which λ and μ's are the Lagrange Multiplier. The first order optimality conditions are:

$$\frac{\partial \mathcal{L}}{\partial p^{S}_{m}} = \sum_{s\in\mathcal{S}} 2A_m p^{S}_{m} + B_m \tag{2.50}$$
$$- \lambda_m + \mu^{\overline{P}}_{m} - \mu^{\underline{P}}_{m} = 0$$

$$\frac{\partial \mathcal{L}}{\partial \theta_m} = \lambda_m \sum_{n\in\Omega_m} Y_{m,n} - \sum_{n\in\Omega_m} \lambda_n Y_{m,n} \tag{2.51}$$
$$+ \sum_{n\in\Omega_m} G^{p}_{m,n}(\mu_{m,n} - \mu_{n,m}) = 0$$

$$\frac{\partial \mathcal{L}}{\partial \lambda_m} = - \sum_{s\in\mathcal{S}} p^{S}_{m} + \sum_{n\in\Omega_m} Y_{m,n}(\theta_m - \theta_n) = 0 \tag{2.52}$$

$$\frac{\partial \mathcal{L}}{\partial \mu_{m,n}} = \sum_{n\in\Omega_m} Y_{m,n}(\theta_m - \theta_n) - \overline{P}_{m,n} \leq 0 \tag{2.53}$$

$$\frac{\partial \mathcal{L}}{\partial \mu_{n,m}} = \sum_{n\in\Omega_m} -Y_{m,n}(\theta_m - \theta_n) - \overline{P}_{m,n} \leq 0 \tag{2.54}$$

$$\frac{\partial \mathcal{L}}{\partial \mu^{\overline{P}}_{m}} = p^{S}_{m} - \overline{P}^{S}_{m} \leq 0 \tag{2.55}$$

$$\frac{\partial \mathcal{L}}{\partial \mu^{\underline{P}}_{m}} = -p^{S}_{m} + \underline{P}^{S}_{m} \leq 0 \tag{2.56}$$

Based on KKT theory for sufficient and optimal condition, it is necessary to include also the complementary slackness condition and positivity condition.

$$\mu_{m,n} \Big(\overline{P}_{m,n} - \sum_{n\in\Omega_m} Y_{m,n}(\theta_m - \theta_n) \Big) = 0 \tag{2.57}$$

$$\mu_{n,m} \Big(- \overline{P}_{m,n} + \sum_{n\in\Omega_m} Y_{m,n}(\theta_m - \theta_n) \Big) = 0 \tag{2.58}$$

$$\mu^{\overline{P}}_{m}(\overline{P}^{S}_{m} - p^{S}_{m}) = 0 \tag{2.59}$$

$$\mu^{\underline{P}}_{m}(p^{S}_{m} - \underline{P}^{S}_{m}) = 0 \tag{2.60}$$

$$\mu_{m,n}, \mu_{n,m}, \mu^{\overline{P}}_{m}, \mu^{\underline{P}}_{m} \geq 0 \tag{2.61}$$

Equation (2.50) to (2.61) are the conditions that have to be met in the solution. A distributed iterative approach will be conducted where each bus only shares and receives information from the connected bus during the iteration.

In [14] a general method for the local update is written as:

$$x_m(l+1) = \mathbb{P}_m[(x_m(l) + \Phi_m g_m(x_n(l)))] \tag{2.62}$$

$$x_m(l) = [\lambda_m(l) \quad \theta_m(l) \quad \mu_{mn}(l) \quad p_m^{\mathrm{S}}]^{\mathrm{T}} \tag{2.63}$$

From (2.63), $x_m(l)$ is the set of variables which are updated every iteration and l is the iteration counter. The function $g_m(x_n(l))$ denotes the first order optimality condition related to bus m wherein some equation, variables from the neighboring bus are included. The term $\mathbb{P}_m$ is the projection operator to keep x_m in its boundaries. Lastly, Φ_m is the vector tuning parameter which plays an essential role in the update. It is a set of constants which determines the speed of the iteration to reach convergence or even if the algorithm reaches its solution.

Therefore update for The Lagrange multipliers is:

$$\begin{aligned}\lambda_m(l+1) &= \lambda_m(l) - \alpha_\theta^\lambda\left(\frac{\partial \mathcal{L}}{\partial \theta_m}\right) + \alpha_\lambda^\lambda\left(\frac{\partial \mathcal{L}}{\partial \lambda_m}\right) \\ &= \lambda_m(l) - \alpha_\theta^\lambda\left(\lambda_m \sum_{n\in\Omega_m} Y_{m,n} - \sum_{n\in\Omega_m} \lambda_n Y_{m,n} + \sum_{n\in\Omega_m} G_{m,n}^p(\mu_{m,n} - \mu_{n,m})\right) \\ &+ \alpha_\lambda^\lambda\left(-\sum_{s\in\mathcal{S}} p_m^{\mathrm{S}} + \sum_{n\in\Omega_m} Y_{m,n}(\theta_m - \theta_n)\right)\end{aligned} \tag{2.64}$$

The first term which comes from (2.51) reflects the consensus of the Lagrange multipliers where the second term is an innovation term based on the power balance equation in (2.52). If the generation is too high, λ_m should reduces its value [14]. That is the base of the innovation term addition. Moreover, α are the tuning parameters which will be explained later on.

The next variable updated is the power. It is updated as follows:

$$p_m^{\mathrm{S}}(l+1) = \mathbb{P}\left(p_m^{\mathrm{S}}(l) - \frac{1}{2A_m} \cdot \frac{\partial \mathcal{L}}{\partial p_m^{\mathrm{S}}}\right) = \mathbb{P}\left(\frac{\lambda_m(l) - B_m}{2A_m}\right) \tag{2.65}$$

The operator $\mathbb{P}$ limits the result value to be only between $\underline{P}_m^{\mathrm{S}}$ and $\overline{P}_m^{\mathrm{S}}$. It will set the value to one of the limits if $p_m^{\mathrm{S}}(l+1)$ exceeds the respective limit. Due to the projection, there is no need for updating $\mu^{\overline{P}_m}$ and $\mu^{\underline{P}_m}$, thus, those terms are negligible for updates. Equation 2.65 expresses that the decrease of λ_m due to excess of generation will consequently decrease the power itself.

The voltage angles are updated by this following way:

$$\begin{aligned}\theta_m(l+1) &= \theta_m(l) - \alpha_\lambda^\theta\left(\frac{\partial \mathcal{L}}{\partial \lambda_m}\right) \\ &= \theta_m(l) - \alpha_\lambda^\theta\left(-\sum_{s\in\mathcal{S}} p_m^{\mathrm{S}} + \sum_{n\in\Omega_m} Y_{m,n}(\theta_m - \theta_n)\right)\end{aligned} \tag{2.66}$$

With α_λ^θ as the tuning parameter, the power balance equation is used for the update to create a sense that adjustment in the voltage needs to occur due to the power mismatch in a node.

Lastly, since the Lagrange multiplier $\mu_{m,n}$ and $\mu_{n,m}$ appear in (2.64), Having them updated is necessary.

$$\mu_{m,n}(l+1) = \mathbb{P}\left(\mu_{m,n}(l) + \beta_\mu^{\overline{P}_{m,n}}\left(\frac{\partial \mathcal{L}}{\partial \mu_{m,n}}\right)\right) \tag{2.67}$$

$$\mu_{n,m}(l+1) = \mathbb{P}\left(\mu_{n,m}(l) + \beta_\mu^{\overline{P}_{m,n}}\left(\frac{\partial \mathcal{L}}{\partial \mu_{m,n}}\right)\right) \tag{2.68}$$

Due to the positivity condition, $\mathbb{P}$ will force the μ to be zero if they are negative. Based on (2.67) and (2.68), μ can decrease its value if the actual power flow does not exceed the limit.

Using the (2.64) to (2.68), each parameter can now be updated locally with only regarding the required parameter from the neighboring nodes. Using this approach, no central coordinator or database is needed and the algorithm can work in a fully distributed mode.

Regarding the tuning parameters, trial-and-error is used in the related works [14, 15]. In this thesis, different ways of tuning parameter settings will be discussed in order to tackle this DC-OPF problem.

2.5. Asynchronous Distributed Optimal Power Flow

Some distributed optimization techniques rely on data exchange and iteration [11]. As every node plays a role as an agent to spread the computation burden, it is possible to have one node that stalls the whole iteration process. Therefore some researches [23–26] regarding asynchronous distributed optimization have been conducted.

In [23], the network is modeled as several areas comprising several buses. Asynchronous implementation requires the buses in the same area to communicate with each other every iteration, while inter-area communication only occurs after multiple iterations. Moreover, the distributed approach allows other information sharing despite not physically connected areas. This extra information results in a faster agreement between the areas.

The second existing approach for asynchronous algorithm is using local estimations and updating the forecast value at the neighbors [24]. The research worked on the distributed optimization using dual decomposition method [27] as explained in the previous section. The result shows that although it is run asynchronously, it still converges to the solution.

Meanwhile, in [26], another sense of asynchronous optimization is introduced. Chang et al. develop a scheduled-asynchronous algorithm to solve the OPF problem in a distributed way. By applying the SDP convex relaxation, every pair of physically connected nodes does their alternate minimizations using ADMM-like iteration. Every node only performs a local minimization when all connected buses have updated values.

All of the mentioned previous works have a different interpretation for asynchronous algorithms. In [23], asynchronous is defined as different iteration in when the inter-area data sharing occurs. Meanwhile, [24] uses estimation to avoid delay in data sharing. And last, the unnecessary usage of clock synchronization in [26] is how they define the asynchronous algorithm. In this thesis, the asynchronous definition used leans towards [24]. An estimate will be employed when no data sharing occurs between two neighboring nodes.

2.6. Literature Review Relevation to the Thesis

An algorithm based on Consensus and Innovation algorithm will be developed in this thesis. It has been implemented for solving DC distribution grid optimization problems with the losses being accounted for in the previous research [12]. However, it takes up to 200000 iteration to converge. This happens due to the tuning parameter value which has to be set to gain convergence. Therefore, an approach to formulate the tuning parameters will be conducted. Moreover, when the algorithm is implemented in microcomputers, delay occurs during the calculation. Therefore, asynchronous algorithm will be discussed to reduce the delay. Both approach will lead to a plausible implementation of the OPF algortihm.

3

Algorithm for the Distributed Optimal Power Flow: Lossless Optimal Power Flow

3.1. Problem Definition

The objective of the optimization problem is to minimize the cost of power production in the whole grid. It is formed such as:

$$\min \sum_{m \in \mathcal{N}} A_m (p_m^{\mathrm{S}})^2 + B_m p_m^{\mathrm{S}} \tag{3.1}$$

The term B_m and A_m are the linear and quadratic operational price of a generator (m.u/W and m.u/W^2) and p_m^S is the power generated in node m. This problem is subjected to some constraints below:

$$p_m^{\mathrm{S}} = \sum_{n \in \Omega_m} G_{m,n}^p (u_m - u_n) \tag{3.2}$$

$$G_{m,n}^p (u_m - u_n) \leq \overline{P}_{m,n} \tag{3.3}$$

$$\underline{P}_m^{\mathrm{S}} \leq p_m^{\mathrm{S}} \leq \overline{P}_m^{\mathrm{S}} \tag{3.4}$$

The constraints are formulated in a DC system formulation where the current flows due to the voltage difference multiplied by the conductance. While in (2.46), it is a DC approximated AC power flow where the power flows due to the voltage angle difference multiplied by the admittance. The constraints comprise some variables which are voltage in node m or n (u_m or u_n), maximum and minimum power production ($\overline{P}_m^{\mathrm{S}}$ and $\underline{P}_m^{\mathrm{S}}$), maximum power flow in the line m, n ($\overline{P}_{m,n}$), and nominal conductance ($G_{m,n}^p$). The nominal conductance is defined as a nominal voltage times the line conductance ($G_{m,n}^p = u_{\mathrm{nom}} G_{m,n}$) to transform the current representation into power. By using this nominal conductance, there will be no power loss along the line since the power flow leaving node m will be identical to the power flow in the receiving node n.

The first constraint (3.2) is the equality constraint explaining that the power injected in the node m equals the power flowing out from node m to every connected node (Ω_m). This is basically a Kirchoff Current Law, except that the current is transformed to power using the term u_{nom}. The second one (3.3) represents the power flow limit. The last equation (3.4) shows the power production limit for every node m.

This algorithm was derived based on Consensus + Innovation as presented in [14] as well as [12]. This chapter will explain the updates for every variable, emphasizing on the tuning parameters formulation especially.

3.2. Lagrangian Function

The method for solving this optimization problem is Consensus + Innovation. Therefore, dual variables and Lagrangian function will be employed. Based on the objective function and the constrains, Lagrangian function can be written as follows:

$$\begin{aligned}\mathcal{L} = & \sum_{m\in\mathcal{N}}\sum_{s\in\mathcal{S}}\left(A_m(p_m^{\mathrm{S}})^2 + B_m p_m^{\mathrm{S}}\right) \\ & + \sum_{m\in\mathcal{N}}\lambda_m\left(\sum_{n\in\Omega_m} G_{m,n}^{p}(u_m - u_n) - \sum_{m\in\mathcal{N}} p_m^{\mathrm{S}}\right) \\ & + \sum_{m\in\mathcal{N}}\sum_{n\in\Omega_m}\mu_{m,n}\left(G_{m,n}^{p}(u_m - u_n) - \overline{P}_{m,n}\right) \\ & + \sum_{m\in\mathcal{N}}\mu_{\overline{m}}^{\overline{P}}\left(p_m^{\mathrm{S}} - \overline{P}_m^{\mathrm{S}}\right) \\ & + \sum_{m\in\mathcal{N}}\mu_{\underline{m}}^{\underline{P}}\left(-p_m^{\mathrm{S}} + \underline{P}_m^{\mathrm{S}}\right)\end{aligned} \tag{3.5}$$

The λ_m will become the Locational Marginal Price (LMP) in the node m that expresses the sensitivity of the system cost for the system demand in m.u/W (monetary unit per watt). Meanwhile, all the μ is the dual variable that also expresses the sensitivity regarding the inequality constraint.

3.3. Karesh Kuhn Tucker Conditions

The Lagrangian function must follow First Order Optimality Conditions, Complementary Slackness Conditions, and Positivity Conditions.

First Order Optimality Conditions

$$\frac{\partial\mathcal{L}}{\partial p_m^{\mathrm{S}}} = \sum_{s\in\mathcal{S}} 2A_m p_m^{\mathrm{S}} + B_m - \lambda_m + \mu_{\overline{m}}^{\overline{P}} - \mu_{\underline{m}}^{\underline{P}} = 0 \tag{3.6}$$

$$\frac{\partial\mathcal{L}}{\partial u_m} = \lambda_m\sum_{n\in\Omega_m} G_{m,n}^{p} - \sum_{n\in\Omega_m}\lambda_n G_{m,n}^{p} + \sum_{n\in\Omega_m} G_{m,n}^{p}(\mu_{m,n} - \mu_{n,m}) \tag{3.7}$$

$$\frac{\partial\mathcal{L}}{\partial\lambda_m} = -p_m^{\mathrm{S}} + \sum_{n\in\Omega_m} G_{m,n}^{p}(u_m - u_n) = 0 \tag{3.8}$$

$$\frac{\partial\mathcal{L}}{\partial\mu_{m,n}} = \sum_{n\in\Omega_m} G_{m,n}^{p}(u_m - u_n) - \overline{P}_{m,n} \leq 0 \tag{3.9}$$

$$\frac{\partial\mathcal{L}}{\partial\mu_{\overline{m}}^{\overline{P}}} = p_m^{\mathrm{S}} - \overline{P}_m^{\mathrm{S}} \leq 0 \tag{3.10}$$

$$\frac{\partial\mathcal{L}}{\partial\mu_{\underline{m}}^{\underline{P}}} = -p_m^{\mathrm{S}} + \underline{P}_m^{\mathrm{S}} \leq 0 \tag{3.11}$$

Complementary Slackness Condition

The complementary slackness conditions taken from the constraints are:

$$\mu_{m,n}\left(\overline{P}_{m,n} - \sum_{n\in\Omega_m} G^p_{m,n}(u_m - u_n)\right) = 0 \tag{3.12}$$

$$\mu_{n,m}\left(-\overline{P}_{m,n} + \sum_{n\in\Omega_m} G^p_{m,n}(u_m - u_n)\right) = 0 \tag{3.13}$$

$$\mu^{\overline{P}}_m\left(\overline{P}^{\mathrm{S}}_m - p^{\mathrm{S}}_m\right) = 0 \tag{3.14}$$

$$\mu^{\underline{P}}_m\left(p^{\mathrm{S}}_m - \underline{P}^{\mathrm{S}}_m\right) = 0 \tag{3.15}$$

Positivity Condition

All the dual variable regarding the limits have to be positive. It is written as:

$$\mu_{m,n}, \mu_{n,m}, \mu^{\overline{P}}_m, \mu^{\underline{P}}_m \geq 0 \tag{3.16}$$

3.4. LMP and Power Updates

Power is the vital parameter in this optimization. The most power generated should be coming from all the cheapest generators. The more expensive generators can only produce if all the cheaper units have reached their maximum generation or there are other constraints. Meanwhile, the Locational Marginal Price (LMP) explains the price in the node and will be identical for every node as long as no losses and/or congestion occurs. The LMP is expressed as m.u/W, a monetary unit (m.u) over a power unit (watt). To avoid oscillation between LMP and power during both updates, a new update mechanism is proposed which links the updates of the price and power. Figure 3.1 and 3.2 depicts how the power relates to the LMP. Throughout the iteration, either the LMP or the power should be forced to follow the trajectory. The generator can only produce power if its LMP reaches its cost coefficient which is denoted by B_m in (3.1). It stays at its minimum power (normally equals to 0) if the LMP is less than its cost coefficient. When the LMP equals its cost coefficient, the generator will produce power as long as it can until it reaches its maximum power. Along the power changes, the price will vary if the generator has a quadratic cost function ($A_m > 0$) is present or stay constant if it has a linear cost function ($A_m = 0$). If it reaches the maximum power without satisfying the demand, the LMP will continue in going higher to find another generator with a higher price. It makes an intuitive sense as in a market, if the price is lower than the price set for a product, the producer cannot sell anything. When the price equals, the products can be sold until they are sold out. If there is no product left, the price will continue going higher until it equals the other price from other producers.

Figure 3.1 and 3.2 divides the update into two meaningful region. The first region is the constant power where the LMP is below the minimum marginal price (LMP $< B_m + 2A_m(\underline{P}_m)$) and above the maximum marginal price (LMP $> B_m + 2A_m(\overline{P}_m)$). The other region is called marginal generator where the power can vary between its boundaries while LMP $= B_m + 2A_m(p^{\mathrm{S}}_m)$. In the upcoming cases, it is chosen for the generator's minimum power as 0 ($\underline{P}_m = 0$) for simplicity.

3.4.1. Constant Power Region

Intuitively, the load will inform its demand to other nodes, creating a power mismatch in the node, which can be found in (3.8). Due to this power mismatch, the generator should produce the desired amount of power. However, the LMP should be equal to its price first to produce power. Therefore, it is necessary to increase the LMP due to power mismatch. Meanwhile, one grid should have the similar price if there is no congestion. Equation (3.7) in the LMP update represents the LMP agreement of a node with its neighboring node(s). Therefore, the LMP should update like the following way:

$$\lambda_m(l+1) = \lambda_m(l) - \alpha^{\lambda}_u \frac{\partial \mathcal{L}}{\partial u_m} + \alpha^{\lambda}_{\lambda} \frac{\partial \mathcal{L}}{\partial \lambda_m} \tag{3.17}$$

where α^{λ}_u and $\alpha^{\lambda}_{\lambda}$ are the tuning parameters that will be explained in the following subsections.

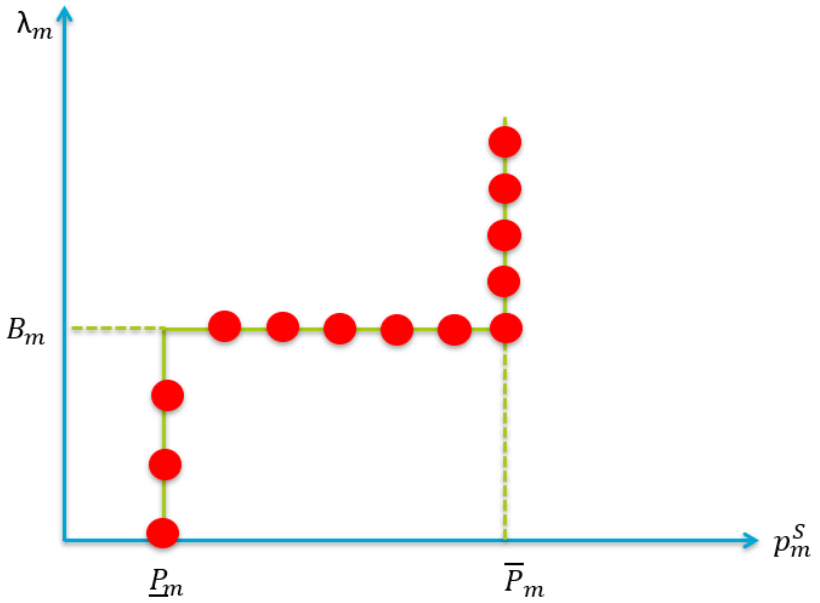

Figure 3.1: Relation between power (x-axis) and LMP (y-axis) when the generator has a linear cost function. Each red dot represents the power and LMP for every iteration. The result of LMP and power calculation is bounded by this graph. In the upcoming cases, it is chosen for the generator's minimum power as 0 ($\underline{P}_m = 0$) for simplicity.

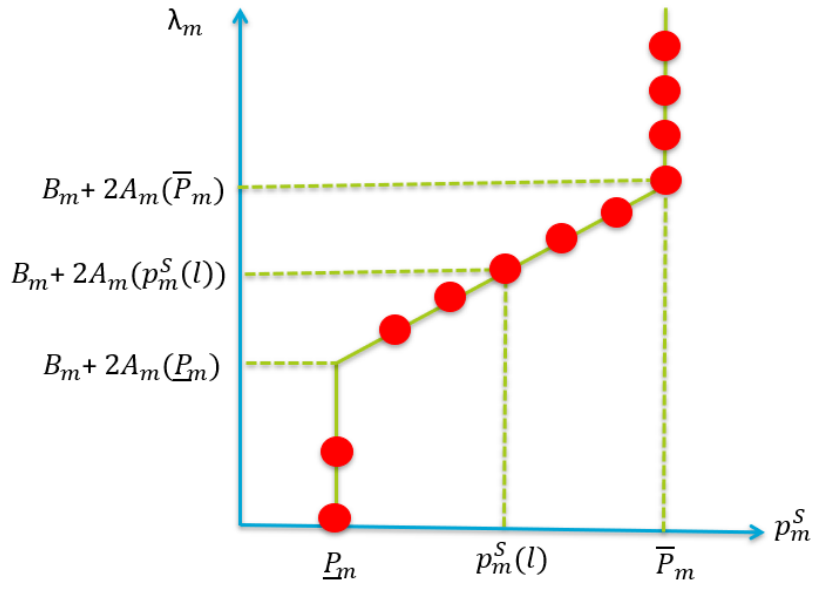

Figure 3.2: Relation between power (x-axis) and LMP (y-axis) when the generator has a quadratic cost function. The symbol l denotes the iteration counter. During the marginal generator region, the LMP changes according to the power generation value. In the upcoming cases, it is chosen for the generator's minimum power as 0 ($\underline{P}_m = 0$) for simplicity.

Formulation for α_u^λ

The term α_u^λ is formulated so that λ_m as this node's LMP can resemble λ_n, the other nodes' (or node's) LMP. If it occurs, it means that the lambda reaches a consensus. To attempt this approach, (3.17) is rewritten by neglecting $\frac{\partial \mathcal{L}}{\partial \lambda_m}$ and expanding $\frac{\partial \mathcal{L}}{\partial u_m}$:

$$\lambda_m(l+1) = \lambda_m(l) - \alpha_u^\lambda \left(\lambda_m \sum_{n \in \Omega_m} G_{m,n}^p - \sum_{n \in \Omega_m} \lambda_n G_{m,n}^p + \sum_{n \in \Omega_m} G_{m,n}^p (\mu_{m,n} - \mu_{n,m}) \right) \tag{3.18}$$

To simplify things, there is no congestion in the grid. Hence, all the μ can be ignored:

$$\lambda_m(l+1) = \lambda_m(l) - \alpha_u^\lambda \left(\lambda_m \sum_{n \in \Omega_m} G_{m,n}^p - \sum_{n \in \Omega_m} \lambda_n G_{m,n}^p \right) \tag{3.19}$$

Since the desired solution is simply $\lambda_m = \lambda_n$, therefore:

$$\alpha_u^\lambda = \frac{k}{\sum_{n \in \Omega_m} G_{m,n}^p} \qquad k = 1 \tag{3.20}$$

$$\lambda_m(l+1) = \lambda_m(l) - \frac{1}{\sum_{n \in \Omega_m} G_{m,n}^p} \left(\lambda_m \sum_{n \in \Omega_m} G_{m,n}^p - \sum_{n \in \Omega_m} \lambda_n G_{m,n}^p \right) \tag{3.21}$$

$$\lambda_m(l+1) = \lambda_m(l) - \lambda_m + \lambda_n \tag{3.22}$$

$$\lambda_m(l+1) = \lambda_n \tag{3.23}$$

However, if k = 1 as stated in (3.20), λ_m will directly become λ_n and the node m update oscillates against n. To overcome the problem, k should be set to 0.5 to give a sense that node m does half and so does node n. It can be concluded that:

$$\alpha_u^\lambda = \frac{0.5}{\sum_{n \in \Omega_m} G_{m,n}^p} \left[\frac{\mathrm{V}}{\mathrm{W}} \right] \tag{3.24}$$

The equations hold for the region where the generator is at its maximum power without satisfying the demand. The LMP will continue to search for another generator which has the next low price.

Equation (3.24) partly answers the research question 1. The tuning parameter is formulated based on a physical interpretation that in the solution, the LMP has to be identical for a connected two nodes without any congestion and losses.

Formulation for α_λ^λ

The second derivation term in (3.17) expresses the power mismatch in the node, referred to (3.8). The tuning parameter α_λ^λ then represents the rate of change in the LMP regarding power mismatch. The value is estimated as the ratio between the order of the LMP and power. In this thesis' case, the order of the power is in kilowatts (kW). It is desired that the LMP will change 0.00001 m.u/W due to 1 W power mismatch or equivalent with 0.01 m.u/W change due to 1 kW power mismatch. Thus:

$$\alpha_\lambda^\lambda = 0.00001 \ \frac{\mathrm{m.u}}{\mathrm{W}^2} \tag{3.25}$$

The tuning parameter α_λ^λ determines the sensitivty of LMP change due to the power mismatch. Note that this tuning factor can still be tuned and maybe ten times smaller if the power mismatch is too high. The tuning parameter is set that way so the iteration result can follow Figure 3.1 in updating LMP to reach its linear cost coefficient. Every case may have its faster tuning for this parameter by setting it to a higher number.

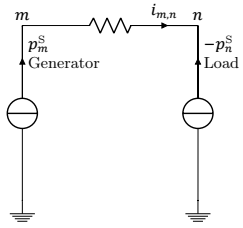

Figure 3.3: A simple load and generator grid.

3.4.2. Marginal Generator Region

After the LMP reaches the node's marginal cost, the generator is allowed to produce power. The power produced needs to follow the demand by detecting the power mismatch in that node. Observing Figure 3.3, the power mismatch in the Load node triggers the Generator node to produce power. The load in node n will create voltage drop resulting u_m higher than u_n as explained in Chapter 3.5. This condition triggers power flowing from m to n. Based on (3.8), the generator should produce power as much as the power flowing to satisfy the equation. Aside from the power mismatch, the LMP consensus in (3.7) should also be taken into account. Thus:

$$p_m^S(l+1) = p_m^S(l) + \alpha_\lambda^p \frac{\partial \mathcal{L}}{\partial \lambda_m} + \alpha_u^p \frac{\partial \mathcal{L}}{\partial u_m} \tag{3.26}$$

Formulation for α_λ^p

Adding the term $\frac{\partial \mathcal{L}}{\partial \lambda_m}$ for the power update creates the sense on how much power should be dispatched regarding the power mismatch. To get a smooth result, the update only needs to go half the necessary step, resembling the LMP update in (3.24). Since the updates are done simultaneously with the voltage, which will be discussed in the next section, the power only needs to increase a quarter from what is required ad the voltage update will take care the other quarter.

$$\alpha_\lambda^p = 0.25 \tag{3.27}$$

Formulation for α_u^p

The second derivation term in the power updates helps the power to increase or decrease power regarding the lambda difference between nodes. By referring to (3.26), neglecting the power mismatch term, and applying no congestion event, the power update would be:

$$p_m^S(l+1) = p_m^S(l) + \alpha_u^p \left(\lambda_m \sum_{n \in \Omega_m} G_{m,n}^p - \sum_{n \in \Omega_m} \lambda_n G_{m,n}^p \right) \tag{3.28}$$

Setting the α_u^p with the same way in α_u^λ in (3.20), it will result:

$$p_m^S(l+1) = p_m^S(l) + (\lambda_m - \lambda_n) \tag{3.29}$$

Therefore, k has to be set as the ratio of the order of the power (in W) with the LMP (expressed in m.u/W). This formulation resemblance α_u^λ in subsection 3.4.1 except that it is the inverse ratio. It is desired that the power should change by 1 kW with respect to 1 m.u/W LMP difference. Hence, the formulation is:

$$\alpha_u^p = \frac{1000 \frac{\mathrm{W}^2}{\mathrm{m.u}}}{\sum_{n \in \Omega_m} G_{m,n}^p} \left[\frac{\mathrm{V}}{\mathrm{W}} \right] \tag{3.30}$$

3.5. Voltage Updates

A voltage difference makes current and power flow possible. If we see Figure 3.3 for a simple model, the current needs to flow from the generator to the load by making the voltage in the load lower than the generator. This will happen if the load node reduces its voltage. The suitable differential is (3.8)

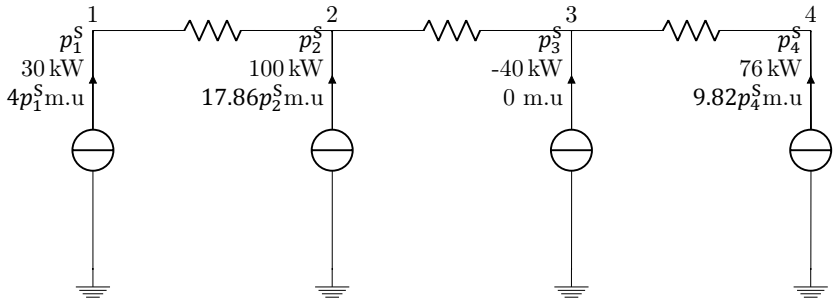

Figure 3.4: Simple four node radial grid with one load and three distributed generators. Without any losses and congestion, the load should be satisfied from the generator in node one first (the cheapest) and take the remaining from the generator in node 4 (the next cheapest). The generation cost has a unit of m.u which stands for monetary unit. The notes in the units from top to bottom are: unit's name, unit's capacity (positive for generator and negative for the load), and unit's cost function.

which represents the power mismatch. The load with negative p_m^S will turn (3.8) to a positive value. Therefore, the existing voltage value should be subtracted by (3.8).

$$u_m(l+1) = u_m(l) - \alpha_\lambda^u \frac{\partial \mathcal{L}}{\partial \lambda_m} \tag{3.31}$$

Formulation for α_λ^u

The voltage update is basically the reverse approach of the power update. In the power update, If (3.8) is positive, meaning to much power flowing from node m, the power increase its value. In the voltage update, the voltage reduces its value to decrease the power flow and ultimately satisfy the nodal power (zero power mismatch). As mentioned in subsection 3.4.2, the voltage does a quarter step since the power also does a quarter step in the update. Together, they go half to the solution.

$$\alpha_\lambda^u = \frac{0.25}{\sum_{n\in\Omega_m} G_{m,n}^p} \left[\frac{\mathrm{V}}{\mathrm{W}}\right] \tag{3.32}$$

3.6. Dual Variable for Power Limit

The lambda consensus results in identical figures for every node (without congestion in any line). To satisfy (3.6), $\mu_m^{\overline{P}}$ and $\mu_m^{\underline{P}}$ should active as the difference between its price (B_m) and the LMP. Both dual variables are calculated by the equations below:

$$\mu_m^{\overline{P}}(l+1) = \begin{cases} 0 & \text{if } p_m^S(l+1) \le \overline{P}_m^S \\ \mu_m^{\overline{P}}(l) - \beta_p^{\overline{P}} \frac{\partial \mathcal{L}}{\partial p_m^S} & \text{if } p_m^S(l+1) > \overline{P}_m^S \end{cases} \tag{3.33}$$

$$\mu_m^{\underline{P}}(l+1) = \begin{cases} 0 & \text{if } p_m^S(l+1) \ge \underline{P}_m^S \\ \mu_m^{\underline{P}}(l) + \beta_p^{\underline{P}} \frac{\partial \mathcal{L}}{\partial p_m^S} & \text{if } p_m^S(l+1) < \underline{P}_m^S \end{cases} \tag{3.34}$$

$$\beta_p^{\overline{P}} = \beta_p^{\underline{P}} = 0.5 \tag{3.35}$$

Both parameters have value if the power in the node exceeds the upper and lower limit.

Sample Case for Non-Congested Line

The development of the algorithm is valid for a lossless case without congestion. For a simple case, Figure 3.4 shows a grid with one load and three distributed generators with a different price. The desired solution is that the cheapest generator (node 1) dispatches all its power. Since its capacity is below the load capacity, the remaining power should be transferred from the next cheapest generator (node 4). The algorithm works as desired. The converged solution presented in Figure 3.5 and Figure 3.6 follow exactly the dersired result. Moreover, no oscillation occurs between the LMP and power. Power changes only occur when the LMP stays constant, following Figure 3.1. From Figure 3.5, the speed of

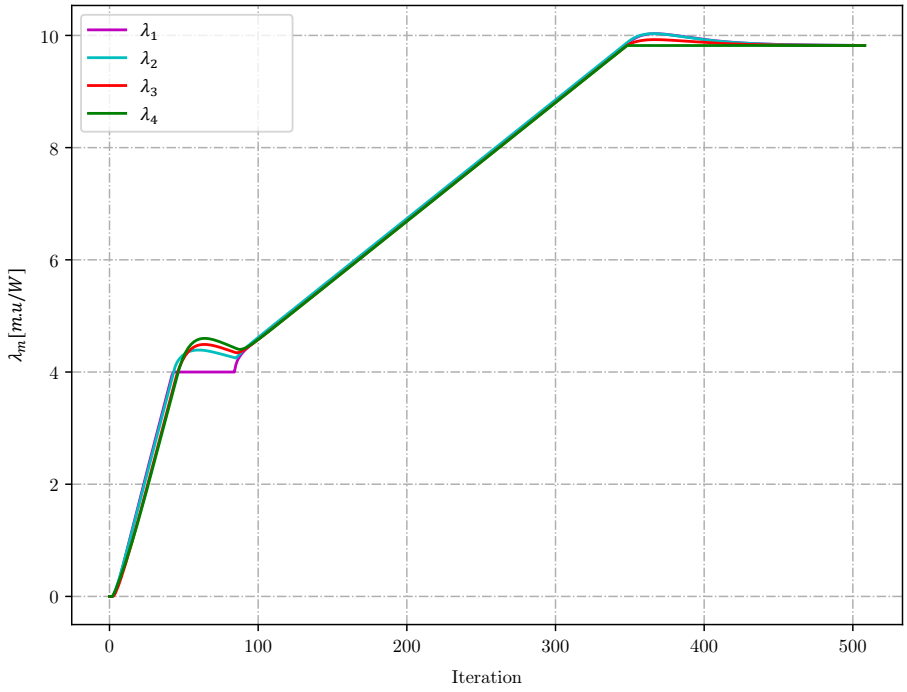

Figure 3.5: Locational Marginal Price (LMP) at every node for the grid in Figure 3.4. The values only rise during constant power region (maximum or minimum power).

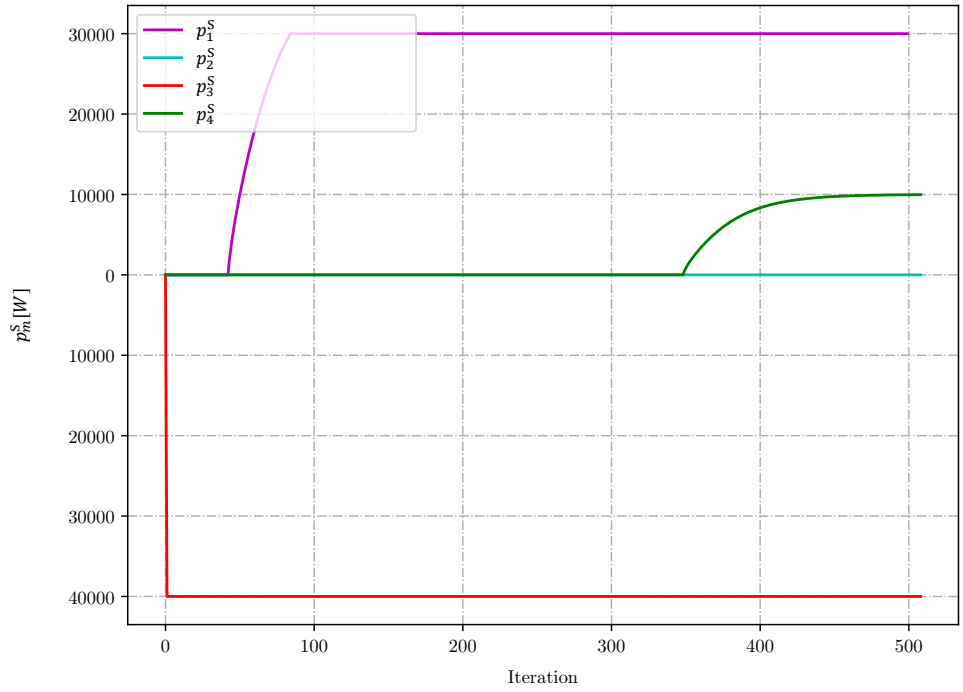

Figure 3.6: Power generation in each node for the grid in Figure 3.4. The power only updates when the LMP has reached the marginal price. For instance, p_1^S only updates when in Figure 3.5, λ_1 is constant.

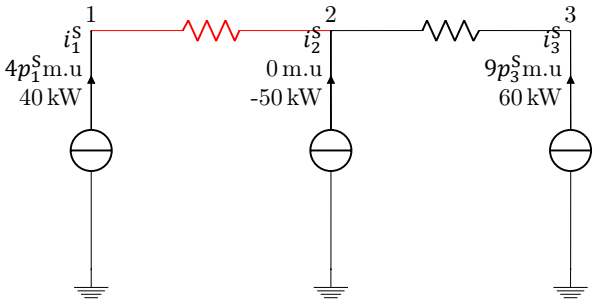

Figure 3.7: Simple three node serial case as an example. The red line depicts a limited power transfer of 25kW. The $4p_1^S$ m.u unit (cheaper) cannot produce power more than 25kW, and the remaining 15kW will be handled by the $9p_3^S$ m.u unit (more expensive), making both of them marginal generators.

rise of the value from 0 to the iteration where the power starts updating is determined by α_λ^λ. Increasing this tuning parameter may lead to a faster rise of the LMP, but it can cause the LMP from the more expensive generator to reach its marginal price. If that happens, there will be two marginal generators, and it will need some time for the expensive generator to turn the power off.

Up until this point, Figure 3.1-3.2 alongside with the equations of LMP, power, and voltage update including their respective tuning parameters have answered the research question 1 for the lossless and non-congested case. In Figure 3.1 and 3.2, the generator can produce power only when the LMP is more or equal the linear cost coefficient or the market price. This is how the physical interpretation is used to update the power and the LMP. As a result, the no oscillation occurs between the LMP and power. In the LMP update itself, the LMP between nodes should be the same in the absence of losses and congestion. Therefore, the tuning parameter is formulated as (3.24) so the derivation in (3.19)-(3.23) works. In the voltage update, the tuning parameter (3.32) is formulated so that the voltage increase or decrease its value due to power mismatch (3.8). The coefficient 0.25 is taken so the voltage only solves 0.25 part and the power does also 0.25 in (3.26). The first order of Karesh Kuhn Tucker conditions are studied to produce an oscillation-free result in Fig 3.5 and 3.6.

The results show that it takes 500 iterations to reach the convergence. The convergence is relatively slow compared to [14, 15] since the algorithm works conservatively. It means that combined, the power and the voltage solves 50% of the mismatch instead of going too high and reduce it afterward. Moreover, the LMP increases slowly to make sure that the cheap generator reaches its maximum power and let the more expensive one produce. Besides, it also avoids the LMP from another generator which has a higher price reaches its price before the cheaper generator produces its maximum power. Consequently, the calculation needs some extra iteration to eliminate the unnecessary generated power.

3.7. Congestion Management

Since there is always a current limitation (in the lossless case, power), congestion in a line needs to be considered. In Figure 3.7 the load can be fulfilled by activating the cheaper unit only. However, it is not possible since the line limits the power transfer. The only solution is to enable and get the power from the more expensive unit after updating the price up to the more expensive unit's LMP. With the cheaper unit still being a marginal generator (supplying power within its range), the LMP for the cheaper unit has to remain constant. Therefore, there will be an LMP difference between both generators and $\mu_{m,n}$ will be higher than zero.

3.7.1. Area Separation

In the case of Figure 3.7, both generators will become marginal which means they both operate at their marginal price. Ultimately it would divide the grid into two areas. The first area consists of node 1 only, operating at its own price while the other area consists of node 2 and 3 operating at node 3's price.

Based on that fact, a new approach to treat this congestion is purposed. Whenever the congestion is sensed from the sending end (node 1), node 1 is no longer consider node 2 as its neighbor for LMP consensus. In (3.7), node 2 will be excluded from $n \in \Omega_{m=1}$. The exclusion does not occur for the power mismatch in (3.8) since they are still physically connected. This condition also applies to node 1 from

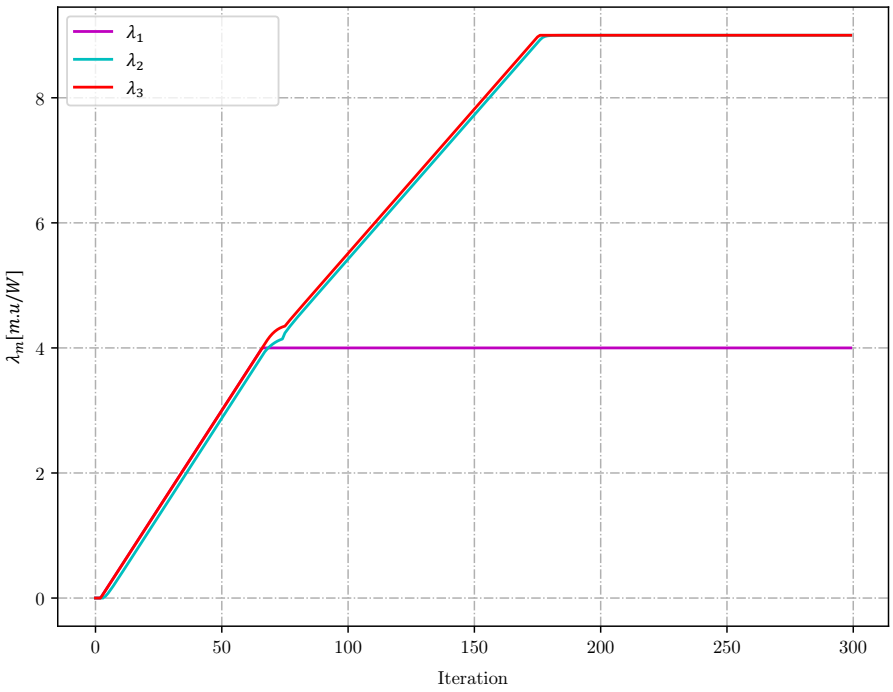

Figure 3.8: Locational Marginal Price (LMP) at every nodes for the grid in Figure 3.7. In the solution, the grid is divided into two areas with different price to keep the generators as marginal generators

node 2 point of view.

When the voltage update results in excessive power flow, the voltage in the sending end adjusts its voltage so the power flow matches the power flow limit.

$$u_m(l+1) = \frac{\overline{P}_{m,n}}{\sum_{n\in\Omega_m} G^p_{m,n}} + u_n(l) \tag{3.36}$$

By separating these nodes, the LMP consensus happens separately for both areas. The dual variable $\mu_{m,n}$ is no longer useful and can be calculated manually as the LMP difference between both nodes.

$$\mu_{m,n}(l+1) = \begin{cases} 0 & \text{if } u_m < u_n \\ \lambda_m - \lambda_n & \text{if } u_m > u_n \end{cases} \tag{3.37}$$

With a limited power transfer, the three node grid is separated into two areas with different LMP as seen in Figure 3.8. The separation starts happening when the power flow from node 2 to 3 violates the boundary (20 kW) in Figure 3.12 and $\mu_{2,3}$ starts to rise from zero in Figure 3.9. During the separation process, generator in node 1 reduces its power to satisfy the power balance as depicted in Figure 3.10 and the voltage of node 1 adjusts its value as shown in Figure 3.11.

3.7.2. Activation of the Dual Variable

This area separation cannot be applied in a meshed grid where loops exist. Figure 3.13 shows an example of a simple four node meshed grid where congestion occurs in one of the lines. In this case, area separation is not allowed since the connection of node 3-2-1-4 is non-congested and should have the same LMP. When the case is run through a centralized method, it results as in Table 3.1 where all the LMP are different and the dual variable $\mu_{m,n}$ is not the difference between the LMP from the two ends of the congested line. Therefore, the LMP and $\mu_{m,n}$ should be updated naturally. When a congestion occurs between node m and n, the voltage is updated with (3.36) and the node n chosen

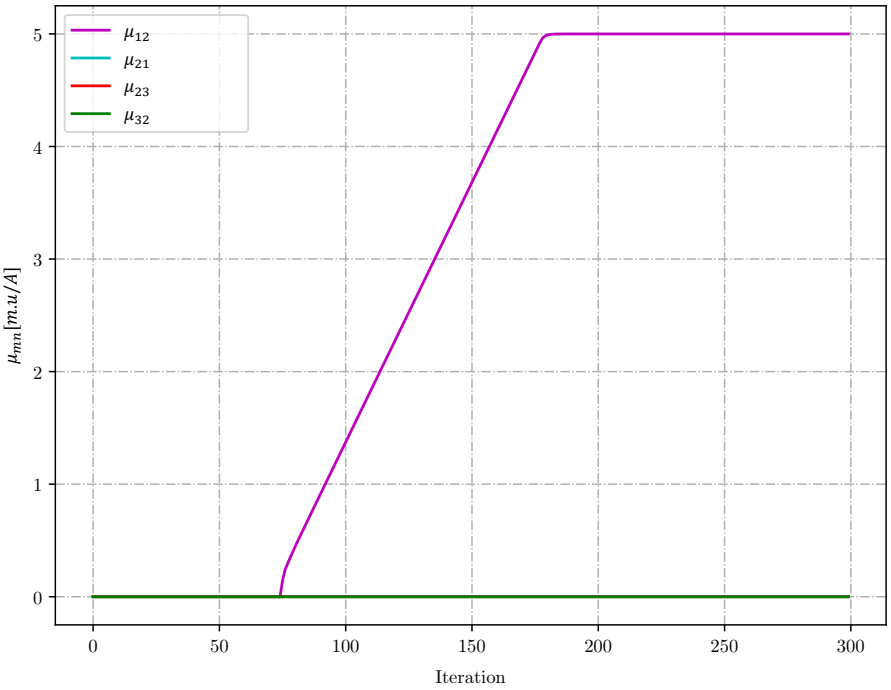

Figure 3.9: Dual variable for the line limit for the grid in Figure 3.7. The value of $\mu_{1,2}$ starts rising when the value of the power flow exceeds the maximum power transfer.

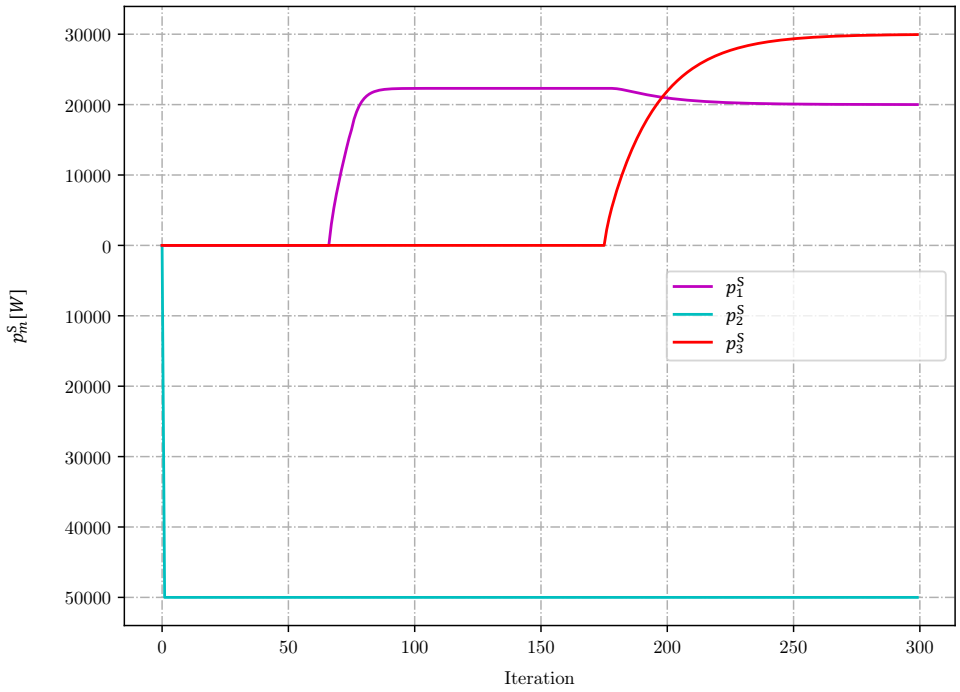

Figure 3.10: The power generation in each node for the grid in Figure 3.7

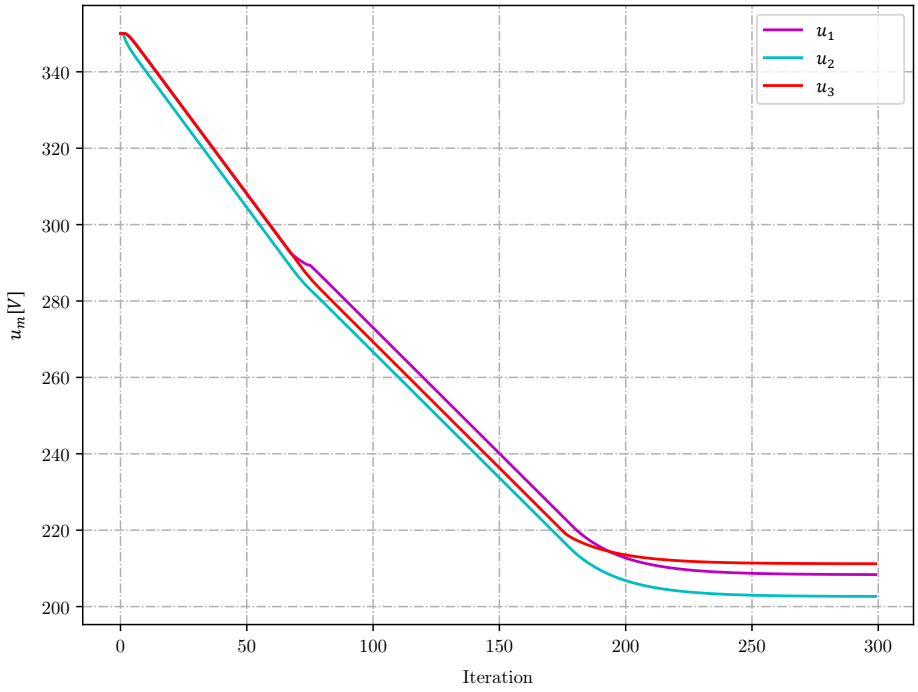

Figure 3.11: The voltage at each node for the grid in Figure 3.7. When the congestion occurs, u_1 is forced to a certain value so the power flow flowing from node 1 and 2 is the power flow limit $\overline{P}_{1,2}$.

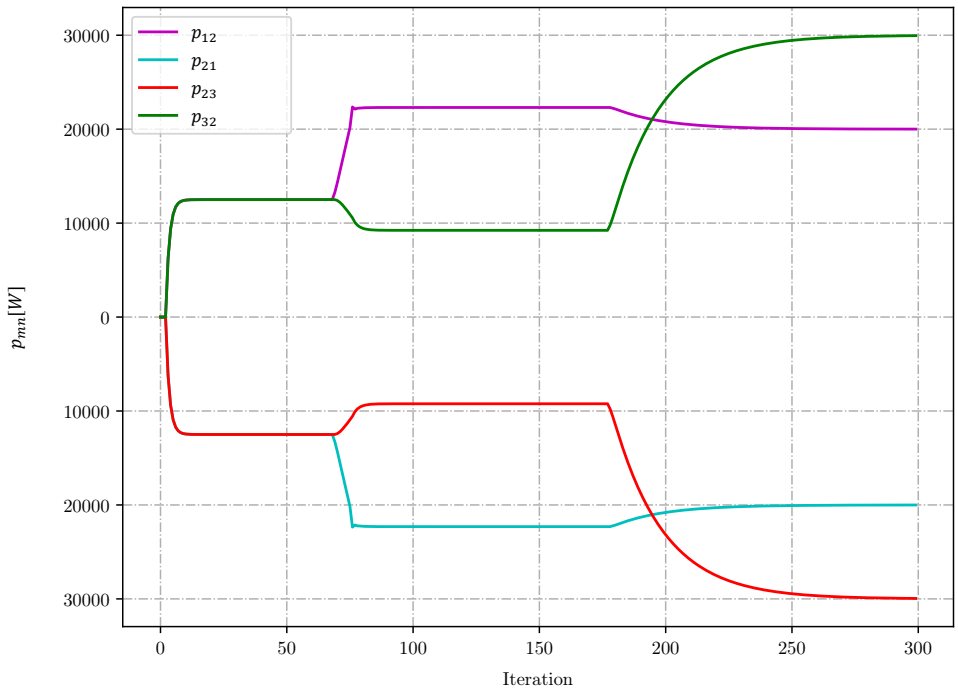

Figure 3.12: The power flowing in the line for the grid in Figure 3.7 where the power in line connecting node 1 and 2 is limited to 20 kW.

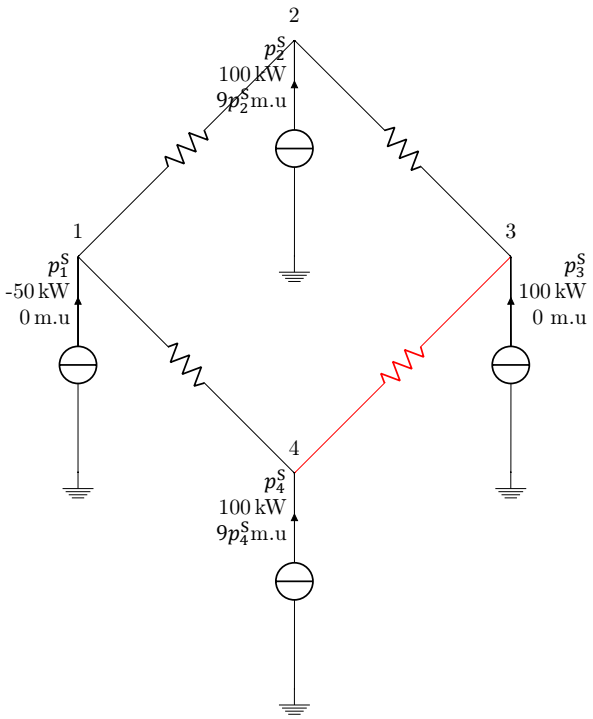

Figure 3.13: Four node mesh with congestion from node 3 to 4 of 20kW. The LMP values for each node is presented in Table 3.1.

is the line that is violated the most if m is connected to multiple congested line to node n. The dual variable $\mu_{m,n}$ is updated such as:

$$\mu_{m,n}(l+1) = \mu_{m,n}(l) + \beta_{m,n}\frac{\partial \mathcal{L}}{\partial \mu_{m,n}} \tag{3.38}$$

It is updated due to the excess power referred to the line limit. The tuning parameter $\beta_{m,n}$ merely is determined by estimating the speed of μ increase because of the excess power flow.

$$\beta^{m,n} = 0.00005 \quad \frac{\text{m.u}}{\text{W}^2} \tag{3.39}$$

Table 3.1: The result of centralized optimal power flow for the case in Figure 3.13, conducted by fmincon function in MATLAB. The result shows different value of LMP for every node.

λ_1	λ_2	λ_3	λ_4	$\mu_{3,4}$
6 m.u/kW	3 m.u/kW	0 m.u/kW	9 m.u/kW	12 m.u/kW

Figure 3.14-3.16 prove that the distributed approach has the same value with the centralized simulation, conducted with fmincon in Matlab. The nodes have different LMP even though only one congestion occurs to satisfy the LMP consensus in (3.7) and the fact that LMP should be equal to the linear cost coefficient for generating power as depicted in Figure 3.1.

The methods Area Separation and Dual Variable Activation answer the research question 2. The new approach is by having the voltage updated, so the power flow is clamped to the power flow limit as in (3.36) for both method. The Area Separation Method is also a new approach to solve a congested case for a radial grid. However, for the meshed grid, the dual variable of the line limit should be updated as the C+I method explained.

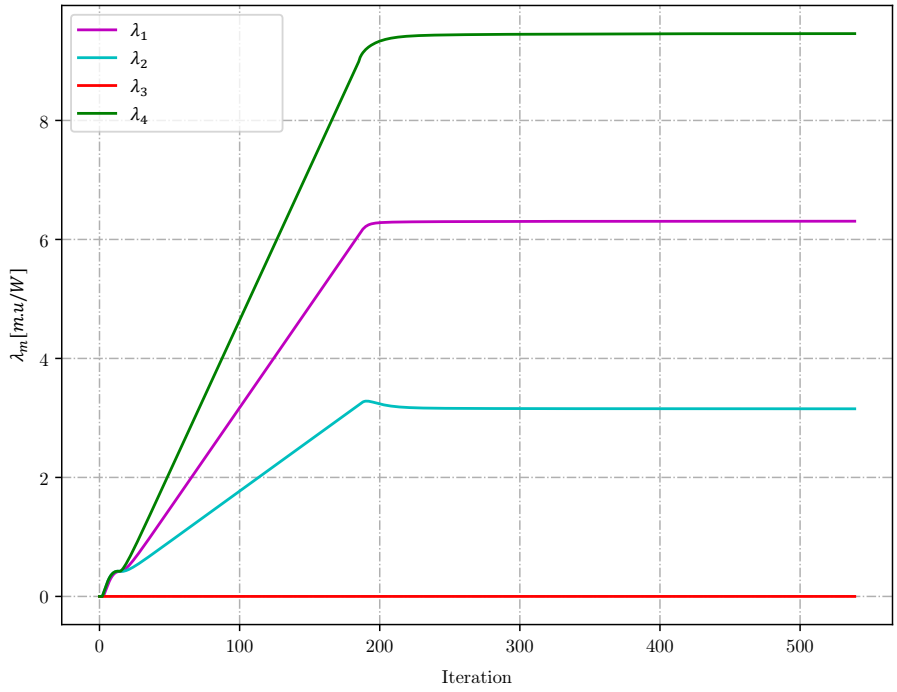

Figure 3.14: Locational Marginal Price (LMP) at every node for the grid in Figure 3.13. The LMP for each node is similar with the result from the centralized simulation presented in Table 3.1.

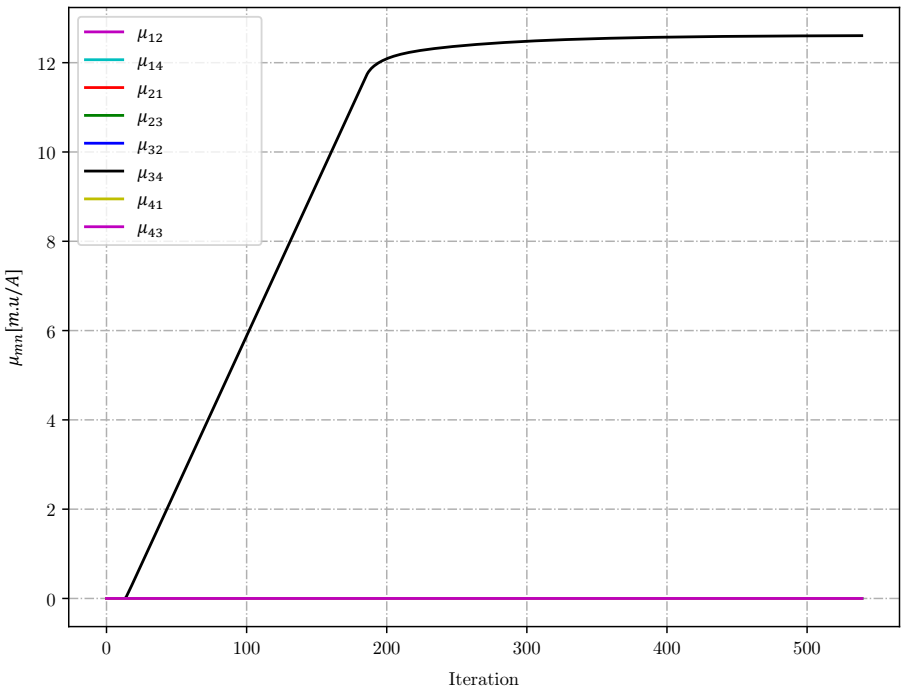

Figure 3.15: The dual variable for the line limit during the congestion in the line connecting node 3 and 4 for the grid in Figure 3.13.

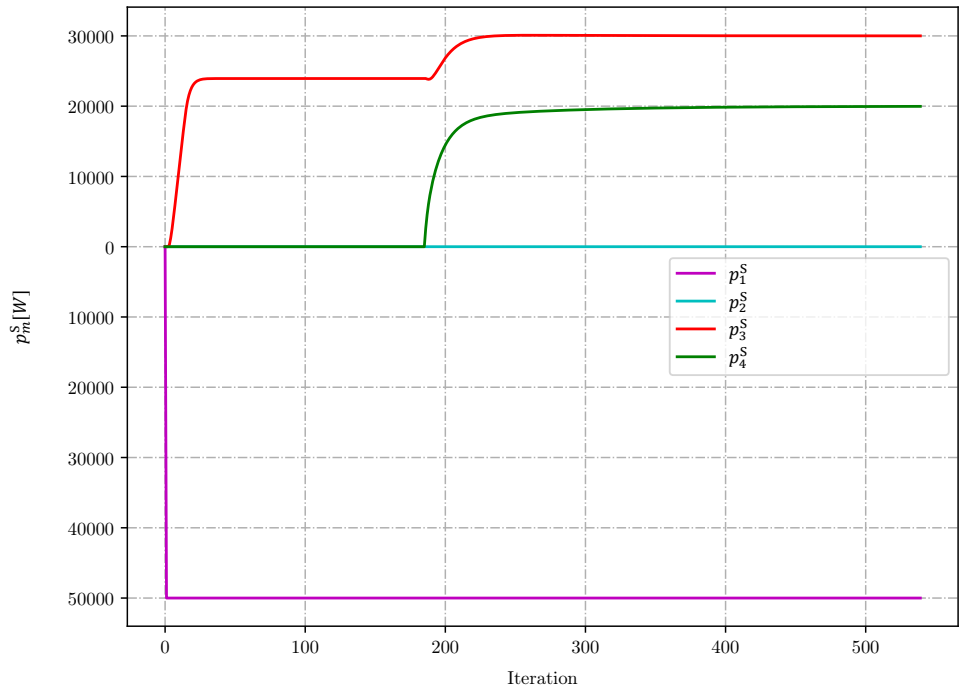

Figure 3.16: The power generation in every node for the grid in Figure 3.13. Node 3 generation is limited due to the power flow limit $\overline{P}_{3,4}$

3.8. Summary of the Tuning Parameters

By having formulated all the tuning parameters, Table 3.2 summarizes the basic tuning parameter for all the Lossless OPF case that will be discussed. Some parameters which are determined by estimation could be changed depending on the situation.

3.9. Sample Cases

This section presents sample cases for the lossless OPF. The cases chosen are a four node radial grid to compare both of the congestion management methods and a six node meshed to show the optimized solution where a bigger loop exists.

The radial case taken as the example is depicted in Figure 3.17. It was a four node grid with various type generators and a fixed load. The load is actually able to be satisfied by the cheap generator. However, the presence of congestion between node 2 and 3 limits the power transfer and the remaining power needs to come from the more expensive generator. In the result, the grid is divided into two areas, indicated by two different lambda values at the end of the iteration.

Figure 3.18 -3.22 depicts the results of this case using area separation method. Compared to Figure 3.5, the LMP, and power have the same curve until a certain point where node 1 is a marginal generator. At some point, node 1 produces too much and is limited by the congestion occurring between node 2 and 3. Therefore, λ_2 in Figure 3.18 changes its value drastically as node 3 is now excluded from node 2 LMP update. In this point, λ_2 only reaches consensus with λ_1. When node 1 produces more than the congestion, the power is decreased due to the lambda difference between node 1 and 2, happening right after the congestion occurs. The rate of change in the power due to the lambda mismatch is determined by α_u^p in (3.26).

When the Dual Variable Activation method is applied, during the event of congestion, the μ increases causing λ_2 to follow λ_1 and neglecting the increase of λ_3 as $\partial\mathcal{L}/\partial u_m = 0$ is satisfied by having $\mu_{2,3}$ in Figure 3.24. The rise of the dual variable μ disturbs the LMP update, hence it creates oscillations in the LMP as shown in Figure 3.23. Area Separation method shows a faster convergence time and smoother

Table 3.2: Tuning parameter for all the Lossless OPF cases.

Tuning Parameter	Purpose	Value
α_u^λ	LMP update regarding the LMP consensus as explained in 3.4.1	$\frac{0.5}{\sum_{n\in\Omega_m} G_{m,n}^p}$ $\left[\frac{\mathrm{V}}{\mathrm{W}}\right]$
α_λ^λ	LMP update regarding the power mismatch in the node as explained in 3.4.1	0.00001 $\frac{\mathrm{m.u}}{\mathrm{W}^2}$
α_λ^p	Power update regarding power mismatch in the node as explained in 3.4.2	0.25
α_u^p	Power update regarding the LMP consensus as explained in 3.4.2	$\frac{1000\frac{\mathrm{W}^2}{\mathrm{m.u}}}{\sum_{n\in\Omega_m} G_{m,n}^p}$ $\left[\frac{\mathrm{V.W}}{\mathrm{m.u}}\right]$
α_λ^u	Voltage update regarding the power mismatch as explained in 3.5	$\frac{0.25}{\sum_{n\in\Omega_m} G_{m,n}^p}$ $\left[\frac{\mathrm{V}}{\mathrm{W}}\right]$
$\beta^{m,n}$	Dual variable update regarding the difference between the line limit and the actual power flow as explained in 3.7.2	0.00005 $\frac{\mathrm{m.u}}{\mathrm{W}^2}$
$\beta^{\overline{P}}$	Dual variable (maximum power) update regarding the LMP difference with the marginal cost as explained in 3.6	0.5
$\beta^{\underline{P}}$	Dual variable (minimum power) update regarding the LMP difference with the marginal cost as explained in 3.6	0.5

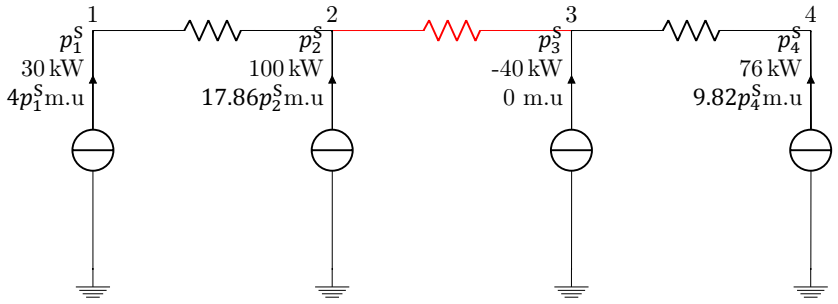

Figure 3.17: Four node serial case with congestion from node 2 to 3.

results. However, this method is not globally useful since it cannot be applied where congestion in a loop exists.

In this meshed case, it is evident that the algorithm works after the case is scaled up to 6 nodes. Figure 3.29-3.33 show that the algorithm is converged. Congestion occurring in a meshed grid causes the nodes to have different LMP value.

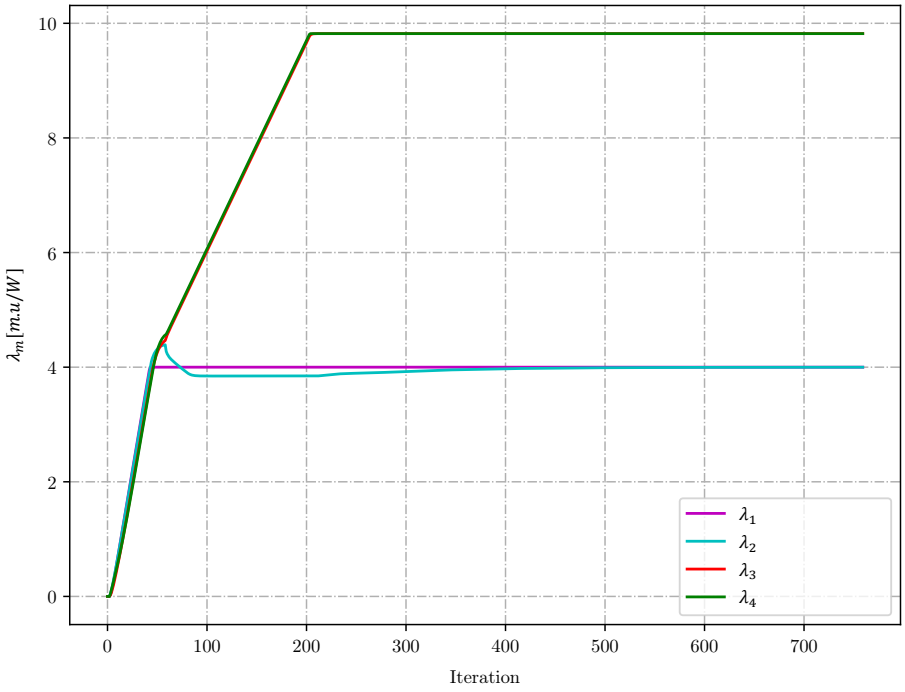

Figure 3.18: Locational Marginal Price (LMP) at every node for a congested four node radial grid using Area Separation Method for the grid in Figure 3.17.

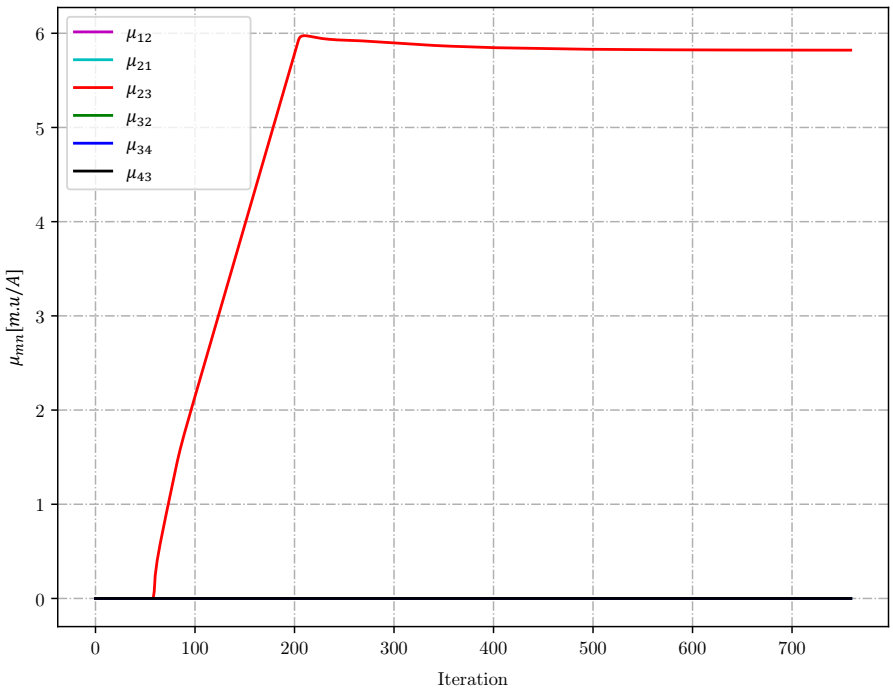

Figure 3.19: Dual variable for the line limit using Area Separation Method for the grid in Figure 3.17. The μ is calculated by taking the difference between the LMP of the nodes at both end of the congested line.

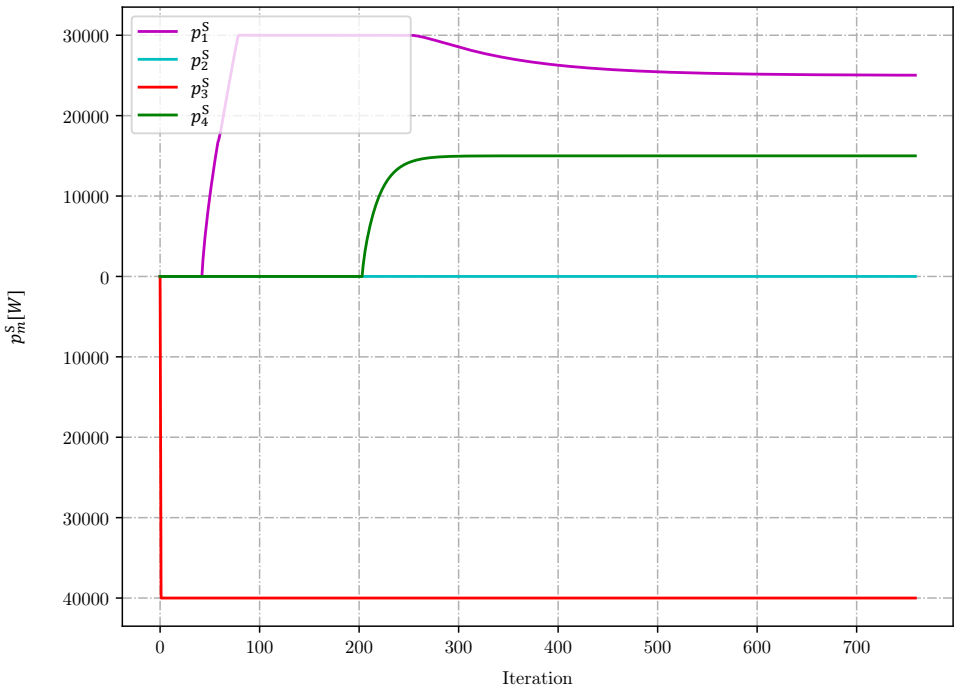

Figure 3.20: Power generation in every node for the grid in Figure 3.17 using Area Separation Method.

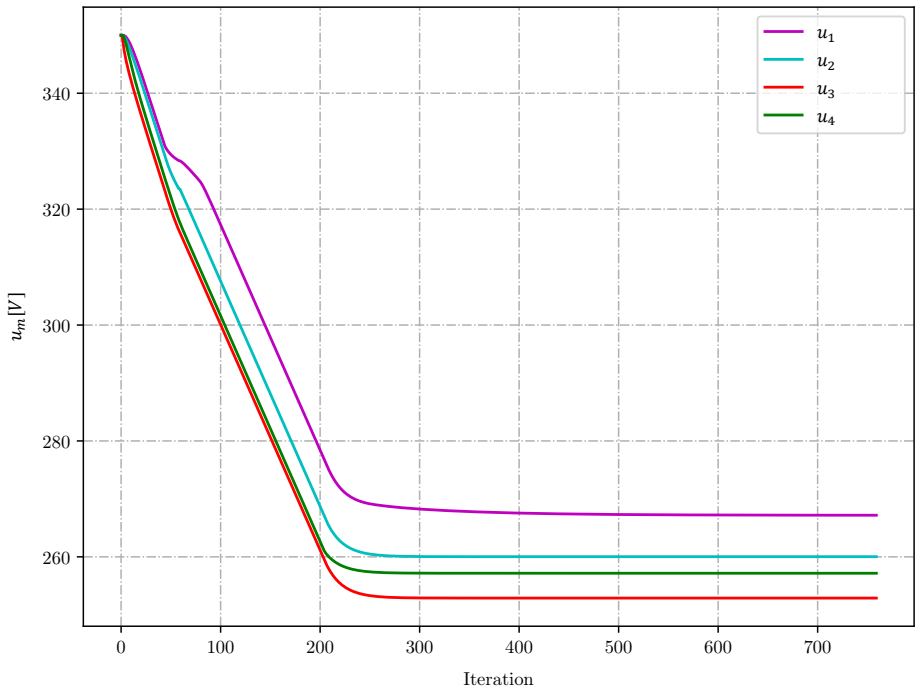

Figure 3.21: Voltage in every node for the grid in Figure 3.17 using Area Separation Method.

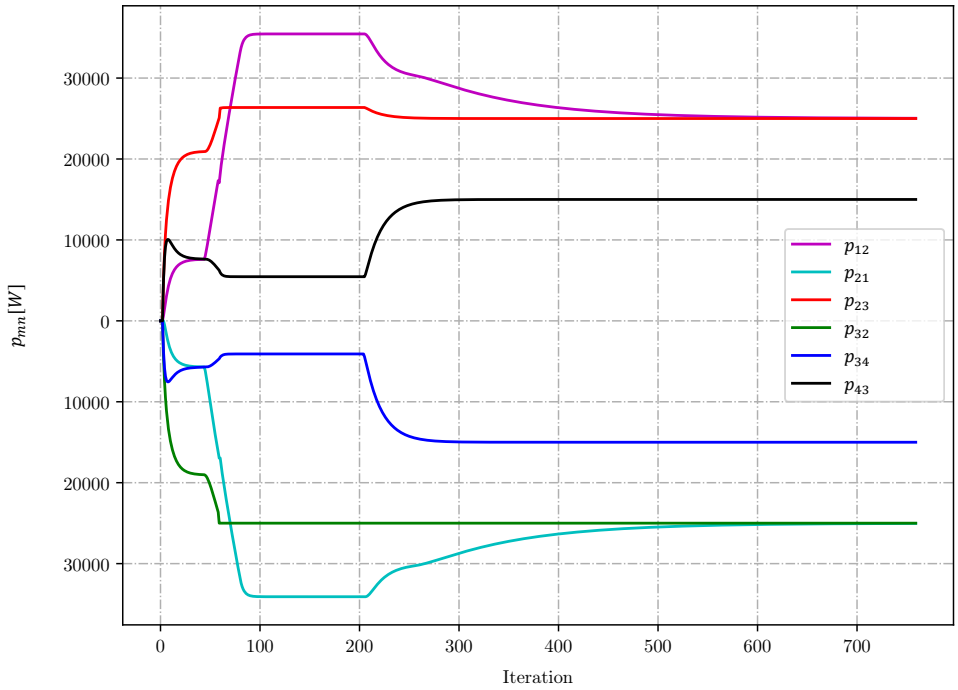

Figure 3.22: The power flow in every line for the grid in Figure 3.17 using Area Separation Method.

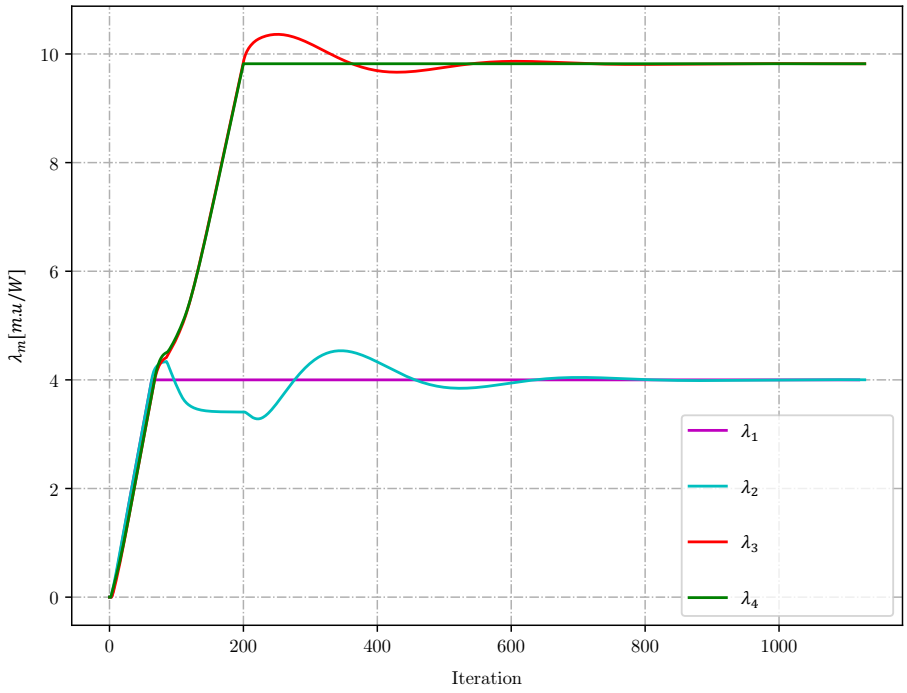

Figure 3.23: Locational Marginal Price (LMP) at every node for the grid in Figure 3.17 using Dual Variable Activation Method.

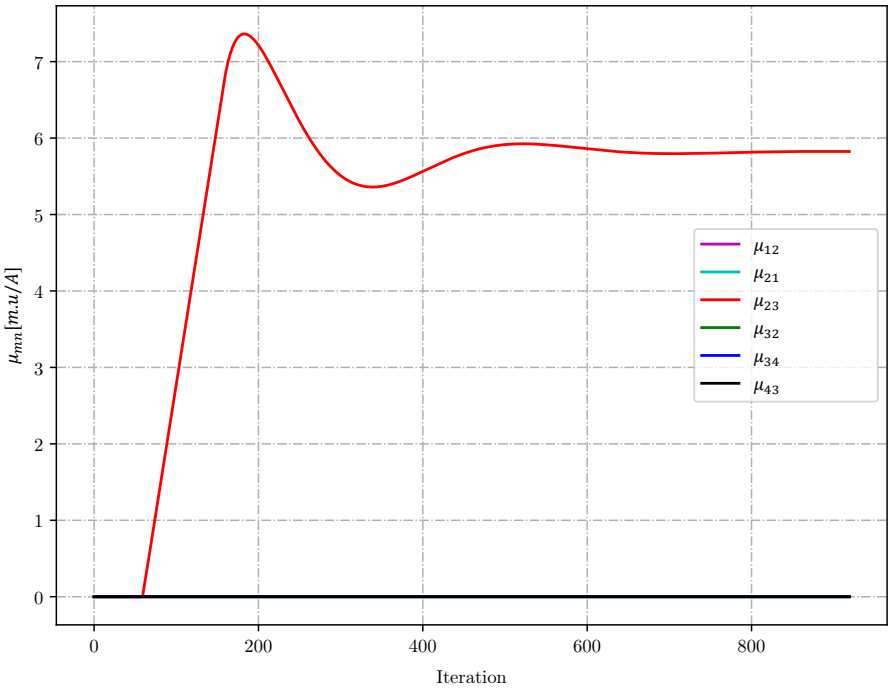

Figure 3.24: Dual variable for the line limit for the grid in Figure 3.17 using Dual Variable Activation Method. The μ is calculated by increasing slowly the value regarding the difference between the actual power flow and its limit.

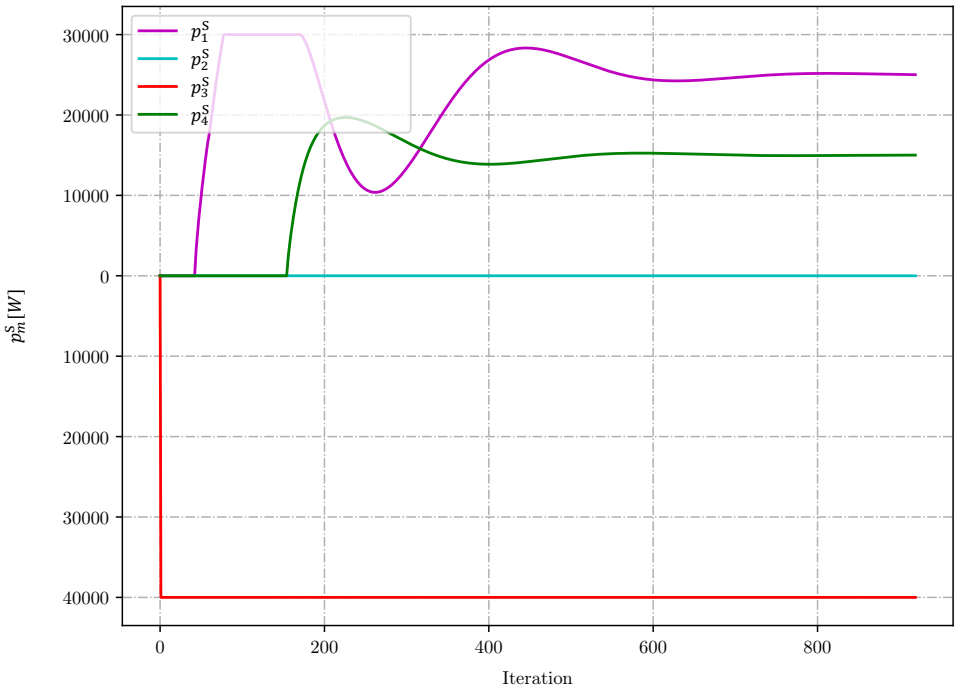

Figure 3.25: Power generation in every node for for the grid in Figure 3.17 using Dual Variable Activation Method.

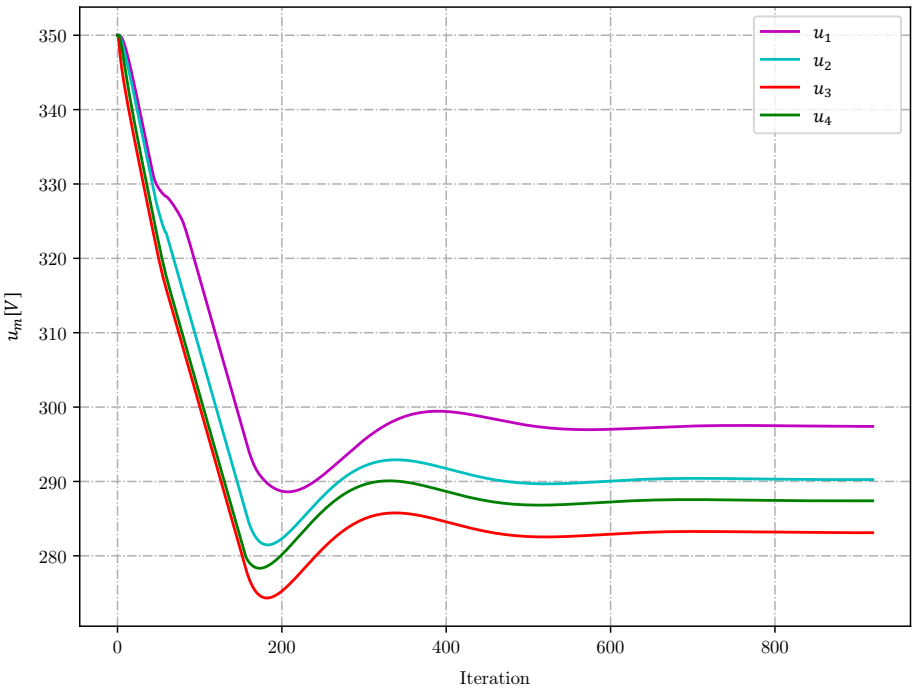

Figure 3.26: The voltage at every node for for the grid in Figure 3.17 using Dual Variable Activation Method.

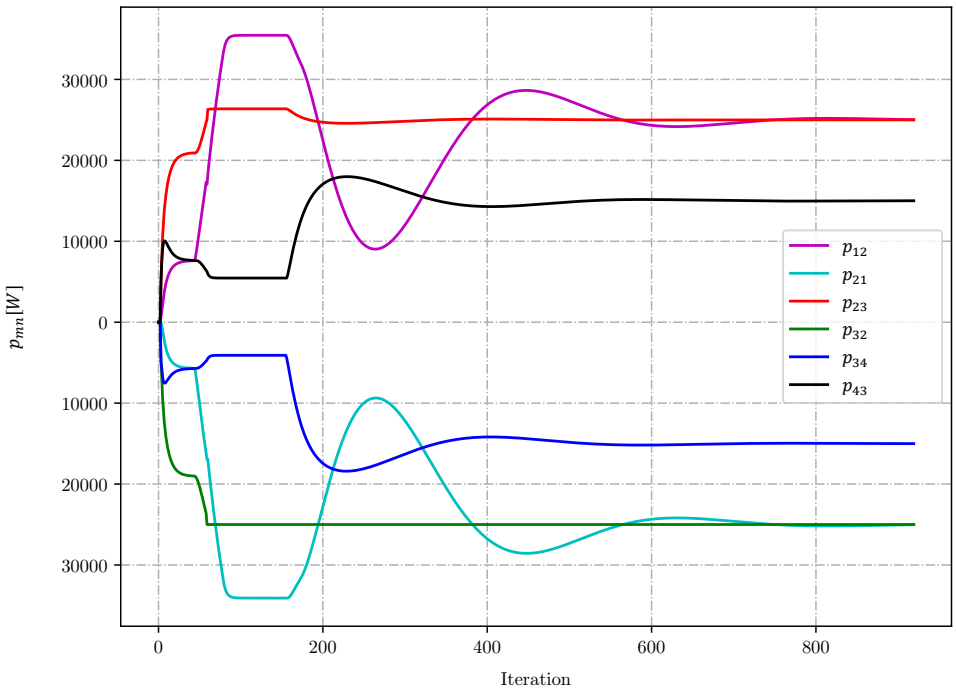

Figure 3.27: The power flow in every line for the grid in Figure 3.17 using Dual Variable Activation Method.

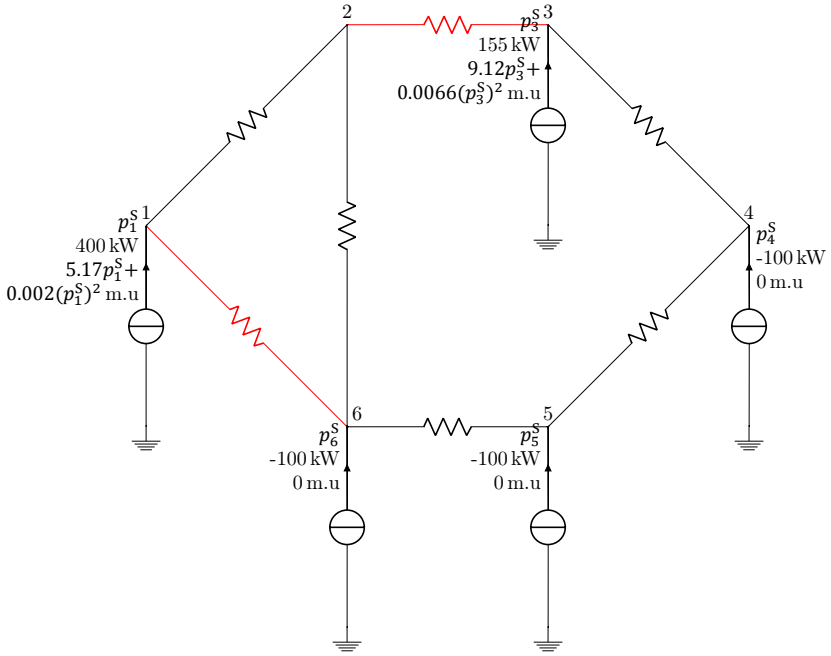

Figure 3.28: A six node mesh topology with several congestion (denoted by the red lines).

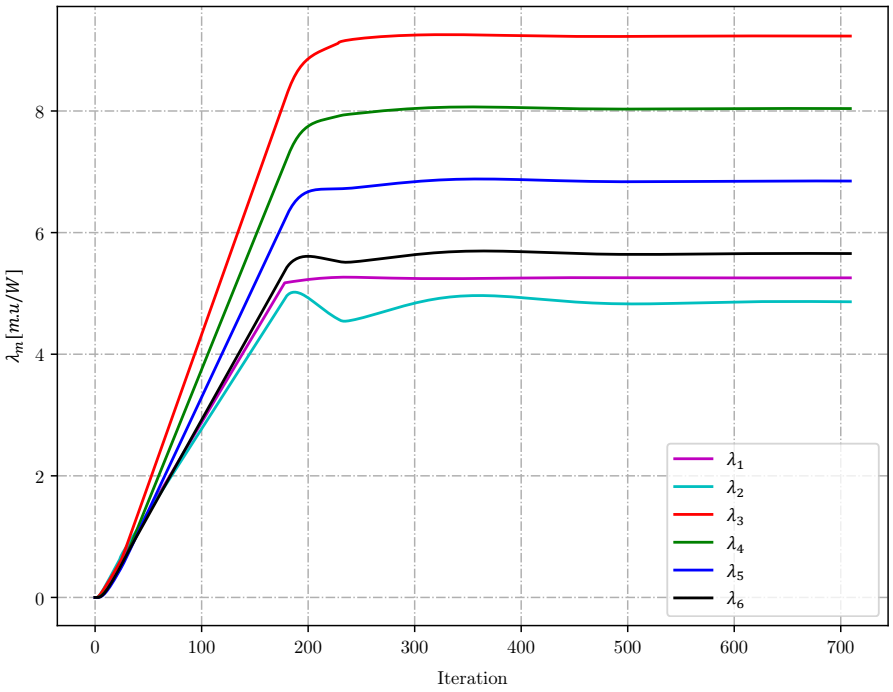

Figure 3.29: Locational Marginal Price (LMP) for the grid in Figure 3.28. Due to the congestion, the LMP are different in every node.

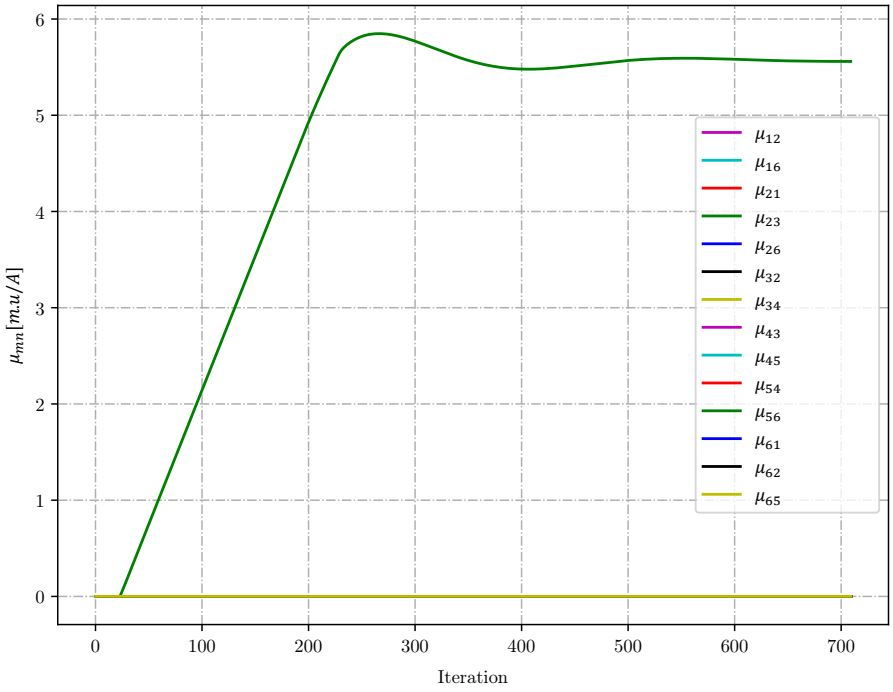

Figure 3.30: Dual variable of the congested line for the grid in Figure 3.28. The congestion occurs in line 2-3 while limit in line 1-6 is not violated.

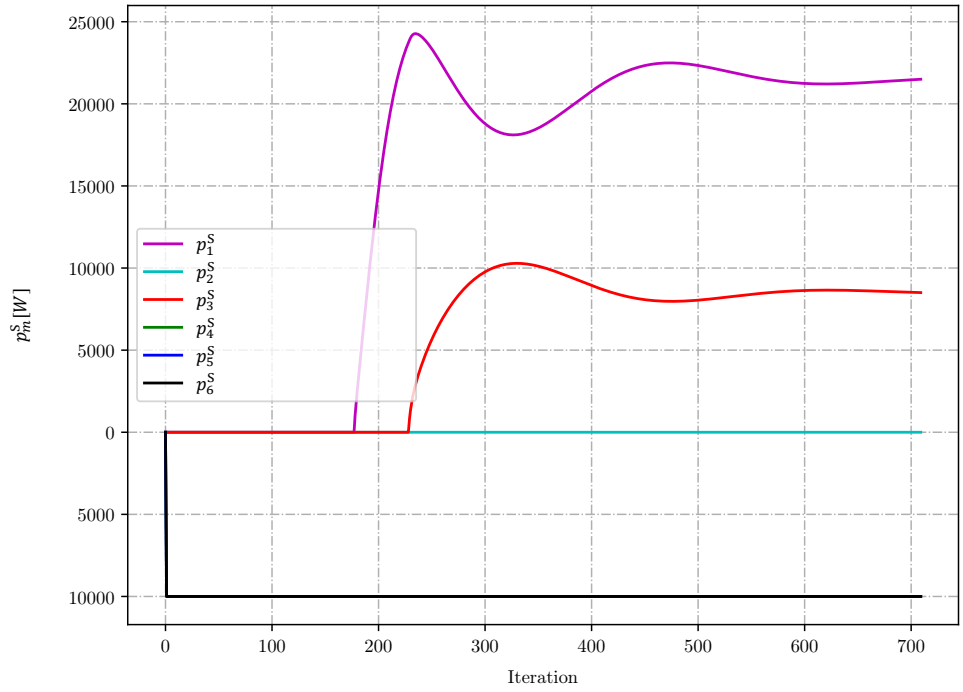

Figure 3.31: The power generation in each node for the grid in Figure 3.28. Due to the congestion, the generator at node 1 does not produce all the power and the unit at node 3 covers the remaining load demand.

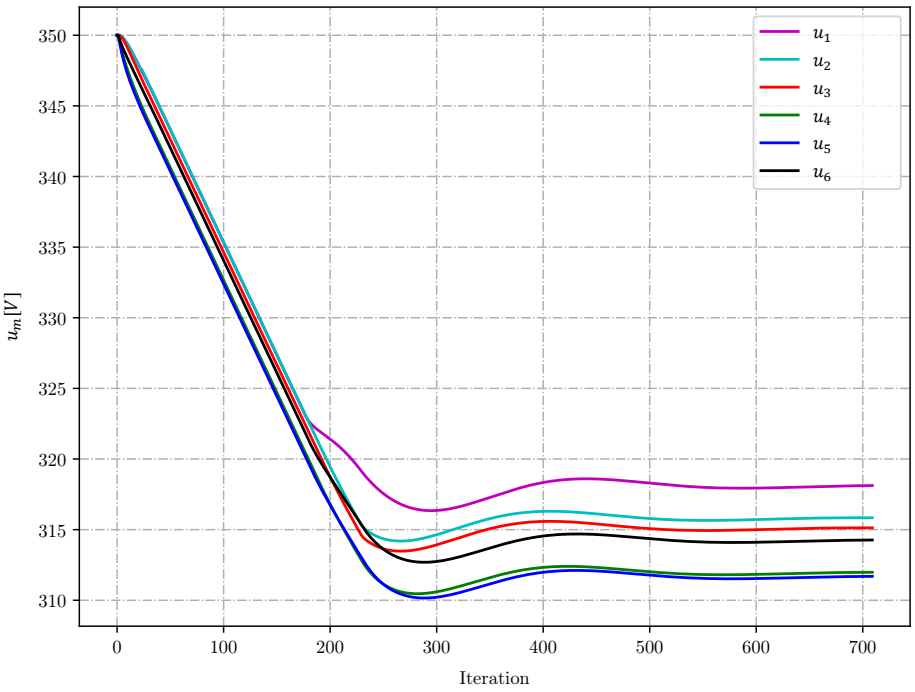

Figure 3.32: Voltage at each node for the grid in Figure 3.28.

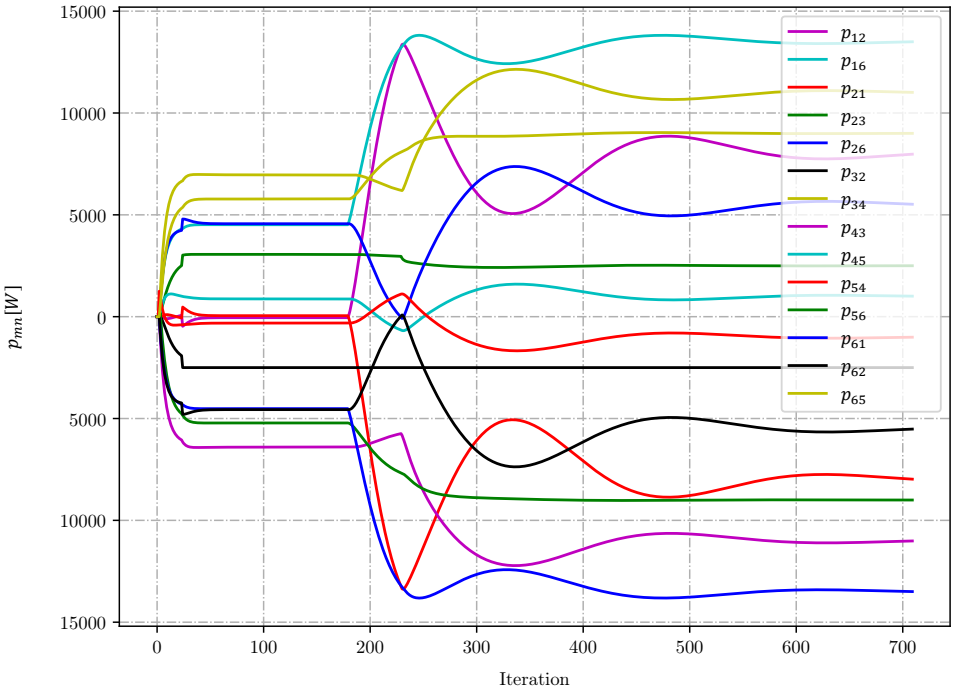

Figure 3.33: The power flow in each line for the grid in Figure 3.28.

4

Algorithm for the Distributed Optimal Power Flow: Exact Optimal Power Flow for DC Distribution Grid

After having covered the lossless case in the previous chapter, this chapter will include the lossless to solve optimization problems in DC grid since a lossless case practically does not exist. The formulation of the grid includes losses in the grid and is defined as the Exact OPF.

4.1. Problem Definition

While the objective stays the same with intrinsically minimizing the losses, (3.1) is rewritten below:

$$\min \sum_{m \in \mathcal{N}} A_m (p_m^{\mathrm{S}})^2 + B_m p_m^{\mathrm{S}} \tag{4.1}$$

subject to

$$p_m^{\mathrm{S}} = u_m \sum_{n \in \Omega_m} G_{m,n}(u_m - u_n) \tag{4.2}$$

$$G_{m,n}(u_m - u_n) \leq \bar{I}_{m,n} \tag{4.3}$$

$$\underline{P}_m^{\mathrm{S}} \leq p_m^{\mathrm{S}} \leq \overline{P}_m^{\mathrm{S}} \tag{4.4}$$

$$\underline{U}_m \leq u_m \leq \overline{U}_m \tag{4.5}$$

The first constraint is the modified representation of the nodal power. Instead of using nominal voltage to transform current to power, the actual voltage of the node is applied. Consequently, the power flowing out in the sending node will be different than the power in the receiving end. Additionally, to get the least amount of losses, the voltage should be as high as possible to reduce the current. Therefore, an absolute limit of voltage level should be set as in (4.5).

4.2. Lagrangian Function

The Lagrangian function is formulated as the lossless OPF. In the exact OPF, two addition of the dual variable of the inequality condition appear.

$$
\begin{aligned}
\mathcal{L} = & \sum_{m\in\mathcal{N}} \left(A_m (p_m^{\mathrm{S}})^2 + B_m p_m^{\mathrm{S}} \right) \\
& + \sum_{m\in\mathcal{N}} \lambda_m u_m \left(\sum_{n\in\Omega_m} G_{m,n}(u_m - u_n) - p_m^{\mathrm{S}} \right) \\
& + \sum_{m\in\mathcal{N}} \sum_{n\in\Omega_m} \mu_{m,n} \left(G_{m,n}(u_m - u_n) - \bar{I}_{m,n} \right) \\
& + \sum_{m\in\mathcal{N}} \mu_m^{\overline{P}} (p_m^{\mathrm{S}} - \overline{P}_m^{\mathrm{S}}) \\
& + \sum_{m\in\mathcal{N}} \mu_{\underline{m}}^{P} (- p_m^{\mathrm{S}} + \underline{P}_{-m}^{\mathrm{S}}) \\
& + \sum_{m\in\mathcal{N}} \mu_m^{\overline{U}} (u_m - \overline{U}_m) \\
& + \sum_{m\in\mathcal{N}} \mu_{\underline{m}}^{U} (- u_m + \underline{U}_m)
\end{aligned}
\tag{4.6}
$$

4.3. Karesh Kuhn Tucker Conditions

First Order Optimality Conditions

The first order conditions have a different derivation for the $\partial\mathcal{L}/\partial u_m$ in (4.9). Another term appears due to the non-linearity of the equality constraint (4.2).

$$\frac{\partial \mathcal{L}}{\partial p_m^{\mathrm{S}}} = 2A_m p_m^{\mathrm{S}} + B_m \tag{4.7}$$

$$- \lambda_m + \mu_m^{\overline{P}} - \mu_{\underline{m}}^{P} = 0 \tag{4.8}$$

$$
\begin{aligned}
\frac{\partial \mathcal{L}}{\partial u_m} = & \lambda_m \sum_{n\in\Omega_m} G_{m,n}(u_m - u_n) \\
& + \lambda_m u_m \sum_{n\in\Omega_m} G_{m,n} - \sum_{n\in\Omega_m} \lambda_n u_n G_{m,n} \\
& + \sum_{n\in\Omega_m} G_{m,n}(\mu_{m,n} - \mu_{n,m}) + \mu_m^{\overline{U}} - \mu_{\underline{m}}^{U}
\end{aligned}
\tag{4.9}
$$

$$\frac{\partial \mathcal{L}}{\partial \lambda_m} = -p_m^{\mathrm{S}} + u_m \sum_{n\in\Omega_m} G_{m,n}(u_m - u_n) = 0 \tag{4.10}$$

$$\frac{\partial \mathcal{L}}{\partial \mu_{m,n}} = \sum_{n\in\Omega_m} G_{m,n}(u_m - u_n) - \bar{I}_{m,n} \leq 0 \tag{4.11}$$

$$\frac{\partial \mathcal{L}}{\partial \mu_m^{\overline{P}}} = p_m^{\mathrm{S}} - \overline{P}_m^{\mathrm{S}} \leq 0 \tag{4.12}$$

$$\frac{\partial \mathcal{L}}{\partial \mu_{\underline{m}}^{P}} = -p_m^{\mathrm{S}} + \underline{P}_{-m}^{\mathrm{S}} \leq 0 \tag{4.13}$$

$$\frac{\partial \mathcal{L}}{\partial \mu_m^{\overline{U}}} = u_m - \overline{U}_m \leq 0 \tag{4.14}$$

$$\frac{\partial \mathcal{L}}{\partial \mu_{\underline{m}}^{U}} = -u_m + \underline{U}_m \leq 0 \tag{4.15}$$

Complementary Slackness Conditions

The complementary slackness conditions taken from the constraints are:

$$\mu_{m,n}\left(\bar{I}_{m,n} - \sum_{n\in\Omega_m} G_{m,n}(u_m - u_n)\right) = 0 \tag{4.16}$$

$$\mu_{n,m}\left(-\bar{I}_{m,n} + \sum_{n\in\Omega_m} G_{m,n}(u_m - u_n)\right) = 0 \tag{4.17}$$

$$\mu^{\overline{P}}_m(\overline{P}^{\mathrm{S}}_m - p^{\mathrm{S}}_m) = 0 \tag{4.18}$$

$$\mu^{\underline{P}}_m(p^{\mathrm{S}}_m - \underline{P}^{\mathrm{S}}_m) = 0 \tag{4.19}$$

$$\mu^{\overline{P}}_m(\overline{U}_m - u_m) = 0 \tag{4.20}$$

$$\mu^{\underline{U}}_m(u_m - \underline{U}_m) = 0 \tag{4.21}$$

$$\tag{4.22}$$

Positivity Conditions

All the dual variable regarding the limits have to be positive. It is written as:

$$\mu_{m,n}, \mu_{n,m}, \mu^{\overline{P}}_m, \mu^{\underline{P}}_m, \mu^{\overline{U}}_m, \mu^{\underline{U}}_m \geq 0 \tag{4.23}$$

4.4. LMP and Power Updates

4.4.1. Constant Power Region

The way in updating LMP in the exact opf is the same with the lossless one. Readers can refer to subsection 3.4.1 for the discussion about the tuning parameters formulation in the region where the power remain constant at the minimum or the maximum. However, multiplication of the actual voltage in the l^{th} iteration for $(u_m(l))$ and the conductivity $(G_{m,n})$ is used instead of $G^p_{m,n}$. Below are the updates and the respective tuning parameters for the LMP updates.

$$\lambda_m(l+1) = \lambda_m(l) - \alpha^{\lambda}_u \frac{\partial \mathcal{L}}{\partial u_m} + \alpha^{\lambda}_{\lambda} \frac{\partial \mathcal{L}}{\partial \lambda_m} \tag{4.24}$$

Tuning Parameters

$$\alpha^{\lambda}_u = \frac{0.5}{u_m(l)\sum_{n\in\Omega_m} G_{m,n}} \left[\frac{\mathrm{V}}{\mathrm{W}}\right] \tag{4.25}$$

$$\alpha^{\lambda}_{\lambda} = 0.000001 \left[\frac{\mathrm{m.u}}{\mathrm{W}^2}\right] \tag{4.26}$$

Through some trials, the algorithm produces better result when the LMP sensitivity regarding the power mismatch is reduced 10 times smaller. Therefore the figure 0.000001 is chosen.

4.4.2. Marginal Generator Region

In this region, only the power should be updated while the value of the LMP depends on the power generated. The power is updated as:

$$p^{\mathrm{S}}_m(l+1) = p^{\mathrm{S}}_m(l) + \alpha^{p}_{\lambda} \frac{\partial \mathcal{L}}{\partial \lambda_m} + \alpha^{p}_u \frac{\partial \mathcal{L}}{\partial u_m} \tag{4.27}$$

with the tuning parameter:

$$\alpha^{p}_{\lambda} = 0.25 \tag{4.28}$$

$$\alpha^{p}_u = \frac{10\frac{\mathrm{W}^2}{\mathrm{m.u}}}{u_m(l)\sum_{n\in\Omega_m} G_{m,n}} \left[\frac{\mathrm{V}}{\mathrm{W}}\right] \tag{4.29}$$

There is a change in the numerator of α_u^p compared to the lossless case. The change is made through trial and error since setting up the numerator to 1000 makes the power to increase rapidly.

as discussed in 3.4.2.

4.5. Voltage Update

In the lossless OPF, the value of the nodal voltage can be arbitrary as long as the voltage differences satisfy the power flow constraint. In the exact OPF, the value of voltage is paramount since higher voltage means lower current and lower power losses. Having a minimized power losses will ultimately meet the objective of minimizing production cost.

In the exact OPF, it is necessary to bring the voltage up to the upper limit. Hence, using only power mismatch in a node is not enough since it can be satisfied in any level of voltage. Therefore, the term $\partial\mathcal{L}/\partial u_m$ from (4.9) has to be utilized. Similarly with the lossless opf, (4.9) explains the LMP consensus between neighboring nodes except that it now has the addition term of $\mu_m^{\overline{U}}$ and $\mu_m^{\underline{U}}$. Both terms will be non zero when the voltage is at the limit. In (4.9), if $\lambda_m < \lambda_n$, when both voltages are not in the limit ($\mu_m^{\overline{U}} = \mu_m^{\underline{U}} = 0$) and no congestion occurs ($\mu_{m,n} = 0$), the term $\partial\mathcal{L}/\partial u_m$ will be less than 0 (assuming power flowing from m to n) and the voltage should become higher. This is due to the fact that $\lambda_m < \lambda_n$. Therefore, with a proper tuning and a negative sign, (4.9) brings the voltage up to the limit.

$$u_m(l+1) = u_m(l) - \alpha_\lambda^u \frac{\partial\mathcal{L}}{\partial\lambda_m} - \alpha_u^u \frac{\partial\mathcal{L}}{\partial u_m} \tag{4.30}$$

$$\alpha_\lambda^u = \frac{0.25}{u_m(l)\sum_{n\in\Omega_m} G_{m,n}} \quad \left[\frac{\mathrm{V}}{\mathrm{W}}\right] \tag{4.31}$$

$$\alpha_u^u = \frac{5\frac{\mathrm{V.W}}{\mathrm{m.u}}}{u_m(l)\sum_{n\in\Omega_m} G_{m,n}} \quad \left[\frac{\mathrm{V}^2}{\mathrm{m.u}}\right] \tag{4.32}$$

The updated value is then forced to be equal to the limit if it violates the boundaries. The voltage for DC microgrids is expected to have a value in a range around 350 V (as 1 p.u) [6]. Therefore, the voltage is limited to 325 V (0.93 p.u) and 375 V (1.07 p.u) for the lowest and the highest voltage respectively.

Formulation for α_λ^u

The reason behind this tuning parameter is the same as the lossless OPF. Similarly with the LMP update, multiplication of the actual voltage in the l^{th} ($u_m(l)$) and the conductivity ($G_{m,n}$) is used instead of $G_{m,n}^p$.

$$\alpha_\lambda^u = \frac{0.25}{u_m(l)\sum_{n\in\Omega_m} G_{m,n}} \quad \left[\frac{\mathrm{V}}{\mathrm{W}}\right] \tag{4.33}$$

Formulation for α_u^u

The new term in the voltage update should bring up the voltage based on the lambda difference. For a simple two-node case, the desired last term in (4.30) can be written as:

$$\alpha_u^u \frac{\partial\mathcal{L}}{\partial u_m} \approx k(\lambda_m - \lambda_n) \tag{4.34}$$

The LHS of the above equation is expanded into α_u^u multiplied by the RHS of (4.9) with all the μ is assumed to be zero:

$$\alpha_u^u \frac{\partial\mathcal{L}}{\partial u_m} = \alpha_u^u \left(\lambda_m \sum_{n\in\Omega_m} G_{m,n}(u_m - u_n) + \lambda_m u_m \sum_{n\in\Omega_m} G_{m,n} - \sum_{n\in\Omega_m} \lambda_n u_n G_{m,n} \right) \tag{4.35}$$

To yield (4.34), the tuning parameter should be:

$$\alpha_u^u = \frac{k}{u_m(l)\sum_{n\in\Omega_m} G_{m,n}} \tag{4.36}$$

Note that the result of the above equation is only an approximation. The first term is neglected due to the relatively small value and the division between u_m and u_n with u_m is approximated to become 1. The value of k is determined by trial and error. Smaller value of k causes unending oscillation and higher value leads to a very sensitive voltage variation. Ultimately, it is chosen $k = 5\frac{\text{V.W}}{\text{m.u}}$ and (4.36) is written as:

$$\alpha_u^u = \frac{5\frac{\text{V.W}}{\text{m.u}}}{u_m(l)\sum_{n\in\Omega_m} G_{m,n}} \quad \left[\frac{\text{V}^2}{\text{m.u}}\right] \tag{4.37}$$

Equation 4.30 with its tuning parameter formulation in (4.33) and (4.36) answer the third research question 3. The voltage is updated by having the power mismatch and LMP consensus in a node to aim the maximum voltage possible. The tuning parameter associated with the power mismatch in (4.33) is formulated for the voltage to go up or down a quarter step. Meanwhile, the other tuning parameter (4.36) is formed to have the voltage increase or decrease due to the LMP consensus and to keep the voltage once one of the node reaches its maximum voltage.

4.6. Congestion Management

The congestion management in the exact OPF is similar with the one in the lossless OPF. The only difference here is that instead of using power flow limit, the boundaries considered is the current flow limit. In the real grid, power flow along the line is not the same due to the losses, but the current remains identical. In principle, during congestion, the sending node is forced to have its voltage so that the current flowing is precisely at the limit, $\bar{I}_{m,n}$.

$$u_m(l+1) = \frac{\bar{I}_{m,n}}{\sum_{n\in\Omega_m} G_{m,n}} + u_n(l) \tag{4.38}$$

$$\mu_{m,n}(l+1) = \mu_{m,n}(l) + \beta^{m,n}\frac{\partial \mathcal{L}}{\partial \mu_{m,n}} \tag{4.39}$$

$$\beta^{m,n} = 5 \quad \frac{\text{V}^2\text{m.u}}{\text{W}^2} \tag{4.40}$$

The value of the tuning parameter $\beta^{m,n}$ is estimated, so it does not go too slow or too fast. The Dual Variable Activation Method has to be used for solving the congestion problems. The Area Separation Method cannot be applied even for the radial grid since the $\mu_{m,n}$ in the congested line is not directly the difference between the LMPs. Additionally, without any congestion, every LMP is different in every node due to the losses. Therefore, the dual variable $\mu_{m,n}$ should be updated step by step.

4.7. Dual Variable for Voltage Limit

Same as in Section 3.6, every inequality constraint leads to the presence of its respective μ. In the power limit, the $\mu_m^{\overline{U}}$ and $\mu_m^{\underline{U}}$ only appear in $\partial\mathcal{L}/\partial p_m^{\text{S}}$ which is not used in any updates. For the voltage limit, $\mu_m^{\overline{U}}$ and $\mu_m^{\underline{U}}$ appear in $\partial\mathcal{L}/\partial u_m$ which appears in the important updates. The value should be increased slowly until it is converged to the solution. Therefore, the update for these μ's resembles the $\mu_{m,n}$ update.

$$\mu_m^{\overline{U}}(l+1) = \mathbb{P}[\mu_m^{\overline{U}}(l) + \beta^{\overline{U}}\frac{\partial \mathcal{L}}{\partial \mu_m^{\overline{U}}}] \tag{4.41}$$

$$\mu_m^{\underline{U}}(l+1) = \mathbb{P}[\mu_m^{\underline{U}}(l) + \beta^{\underline{U}}\frac{\partial \mathcal{L}}{\partial \mu_m^{\underline{U}}}] \tag{4.42}$$

$$\beta^{\overline{U}} = \beta^{\underline{U}} = 15 \quad \frac{\text{m.u}}{\text{V}^2} \tag{4.43}$$

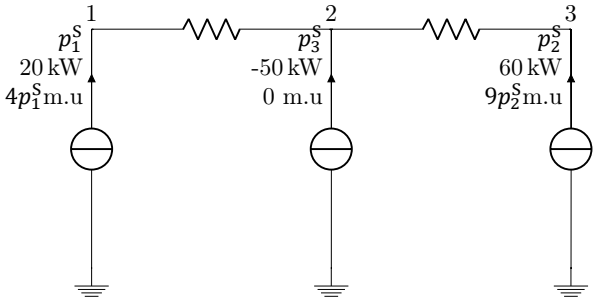

Figure 4.1: A three node radial grid with two different price generators and a load.

The tuning parameters value for $\beta^{\overline{U}}$ and $\beta^{\underline{U}}$ are determined by some trials and the results are then observed. A lower value may decelerate the convergence rate, and higher value could disturb the updates which employ (4.9) since it contains $\mu_m^{\underline{U}}$ and $\mu_m^{\overline{U}}$. At the end, the number 15 is chosen.

4.8. Limitation

The updates for all variables look the same with the lossless case except for the voltage update and the addition of the dual variable of the voltage limit. The algorithm is then implemented for a simple three-node radial case as in Figure 4.1.

Figure 4.2-4.5 show some converged and correct results as validated with the centralized approach. Some parameters are then changed. The cheap generator is then set to 40kW, making it the highest voltage at its maximum power while the marginal generator (the generator in node 3) has a lower voltage. Figure 4.2-4.5 show unending oscillation for every parameters.

It is concluded that there is one condition that makes the problem remain unsolved. It happens when the marginal generator is not at the highest voltage and has a linear function ($A_m = 0$, assuming the marginal generator is node m). When a generator has a linear function, (4.27) is used for the power update. The marginal power will oscillate while the LMP remains constant. It started when the other node (node n) with constant maximum power hits the highest voltage. As it happens, the respective $\mu_n^{\overline{U}}$ starts to have value and taken into account in the LMP update. It causes oscillation in λ_n and tries to change the value of λ_m. This is not possible since node m is still in the marginal node region. Consequently, the power oscillates due to the LMP mismatch. In the end, λ_n remains in oscillation.

The problem is overcome by letting λ_m to change due to the variation of λ_n when node m is in the marginal generator region. The old approach (4.44) based on [14] is employed. The updated LMP determines the power. The LMP is updated with (4.24) since power mismatch is still considered to determine the amount of power necessary. Based on this fact, only cases with a quadratic cost function can be implemented.

$$p_m^S(l+1) = \frac{\lambda_m(l+1) - B_m}{2A_m} \tag{4.44}$$

As a consequence, the power p_m^S is set with respect to the updated λ_m. Ultimately, λ_n and λ_m can converge to the solution. Figure 4.11-4.14 show the solution result for the case in Figure 4.10 which resembles the case in Figure 4.1 with the updated node 1 generator capacity and modified cost function of the generators.

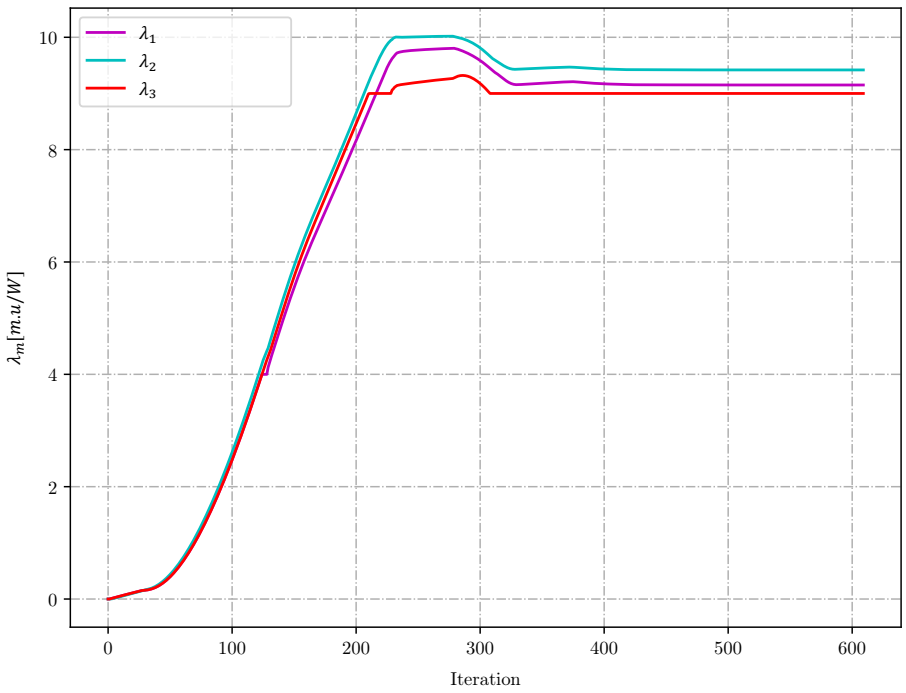

Figure 4.2: Locational Marginal Price (LMP) at every nodes for the grid in Figure 4.1. The LMP are different in every nodes due to the losses as discussed in Chapter 2 and the receiving node has the highest price to pay for the losses.

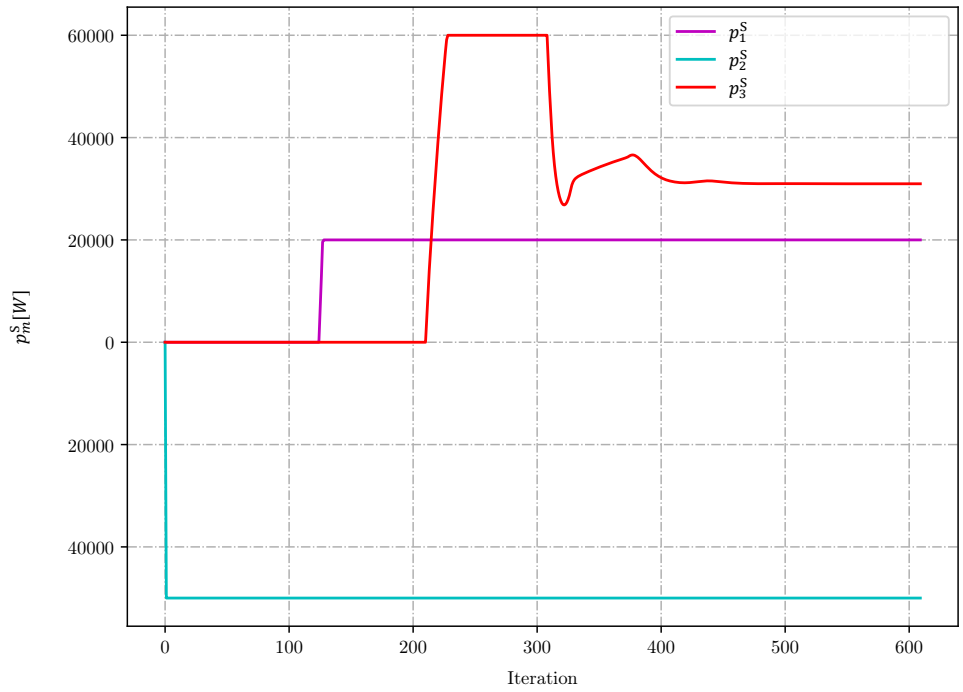

Figure 4.3: The power generated in every nodes for the grid in Figure 4.1. The overall power generated is slightly more than the load to compensate the losses.

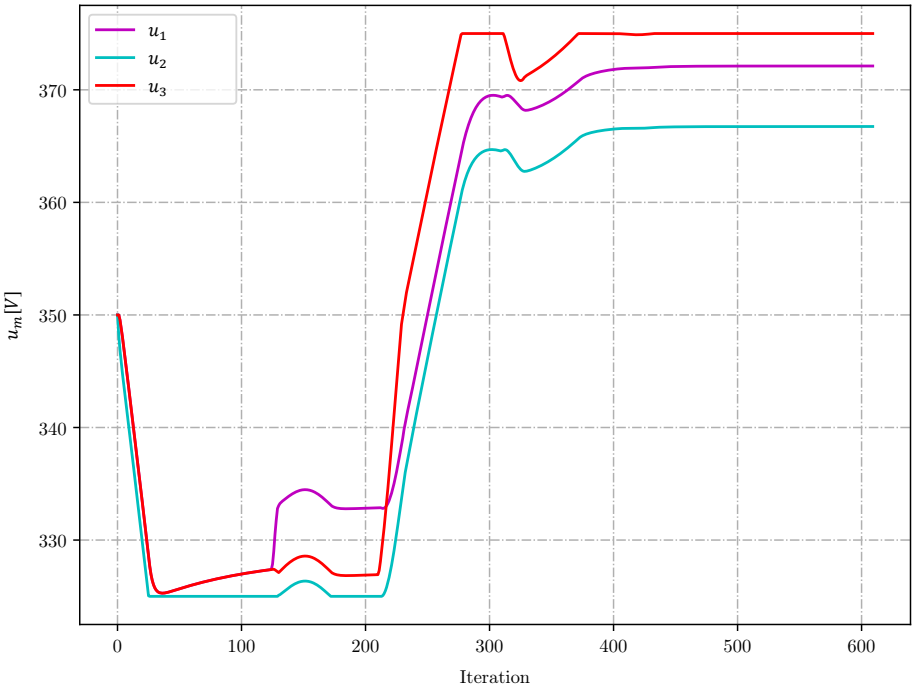

Figure 4.4: The voltage of every node for the grid in Figure 4.1. To minimize the losses, the voltage needs be at the higher limit so the current is as minimized as possible.

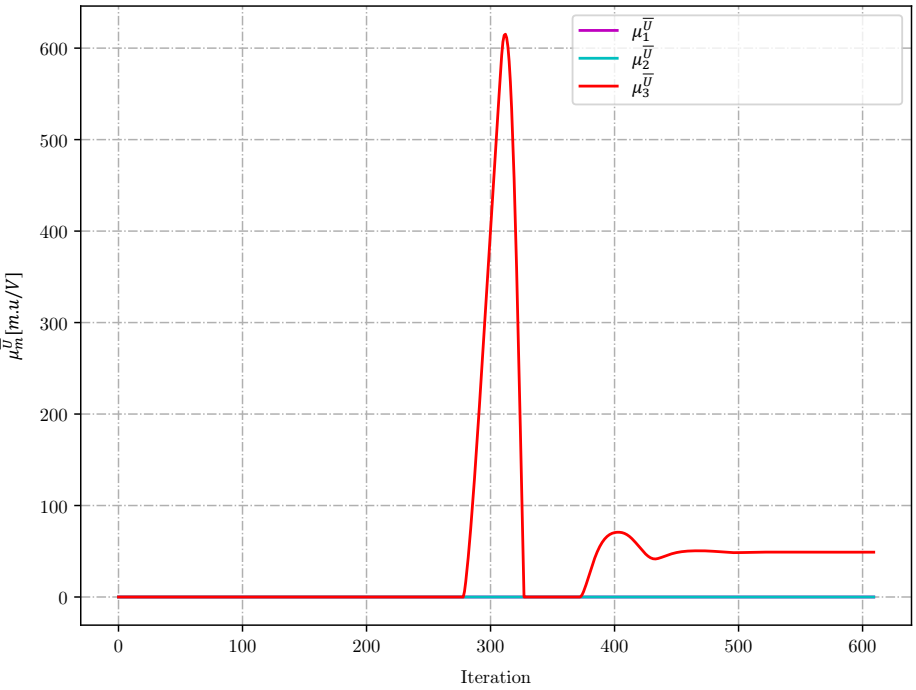

Figure 4.5: The dual variable of the voltage limit for the grid in Figure 4.1.

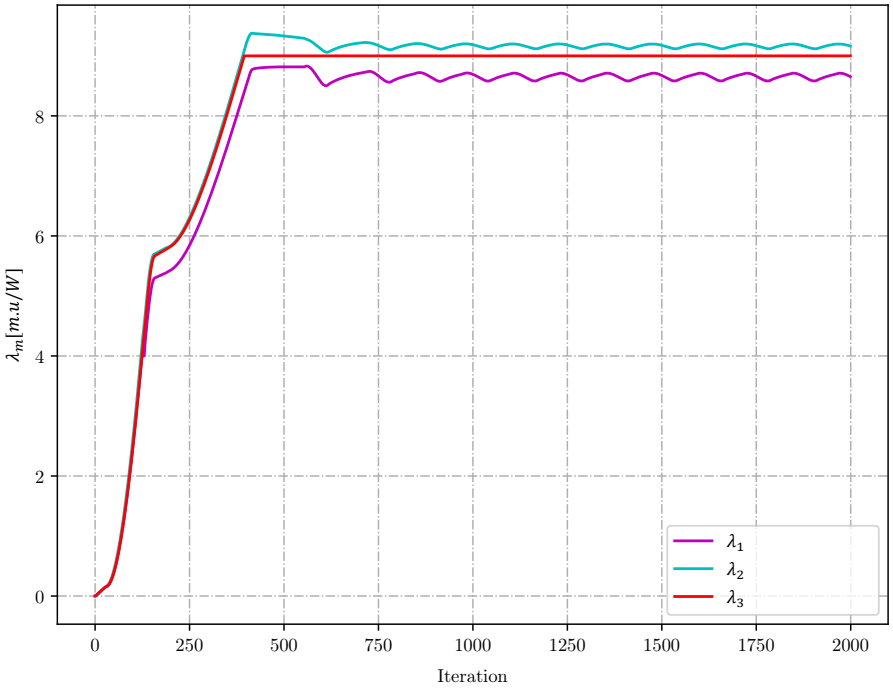

Figure 4.6: Locational Marginal Price (LMP) at every nodes for the grid in Figure 4.1 with increased node 1 generator capacity to 40 kW. Oscillation occurs for all the nodes which are not in the marginal generator region.

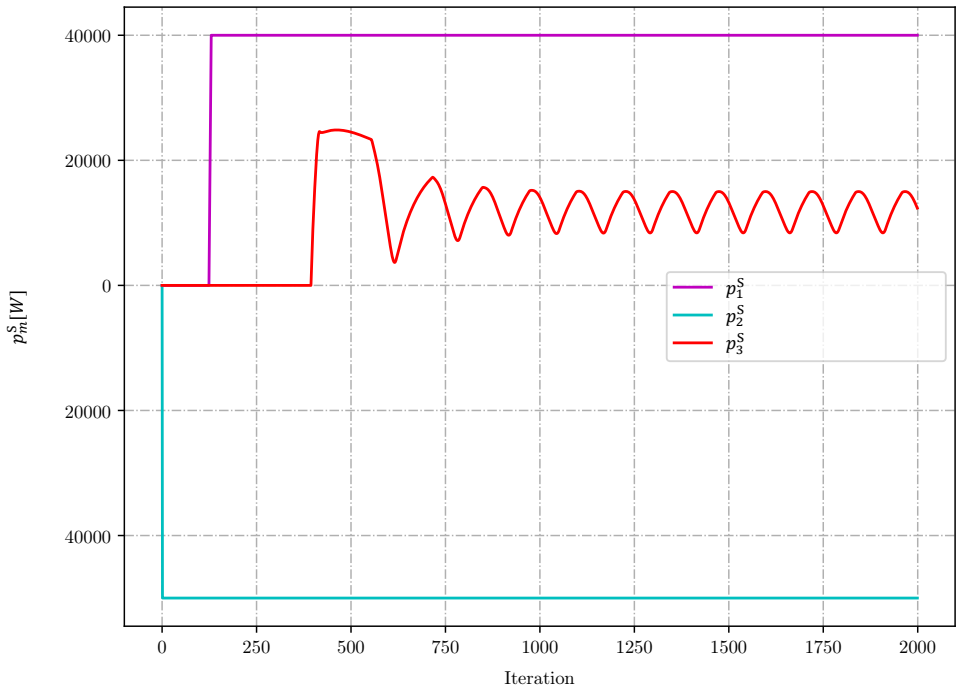

Figure 4.7: The power generation in every node for the grid in Figure 4.1 with increased node 1 generator capacity to 40 kW. Oscillation occurs for the node which is in the marginal generator region to follow the oscillation in the LMP.

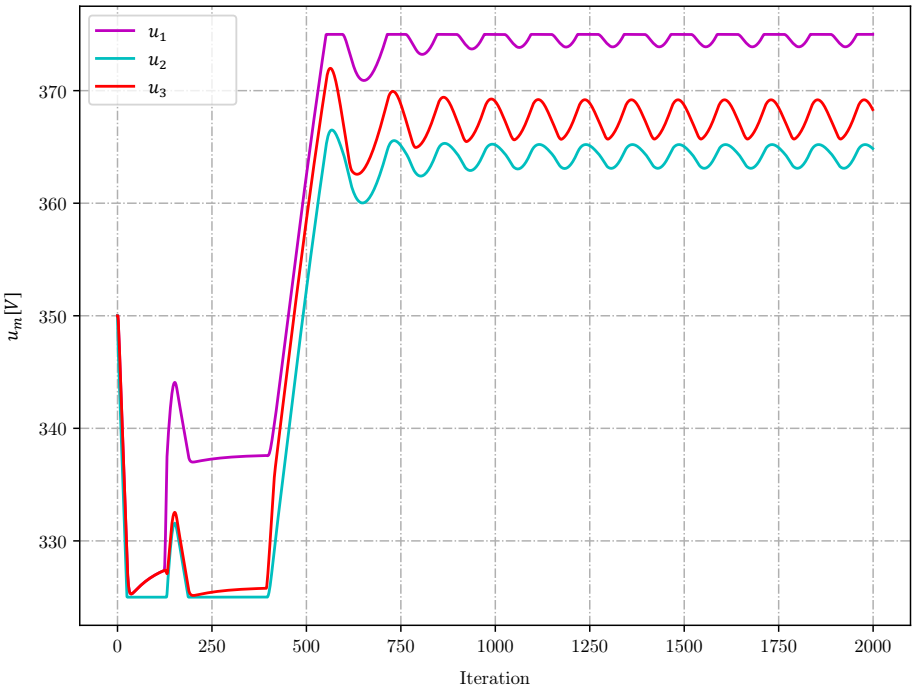

Figure 4.8: The voltage at every node which show unending oscillation for the grid in Figure 4.1 with increased node 1 generator capacity to 40 kW. When the highest voltage (u_1) reaches the limit, the corresponding dual variable $\mu_1^{\overline{U}}$ appears and gets involved in the LMP calculation.

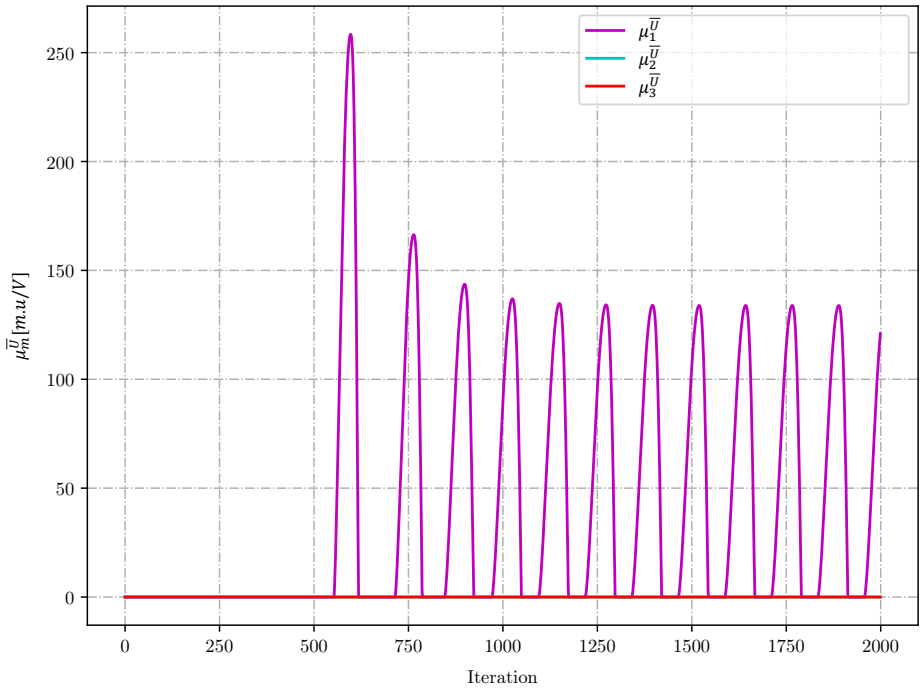

Figure 4.9: The dual variable for the voltage limit for the grid in Figure 4.1 with increased node 1 generator capacity to 40 kW.

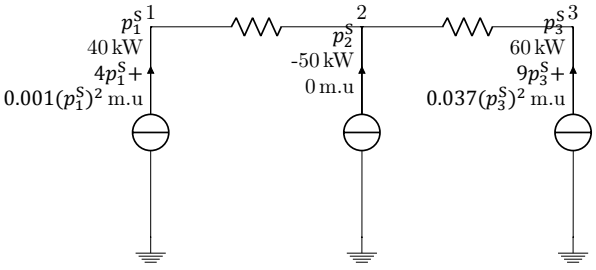

Figure 4.10: A three node radial grid with two different price generators and a load. The generator in node 1 has a higher capacity and both the generators have a quadratic cost function.

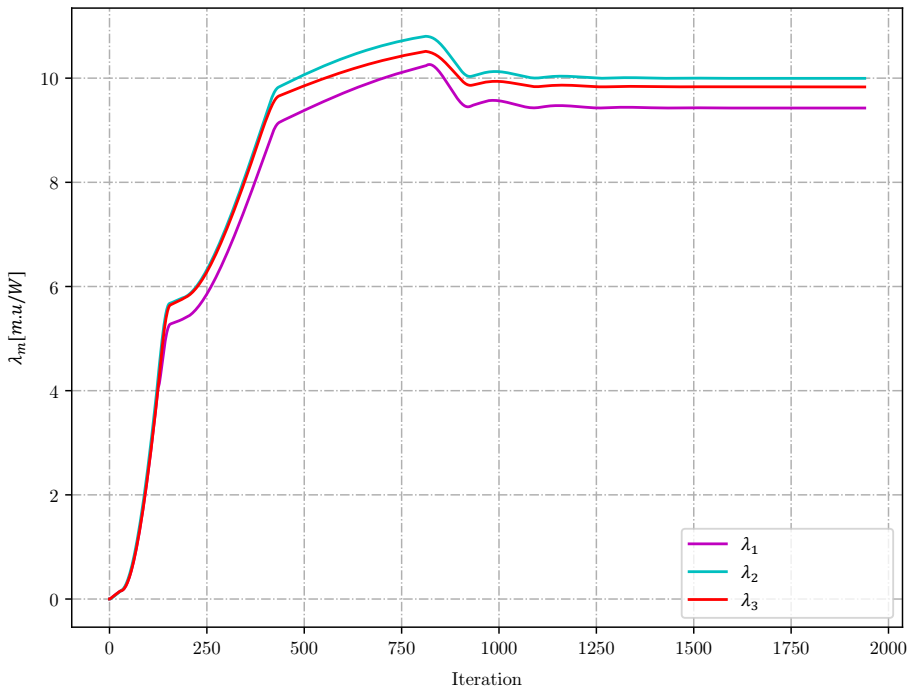

Figure 4.11: Locational Marginal Price (LMP) at every nodes for the grid in Figure 4.10. By letting the LMP to oscillate, all the parameters are converged to the solution.

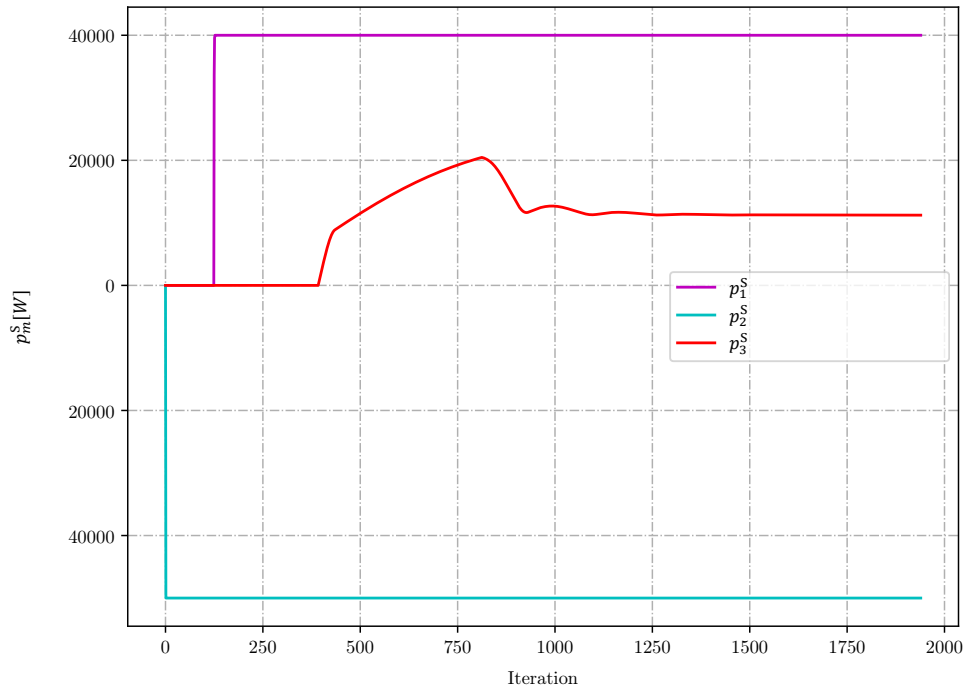

Figure 4.12: The power generation in every node for the grid in Figure 4.10. As for the marginal generator in node 3, the power generation is set with respect to its LMP.

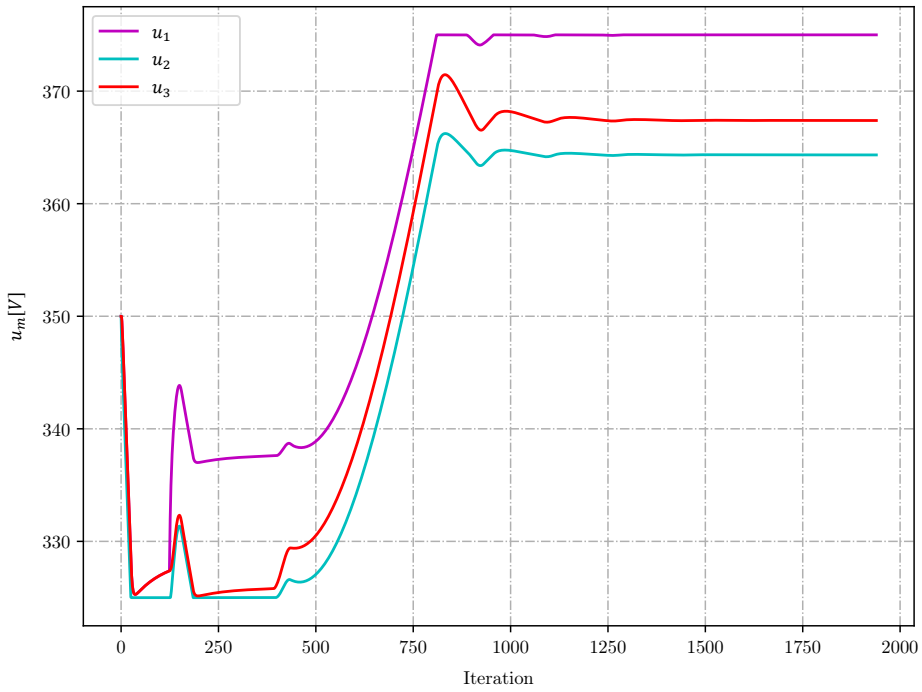

Figure 4.13: The voltage at every node for the grid in Figure 4.10.

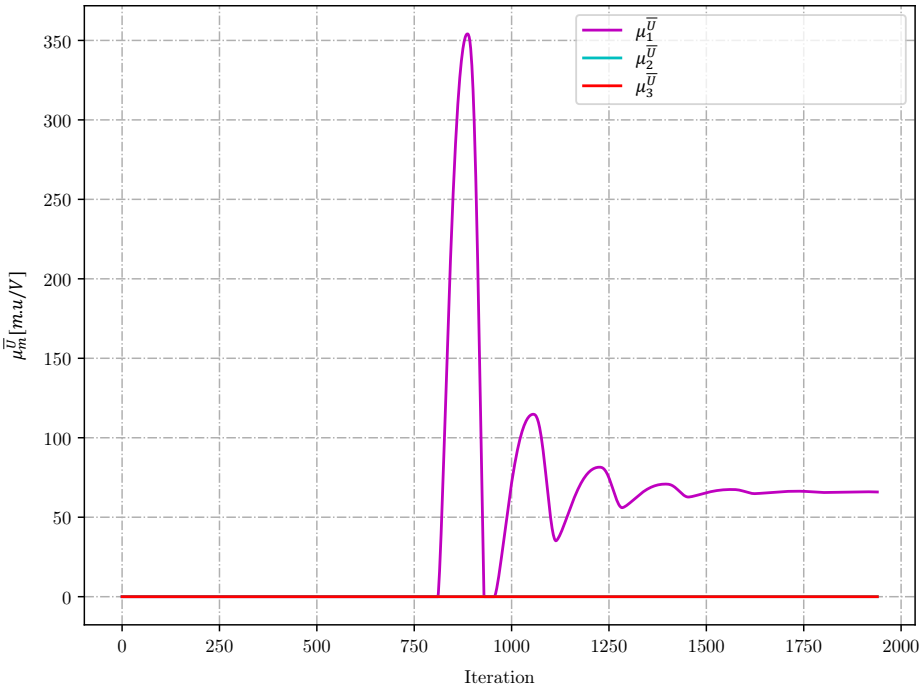

Figure 4.14: The dual variable for the voltage limit for the grid in Figure 4.10.

4.9. Summary of the Tuning Parameters

Based on the discussion in this chapter, the tuning parameters can now be summarized in Table 4.1.

Table 4.1: Tuning parameter for all the Exact OPF cases.

Tuning Parameter	Purpose	Value
α_u^λ	LMP update regarding the LMP consensus as explained in 4.4.1	$\frac{0.5}{u_m(l)\sum_{n\in\Omega_m} G_{m,n}}$ $\left[\frac{\text{V}}{\text{W}}\right]$
α_λ^λ	LMP update regarding the power mismatch in the node as explained in 4.4.1	0.000001 $\frac{\text{m.u}}{\text{W}^2}$
α_λ^p	Power update regarding power mismatch in the node as explained in 4.4.2	0.25
α_u^p	Power update regarding the LMP consensus as explained in 4.4.2	$\frac{10\frac{\text{W}^2}{\text{m.u}}}{u_m(l)\sum_{n\in\Omega_m} G_{m,n}}$ $\left[\frac{\text{V.W}}{\text{m.u}}\right]$
α_λ^u	Voltage update regarding the power mismatch as explained in 4.5	$\frac{0.25}{u_m(l)\sum_{n\in\Omega_m} G_{m,n}}$ $\left[\frac{\text{V}}{\text{W}}\right]$
α_u^u	Voltage update regarding the LMP update as explained in 4.5	$\frac{5\frac{\text{V.W}}{\text{m.u}}}{u_m(l)\sum_{n\in\Omega_m} G_{m,n}}$ $\left[\frac{\text{V}^2}{\text{m.u}}\right]$
$\beta^{m,n}$	Dual variable update regarding the difference between the line limit and the actual power flow as explained in 4.6	5 $\frac{\text{V}^2\text{m.u}}{\text{W}^2}$
$\beta^{\overline{P}}$	Dual variable (maximum power) update regarding the LMP difference with the marginal cost as explained in 3.6	0.5
$\beta^{\underline{P}}$	Dual variable (minimum power) update regarding the LMP difference with the marginal cost as explained in 3.6	0.5
$\beta^{\overline{U}}$	Dual variable (maximum voltage) update regarding the voltage different with the maximum limit as explained in 4.7	15 $\frac{\text{m.u}}{\text{V}^2}$
$\beta^{\underline{U}}$	Dual variable (minimum voltage) update regarding the voltage different with the minimum limit as explained in 4.7	15 $\frac{\text{m.u}}{\text{V}^2}$

4.10. Voltage Limit in the DC Distribution Grid

Being different with the lossless OPF, the losses value needs to be considered. In the lossless OPF, a load can take power from any cheapest generator wherever it is located. In the exact OPF, taking power from a remote generator leads to higher production to overcome the losses. As a consequence,

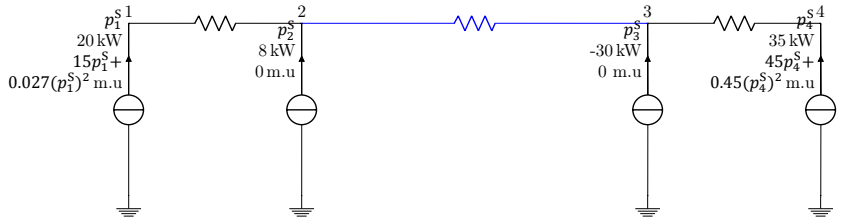

Figure 4.15: Four node serial case with a long line connecting node 2 and 3 (depicted in blue). The line is very long, and due to the voltage limits and losses, all the required power cannot be delivered from the cheapest generator in node 2.

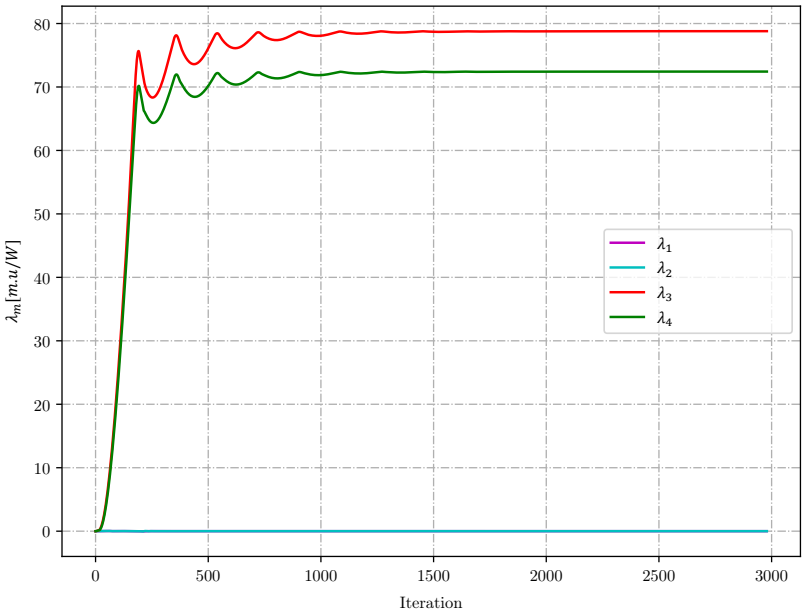

Figure 4.16: Locational Marginal Price (LMP) at every nodes for the grid in Figure 4.15. In the solution, the grid is divided into two areas with different price to keep the generators as marginal generators.

the unnecessary extra cost has to be spent for this extra power. Taking power from an expensive yet close generator may be a cheaper solution. Moreover, due to the presence of the voltage limit, the power transfer is limited. The case in Figure 4.15 show a grid in where a long line cable is present. In this case the numerator in α_u^u is set to be $1\frac{\text{V.W}}{\text{m.u}}$ to avoid the voltage to change quickly. The results in Figure 4.16-4.21 show the result. The LMP shows a significant difference as in congestion case as there are two marginal generators operated in two different prices. The voltage in Figure 4.18 shows that both there is one generator with the upper voltage limit and another generator with the lower voltage limit. As a consequence, both the dual variables for the voltage limits are active as shown in Figure 4.20 and Figure 4.21.

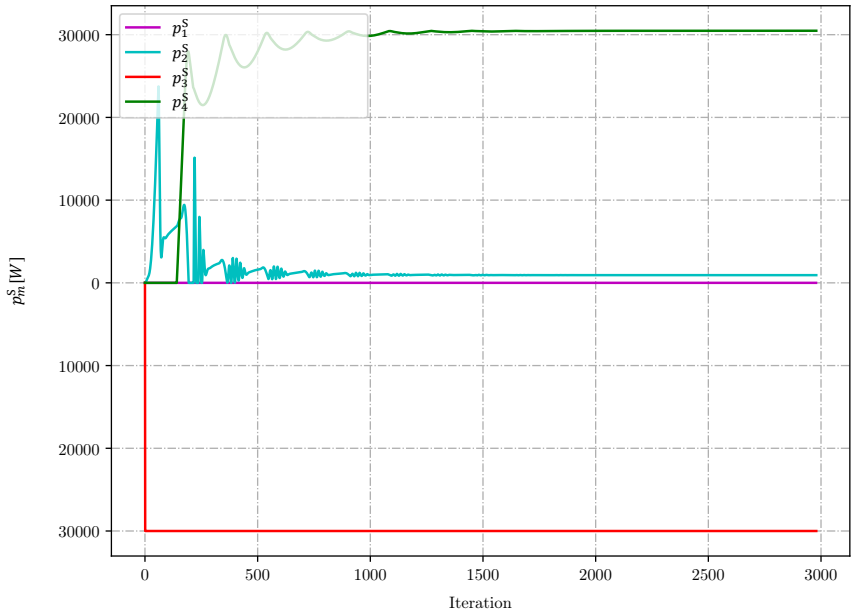

Figure 4.17: The power generation in every node for the grid in Figure 4.15. Although node 2 has the lowest price, the load prefers to take the power from node 4 due to the long distance.

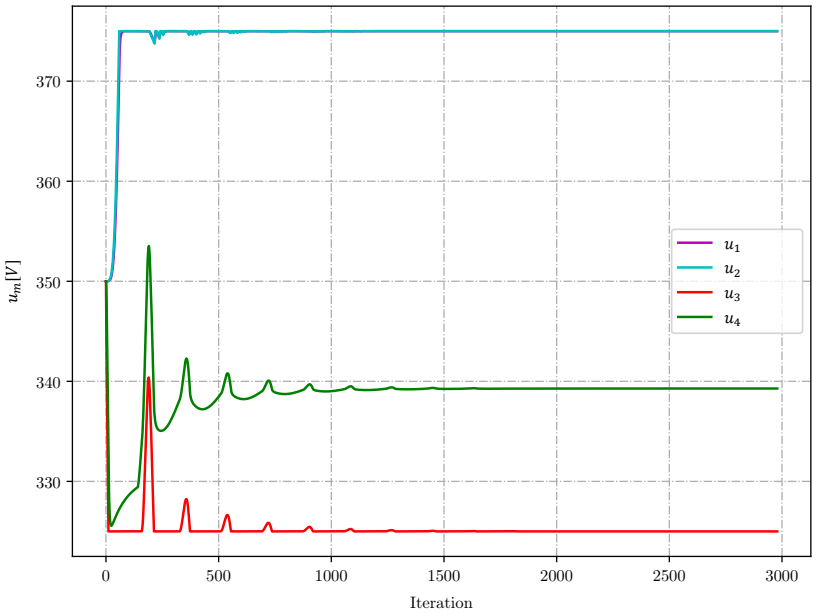

Figure 4.18: The voltage at every node for the grid in Figure 4.15. In the grid, both voltage limits are present. The load has the lowest voltage and the cheapest generator has the highest voltage. The load tries to take as much power as possible from the cheapest generator.

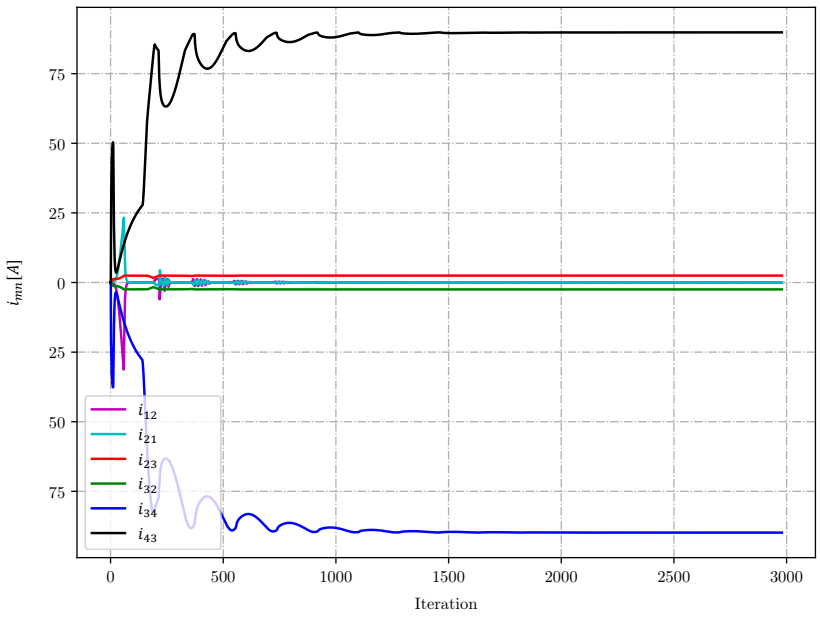

Figure 4.19: The current flowing in the lines for the grid in Figure 4.15. The long line has a very high resistance that leads to a small current transfer from node 2 to node 3.

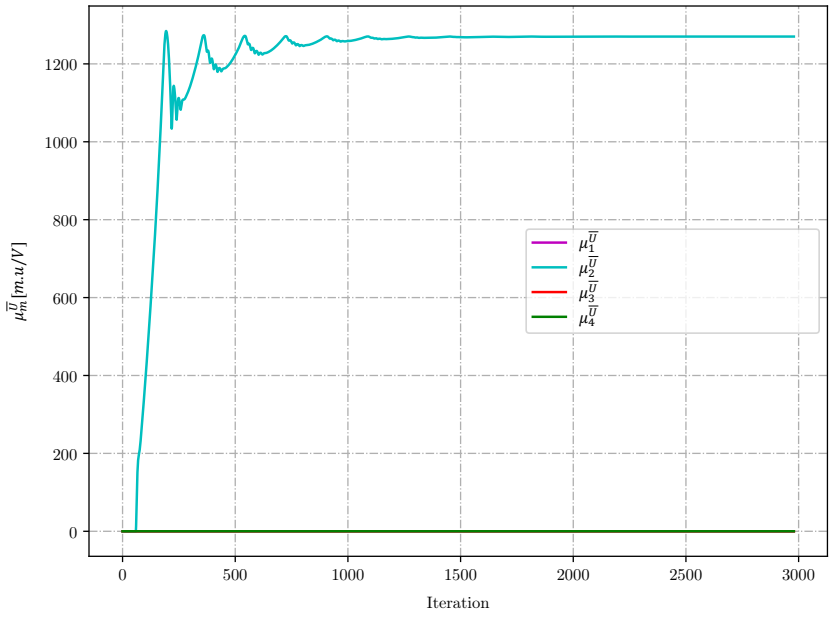

Figure 4.20: The dual variable for the upper voltage limit for the grid in Figure 4.15.

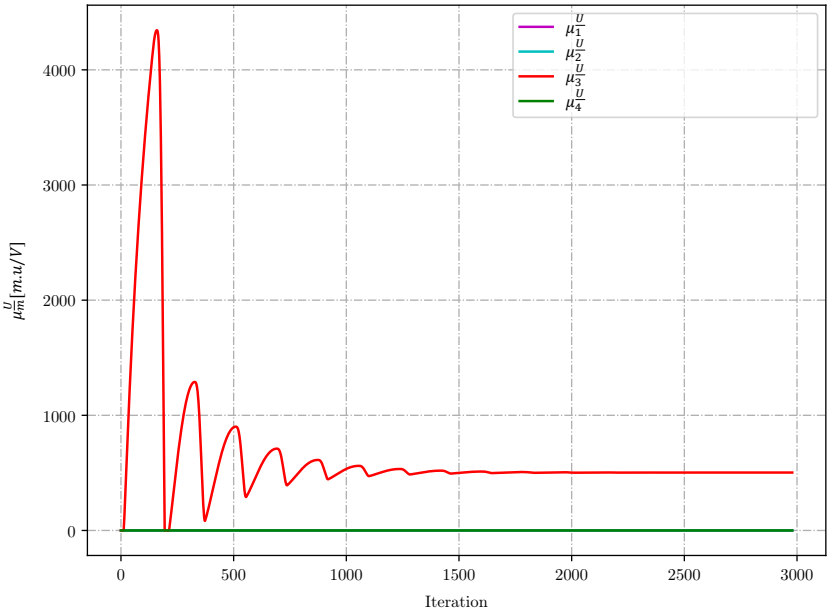

Figure 4.21: The dual variable for the lower voltage limit for the grid in Figure 4.15.

5

Study Case

5.1. Microcomputer Implementation

The algorithm ideally has to be run in a fully distributed manner using several computers where each of which has its own IP address. During the simulation of a four-node grid in Figure 3.4, four computers have to run the algorithm in parallel and exchange all necessary variables (LMP, dual variable of the line limit, and voltage) to their neighboring nodes every iteration.

In the implementation, Raspberry-Pis (raspis) are used to represent the nodes. One extra raspi is employed as a commander to initialize the process and stores all the variable values every iteration for plotting without any interference in the computation. This implementation validates that the algorithm can run without any central coordinator for calculation.

However, simulation using raspis takes some time due to the dependency of the internet connection and the presence of actual data transfer among the raspis. Therefore, for the simulation, the algorithm is run on a single computer. Nevertheless, it is still a fully distributed simulation. For a four-node grid case, the computer activates four terminals, and the IP addresses are changed to local addresses (127.0.0.1-127.0.0.4). Therefore, all information going out are looped back to that computer and the simulation runs faster than the hardware implementation. Using multithreading in Python, all the four terminal runs the algorithm in parallel.

5.2. Comparison with the Previous Research in Exact OPF

The previous research on the Exact OPF [13] used C+I to solve an OPF problem for a DC distribution grid. In the approach, a DC power flow is formulated while the losses are taken into account. The update of every variable uses constants as the tuning parameters. Compared to [13], this thesis has a contribution in studying the meaning for each tuning parameter and aims for a faster convergence rate. A comparison is made using the grid in Figure 5.1. Table 5.1 show the tuning parameter setup for both algorithms and the Figure (5.2)-(5.11) show the result. However, the assumption of having a linear cost function in [13] cannot be used in this work due to the limitation.

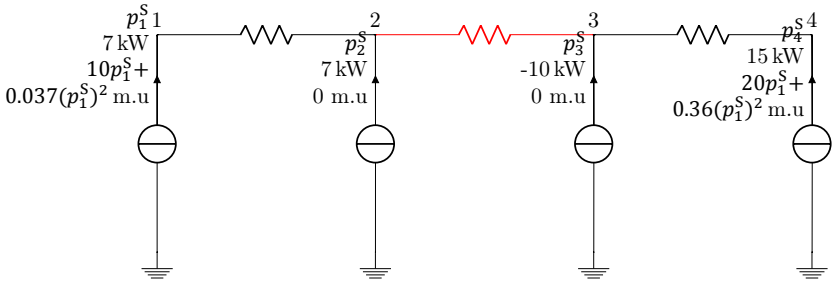

Figure 5.1: Four node serial case with congestion from node 2 to 3. The sample case is taken from [13] with a modification in the generators' cost function. The quadratic cost coefficients are necessary due to the Exact OPF algorithm limitation as explained in Chapter 4.

Table 5.1: Tuning parameter setting for the grid in Figure 5.1 using both algorithm in this work and [13]. The tuning parameters' purpose can be refer to Table 4.1.

Tuning Parameter	Value/Formula from This Work	Value from [13]
α_u^λ	$\frac{0.5}{u_m(l)\sum_{n\in\Omega_m} G_{m,n}}$	0.1485
α_λ^λ	0.000001	0.0052
α_λ^p	N/A	0.007
α_λ^u	$\frac{0.25}{u_m(l)\sum_{n\in\Omega_m} G_{m,n}}$	0.00025
α_u^u	$\frac{5}{u_m(l)\sum_{n\in\Omega_m} G_{m,n}}$	N/A
$\beta^{m,n}$	5	0.004
$\beta^{\overline{P}}$	0.5	0.0001
$\beta^{\underline{P}}$	0.5	0.0001
$\beta^{\overline{U}}$	15	0.004
$\beta^{\underline{U}}$	15	0.002

The results in Figure 5.2-5.11 show that by using the physical interpretation of the first order optimality condition, the tuning parameter can be formulated better and reduce the iteration numbers significantly, compared to use trial and error approach for determining the tuning parameters. This comparison fully answers the research question 1 regarding the convergence rate since it goes from 200000 iterations to 4000 iterations.

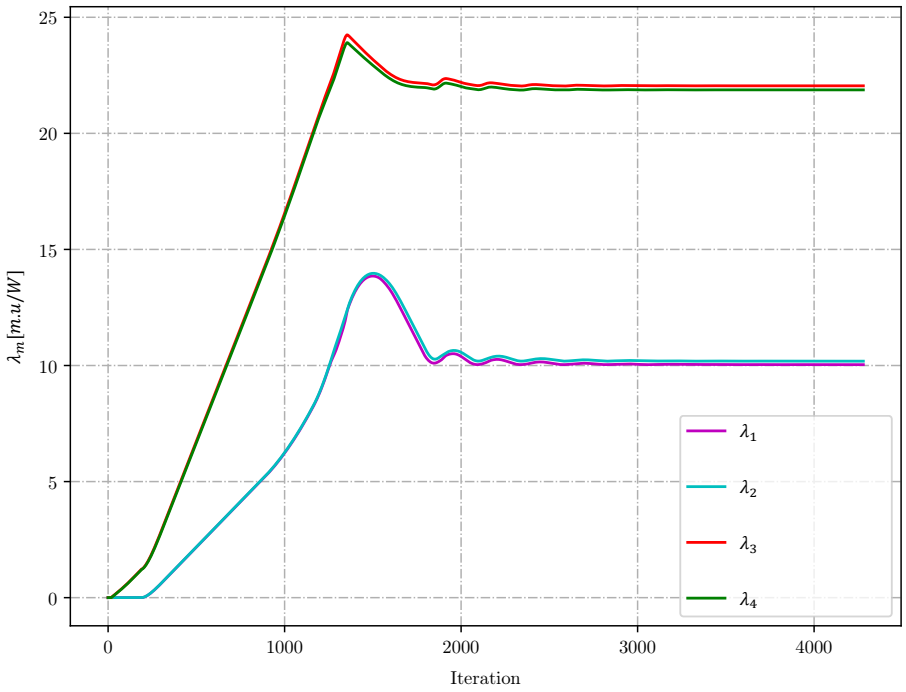

Figure 5.2: Locational Marginal Price (LMP) at every node for the grid in Figure 5.1.

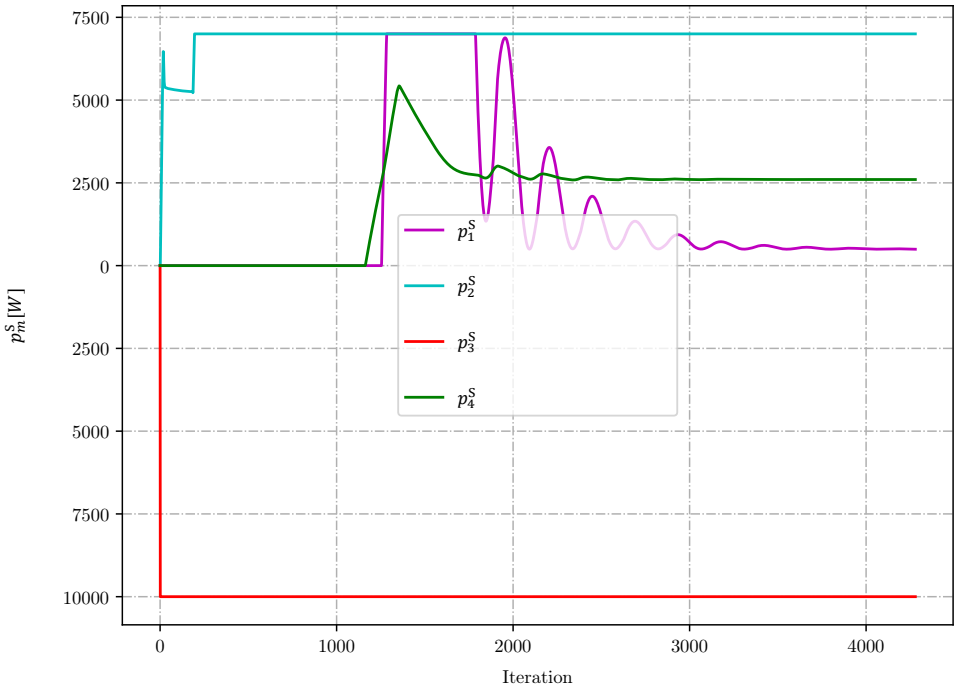

Figure 5.3: The power generation in every node for the grid in Figure 5.1.

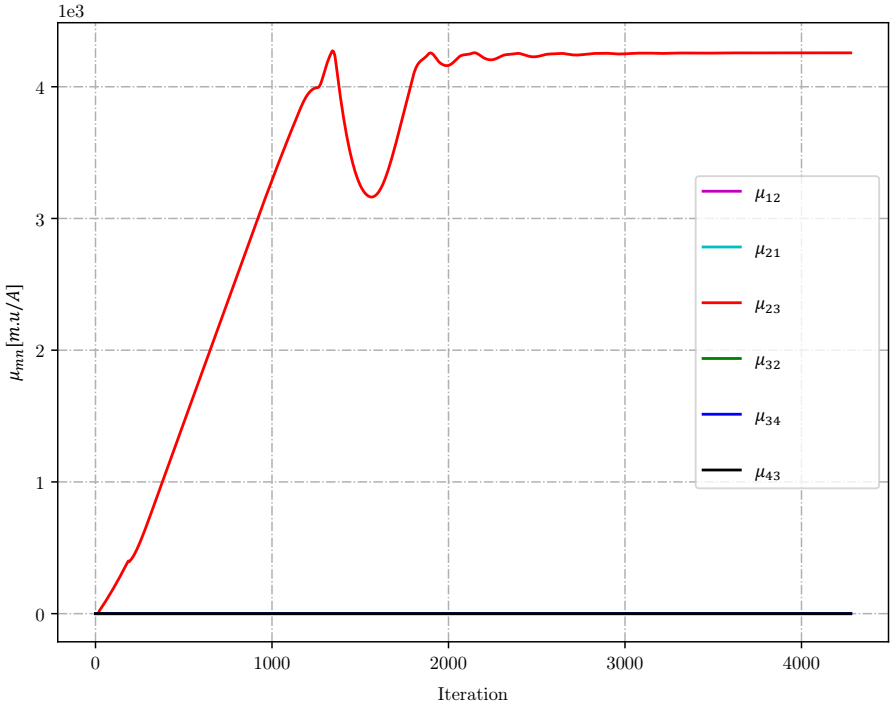

Figure 5.4: Dual variable of the line limit for the grid in Figure 5.1.

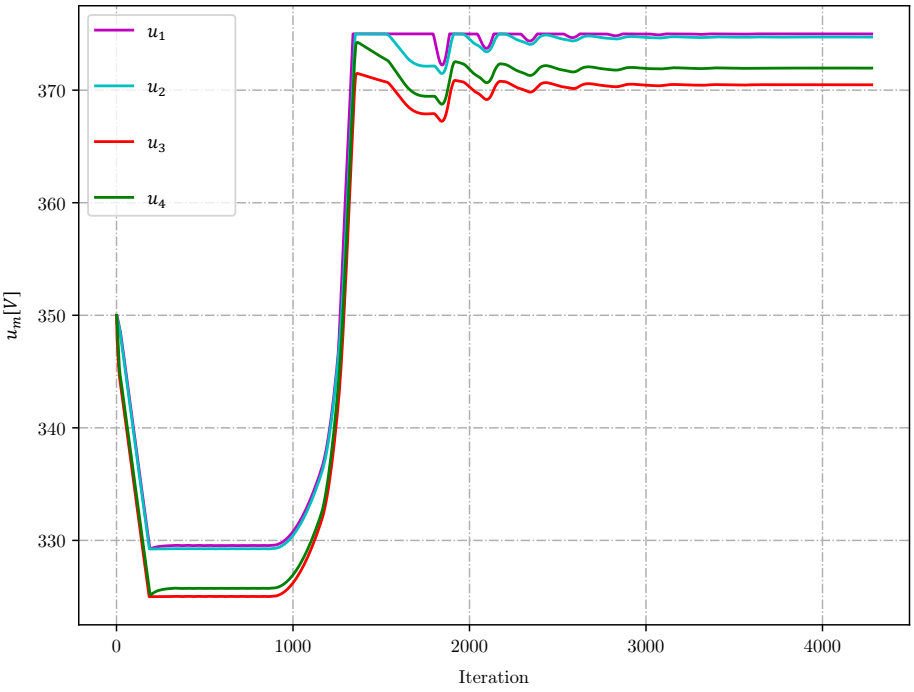

Figure 5.5: Voltage at every node for the grid in Figure 5.1.

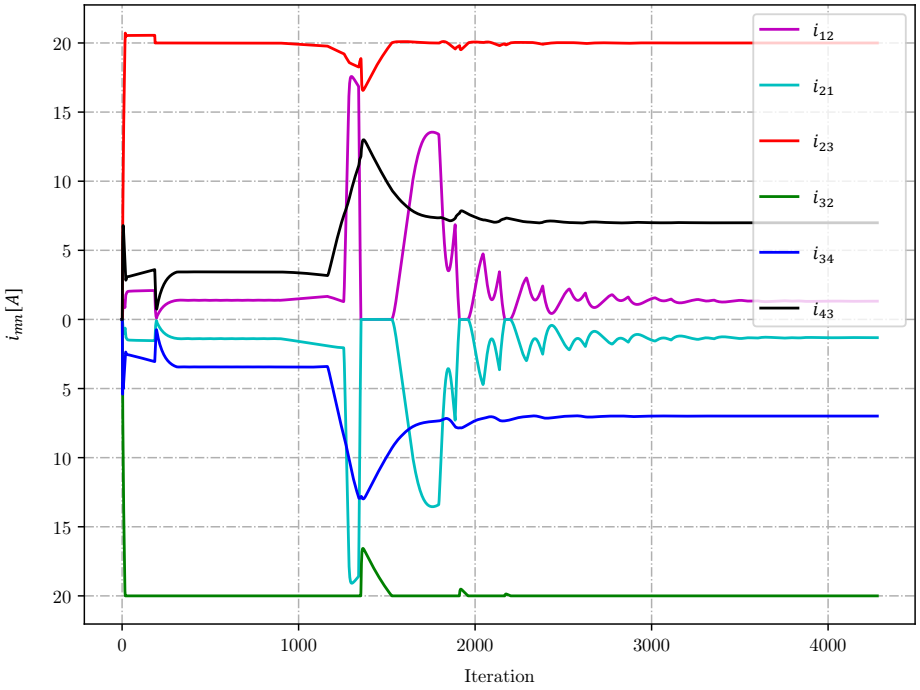

Figure 5.6: The current flowing in every line for the grid in Figure 5.1.

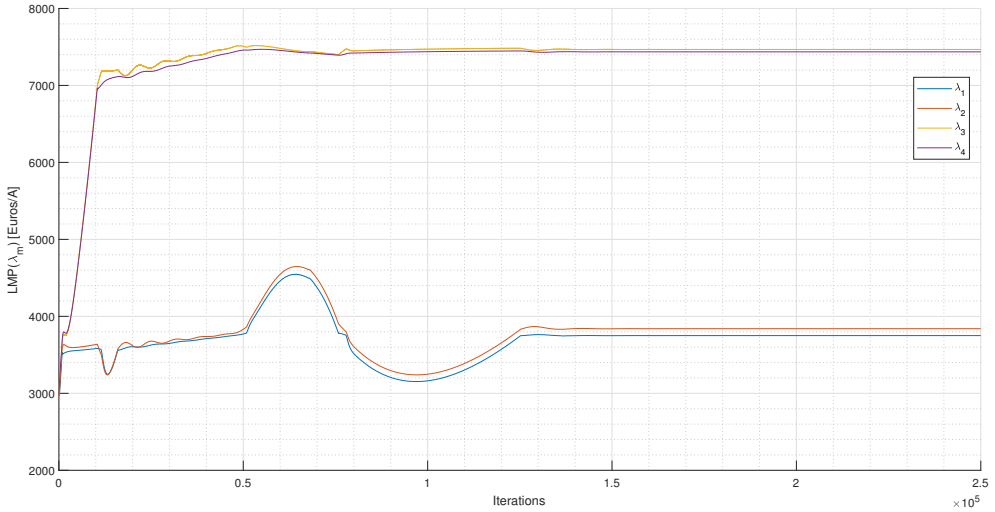

Figure 5.7: Locational Marginal Price (LMP) at every node for the grid in Figure 5.1 using the algorithm from [13].

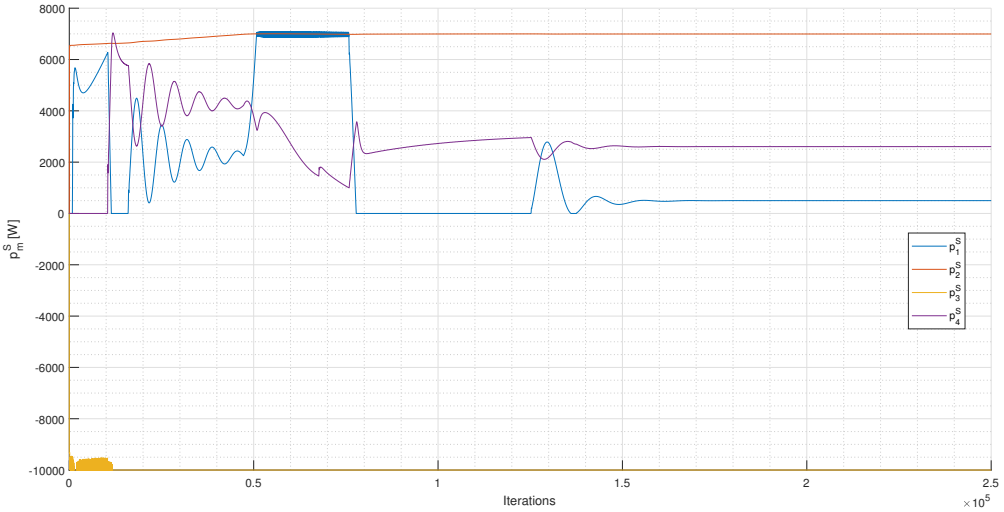

Figure 5.8: The power generation in every node for the grid in Figure 5.1 using the algorithm from [13].

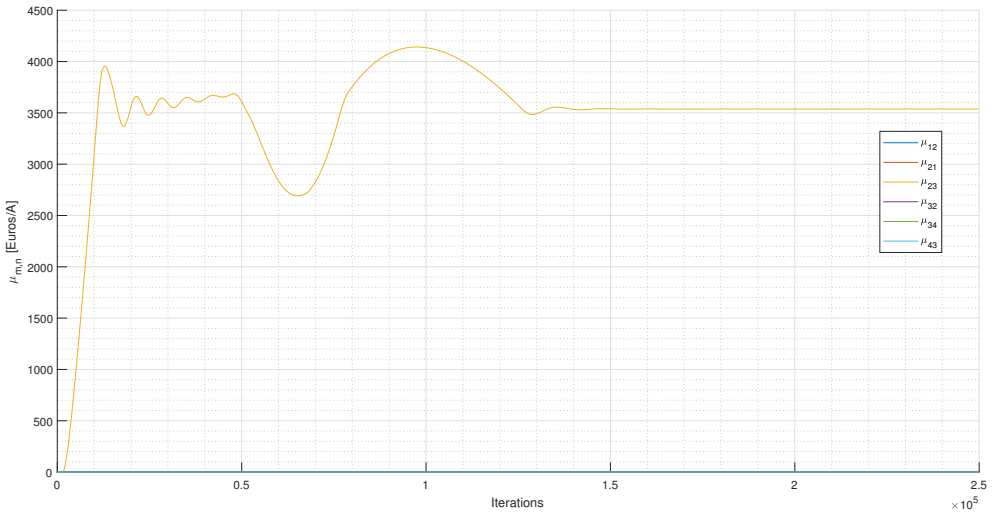

Figure 5.9: Dual variable of the line limit for the grid in Figure 5.1 using the algorithm from [13].

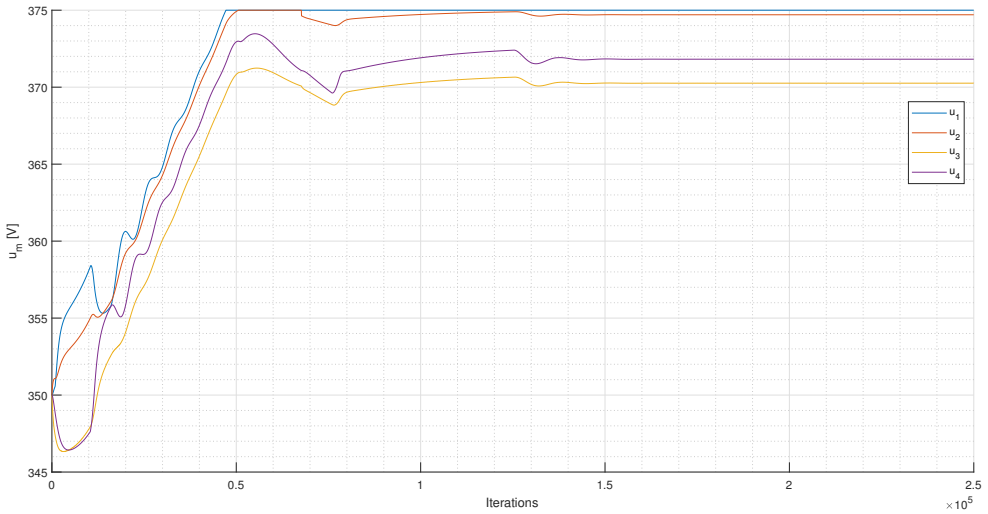

Figure 5.10: Voltage at every node for the grid in Figure 5.1 using the algorithm from [13].

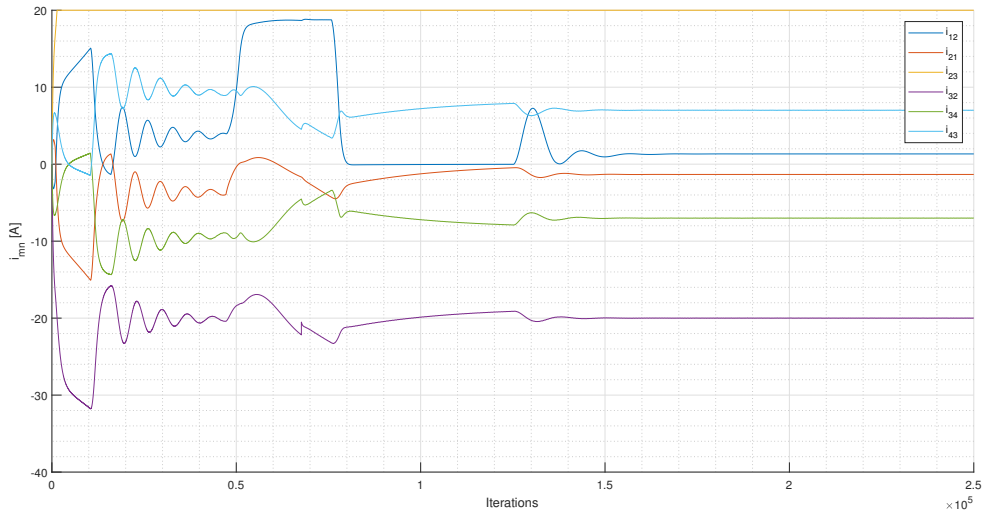

Figure 5.11: The current flowing in every line for the grid in Figure 5.1 using the algorithm from [13]

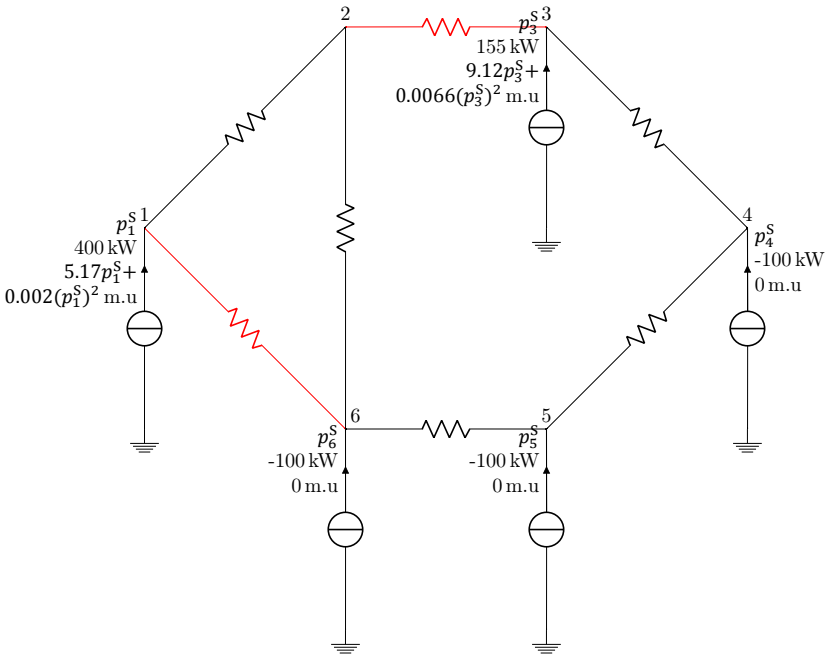

Figure 5.12: A six node meshed grid with line limit (denoted by the red lines), identical with Figure 3.28. The line connecting node 1 to node 6 has a current limit of 50 A while the current flowing in the line from node 2 to node 3 is limited to 20 A

5.3. Simulation with More Nodes

This section shows that the Exact OPF algorithm can work in the case with more generators and loads in the grid. The first case chosen is the 6-node case from Chapter 3, and the other case is a 9-bus IEEE test system.

5.3.1. Meshed 6 Node Case

The meshed grid topology in Figure 5.12 is identical with the grid in Figure 3.28. The difference is that instead of a power transfer capacity, the congestion occurs due to a current transfer capacity since the flow calculation are represented in current. This is for simplicity because the current in the sending end stays the same with the receiving end while the power flow does not. Figure 5.13 - 5.19 depicts the result of the converged calculation. The voltage profile in Figure 5.15 shows that to minimize the losses, the voltage rises to the maximum. This phenomenon does not occur in Figure 3.32 when the losses are not taken into account.

5.3.2. IEEE 9 Bus System

The data are taken from [28] with assuming the cost function for every generator. The original IEEE 9 bus system is a transmission network. In this case, it is modified to be a DC Distribution grid with the power in kilowatts and has voltage boundaries from 325 V to 375 V. Using the Exact OPF algorithm, the results are presented in Figure 5.21-5.25.

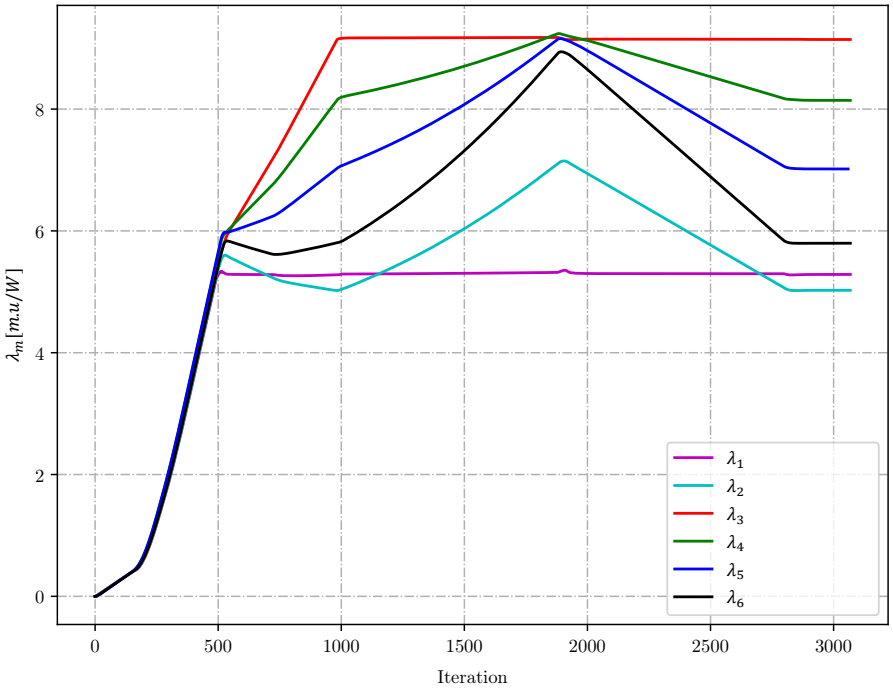

Figure 5.13: Locational Marginal Price (LMP) at every node for the grid in Figure 5.12. Every node has a different value, following the discussion in Section 3.7 regarding the congestion management in a meshed grid.

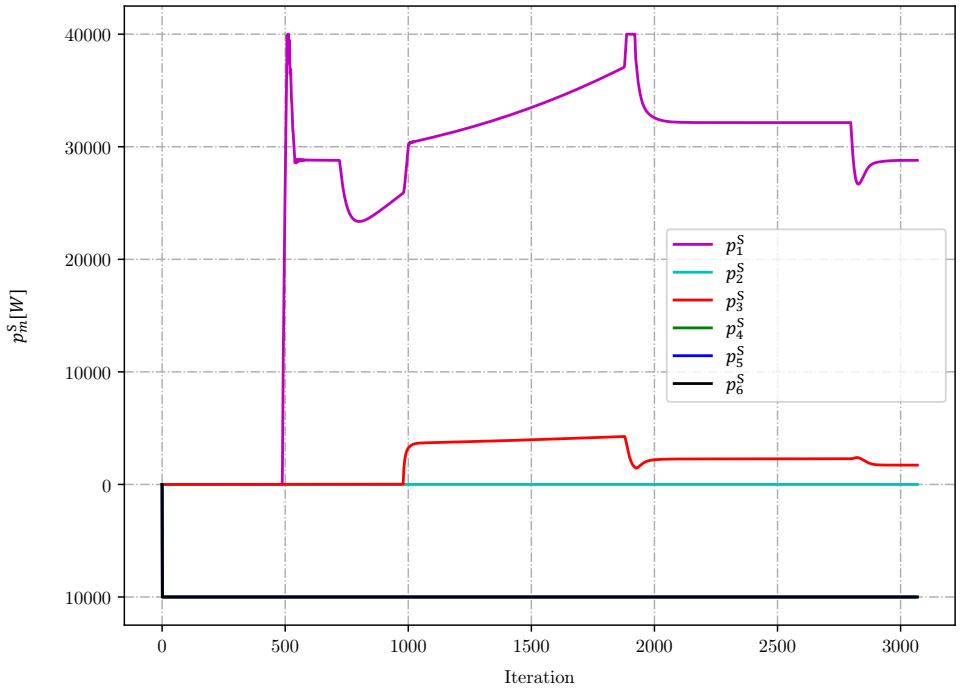

Figure 5.14: The power generation in every node for the grid in Figure 5.12.

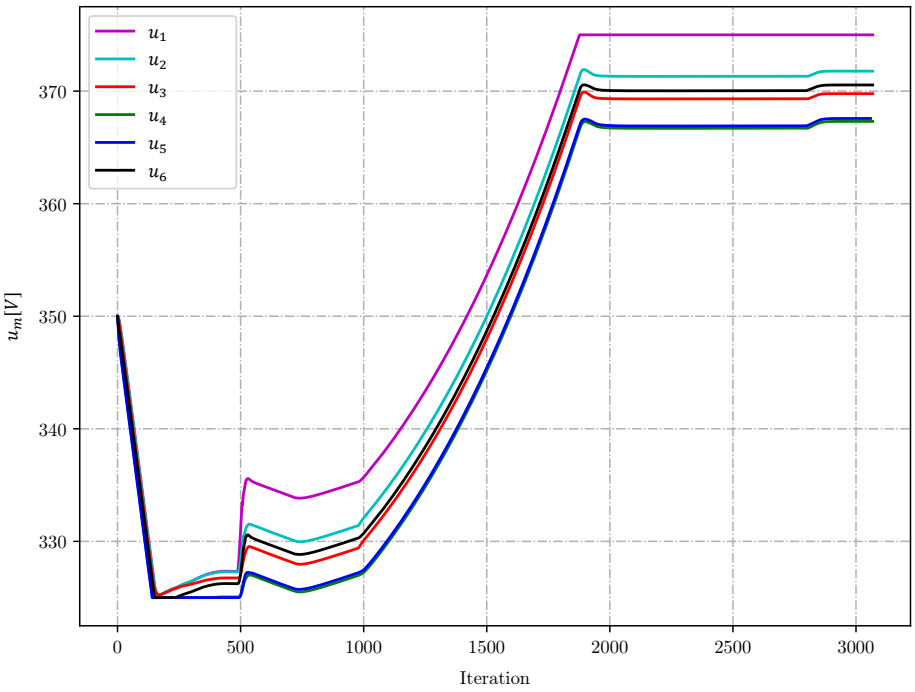

Figure 5.15: The voltage at every node for the grid in Figure 5.12.

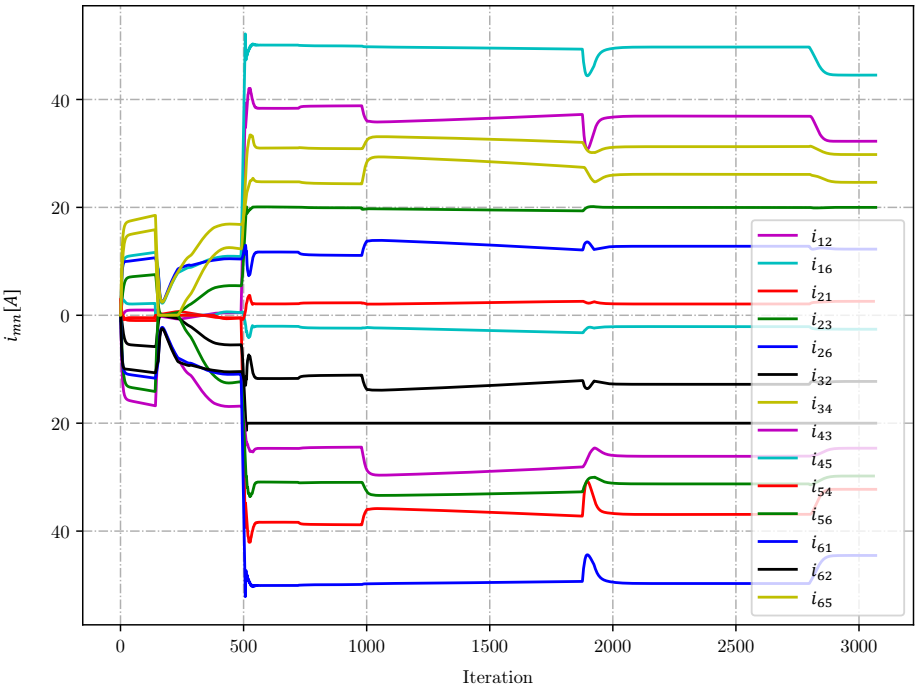

Figure 5.16: The current flowing in the lines for the grid in Figure 5.12.

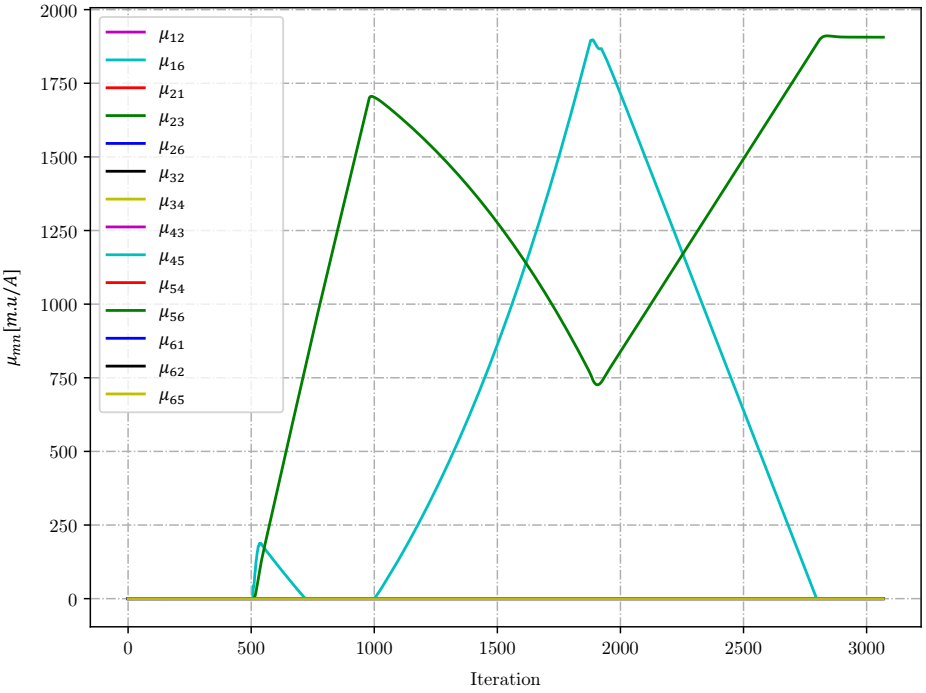

Figure 5.17: The dual variable for current limit in the line for the grid in Figure 5.12.

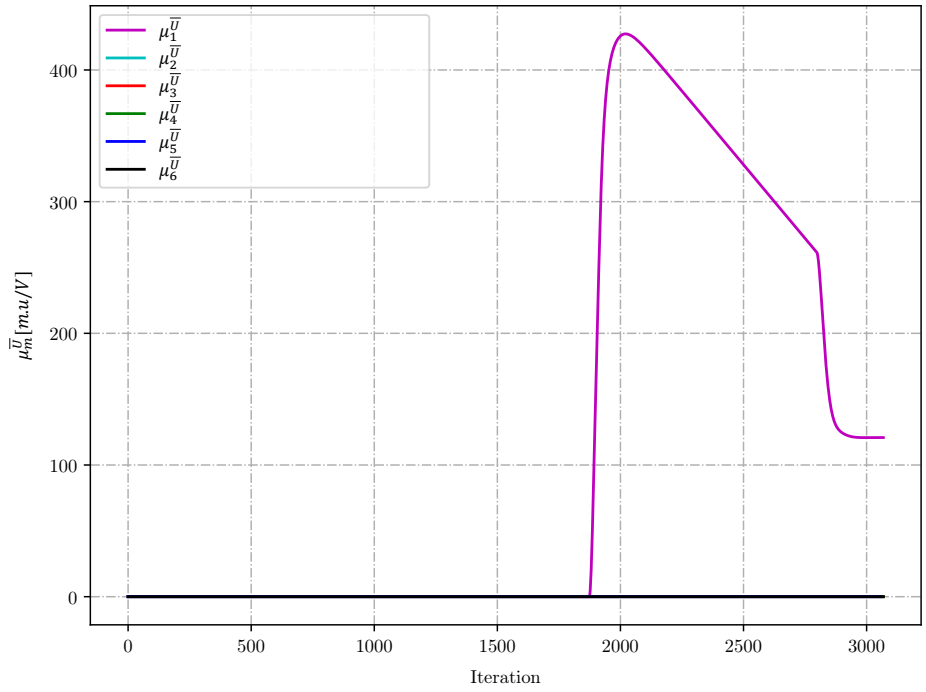

Figure 5.18: The dual variable for the upper voltage limit for the grid in Figure 5.12.

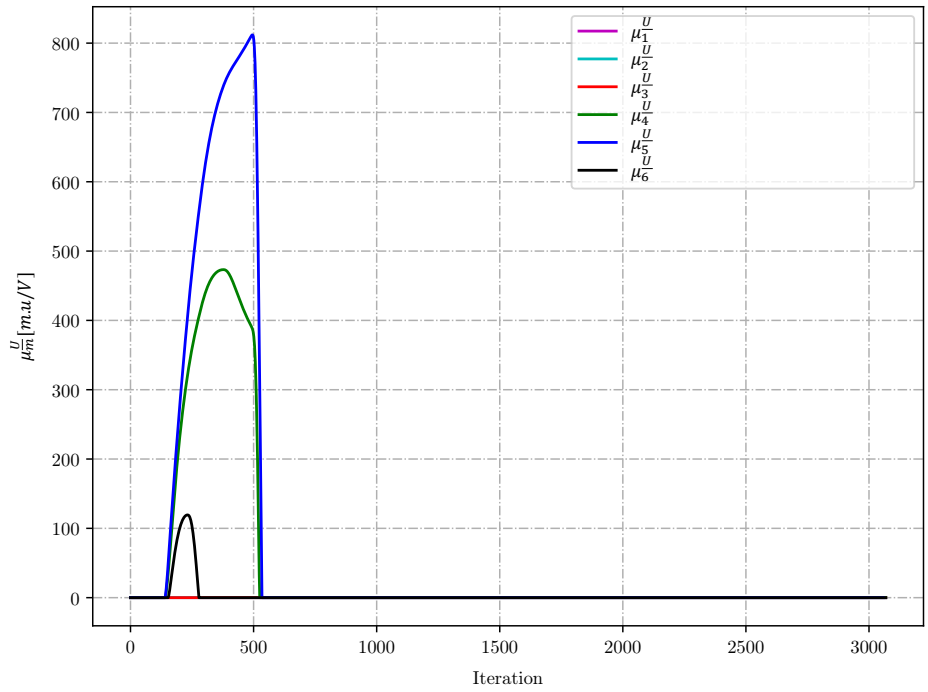

Figure 5.19: The dual variable for the lower voltage limit for the grid in Figure 5.12.

Table 5.2: Line data for the IEEE 9 bus system. The values are modified from the actual line data in [28] by doubling the resistances and state them as ohmic values instead of per unit values.

Line Index	Resistance (Ω)
14	0.1152
27	0.1250
39	0.1772
45	0.184
46	0.184
69	0.34
57	0.322
78	0.144
78	0.2016

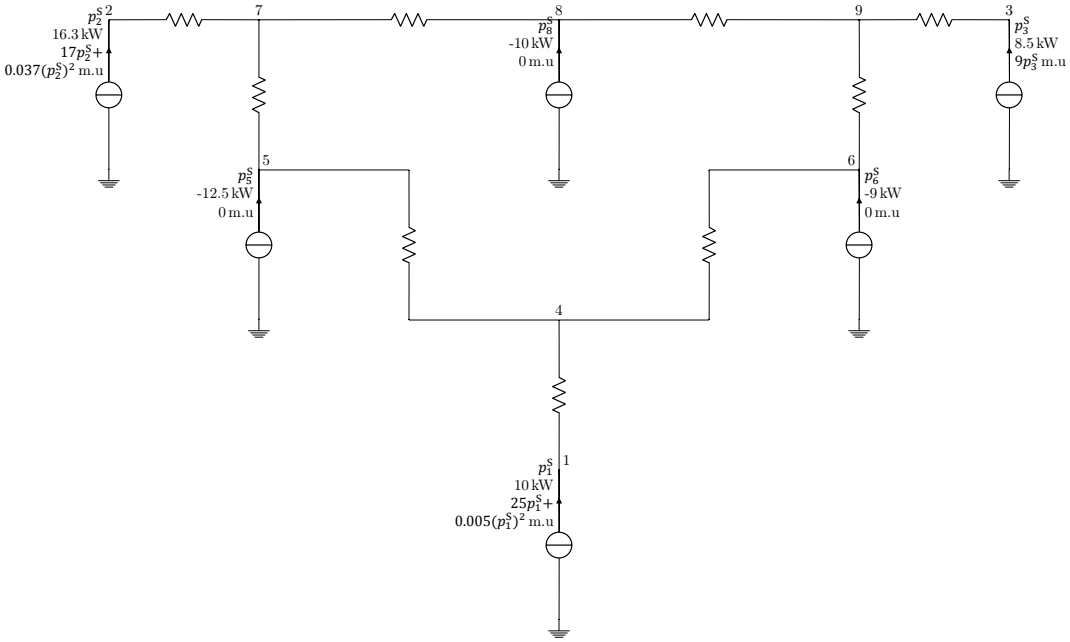

Figure 5.20: The IEEE 9 bus system topology with the modification in the generator and load capacity rating. The resistance values are taken from Table 5.2. Moreover, the generators' cost function are added to create an optimization problem.

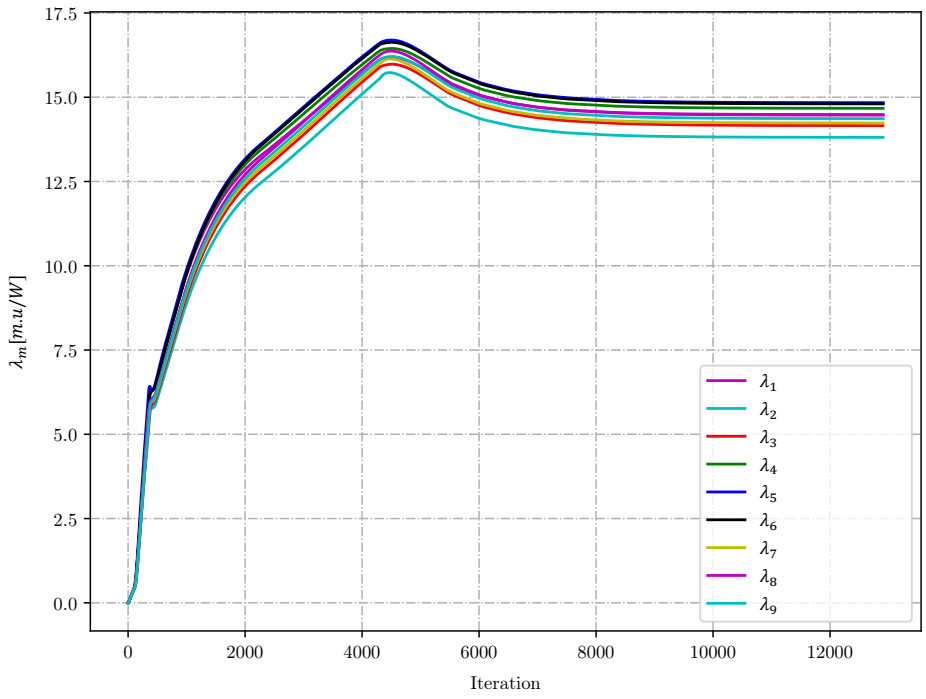

Figure 5.21: Locational marginal price at every node for Figure 5.20. By having the tuning parameters in (4.26) and (4.25), the LMP at all nodes rise conservatively to make sure that the generator produces power sequentially.

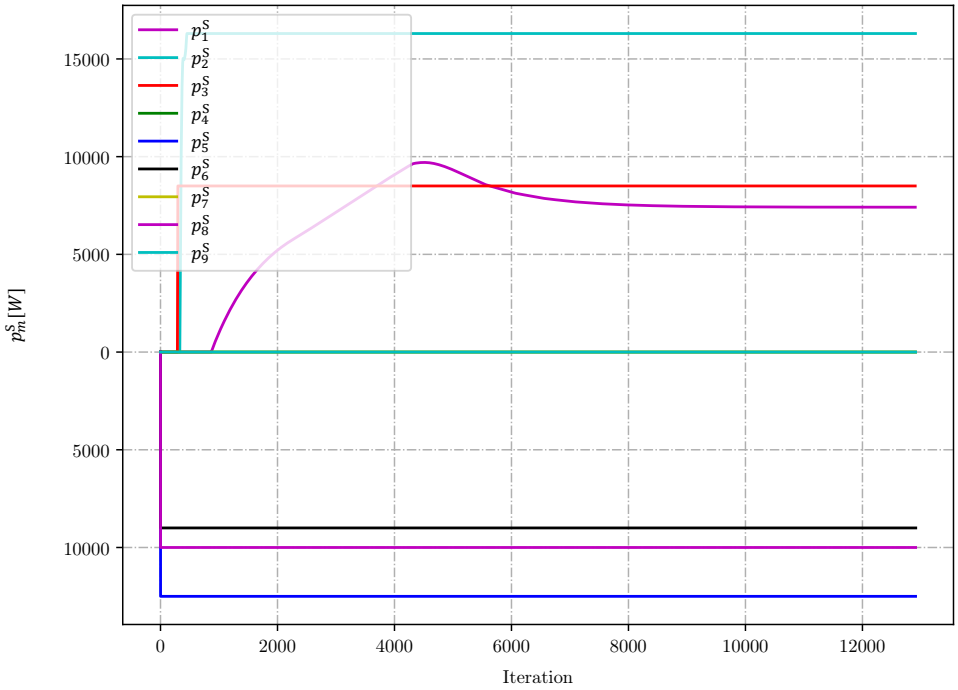

Figure 5.22: The power production at every node for Figure 5.20.

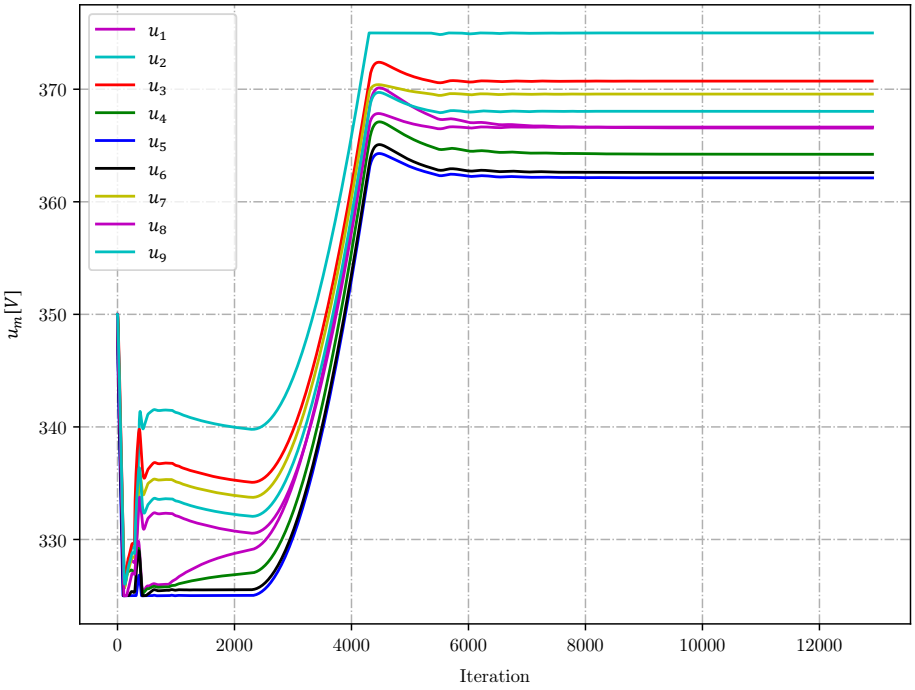

Figure 5.23: The voltage at every node for Figure 5.20. To minimize the losses, every node aims for the highest voltage as possible. Since the generator in node 2 produces more power, node 2 has the maximum voltage.

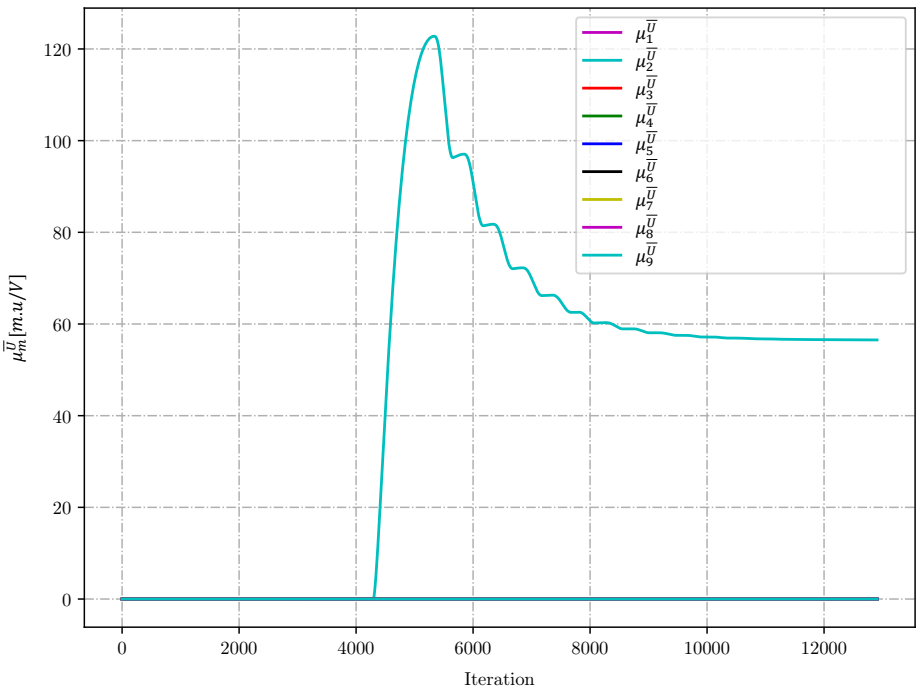

Figure 5.24: The dual variable of the voltage limit at every node for Figure 5.20. Since node 2 reaches its maximum voltage, this parameter increases along with the set tuning parameters. Once it reaches the desired value, the calculation reaches its convergence and stops.

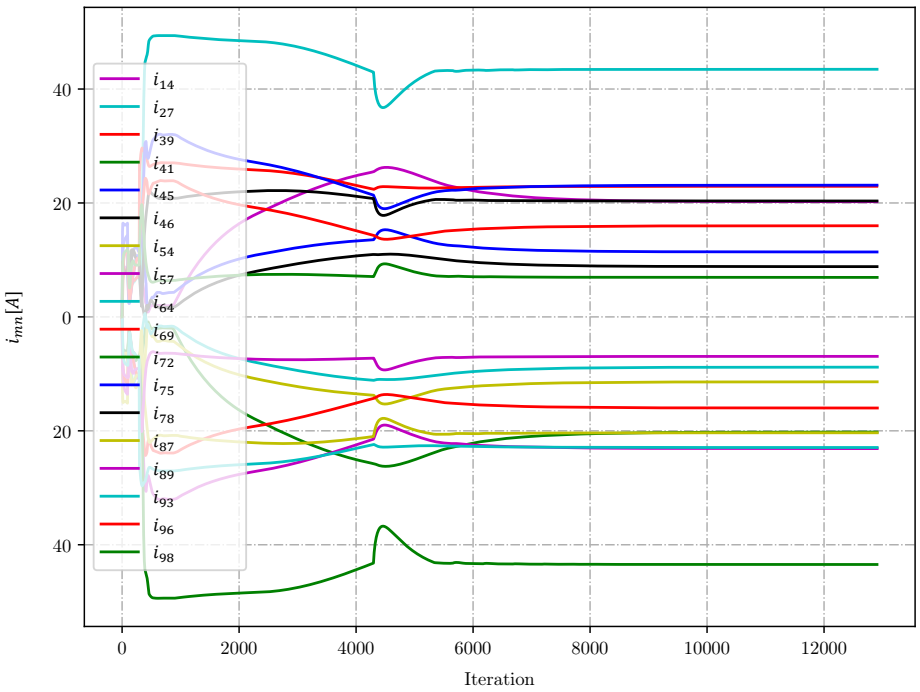

Figure 5.25: The current flowing in every line for Figure 5.20.

6

Asynchronous Update

6.1. Algorithm for Solving the DCOPF in Asynchronous Approach

Being fully distributed means that no central coordinator is necessary and no single point of failure is present. However, as the calculation occurs in every node, a problem in one node can compromise the whole system. The algorithm used in this thesis is based on Consensus and Innovation which relies on data sharing between neighboring nodes. It is possible to have delay during the data sharing. In the Raspberry-Pi implementation, every node must wait for the data shared from its neighbor. The delay occurring in the system is inevitable as it depends on internet connection and there is an actual data transfer between computers.

Based on that problem, it is essential to have an asynchronous update. The asynchronous update in this thesis is different from the one presented in [23] which defines asynchronous as asynchronous inter-area data sharing. The data sharing does not occur every iteration for inter-area connection.

In this thesis, during the synchronous update, the value of the shared parameters (LMP, voltage, and $\mu_{m,n}$) does not vary that much every iteration. Therefore, it is possible to use the previous value for the calculation.

$$[\lambda_n(l), u_n(l), \mu_{n,m}(l)] = \begin{cases} [\lambda_n(l), u_n(l), \mu_{n,m}(l)] & \text{if received} \\ [\lambda_n(l-1), u_n(l-1), \mu_{n,m}(l-1)] & \text{if not received} \end{cases} \tag{6.1}$$

The Raspberry-Pi implementation used socket programming [29] in python for the data sharing. There was no time-out implemented, and the algorithm stops after a determined number of iterations. The implementation is improved by setting a time-out time and execute Eq. 6.1 and also set a convergence criterion to stop the process. The convergence criterion comprises a relatively constant value of power, voltage, and LMP and also satisfied first-order optimality condition.

6.2. Result Comparison between Synchronous and Asynchronous Approach

The grid in Figure 6.1 is simulated to find the optimum solution to the problem. In the hardware validation using microcomputers (Raspberry-Pi), every microcomputer represents as a generator or a load. The first simulation is conducted without setting any time-out time. Figure 6.4 shows that the whole operation takes about 800 s to converge and Figure 6.2 - 6.3 shows the time spent in every iteration. Most of the iterations take 30-40 ms as depicted in Figure 6.2 due to the occurrence of actual data sharing across different microcomputers. However, the time varies due to the quality of the internet connection at a time that can also lead to a longer data sharing time up to 1 s as depicted in Figure 6.3.

Based on Figure 6.4 - 6.7, it is evident that setting a time-out time significantly accelerates the convergence time from 800s to 100s. Each node only waits for the determined timeout duration. As a consequence, in the asynchronous cases, the simulation takes higher iteration numbers since there are lots of data loss that affect the calculation process. Lower timeout duration causes more data loss and leads to a higher iteration number.

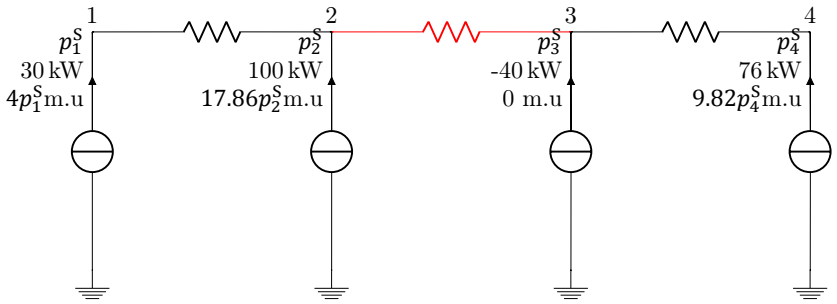

Figure 6.1: Four node serial case with congestion from node 2 to 3. This is a redrawn figure of Figure 3.17.

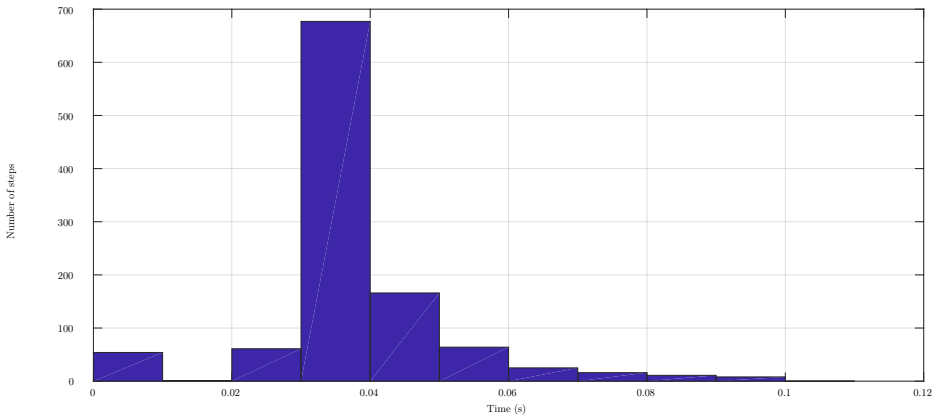

Figure 6.2: The time elapsed for every iteration when Figure 6.1 is simulated in a synchronous way using the microcomputers. It depicts that most of the iterations take around 30-40 ms.

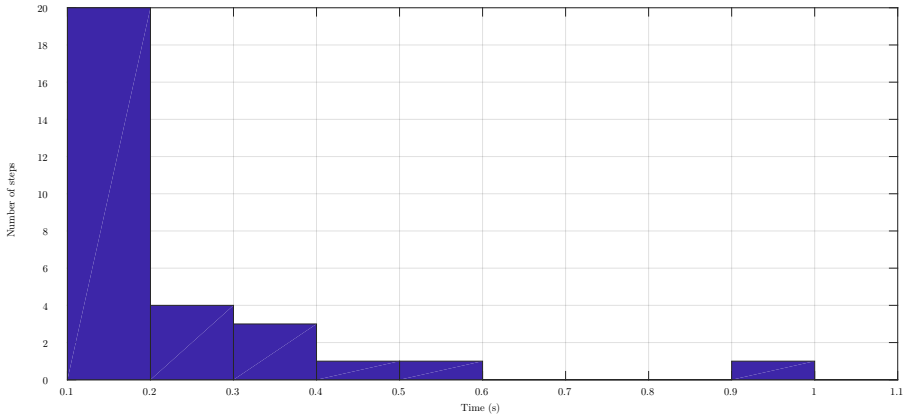

Figure 6.3: The time elapsed for every iteration when Figure 6.1 is simulated in a synchronous way using the microcomputers. It shows the presence of some iterations which take more than 100ms and up to 1s. These cause the algorithm to converge up to 750s.

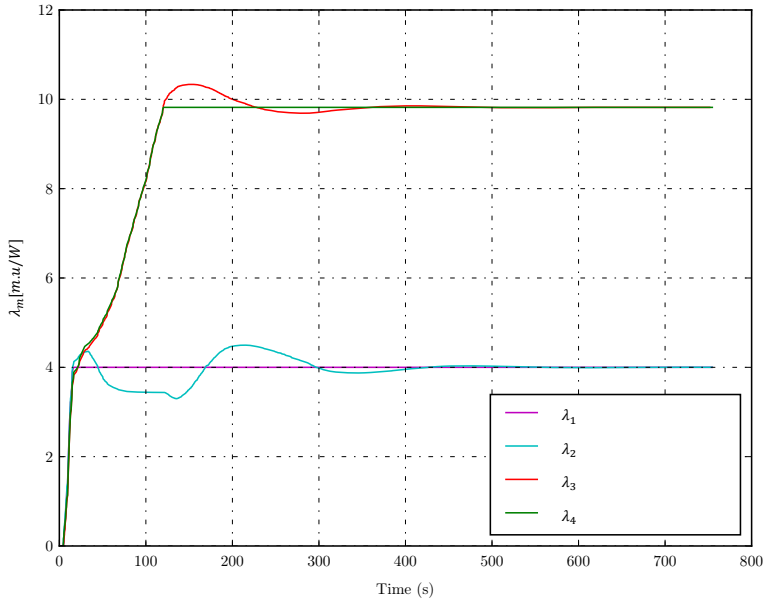

Figure 6.4: Locational Marginal Price (LMP) at every node for the grid in Figure 6.1. The algorithm is run in a synchronous way where every parameter waits for a new value to proceed calculation. It takes 750s and 1112 iterations to converge.

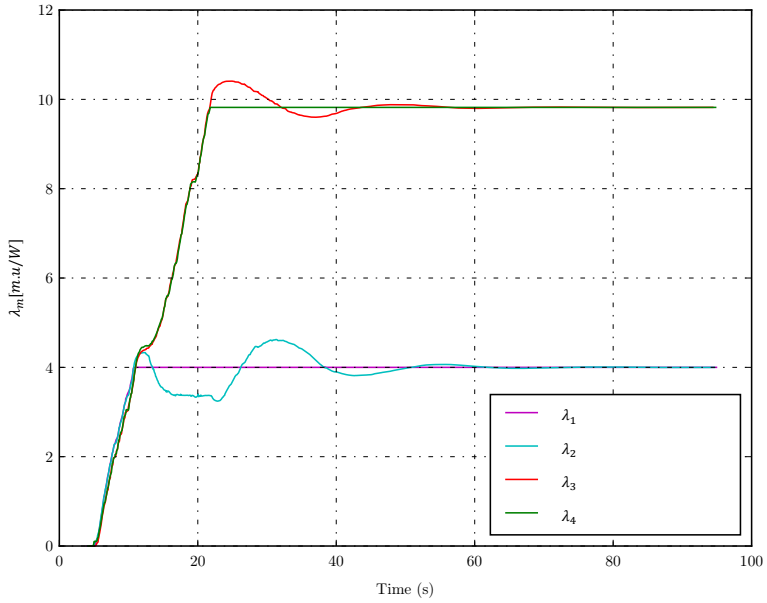

Figure 6.5: Locational Marginal Price (LMP) at every node for the grid in Figure 6.1. The algorithm is run in an asynchronous way where every node only waits for 70ms. In case no new data is received, the calculation continues using the previous value. It takes 95 s and 1360 iterations to converge.

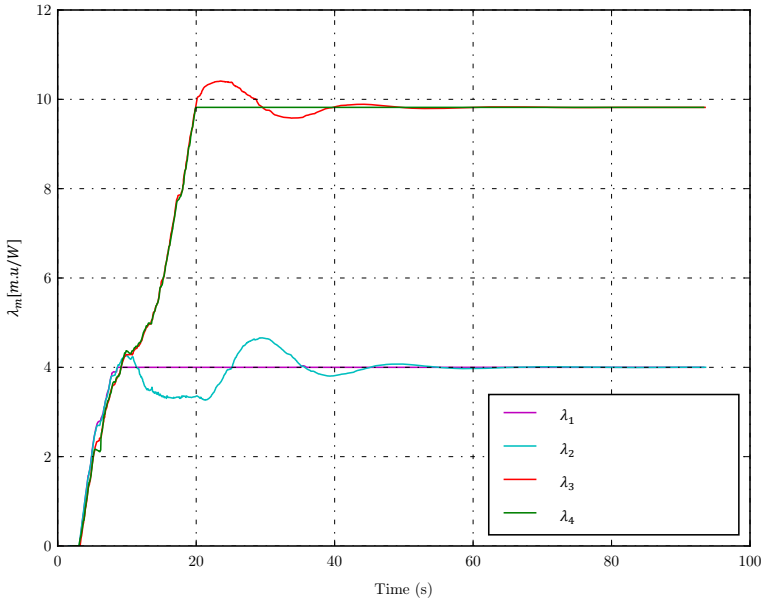

Figure 6.6: Locational Marginal Price (LMP) at every node for the grid in Figure 6.1. The algorithm is run in an asynchronous way where every node only waits for 50ms. In case no new data is received, the calculation continues using the previous value. It takes 92 s and 1550 iterations to converge.

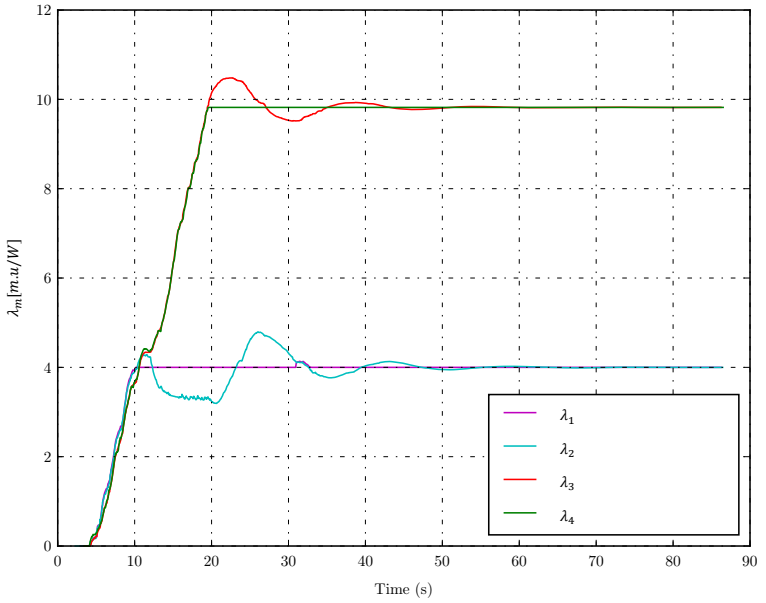

Figure 6.7: Locational Marginal Price (LMP) at every node for the grid in Figure 6.1. The algorithm is run in an asynchronous way where every node only waits for 70ms. In case no new data is received, the calculation continues using the previous value. It takes 83 s and 1800 iterations to converge.

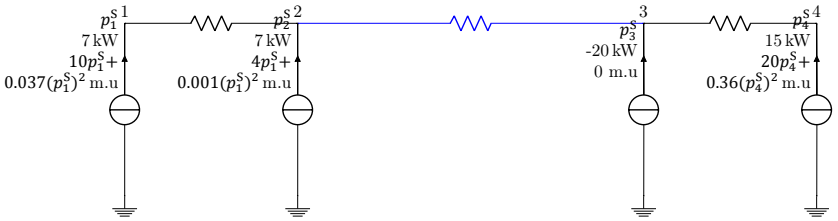

Figure 6.8: Four node serial case with a long line connecting node 2 and 3 (depicted in blue). The line is very long, and due to the voltage limits and losses, all the required power cannot be delivered from the cheapest generator in node 2.

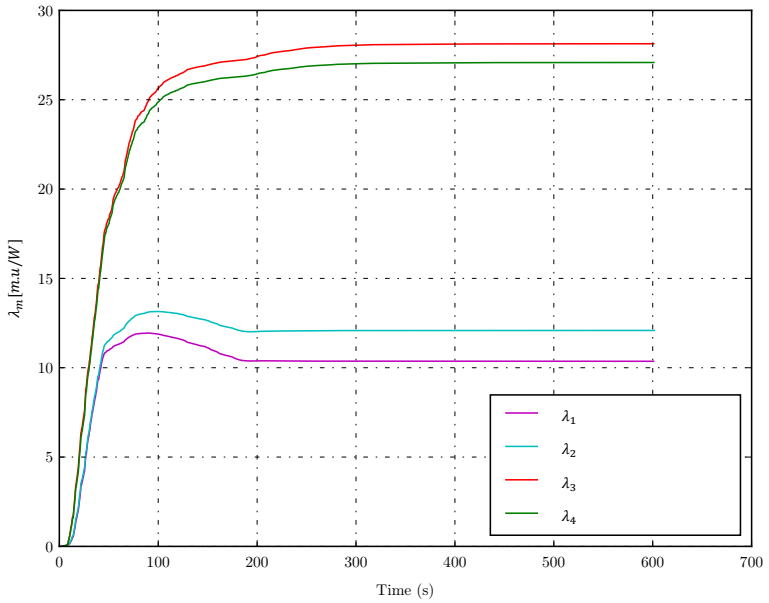

Figure 6.9: Locational Marginal Price (LMP) at every node for the grid in Figure 6.8. The algorithm is run in a synchronous way where every node waits until all data are received. It shows that it took up to 600s to converge.

The time-out time variation does not necessarily work for every case. In the case in Figure 6.8, setting less than 150 ms of time-out time does not result in a converge solution. Although once the time-out time is set right, the convergence time reduces significantly. This happens because, in the Exact OPF, the power generated depends on the LMP value. A difference in LMP value can affect significantly to the power and the other variables. Figure 6.9-6.11 show the result when it is run in a synchronous manner and asynchronous with 100 and 150 ms of time out time.

The discussion in this chapter and (6.1) answer the research question 4 on how the algorithm can be improved to reduce the delay. By setting a time-out time, the node only waits for the desired period. If no data is received, then the neighbor's variables from the previous iteration are used. The algorithm improvement results in faster convergence time, compared to the synchronous algorithm.

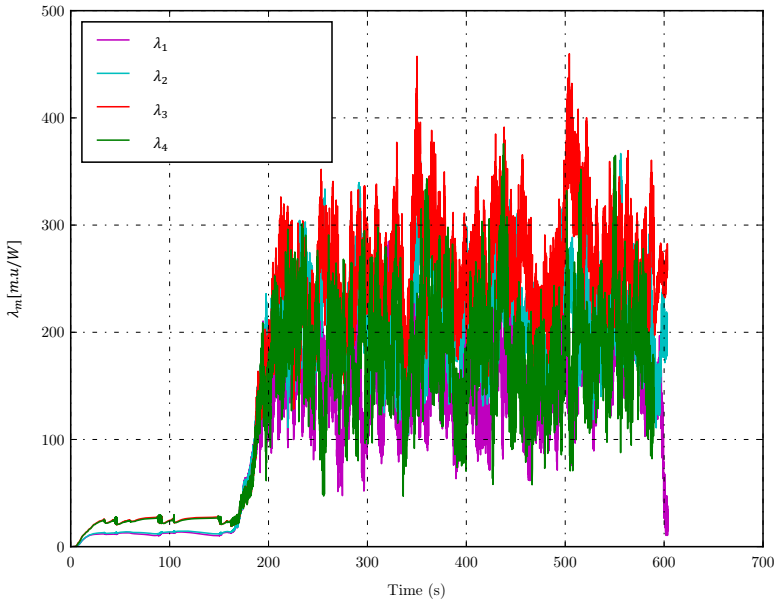

Figure 6.10: Locational Marginal Price (LMP) at every node for the grid in Figure 6.8. The algorithm is run in an asynchronous way where every node only waits for 100ms. In case no new data is received, the calculation continues using the previous value. Due to the sensitivity of the value and poor amount of the updated data received, the problem is not converged to the solution.

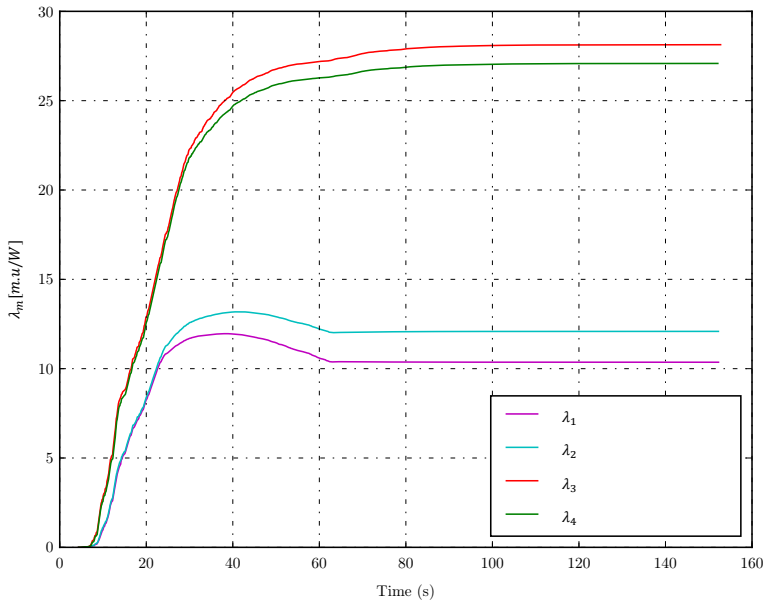

Figure 6.11: Locational Marginal Price (LMP) at every node for the grid in Figure 6.8. The algorithm is run in an asynchronous way where every node only waits for 150ms. In case no new data is received, the calculation continues using the previous value. It takes 160 s to converge.

7

Conclusion, Reflection, and Future Work

7.1. Conclusion

As stated in Chapter 1, the main goal of this thesis is to improve the speed and resilience of the C+I based distributed optimal power flow algorithm by formulating the tuning parameters and asynchronous update. The formulation of the tuning parameters are presented in Table 3.2 and Table 4.1 while the asynchronous algorithm is done by having (6.1). Extensive explanations are discussed through the research questions below.

1. How can the physical interpretation be used to improve the convergence rate?

The use of the physical interpretation started with setting a condition on how the power and the LMP are updated in Figure 3.2 and 3.1. For a linear cost function, the linear coefficient of the generator needs to be the same with the LMP for starting producing power. In the physical meaning, it gives an intuitive sense that a product cannot be sold if the price of the product (represented as the linear coefficient) is higher than the current market price (expressed as the LMP). With that condition, the LMP will stay constant during the power update and the power will remain in the minimum or maximum when the LMP changes to below or above the linear coefficient respectively.

The other exploitation of the physical interpretation is during the tuning parameter formulation. In the previous research [14], the tuning parameters are set through a trial-and-error method and have to change for every case. In this thesis, it is concluded that the physical meaning of the first order KKT condition in 3.3 for a Lossless OPF case and 4.3 for an Exact OPF case can be employed for better tuning parameter determination.

Starting with the LMP update, it follows (3.17) with the tuning parameters in (3.24) and (3.25). For the first tuning parameter α_u^λ, it aims to have the same LMP as its neighbor during the absence of the congestion and losses. Therefore, it is formulated as in (3.24). The equation holds even during the congestion and the presence of the losses. The other tuning parameter α_λ^λ is an estimated constant as in (3.25) by deciding the desired step size of lambda change due to the power mismatch. The equations hold for cases with congested lines since the dual variable will appear in the LMP consensus in (3.8). Moreover, it also holds for an Exact OPF case since in its LMP consensus (4.10), there is an extra term that leads to different LMP across the nodes.

As for the power update, the equations used are (3.26) for the Lossless OPF and (4.44) for the Exact OPF. In (3.26), the tuning parameter is formulated as in (3.27) and (3.30). By having (3.27), it means that the power only solves 25% of compensating the power deficit or surplus. The other tuning parameter in (3.30) estimates the extra generated power necessary when the LMP does not reach consensus.

The voltage is updated by using (3.31) for the lossless OPF and (4.30) for the Exact OPF. Both algorithms use the power mismatch and formulate α_λ^u as in (3.32) and (4.33) to have the voltage change by 25% of the power mismatch. Incorporating the power, the power and voltage move 50% to

the solution every iteration. The Exact OPF has another term in the voltage update which will be discussed in the next subsection.

The Exact OPF case shows a significant improvement in term of the convergence speed from the previous research [13] as shown in Chapter 4. However, it is still assumed that all generators must have a quadratic cost function to be able to calculate the power, following (4.44).

2. How can the line congestion be taken into account for the voltage and the dual variable updates, especially for a meshed grid?

There are two methods in solving a problem where congestion occurs which are Area Separation Method and Dual Variable Activation Method, as discussed in Chapter 3. The congestion is managed by using the Area Separation Method for a radial lossless case. The nodes connected by a congested line exclude each other from their LMP consensus calculation in (3.7). As a consequence, the LMP update of that node does not consider the neighboring nodes to which the line is congested. Moreover, to prevent the power flow from exceeding the limit, the voltage is updated using (3.36) so that the power flow is clamped to the limit to maximize the line utility. The dual variable $\mu_{m,n}$ is updated by taking the LMP difference between the nodes which are separated by the congested line as shown in (3.37).

However, As for the meshed grid and other grids which includes the losses, the dual variable has to be activated by multiplying the difference between the actual power flow (current flow for the Exact OPF) with its respective limit and an estimated constant. Equation 3.38 and 3.39 shows the activation of the dual variable while the voltage is updated using (3.36).

3. How can the losses and the voltage limit be accounted for in the distributed OPF?

The losses and the voltage limit is accounted for by modifying the constraint. The power flow constrain (4.2) uses the actual voltage u_m instead of u_{nom} as in the Lossless OPF. Consequently, all the formulas in Chapter 3 that use $G^p_{m,n}$ are converted into $u_m G^p_{m,n}$. Furthermore, there are some changes in the voltage update. The voltage is updated based on the power mismatch in a node and the LMP consensus between neighboring nodes as discussed in Chapter 4. In (4.30), the voltage is updated by reducing the voltage when the generated power is less than the sum of the power flowing out from the node, indicated by positive power mismatch in (4.10). The tuning parameter α^u_λ is formulated as in (4.33). Regarding the LMP consensus, the power flows from the lesser LMP to the higher LMP. Therefore, the voltage should increase when the LMP is less than the neighboring nodes, indicated by negative LMP consensus (4.9). The voltage change is determined by the tuning parameters α^u_u which is formulated by taking the LMP difference among the nodes and multiply it with an estimated constant as shown in (4.37). This constant determines if the voltage is going to converge. Higher constant will make the voltage changes rapidly, leading to an unending oscillation. On the other hand, the lower constant will also prevent the voltage to converge. By using both terms, the voltage is at the upper limit to minimize the losses.

As a consequence of having one or more nodes with the maximum voltage, the dual variable of the voltage limit $\mu^{\overline{U}}_m$ will have value. It is increased by taking the voltage difference between the limit and the actual voltage and multiply it with a constant in (4.42) and (4.41).

Due to the presence of the voltage limit, during the case where a long line exists in Chapter 4, both upper and lower voltage limit are present. As a consequence, the power transfer is limited and the load takes the power from a closer generator despite the higher price it sets.

4. How can the algorithm be modified in order to run asynchronously for reducing delays?

The algorithm is modified by setting a timeout duration so that the node does not wait for any information received after the timeout duration. It is represented in (6.1). As a consequence, the calculation uses the value from the previous iteration. The number of the iteration increases since the calculation does not use updated value to reach to the solution. However, It leads to a faster convergence time since every iteration has a time limit to wait for the neighbor's information.

Chapter 6 shows that lower time-out time does not necessarily reduce the convergence time. And for another case, when the value changes are too sensitive and the timeout duration is set too low, the solution cannot be reached. Therefore, this would be a recommendation to observe the proper timeout duration for every case.

7.2. Reflection

The model of this work assumes that one node m only contains one unit of a generator or a fixed load. The change in this assumption requires the algorithm to change significantly. Suppose that one node includes loads and generators with different prices, the algorithm must be able to differentiate which generator should supply first. The trajectory of the LMP vs. power update in 3.2 will become different. Moreover, the mathematical formulation holds for DC distribution system with and without losses considered. Problems for AC OPF can be tackled using this algorithm with its DC approximation, and the Lossless OPF is employed. However, when the losses and imaginary part of the AC system are examined, the algorithm and the tuning parameter formulations have to be reformulated since the first order optimality KKT conditions will change and the set of the formulated tuning parameters no longer hold.

The platform of the hardware validation is built in a way that every microcomputer communicate with each other using a Wi-Fi network. In the future development and possible expansion, the system cannot rely on a single network that can cover the whole area. Hence, another infrastructure such as ad-hoc network should be implemented. Moreover, the current platform will also fail during a failure of one node (microcomputer). A more sophisticated approach has to be found to let the system running despite any physical unit loss or communication failure. Furthermore, relying on distance communication is prone to a cyber attack. Therefore, a cybersecurity aspect should be investigated to have better system protection. These reflections would improve the robustness of the system, and the platform is resilient to any internal or external failure.

7.3. Future Work

The current simulation runs a single period problem. In the real implementation, the search of the optimized has to be continuous by being able to adapt to the change of data such as the fluctuation of the load. This feature can later be improved by having storage taking into account in the grid. Moreover, the optimization can also be seen from the demand/load side of the system as a demand response. By having the demand response, the loads can adjust their value so the cost is minimized.

Regarding the iteration numbers, the results shown still have high value of iterations even with a relatively small cases. This causes the implementation to spend a lot of time to solve one problem. Another approach can be thought about to speed up the iteration. For instance, by defining the network topology and make the nodes receive more information, this may enable the calculation converge faster. Moreover, another approach can be used for the asynchronous update since setting up an arbitrary timeout duration does not necessarily work for all cases.

A

Lossless OPF: Remaining Variables and First-Order KKT Conditions

A.1. Four Node Case without Congestion

The case refers to Figure 3.4.

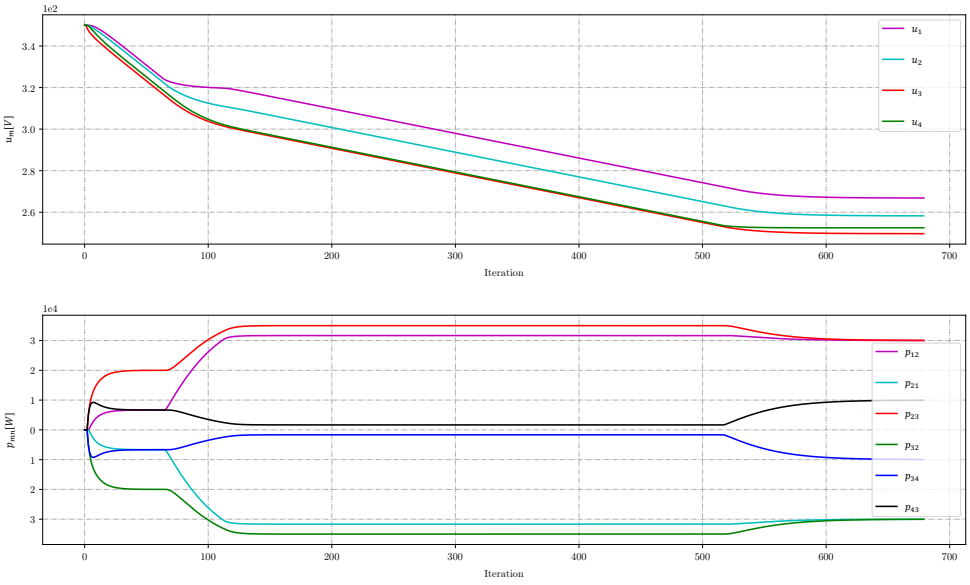

Figure A.1: From top to bottom: The voltage and power flow for the grid in Figure 3.4

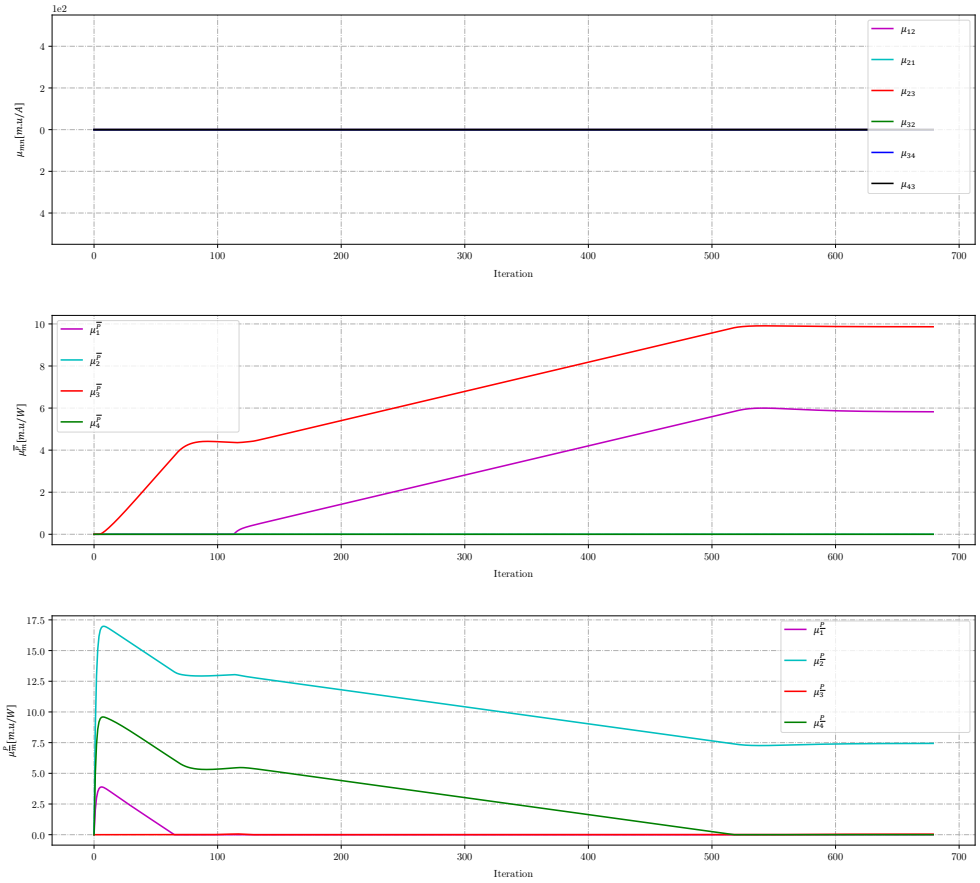

Figure A.2: From top to bottom: Dual variable for line limit, maximum power, and minimum power for the grid in Figure 3.4

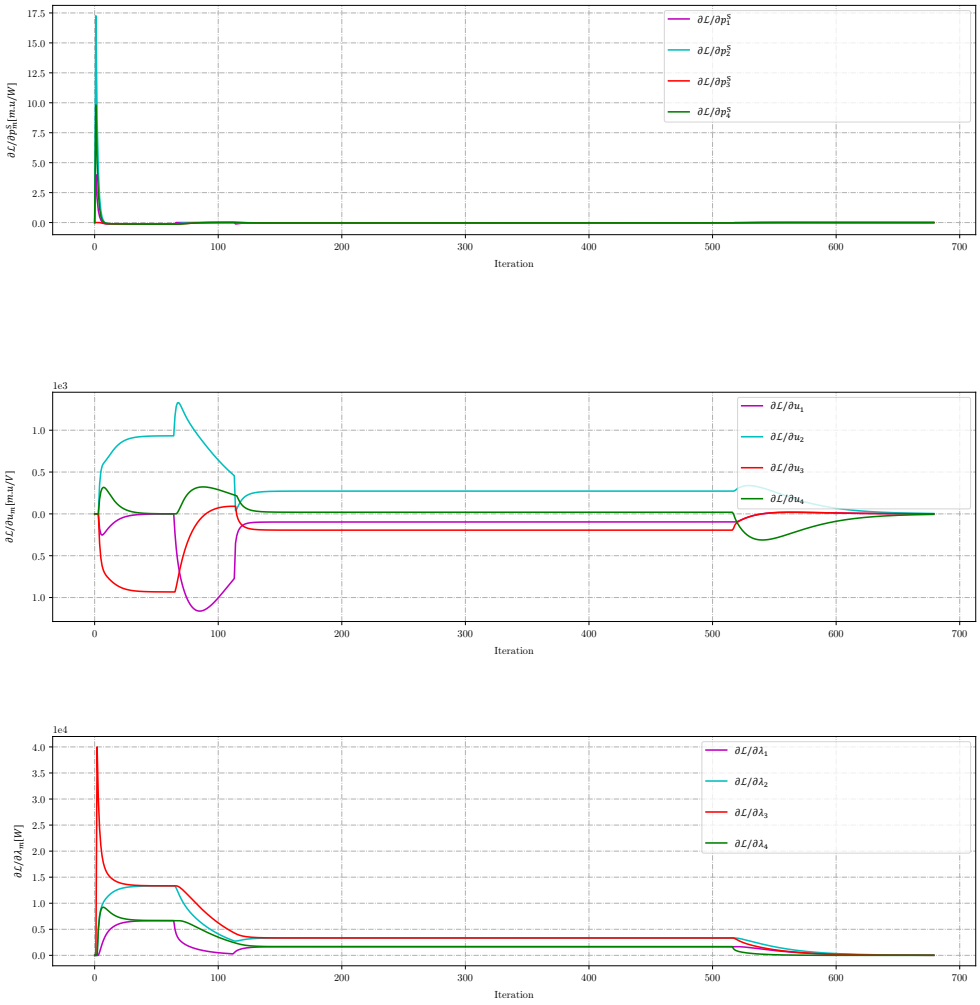

Figure A.3: From top to bottom: Lagrange differentials to power, voltage, and LMP for the grid in Figure 3.4

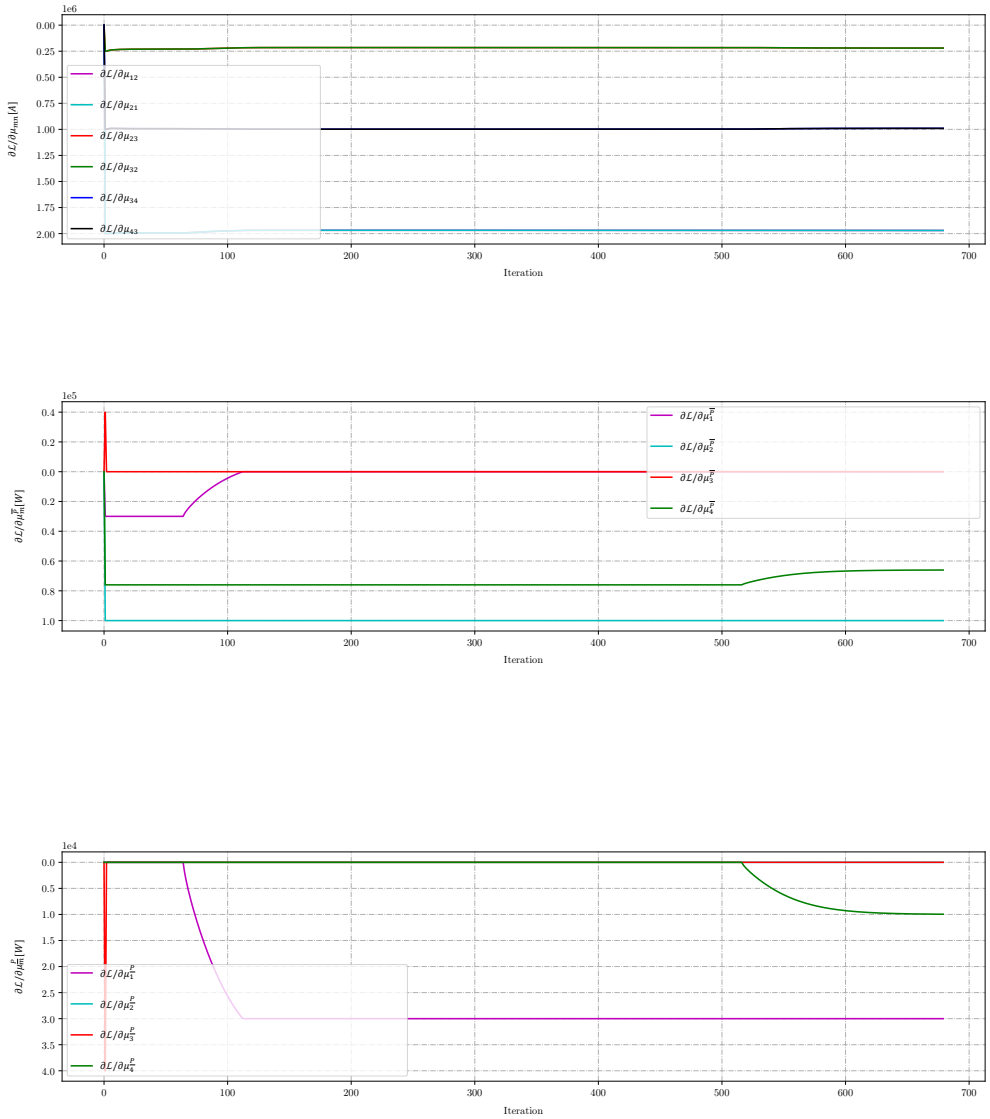

Figure A.4: Lagrange differentials to the dual variables for the grid in Figure 3.4

A.2. Three Node Case with Congestion

The case refers to Figure 3.7.

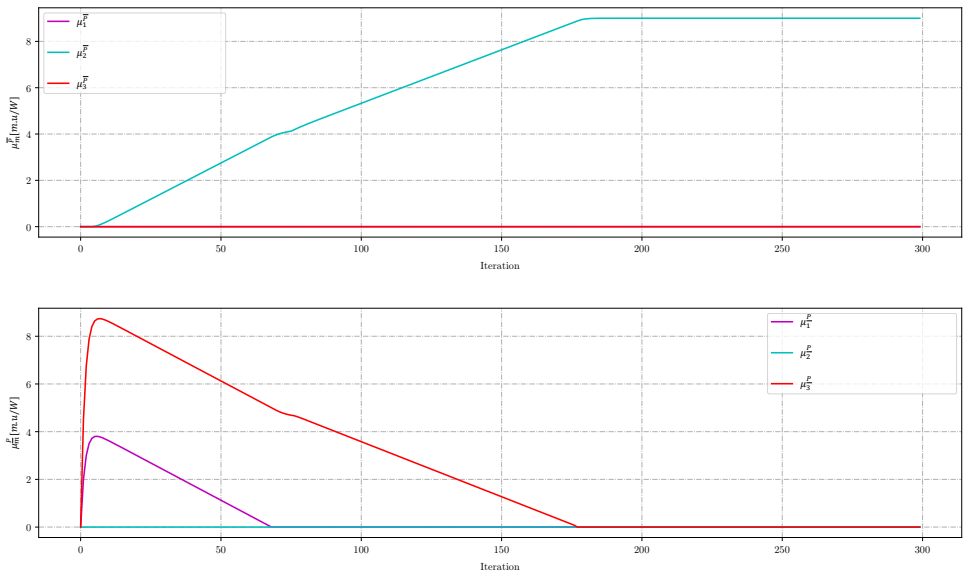

Figure A.5: From top to bottom: Dual variable for maximum and minimum power for the grid in Figure 3.7

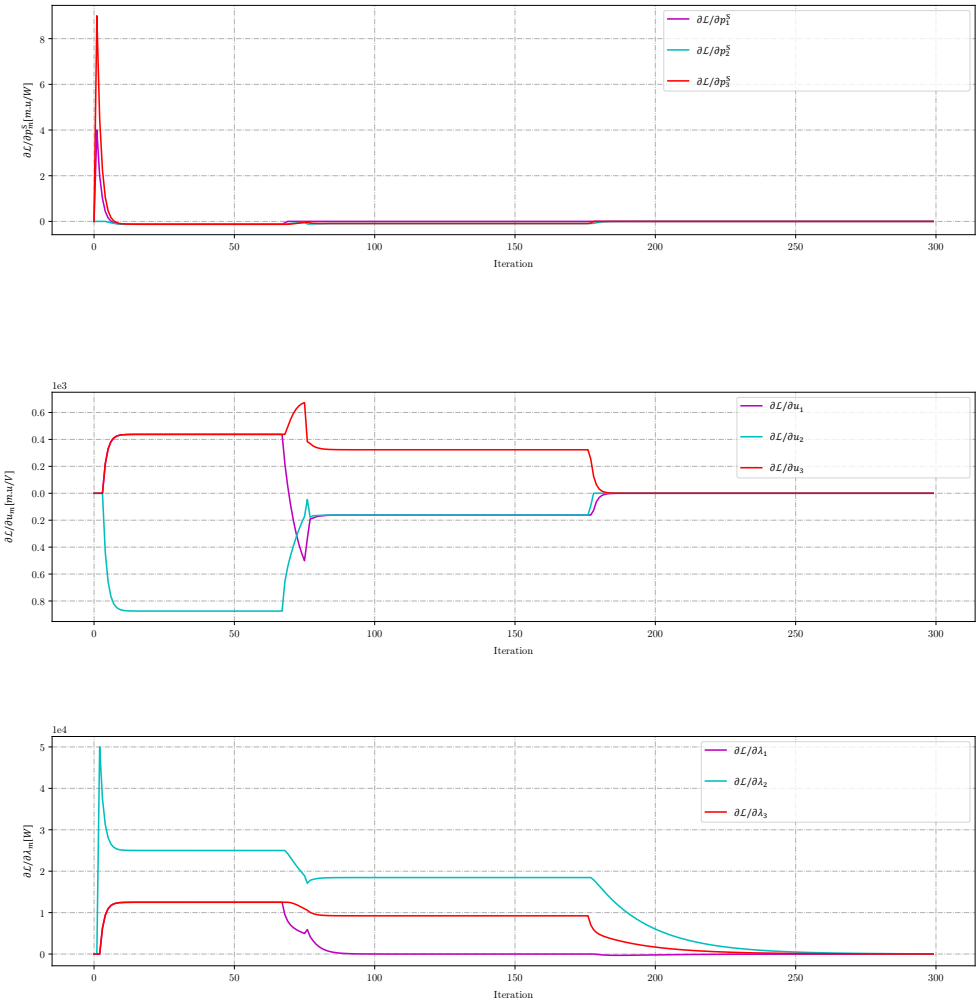

Figure A.6: From top to bottom: Lagrange differentials to the power, voltage, and LMP for the grid in Figure 3.7

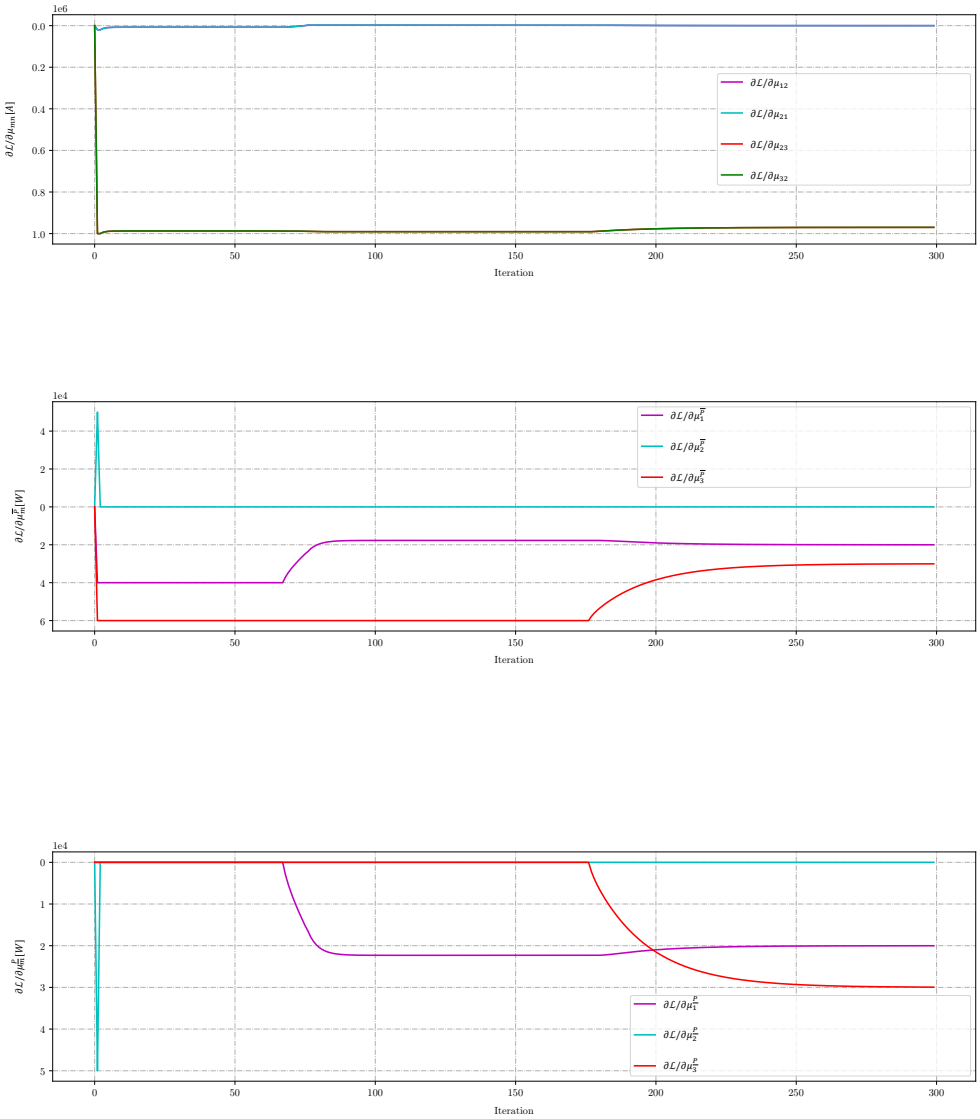

Figure A.7: Lagrange differentials to the dual variables for the grid in Figure 3.7

A.3. Four Node Meshed with Congestion

The case refers to Figure 3.13.

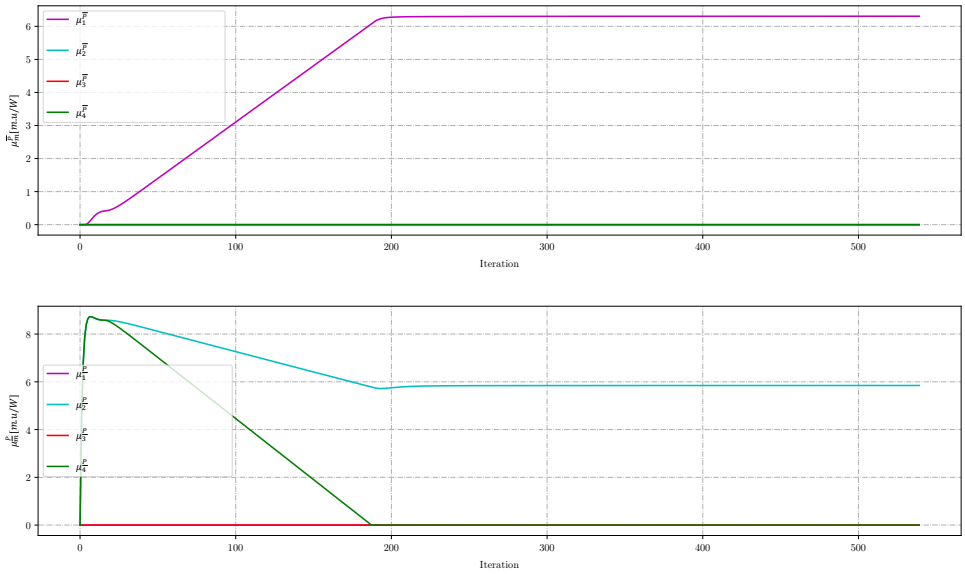

Figure A.8: From top to bottom: Dual variable for maximum and minimum power for the grid in Figure 3.13

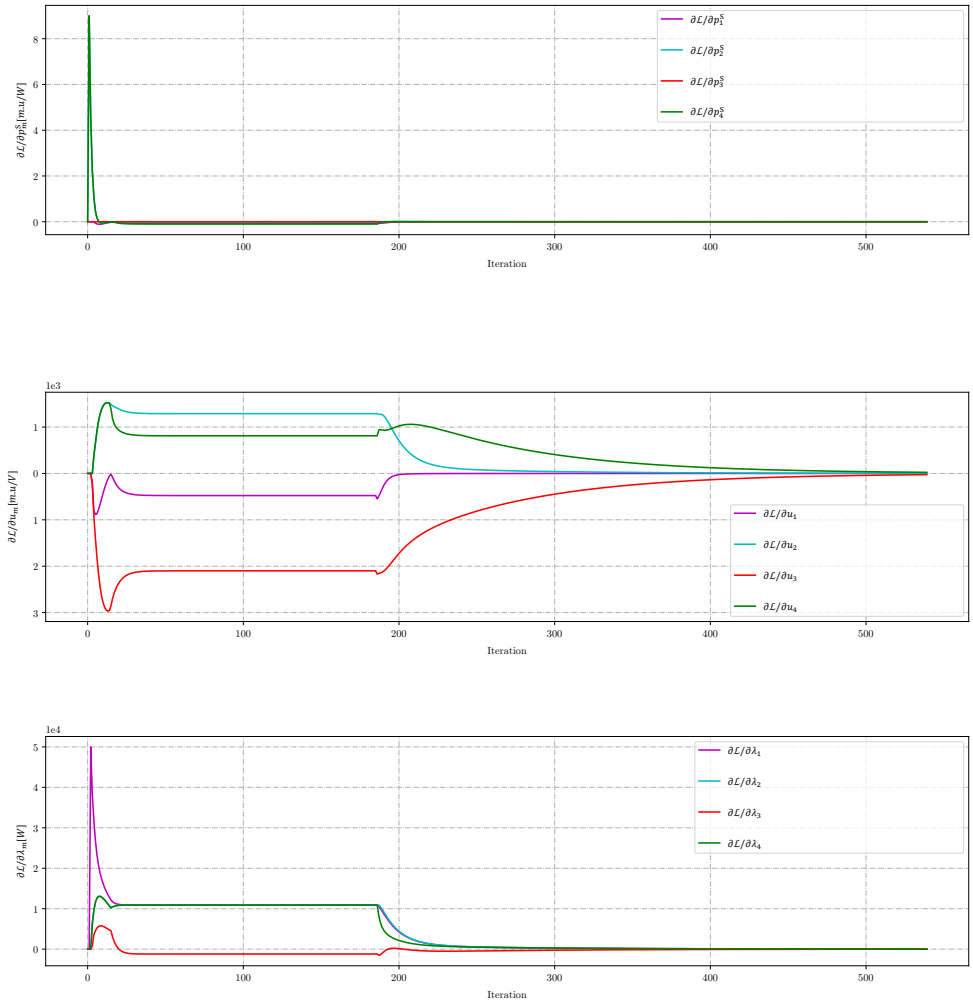

Figure A.9: From top to bottom: Lagrange differentials to the power, voltage, and LMP for the grid in 3.13

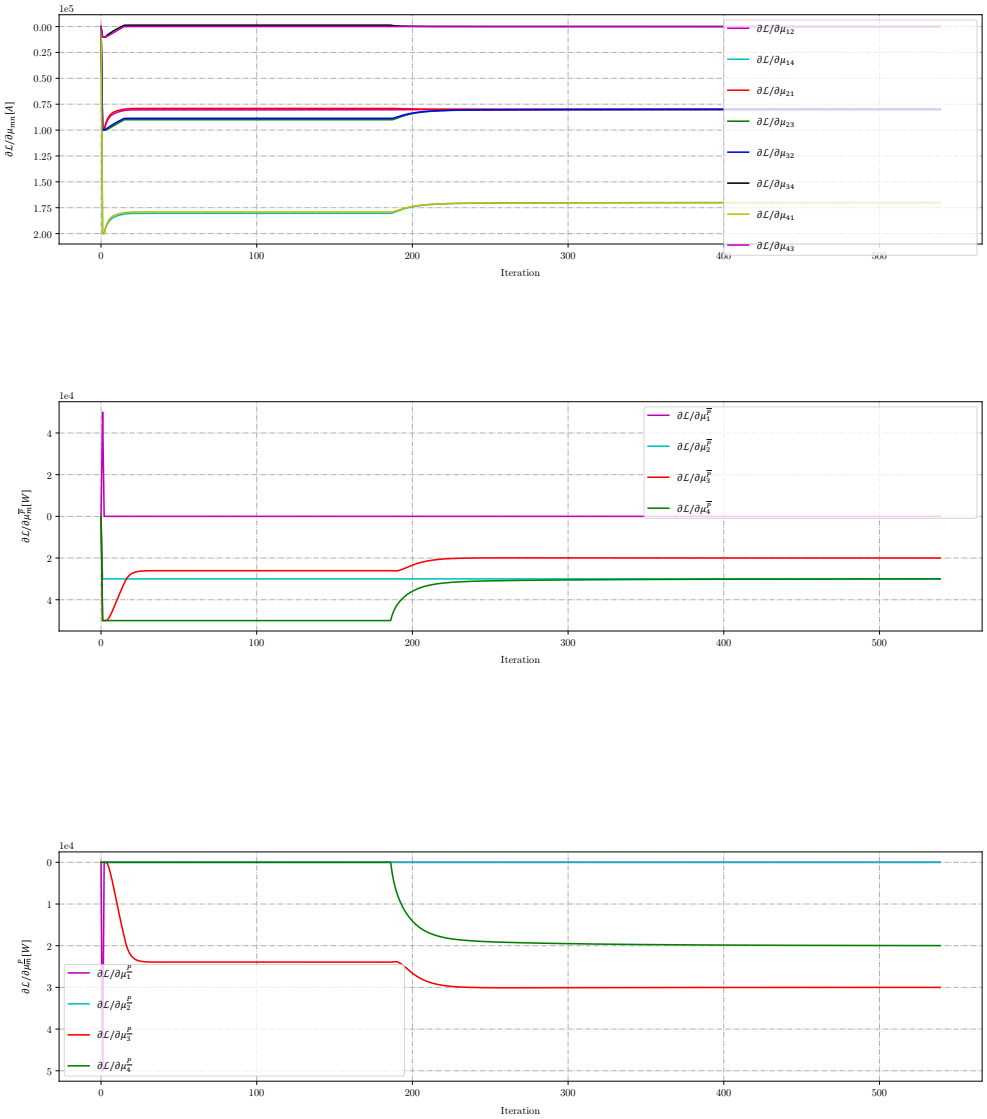

Figure A.10: From top to bottom: Lagrange differentials to the dual variables for the grid in 3.13

A.4. Four Node Serial with Congestion Using Area Separation Method

The case refers to Figure 3.17 which is solved using the Area Separation Method.

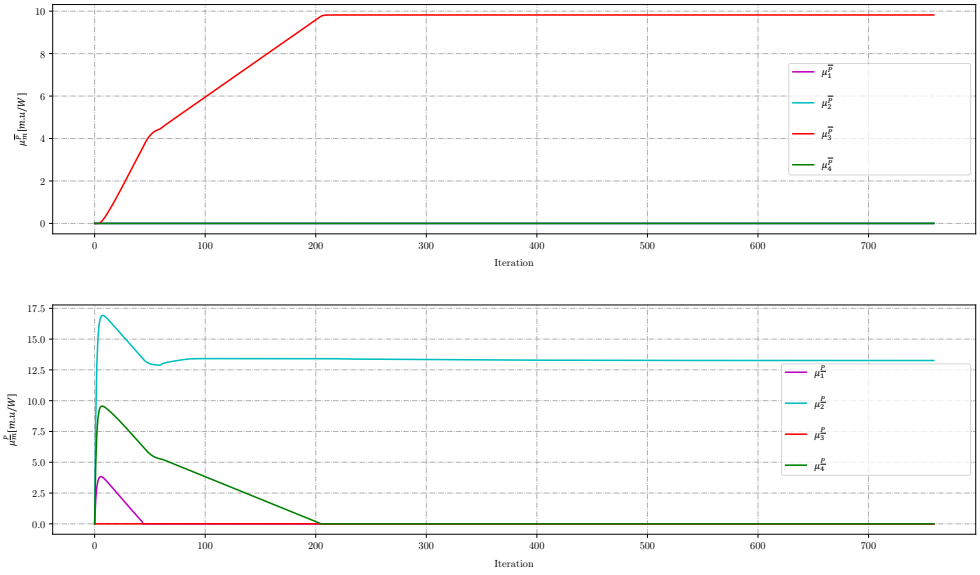

Figure A.11: From top to bottom: Dual variable for maximum and minimum power for the grid in Figure 3.17 using the Area Separation Method

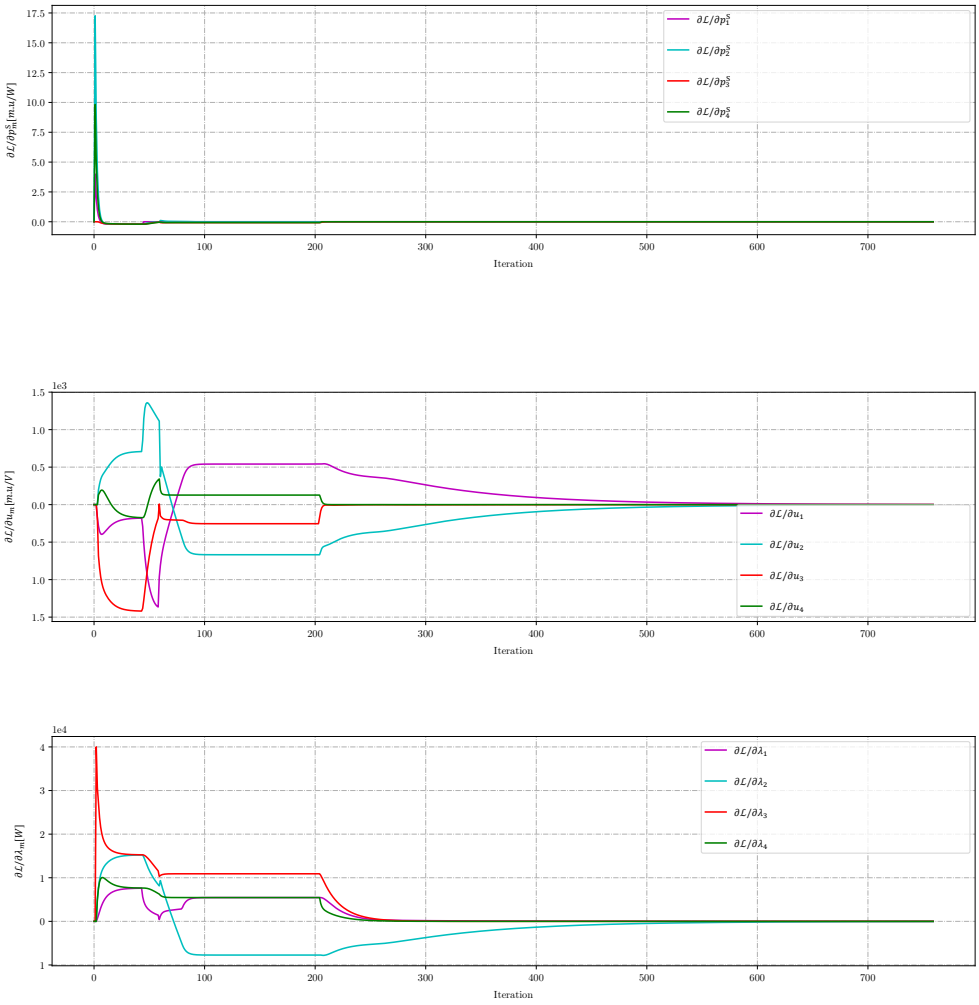

Figure A.12: From top to bottom: Lagrange differentials to the power, voltage, and LMP for the grid in Figure 3.17 using the Area Separation Method

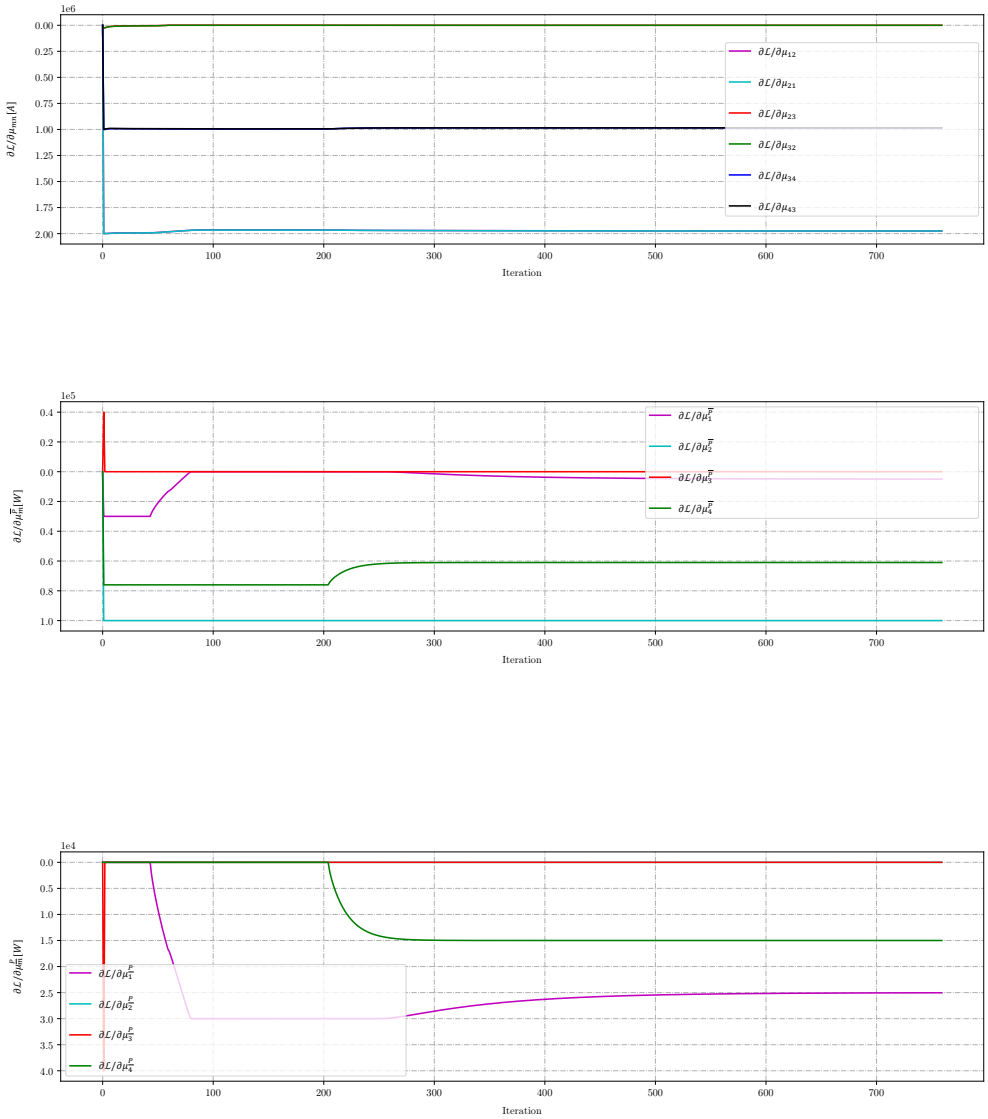

Figure A.13: From top to bottom: Lagrange differentials to the dual variable for the grid in Figure 3.17 using the Area Separation Method

A.5. Four Node Serial with Congestion Using Dual Variable Activation Method

The case refers to Figure 3.17 which is solved using the Dual Variable Activation Method.

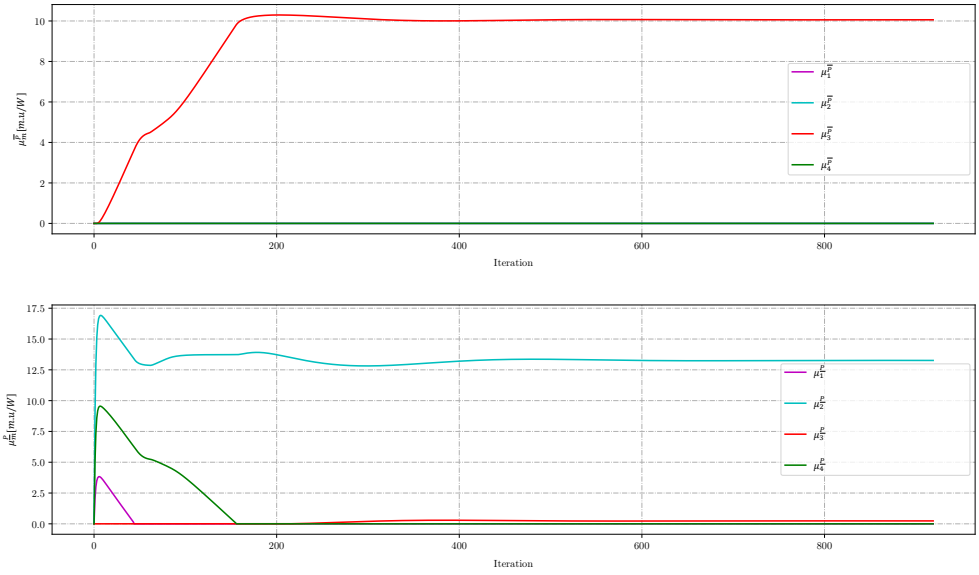

Figure A.14: From top to bottom: Lagrange differentials to the power, voltage, and LMP for the grid in Figure 3.17 using the Dual Variable Activation Method

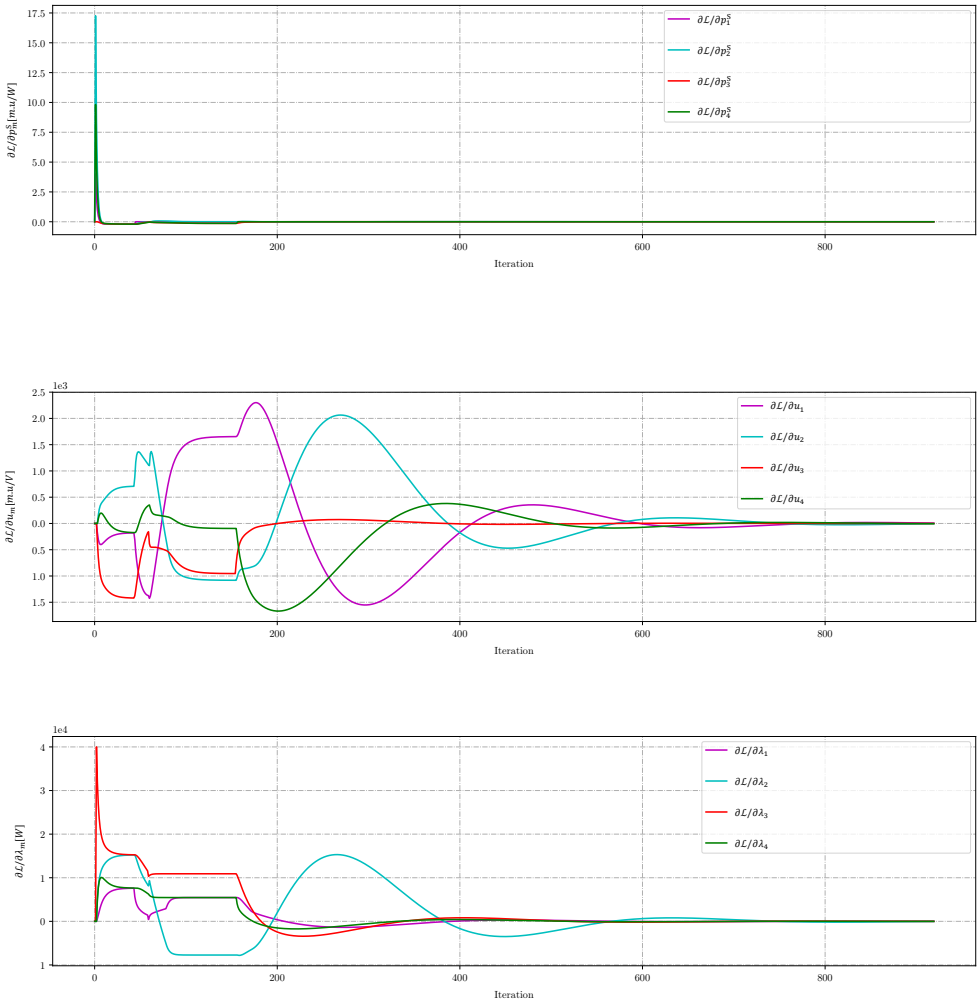

Figure A.15: From top to bottom: Lagrange differentials to the power, voltage, and LMP for the grid in Figure 3.17 using the Dual Variable Activation Method

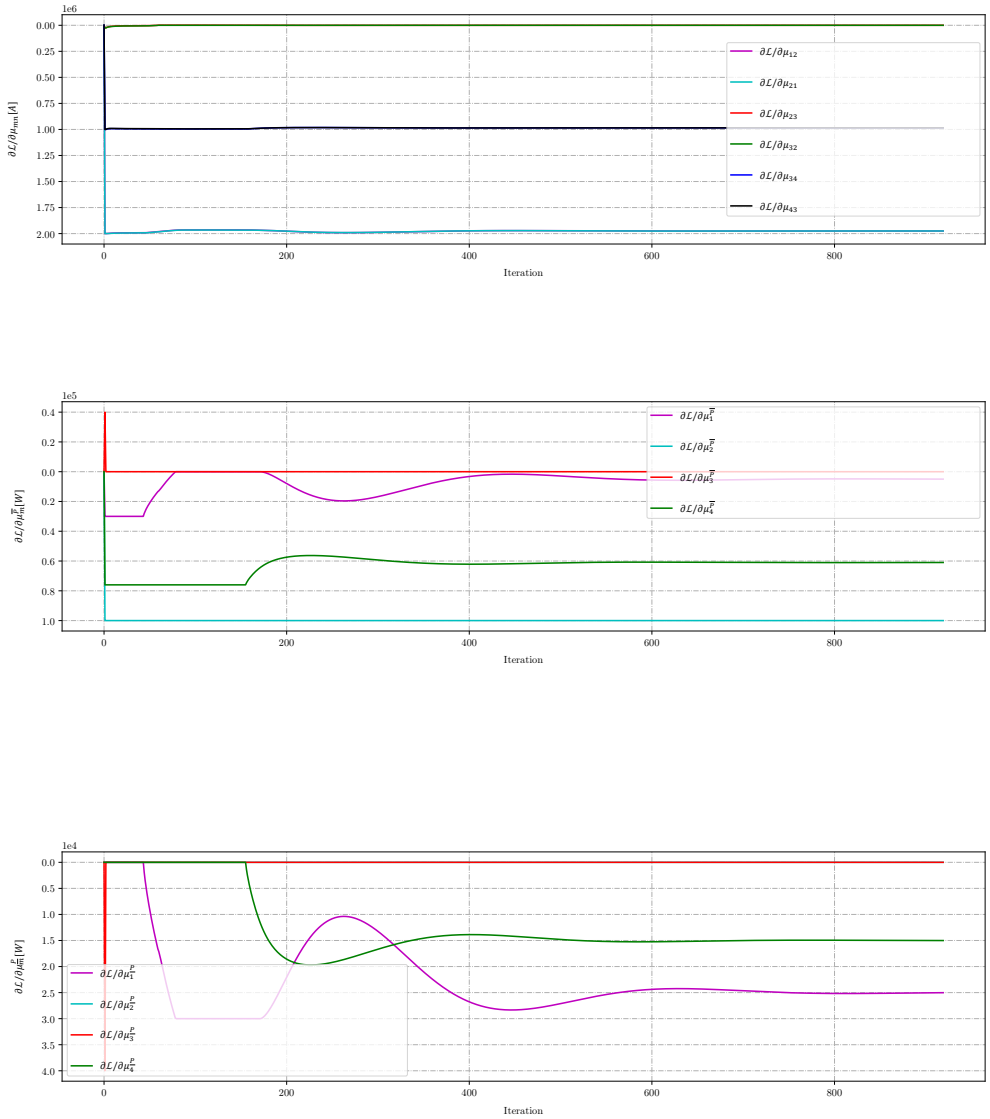

Figure A.16: From top to bottom: Lagrange differentials to the dual variable for the grid in Figure 3.17 using the Dual Variable Activation Method

A.6. Six Node Meshed

The case refers to Figure 3.28.

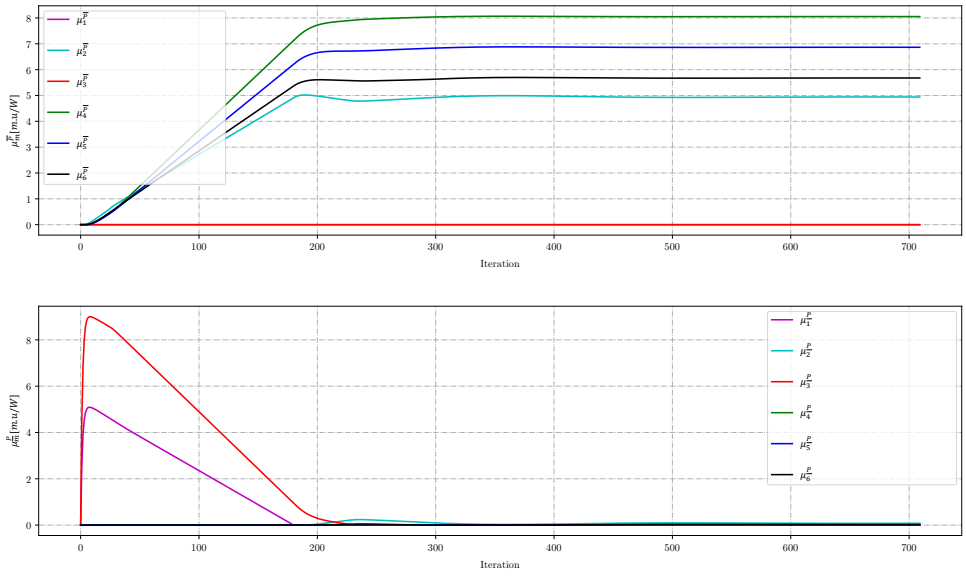

Figure A.17: From top to bottom: Dual variables for the maximum and minimum power for the grid in Figure 3.28

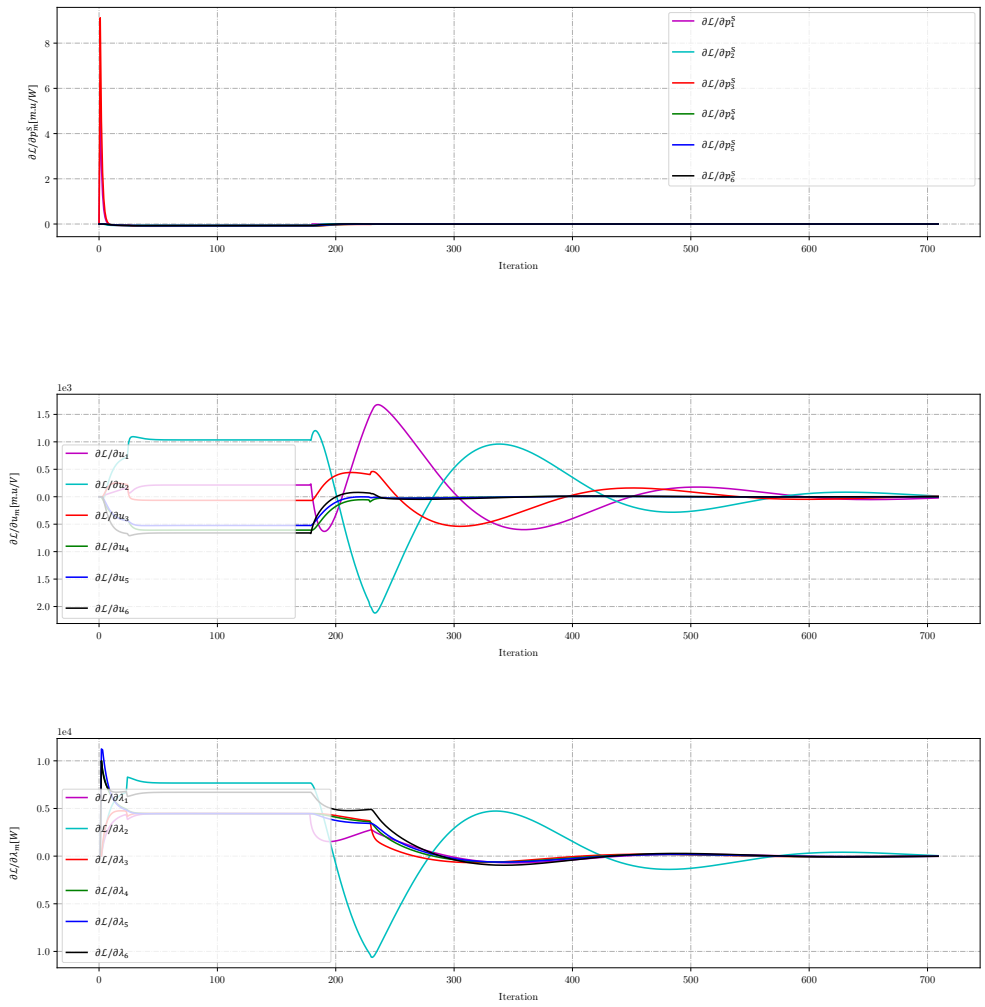

Figure A.18: From top to bottom: Lagrange differentials to the power,voltage, and LMP for the grid in Figure 3.28

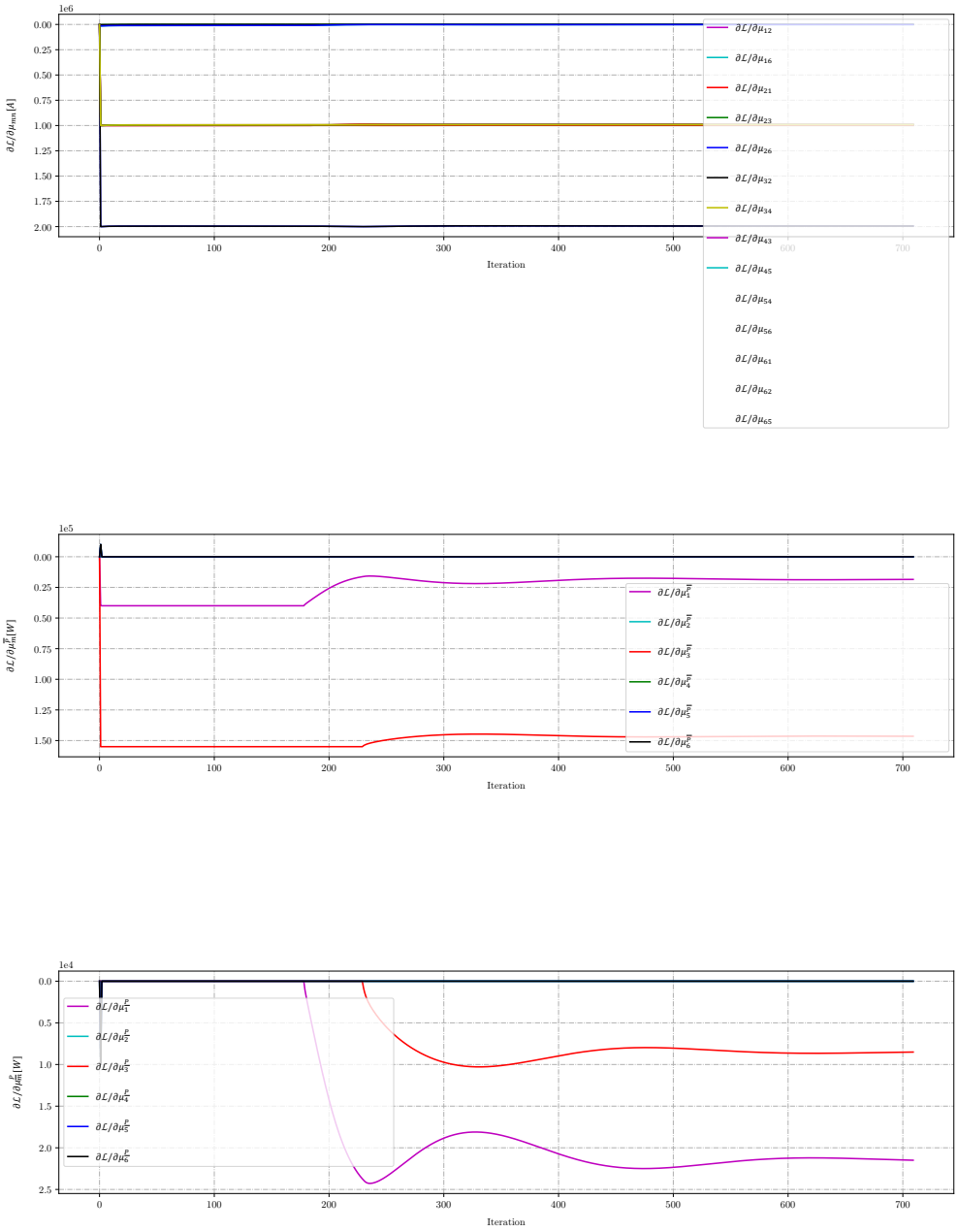

Figure A.19: From top to bottom: Lagrange differentials to the dual variables for the grid in Figure 3.28

B

Exact OPF: Remaining Variables and First-Order KKT Conditions

B.1. Three Node Case I

The case refers to Figure 4.1 when the marginal generator is at the highest voltage.

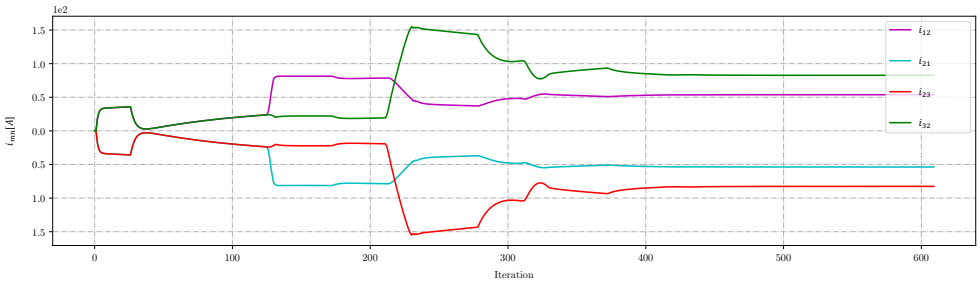

Figure B.1: Current flowing in every line for the grid in Figure 4.1 when the marginal generator is at the highest voltage

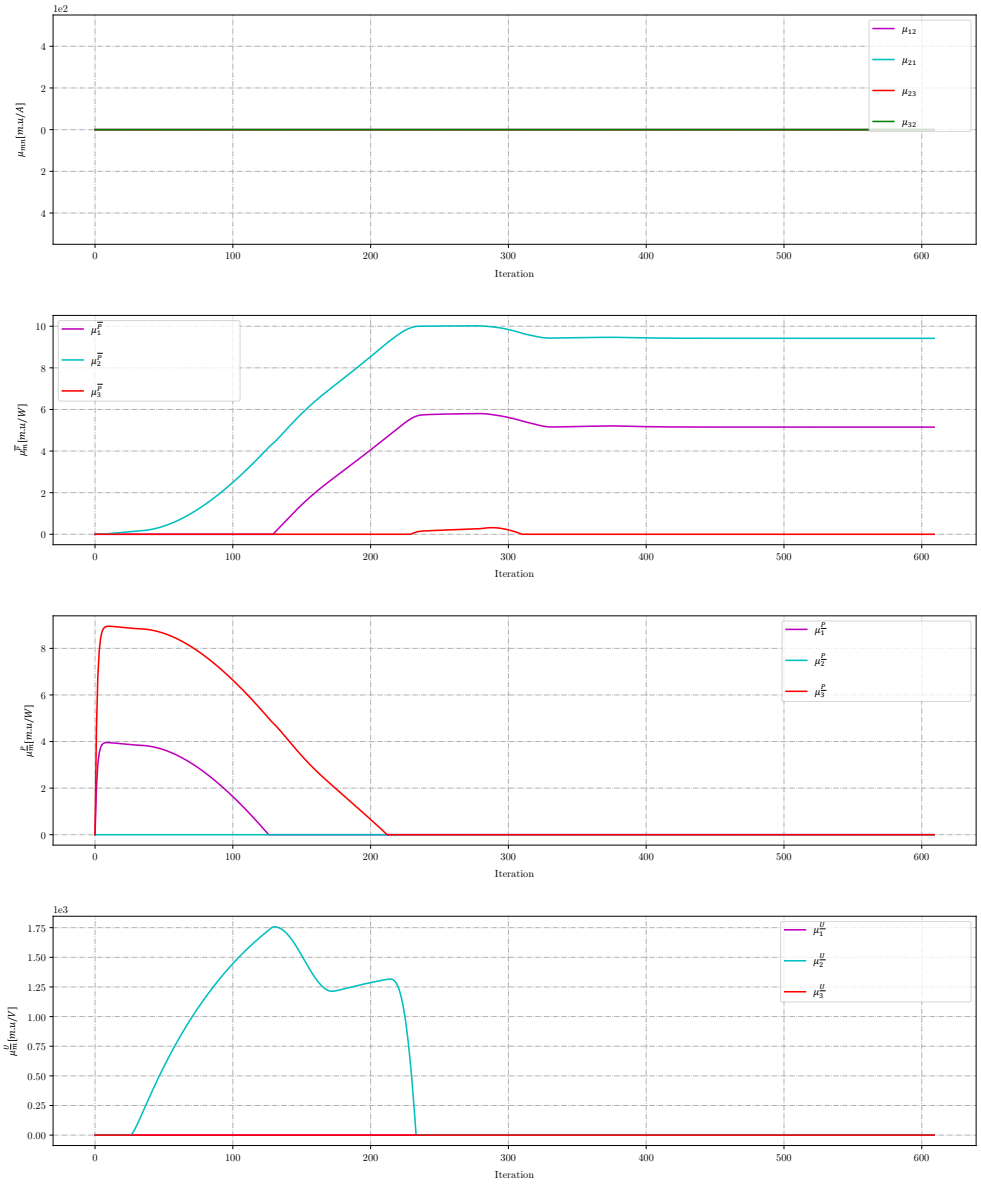

Figure B.2: From top to bottom: Dual variables for the line limit, the maximum and minimum power, and the maximum and minimum voltage for the grid in Figure 4.1 when the marginal generator is at the highest voltage

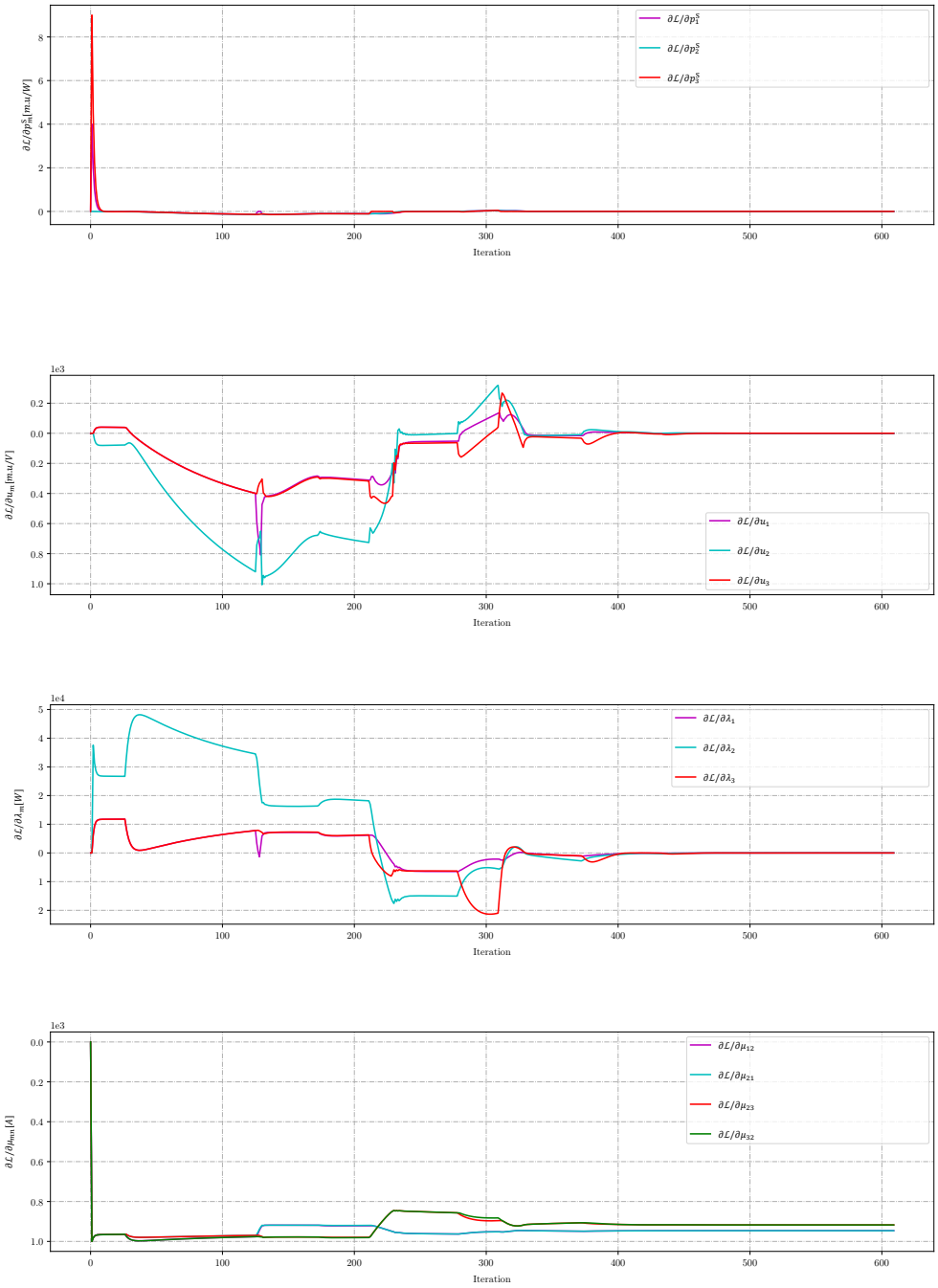

Figure B.3: Lagrange differentials to the power, voltage, lambda, and dual variable for the line limit for the grid in Figure 4.1 when the marginal generator is at the highest voltage

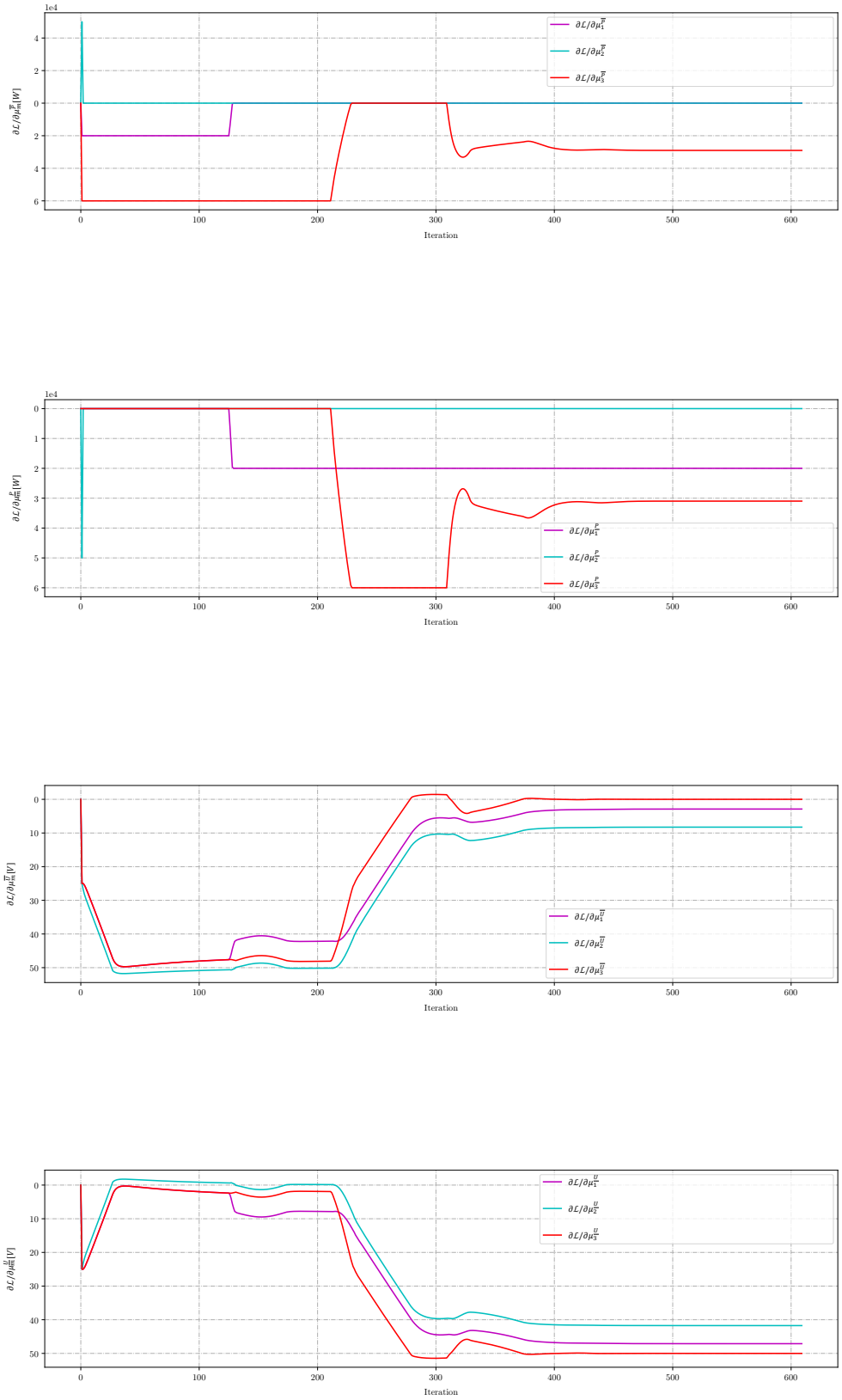

Figure B.4: Lagrange differentials to the dual variables for the grid in Figure 4.1 when the marginal generator is at the highest voltage

B.2. Three Node Case II

The case refers to Figure 4.10 when the marginal generator is not at the highest voltage and the addition of the quadratic cost coefficient.

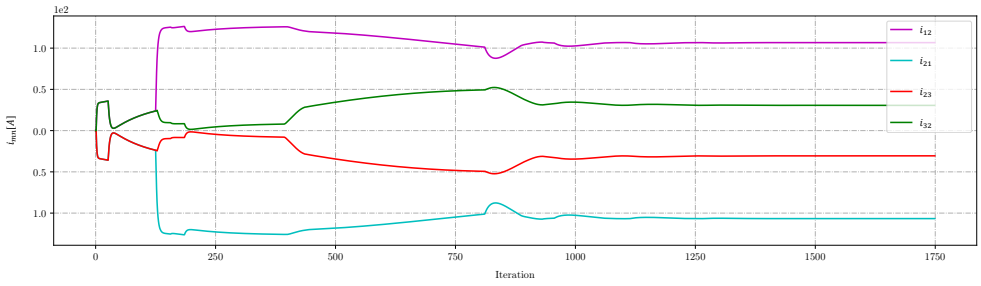

Figure B.5: Current flowing in every line for the grid in Figure 4.10 when the marginal generator is not at the highest voltage

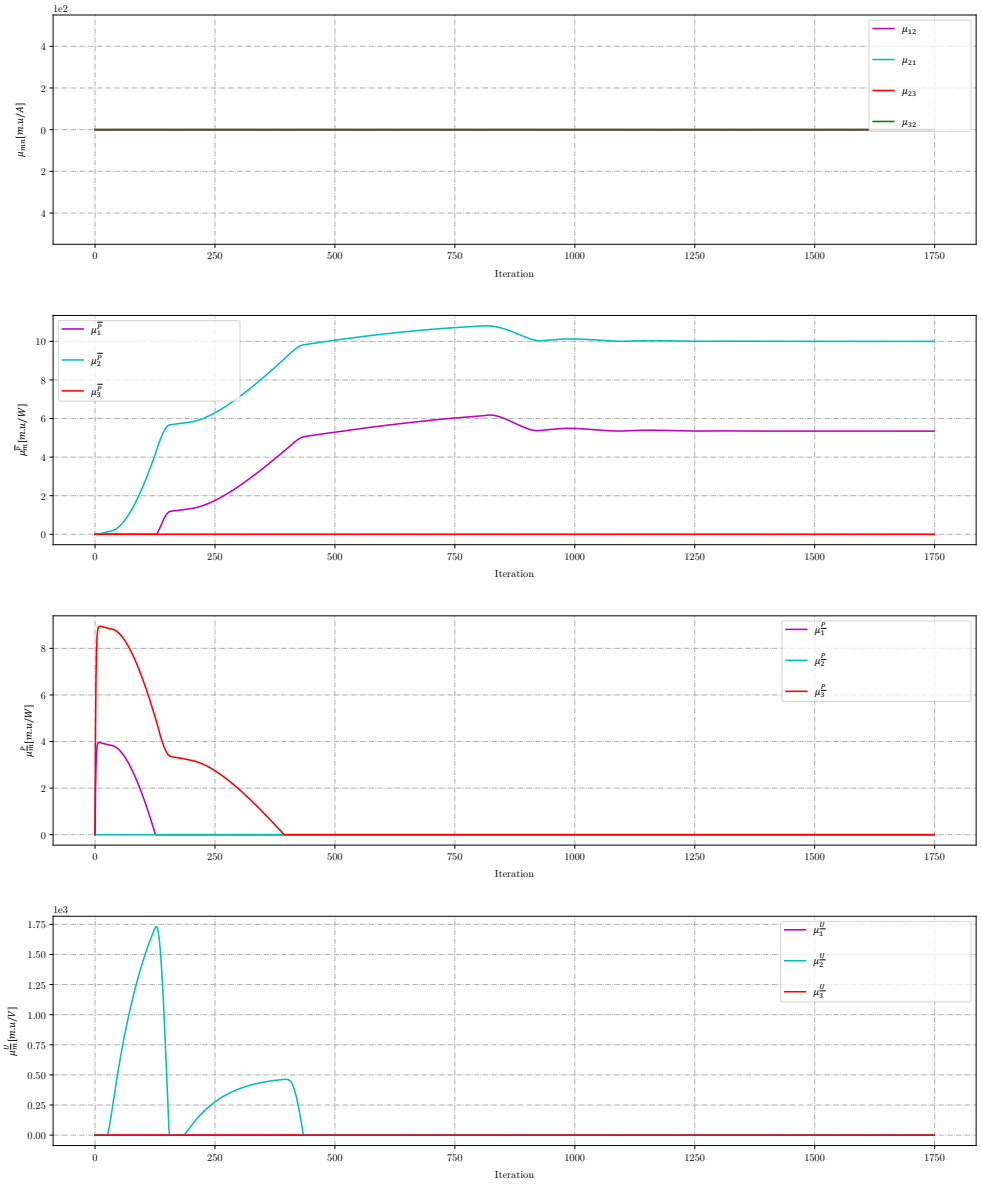

Figure B.6: From top to bottom: Dual variables for the line limit, the maximum and minimum power, and the maximum and minimum voltage for the grid in Figure 4.10 when the marginal generator is not at the highest voltage

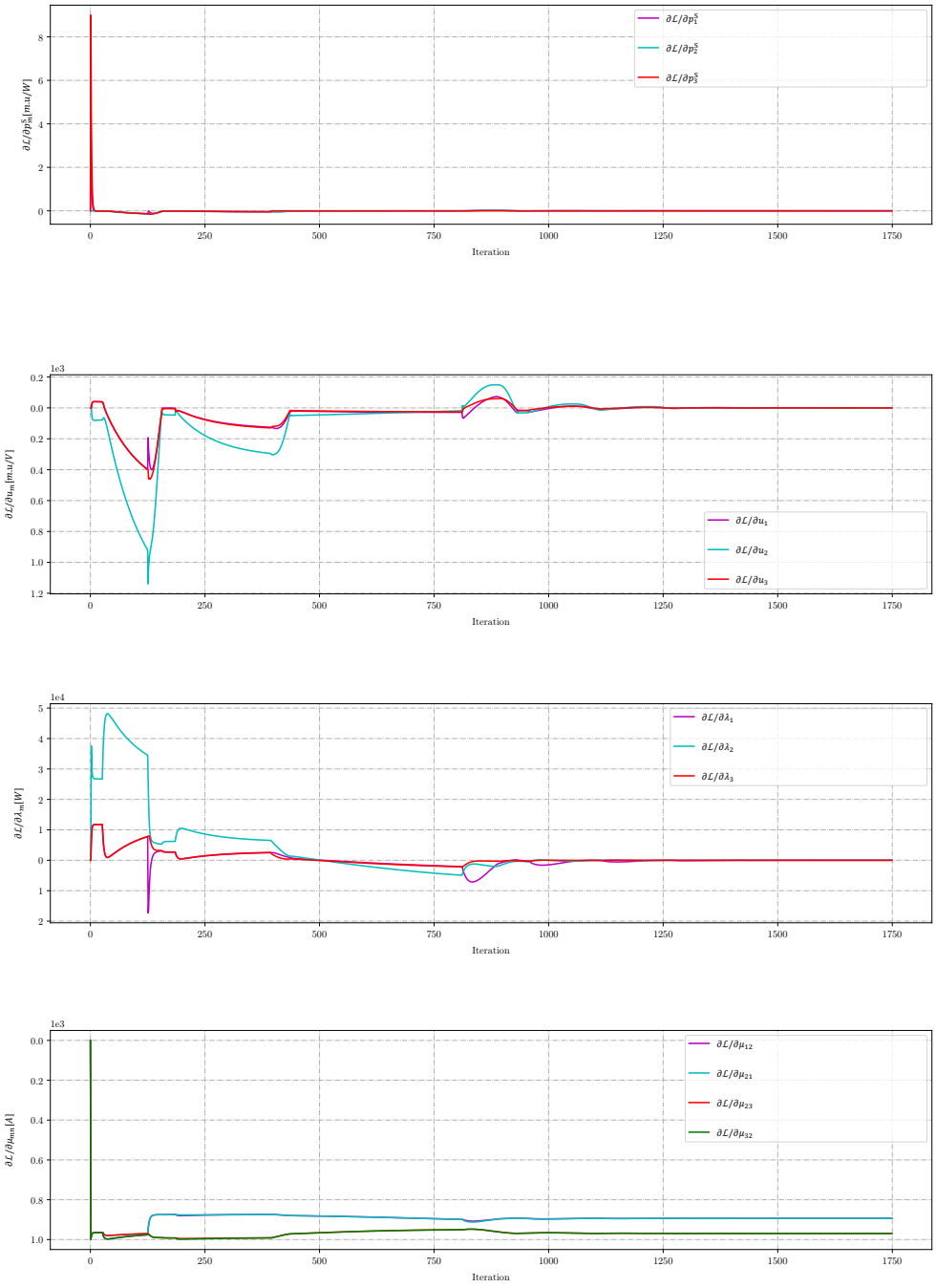

Figure B.7: Lagrange differentials to the power, voltage, lambda, and dual variable for the line limit for the grid in Figure 4.10 when the marginal generator is not at the highest voltage

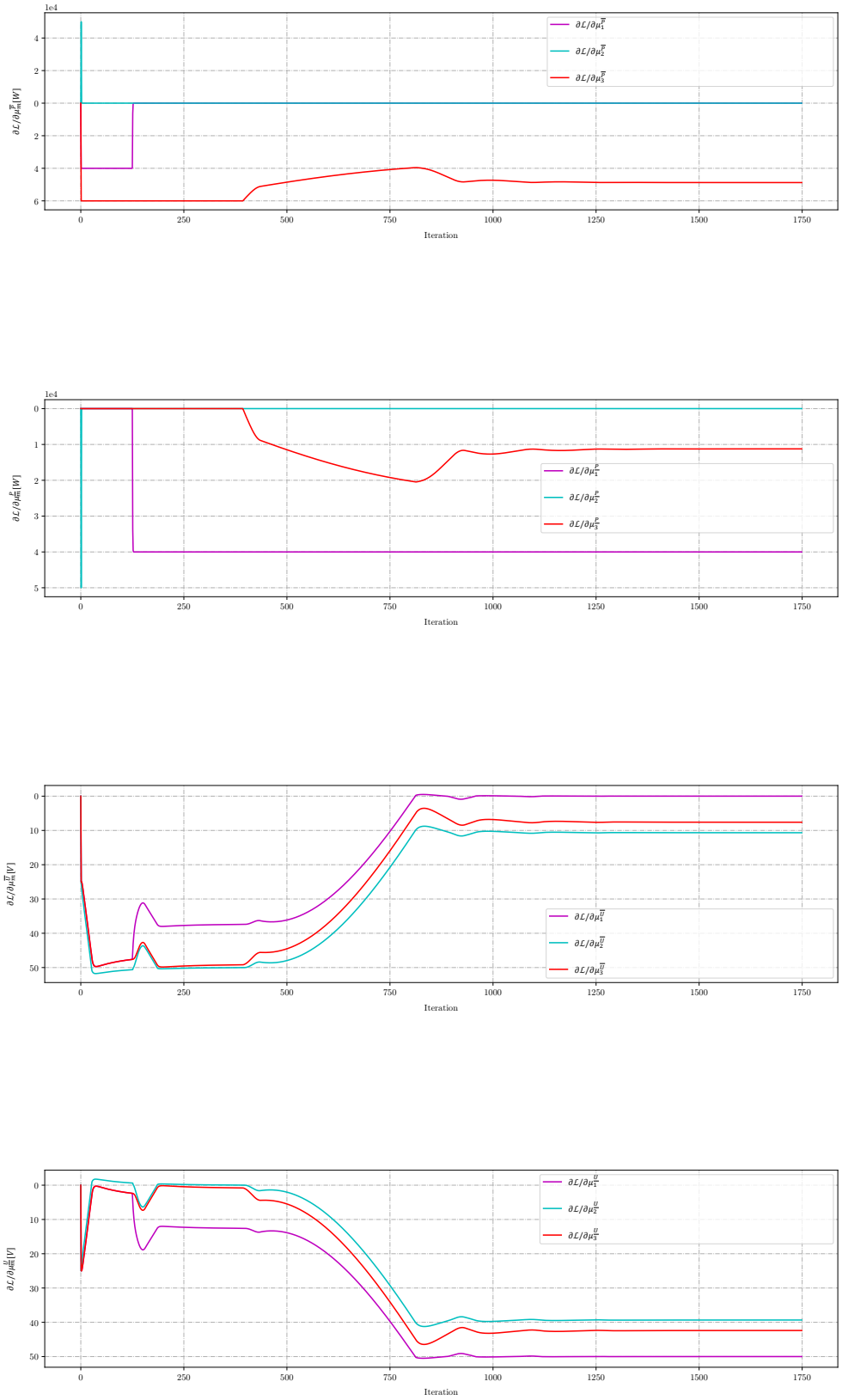

Figure B.8: Lagrange differentials to the dual variables for the grid in Figure 4.10 when the marginal generator is not at the highest voltage

B.3. Four Node Long Line Case

The case refers to Figure 4.15.

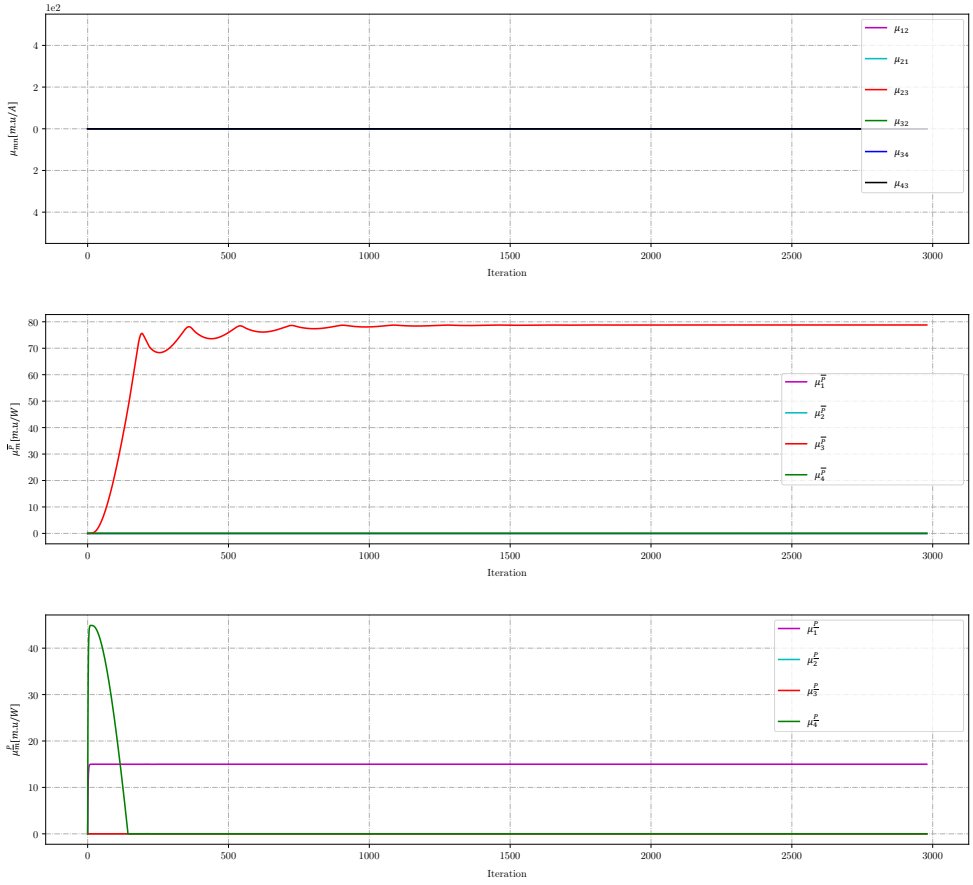

Figure B.9: From top to bottom: Dual variables for the line limit, the maximum power, and the minimum power for the grid in Figure 4.15

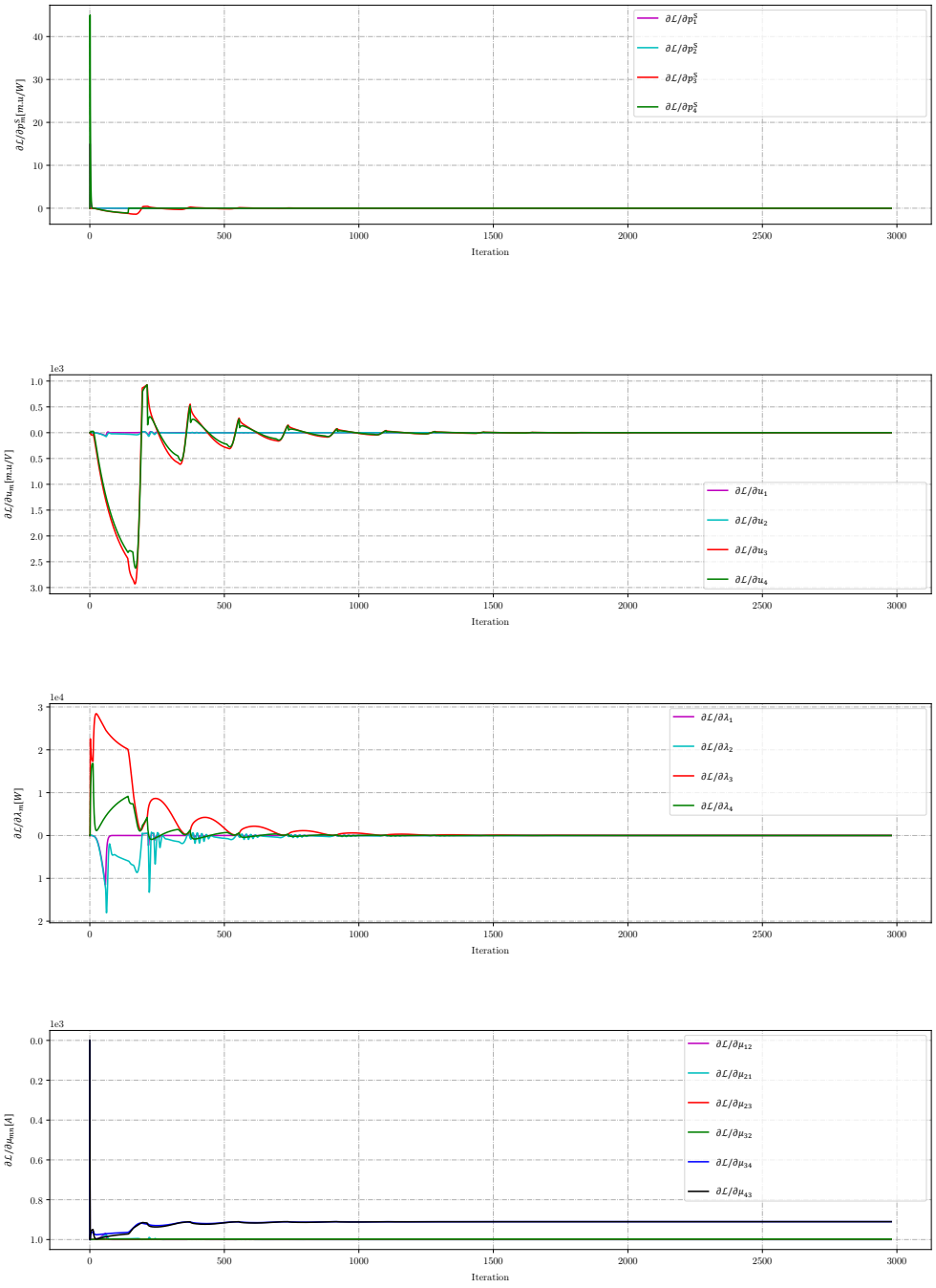

Figure B.10: From top to bottom: Lagrange differentials to the power, voltage, LMP, and the dual variable for the line limit for the grid in Figure 4.15

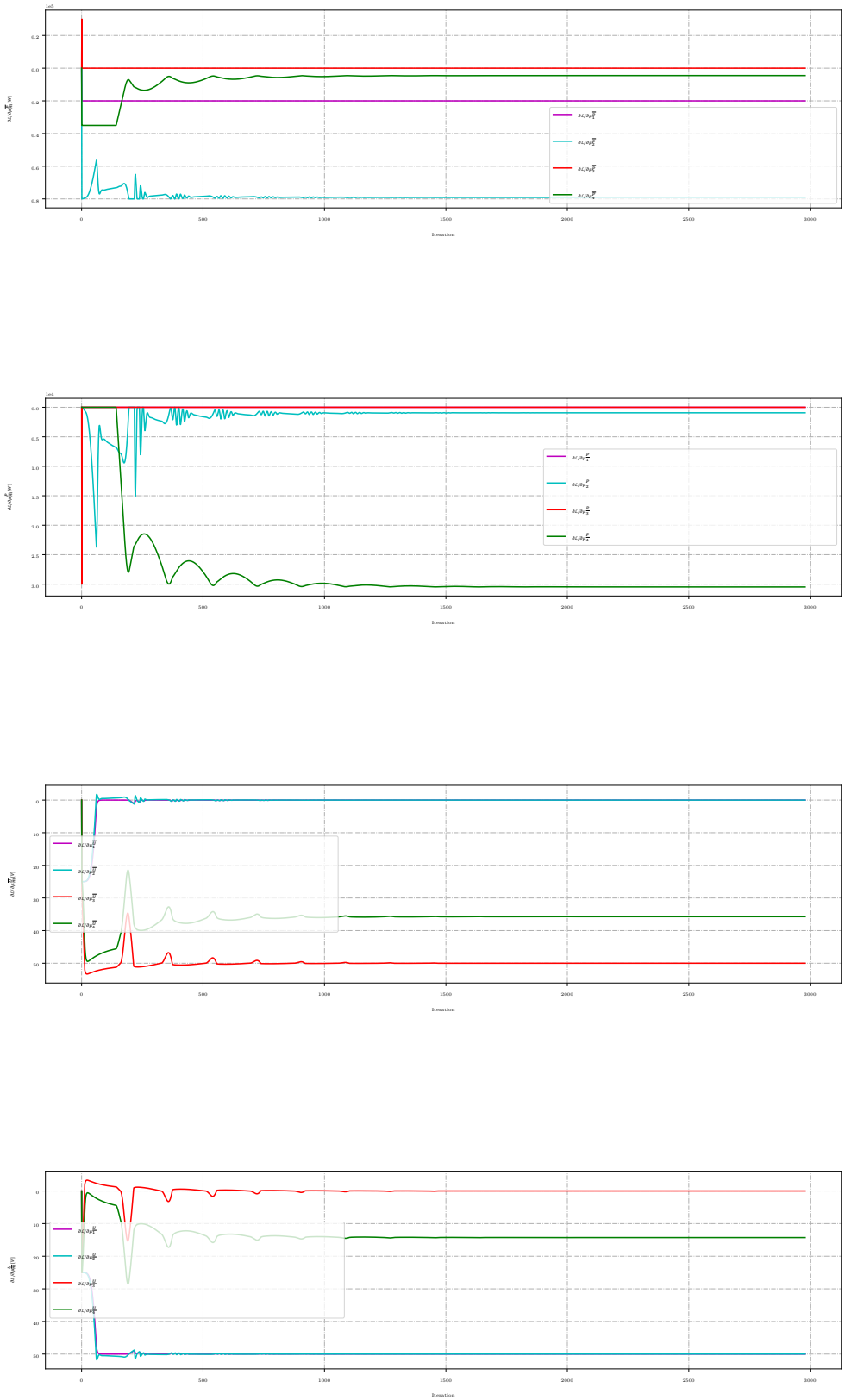

Figure B.11: Lagrange differentials to the dual variables for the grid in Figure 4.15

B.4. Six Node Meshed

The case refers to Figure 5.12.

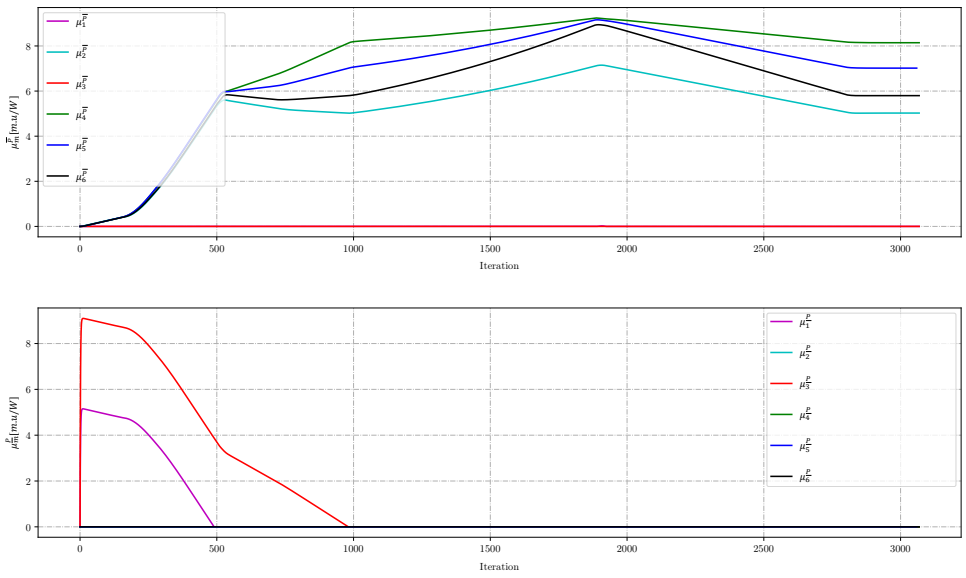

Figure B.12: From top to bottom: Dual variables for the maximum power and the minimum power for the grid in Figure 5.12

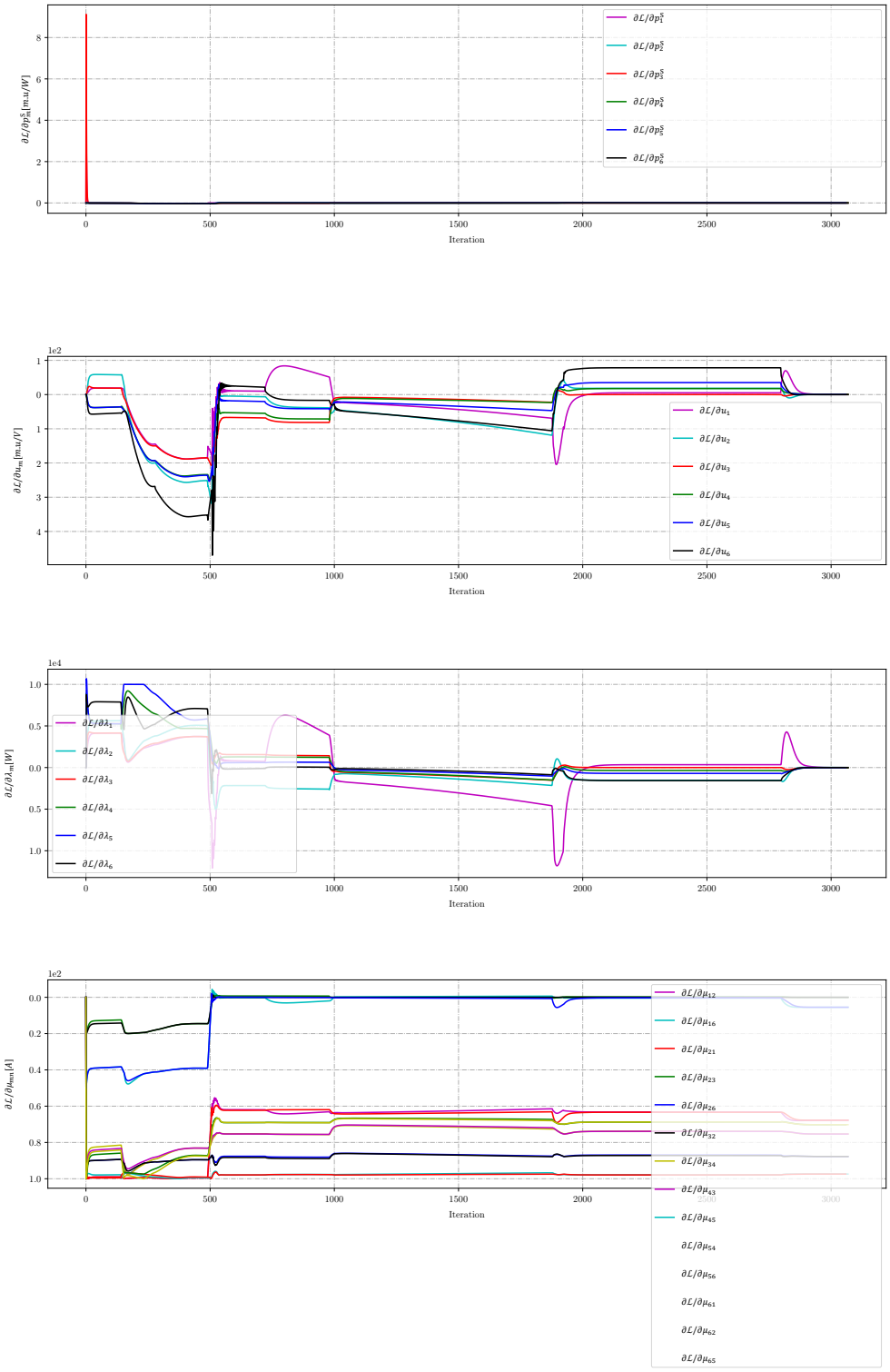

Figure B.13: From top to bottom: Lagrange differentials to the power, voltage, LMP, and dual variable for the line limit for the grid in Figure 5.12

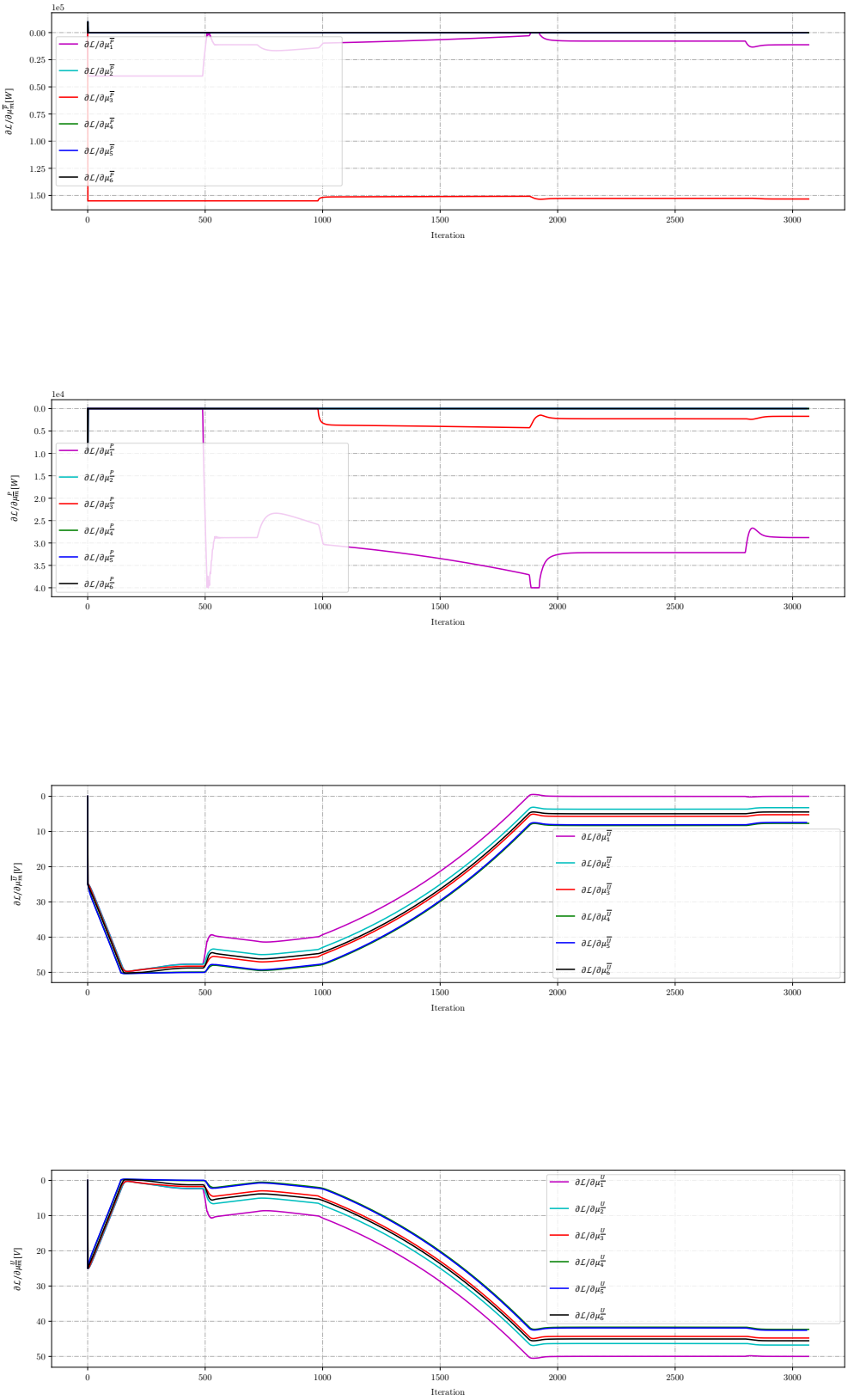

Figure B.14: From top to bottom: Lagrange differentials to the dual variables for the grid in Figure 5.12

B.5. Four Node Serial with Congestion

The case refers to Figure 5.1.

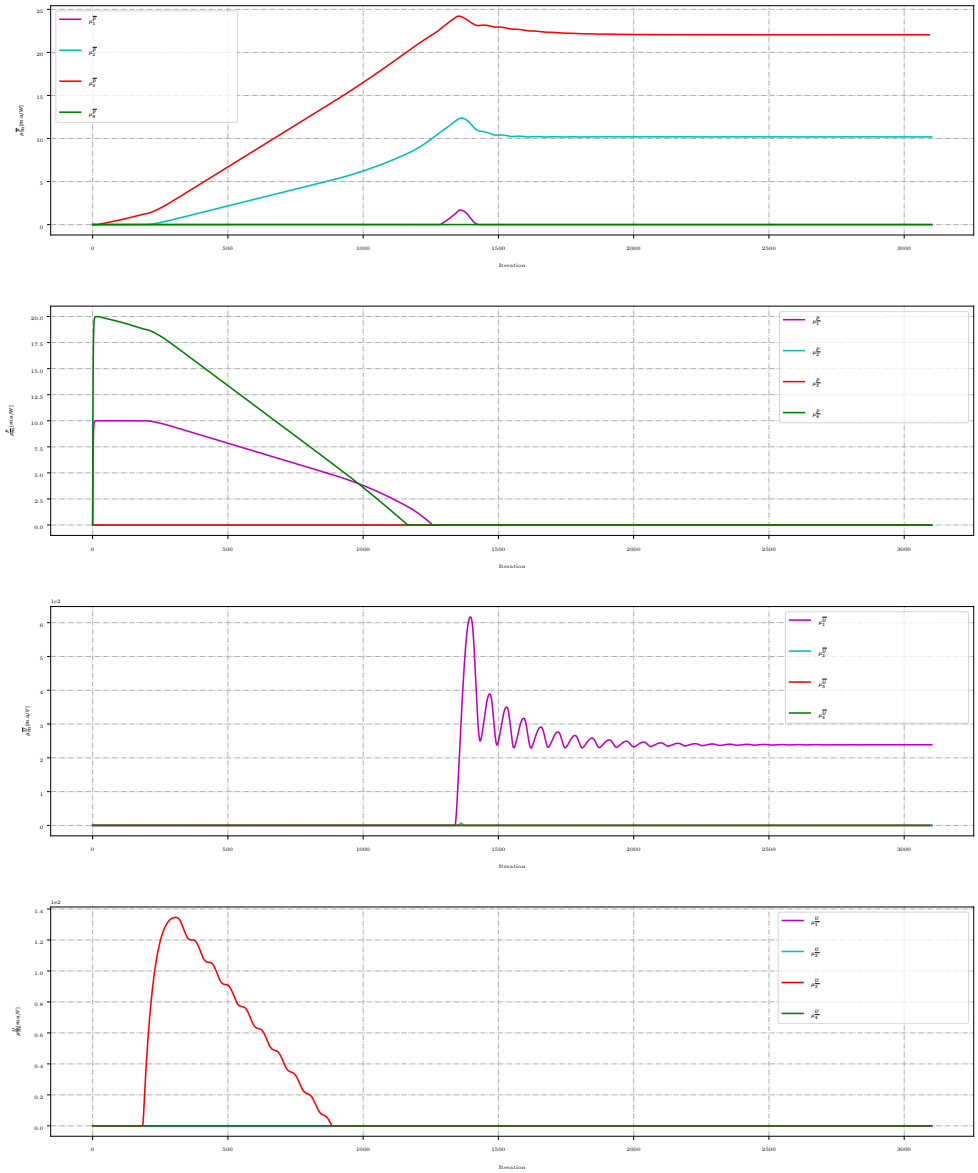

Figure B.15: From top to bottom: Dual variables for the maximum power, minimum power, maximum voltage, and the minimum voltage for the grid in Figure 5.1

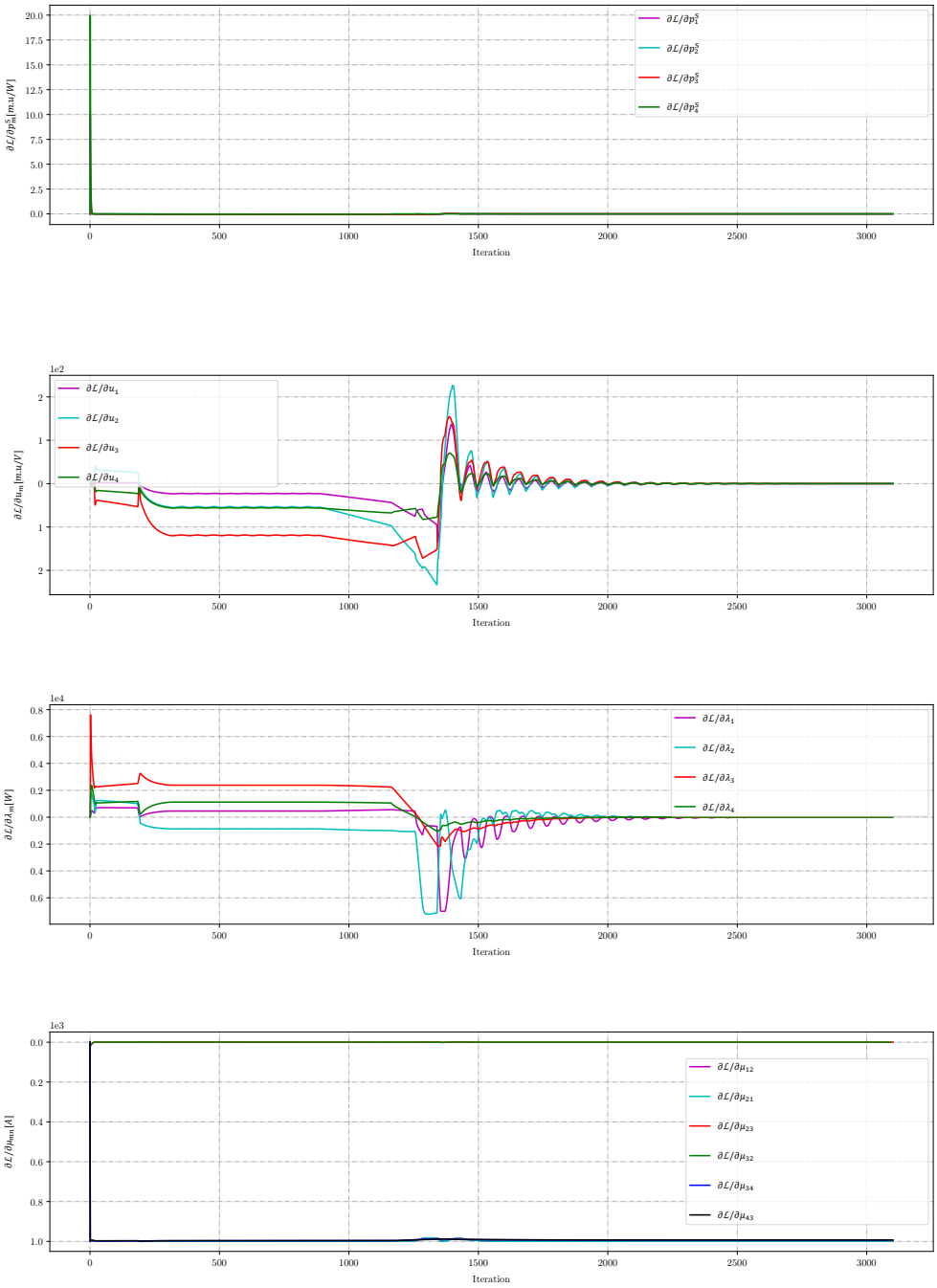

Figure B.16: From top to bottom: Lagrange differentials to the power, voltage, LMP, and dual variable for the line limit for the grid in Figure 5.1

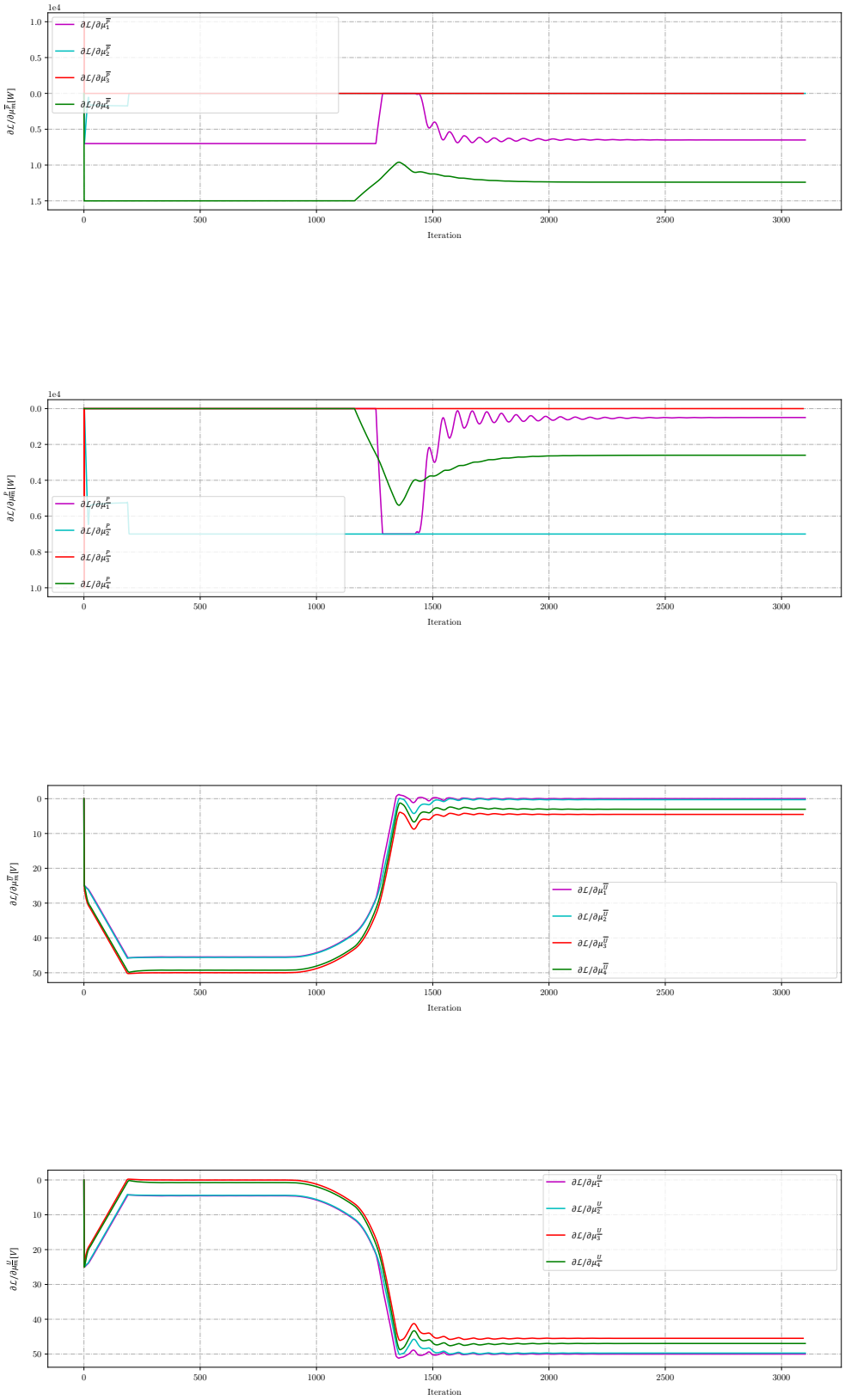

Figure B.17: From top to bottom: Lagrange differentials to the dual variables for the grid in Figure 5.1

B.6. IEEE 9 Bus System

The case refers to Figure 5.20.

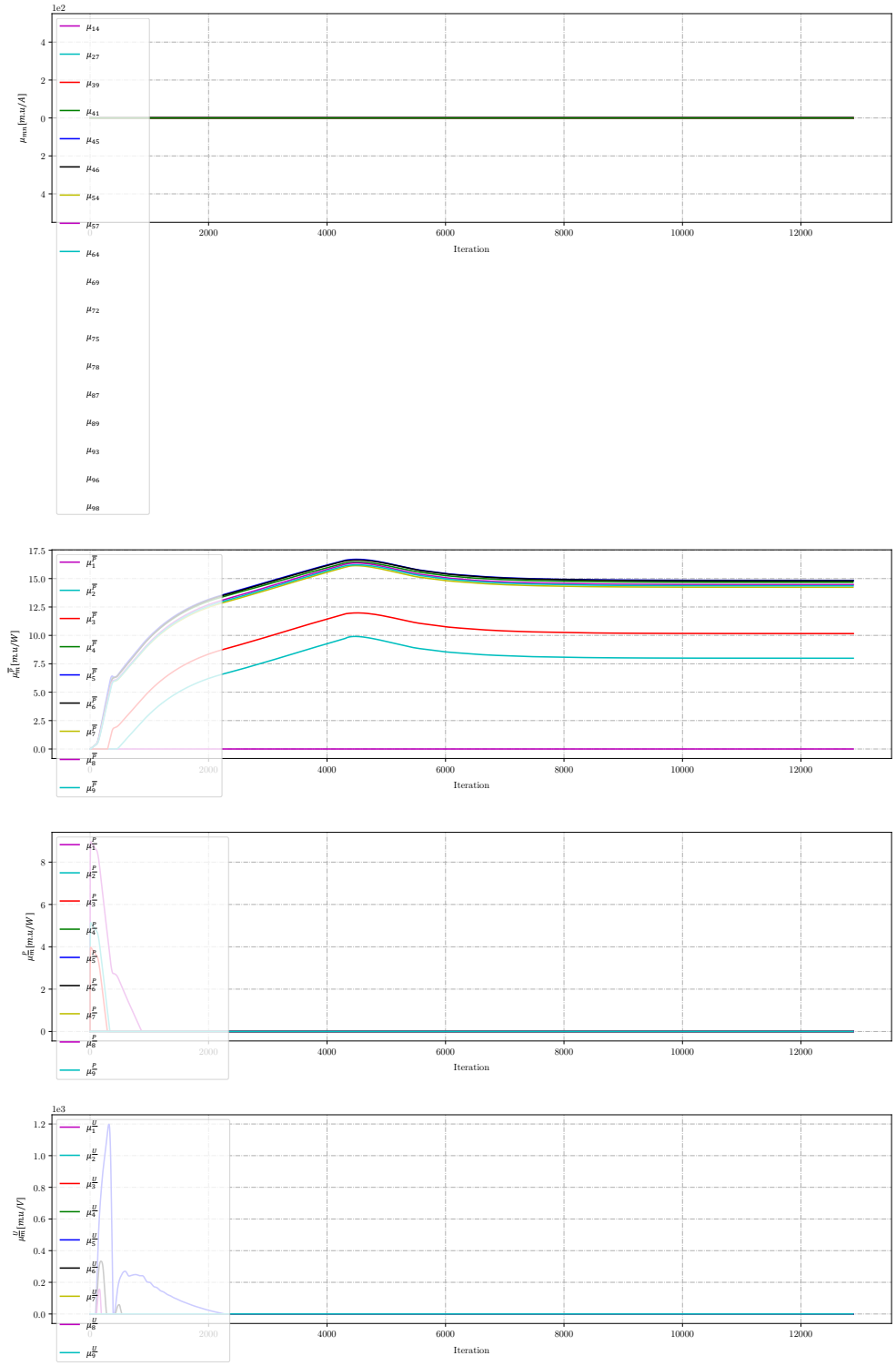

Figure B.18: From top to bottom: Dual variables for the maximum power, minimum power, maximum voltage, and the minimum voltage for the grid in Figure 5.20

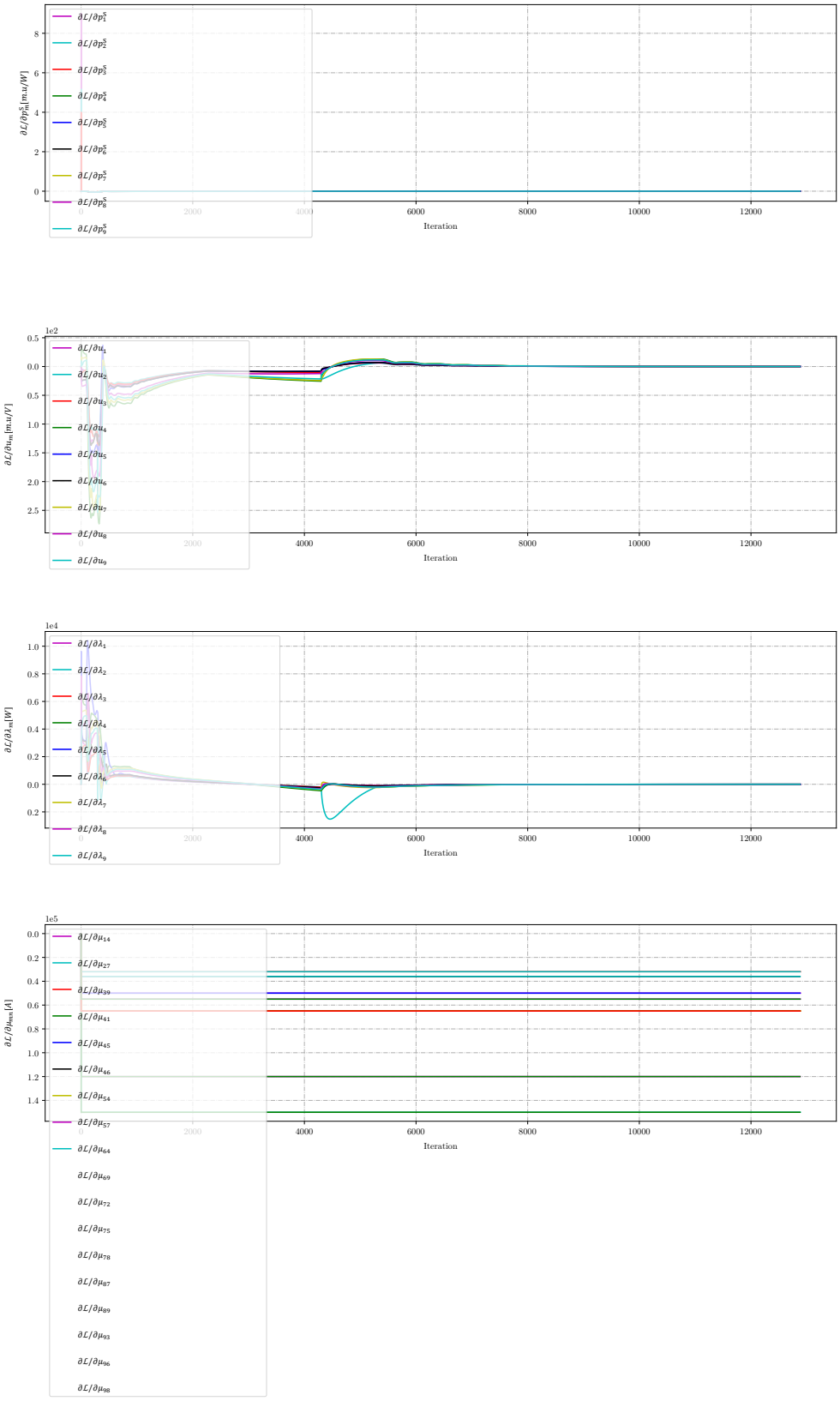

Figure B.19: From top to bottom: Lagrange differentials to the power, voltage, LMP, and dual variable for the line limit for the grid in Figure 5.20

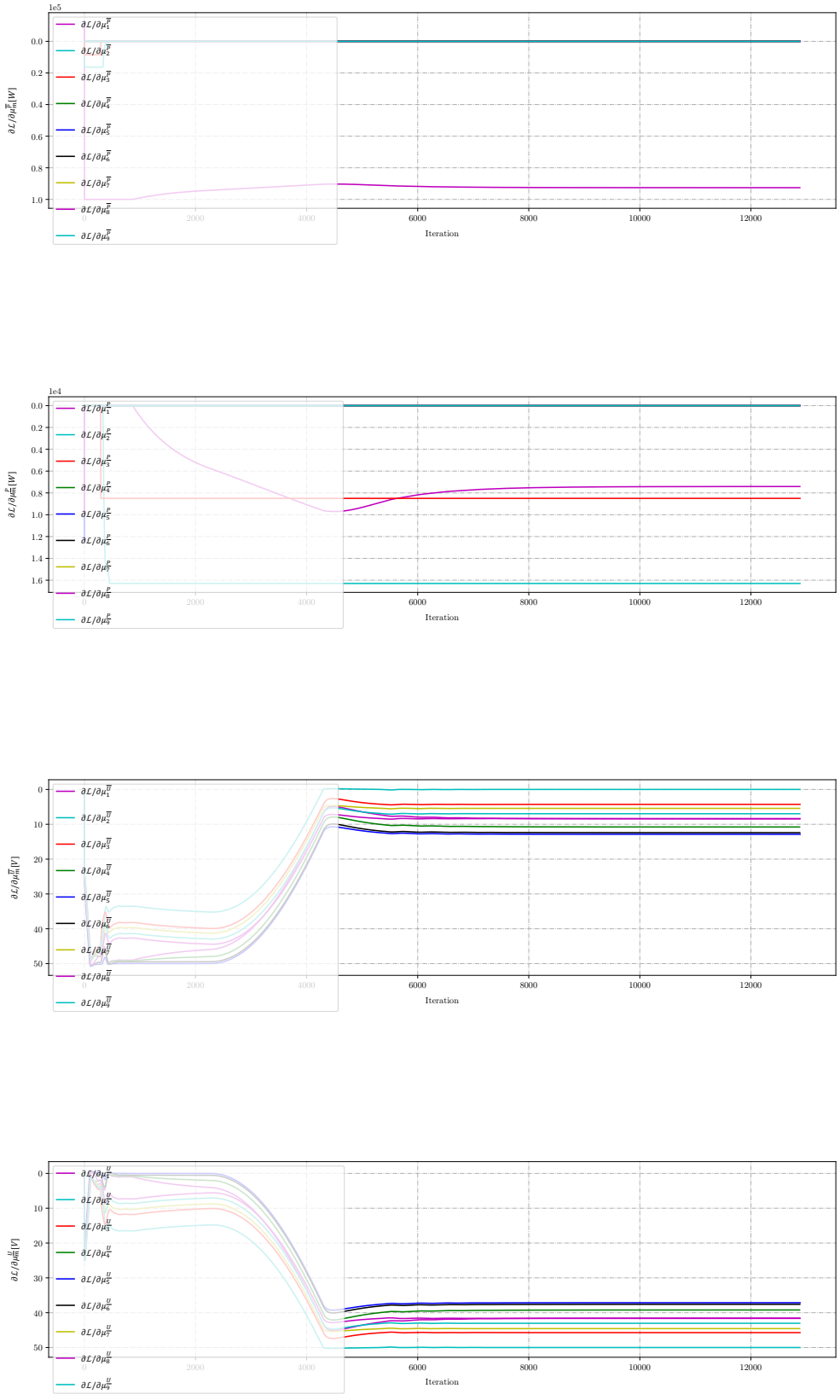

Figure B.20: From top to bottom: Lagrange differentials to the dual variables for the grid in Figure 5.20

C

Asynchronous Algorithm: Remaining Variables

This chapter presents the remaining primary variables such as voltage, power, and power/current flow, and also the dual variable for the line limit for the cases presented in Chapter 6.

C.1. Case I with Synchronous Algorithm

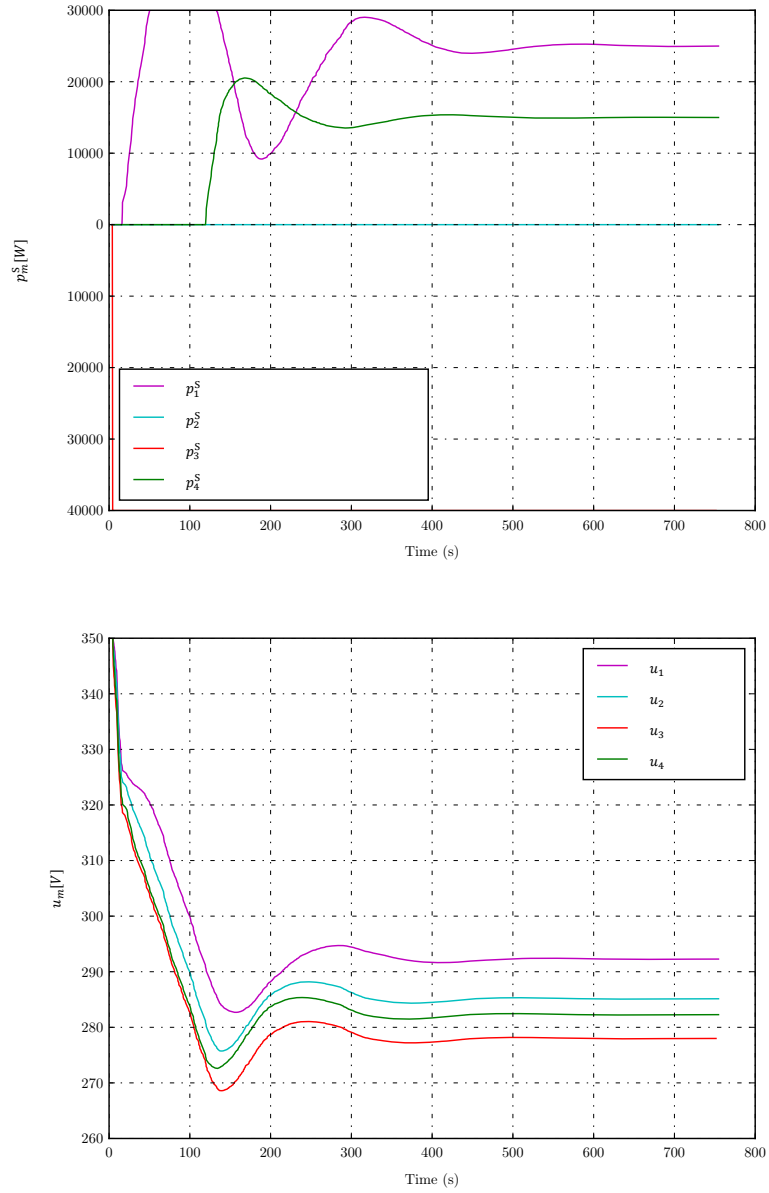

Figure C.1: The power (top) and voltage (bottom) for the grid in Figure 6.1 when the algorithm is run synchronously using the microcomputers.

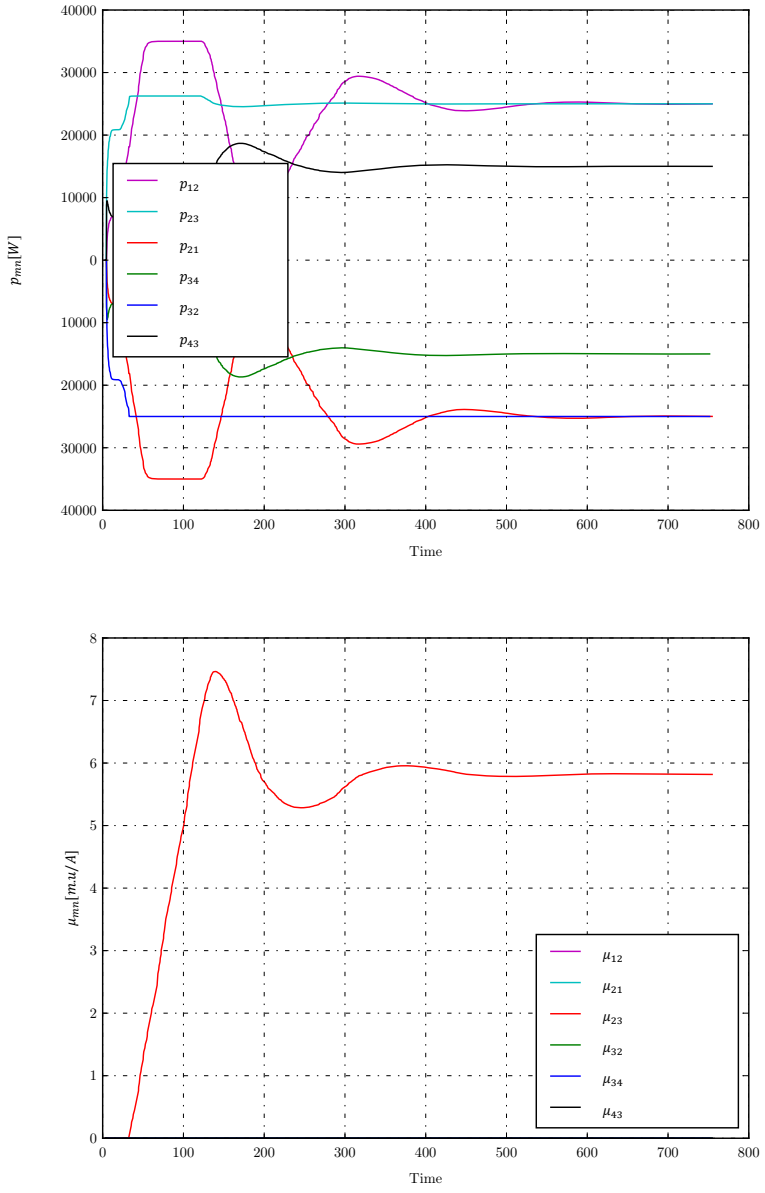

Figure C.2: The power flow (top) and the dual variable for the line limit (bottom) for the grid in Figure 6.1 when the algorithm is run synchronously using the microcomputers.

C.2. Case I with 70 ms Timeout Time

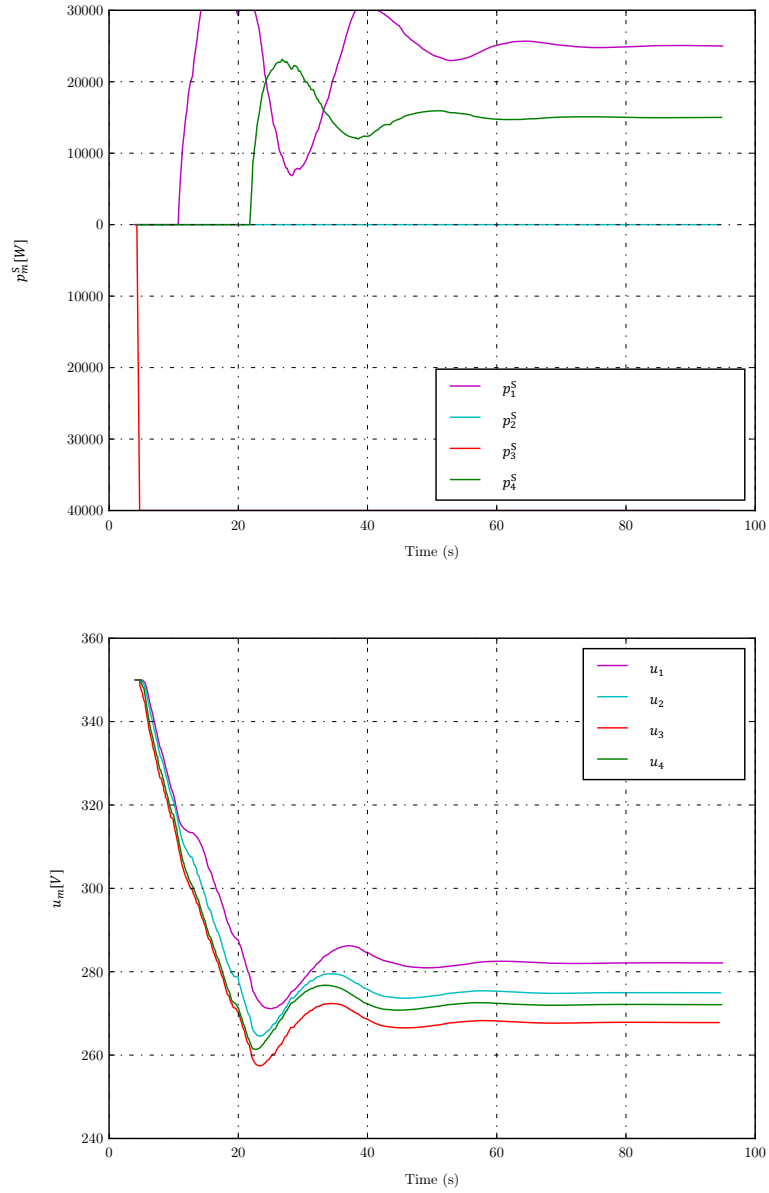

Figure C.3: The power (top) and voltage (bottom) for the grid in Figure 6.1 when the algorithm is run asynchronously with 70 ms timeout time.

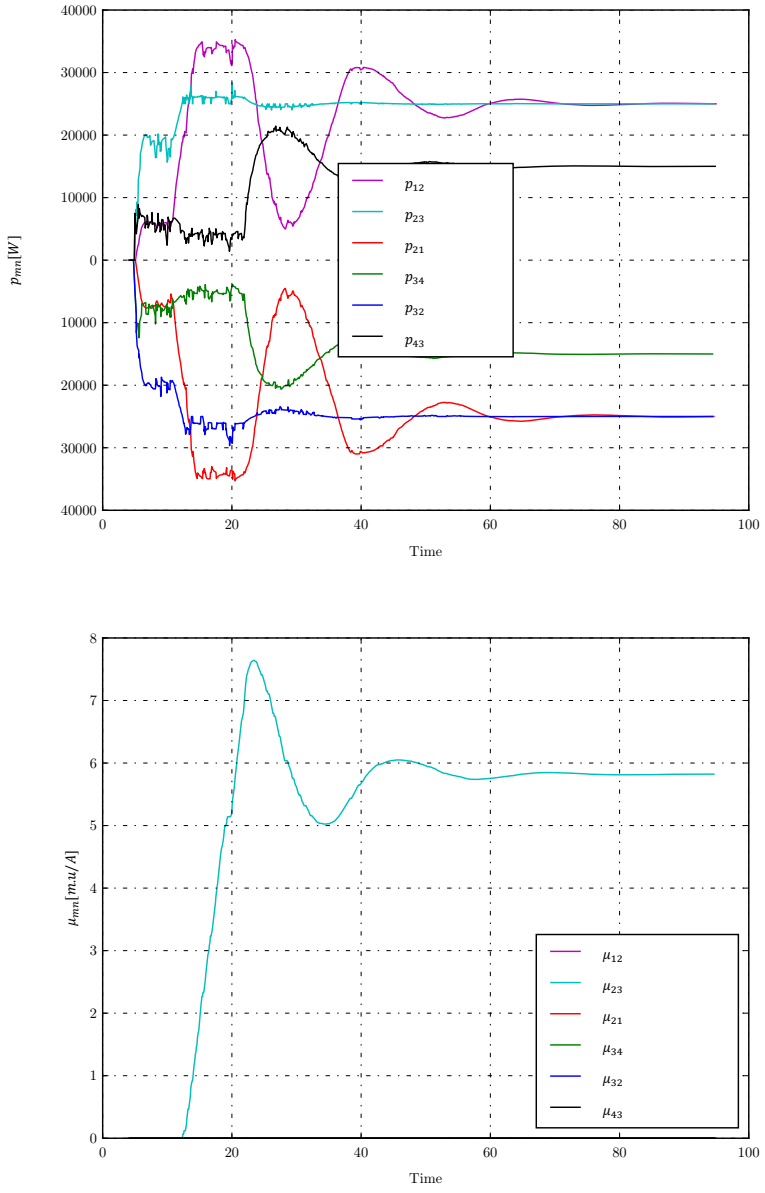

Figure C.4: The power flow (top) and the dual variable for the line limit (bottom) for the grid in Figure 6.1 when the algorithm is run asynchronously with 70 ms timeout time.

C.3. Case I with 50 ms Timeout Time

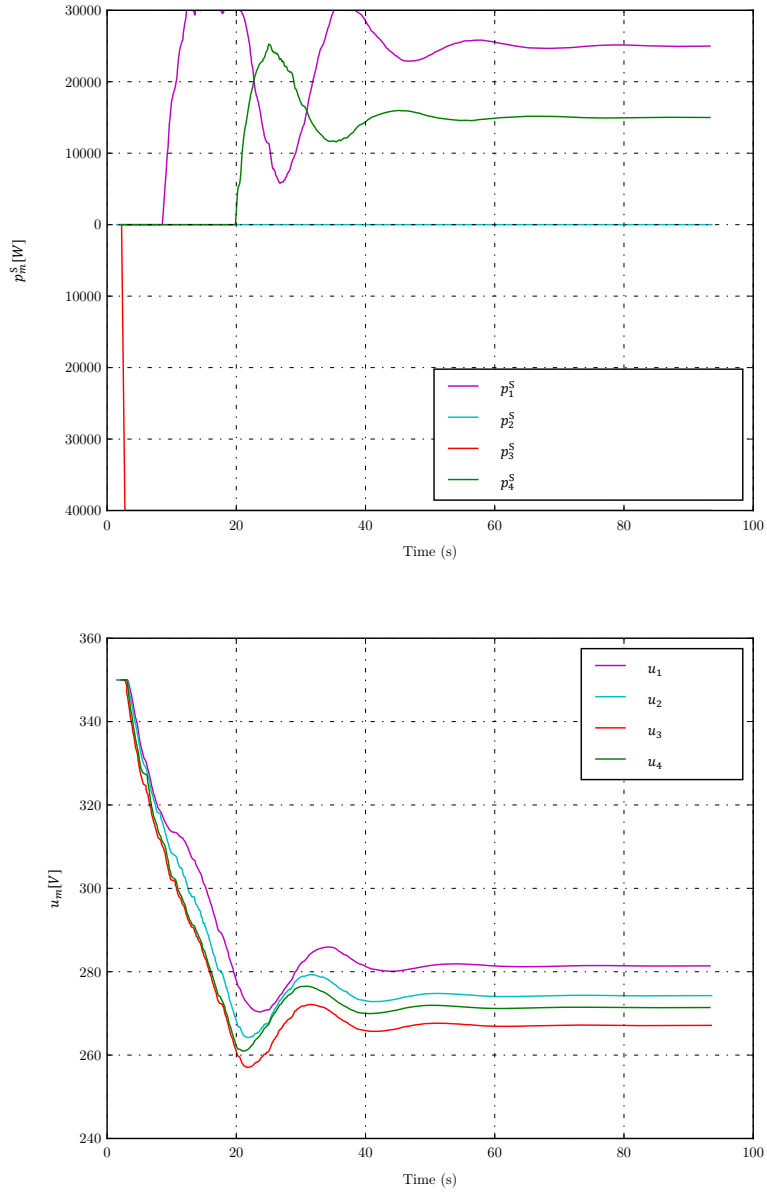

Figure C.5: The power (top) and voltage (bottom) for the grid in Figure 6.1 when the algorithm is run asynchronously with 50 ms timeout time.

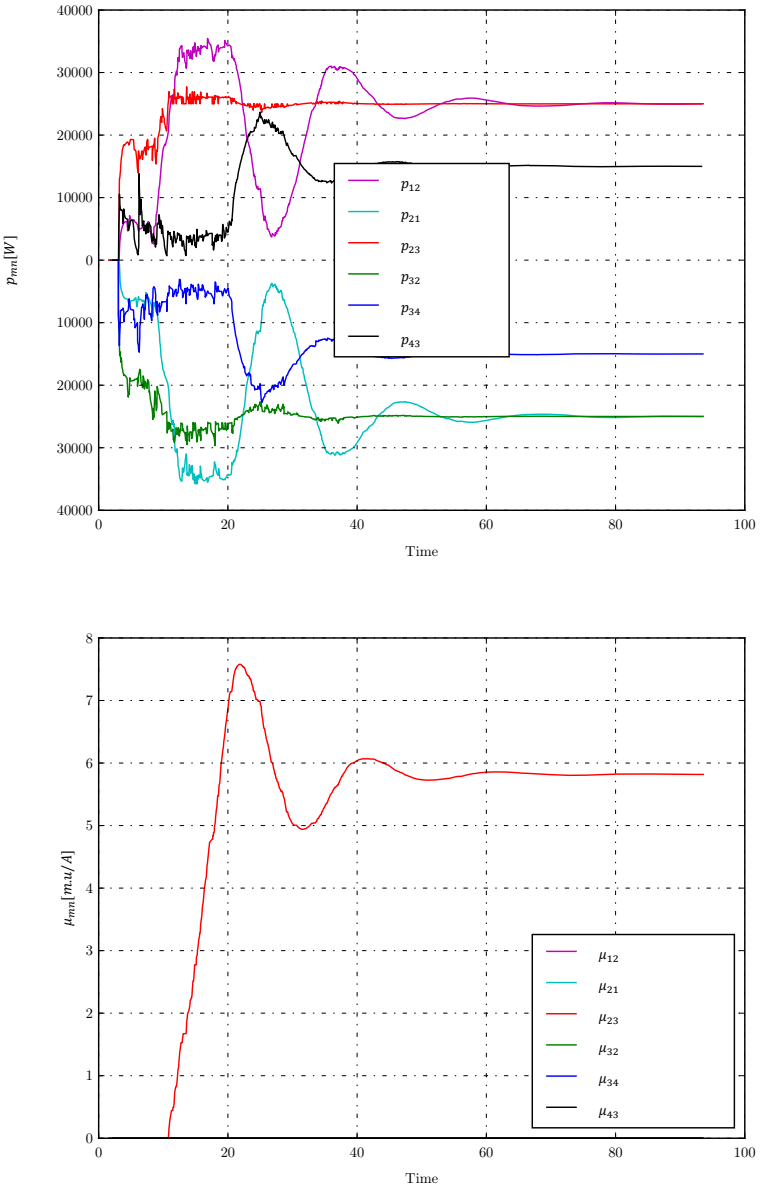

Figure C.6: The power flow (top) and the dual variable for the line limit (bottom) for the grid in Figure 6.1 when the algorithm is run asynchronously with 50 ms timeout time.

C.4. Case I with 30 ms Timeout Time

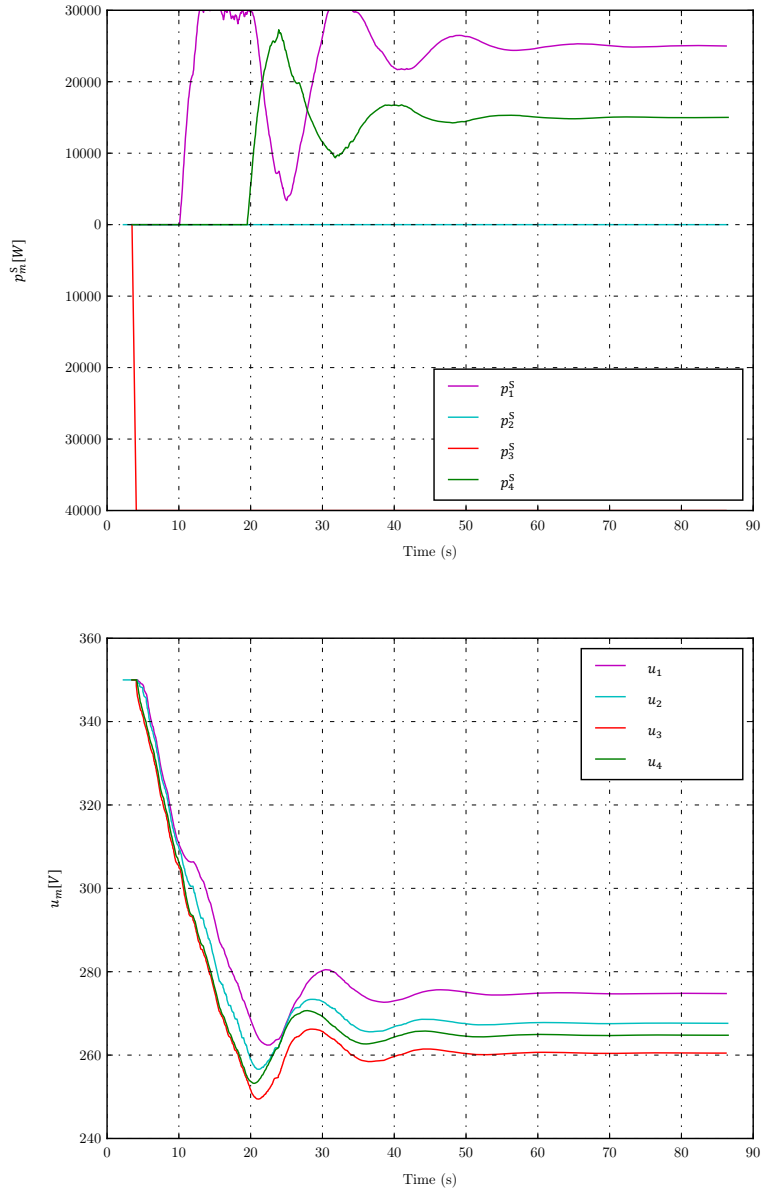

Figure C.7: The power (top) and voltage (bottom) for the grid in Figure 6.1 when the algorithm is run asynchronously with 30 ms timeout time.

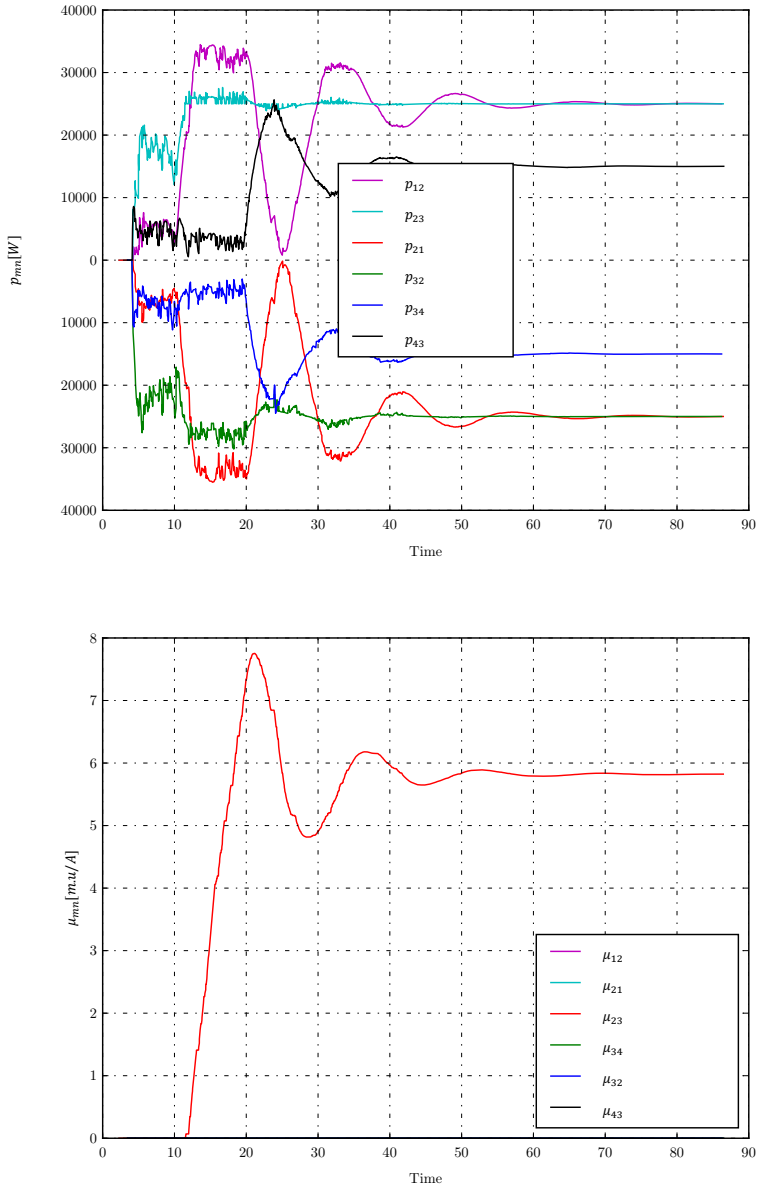

Figure C.8: The power flow (top) and the dual variable for the line limit (bottom) for the grid in Figure 6.1 when the algorithm is run asynchronously with 30 ms timeout time.

C.5. Case II with Synchronous Algorithm

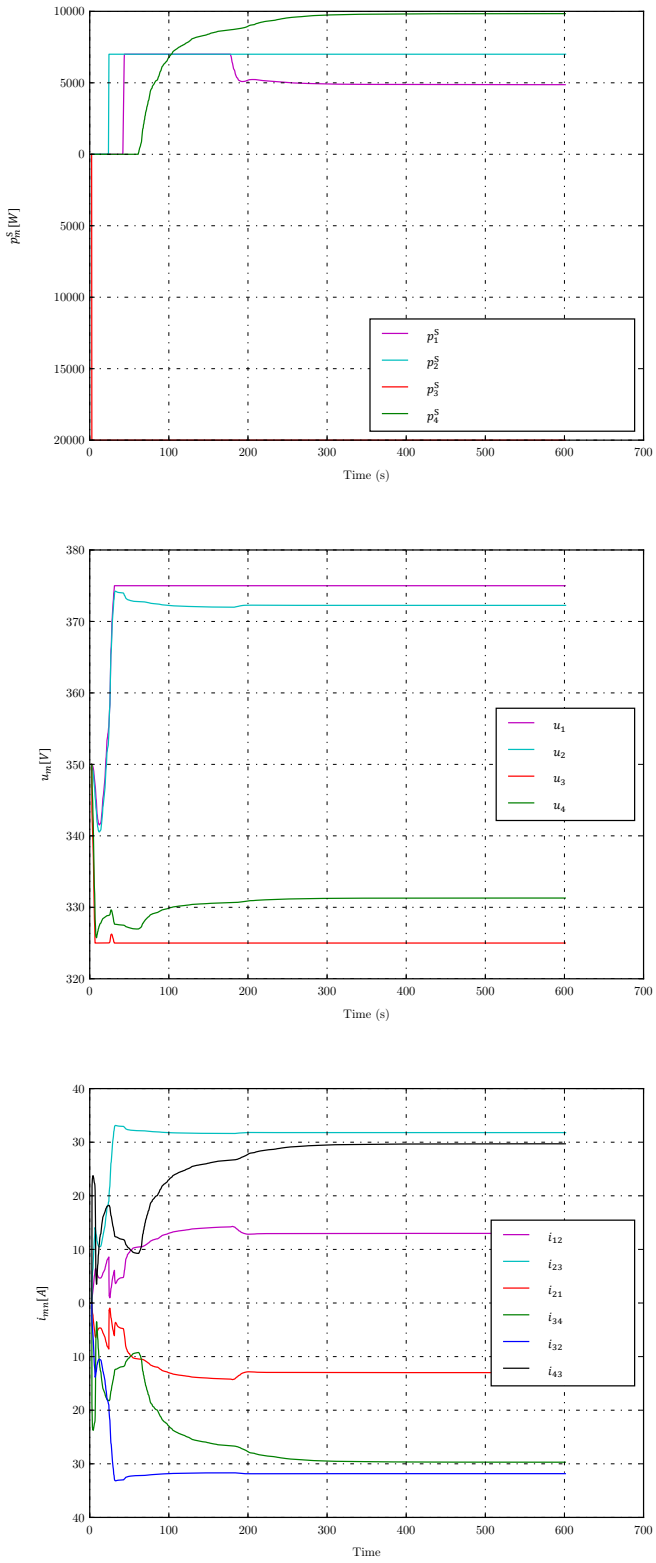

Figure C.9: From top to bottom: The power, voltage, and current flow for the grid in Figure 6.8 when the algorithm is run synchronously using the microcomputers.

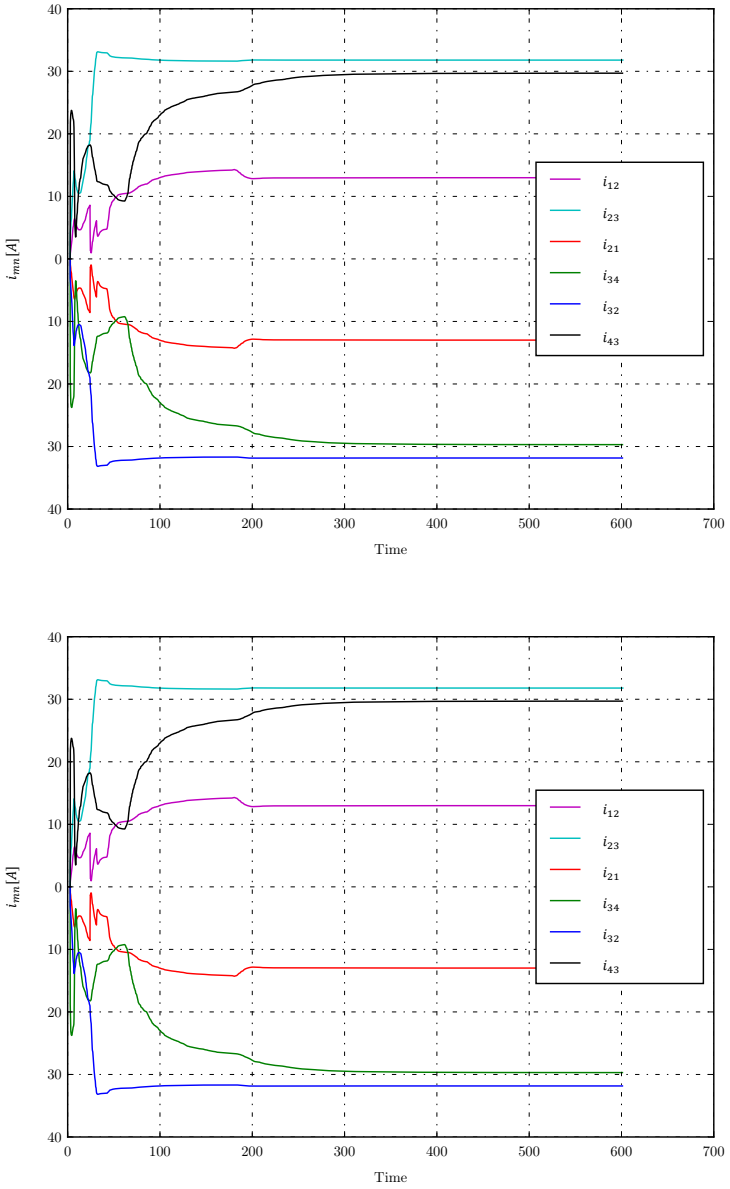

Figure C.10: From top to bottom: The dual variable for the maximum and minimum voltage for the grid in Figure 6.8 when the algorithm is run synchronously using the microcomputers.

C.6. Case II with 150ms Timeout Time

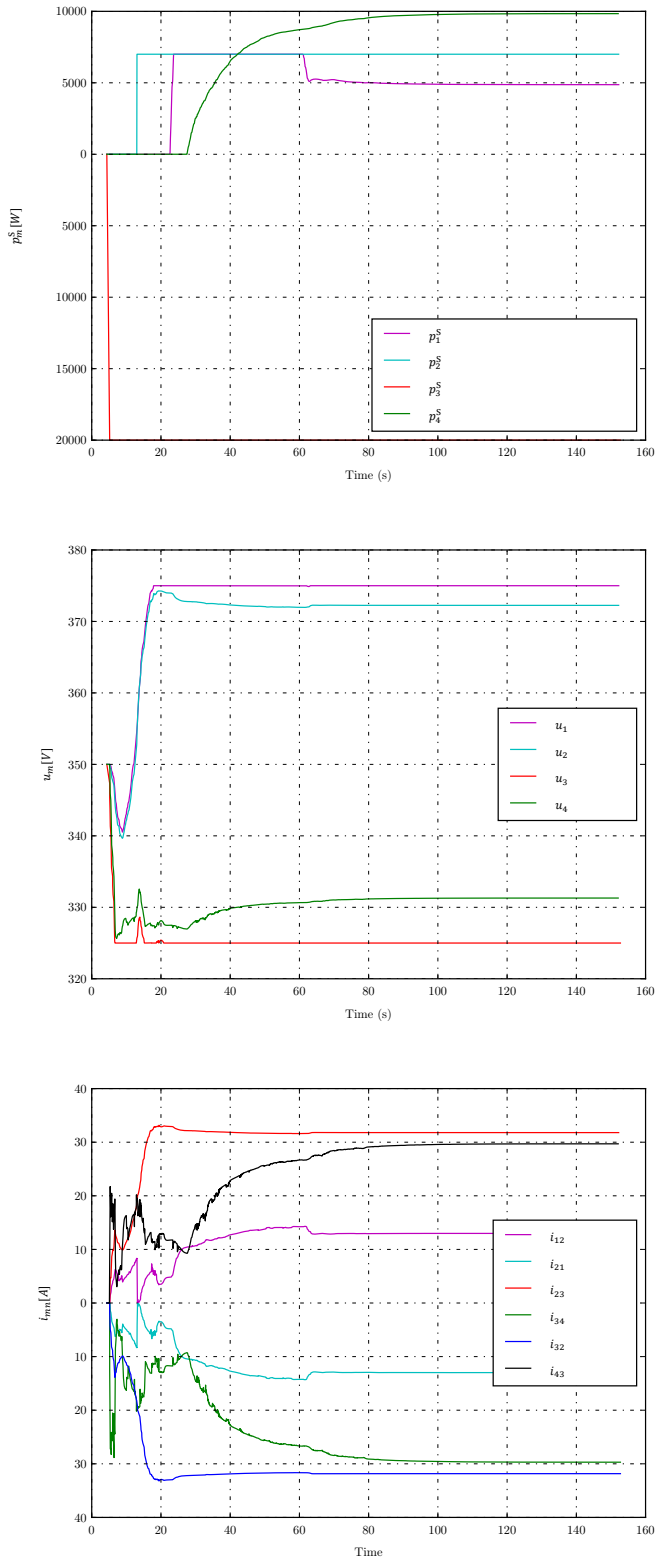

Figure C.11: From top to bottom: The power, voltage, and current flow for the grid in Figure 6.8 when the algorithm is run asynchronously with 150ms timeout time.

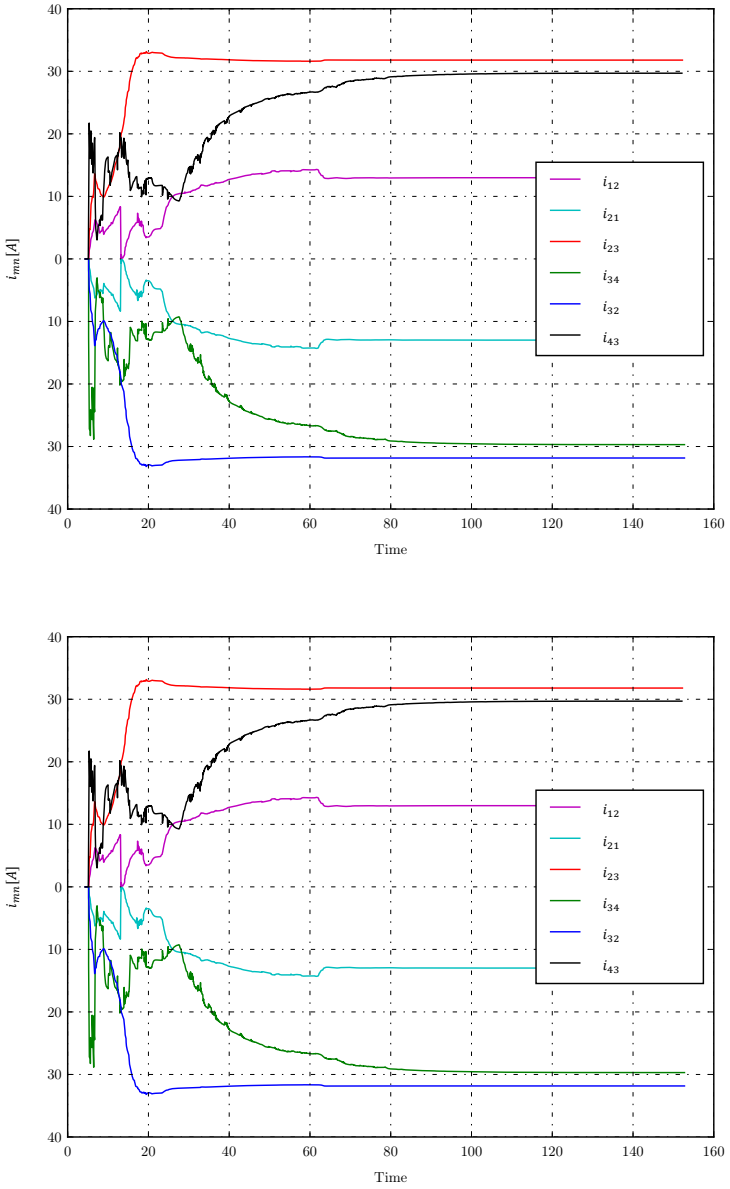

Figure C.12: From top to bottom: The dual variable for the maximum and minimum voltage for the grid in Figure 6.8 when the algorithm is run asynchronously with 150ms timeout time.

Bibliography

[1] A. Alfergani, K. A. Alfaitori, A. Khalil, and N. Buaossa, Control strategies in ac microgrid: A brief review, in 2018 9th International Renewable Energy Congress (IREC) (2018) pp. 1–6.

[2] H. Jiayi, J. Chuanwen, and X. Rong, A review on distributed energy resources and microgrid, Renewable and Sustainable Energy Reviews 12, 2472 (2008).

[3] L. Buono, E. R. Sanseverino, M. L. Di Silvestre, S. Bracco, and F. Delfino, Distributed optimal power flow for islanded microgrids: An application to the Smart Polygeneration Microgrid of the Genoa University, IEEE 2nd International Smart Cities Conference: Improving the Citizens Quality of Life, ISC2 2016 - Proceedings (2016), 10.1109/ISC2.2016.7580793.

[4] J. W. Coltman, The transformer [historical overview], IEEE Industry Applications Magazine 8, 8 (2002).

[5] M. P. Bahrman, Hvdc transmission overview, in 2008 IEEE/PES Transmission and Distribution Conference and Exposition (2008) pp. 1–7.

[6] L. Mackay, N. H. van der Blij, L. Ramirez-Elizondo, and P. Bauer, Toward the universal dc distribution system, Electric Power Components and Systems 45, 1032 (2017), https://doi.org/10.1080/15325008.2017.1318977 .

[7] A. Chakraborty, Advancements in power electronics and drives in interface with growing renewable energy resources, Renewable and Sustainable Energy Reviews 15, 1816 (2011).

[8] L. Mackay, R. Guarnotta, A. Dimou, G. Morales-España, L. Ramirez-Elizondo, and P. Bauer, Optimal power flow for unbalanced bipolar dc distribution grids, IEEE Access 6, 5199 (2018).

[9] D. K. Molzahn, F. Dörfler, H. Sandberg, S. H. Low, S. Chakrabarti, R. Baldick, and J. Lavaei, A Survey of Distributed Optimization and Control Algorithms for Electric Power Systems, IEEE Transactions on Smart Grid 8, 2941 (2017).

[10] Y. Han, L. Chen, Z. Wang, S. Mei, L. Chen, S. Mei, and W. Liu, Fully distributed optimal power flow for unbalanced distribution networks based on admm, in 2016 IEEE International Conference on Power System Technology (POWERCON) (2016) pp. 1–6.

[11] A. Kargarian, J. Mohammadi, S. Member, J. Guo, S. Member, S. Chakrabarti, S. Member, M. Barati, G. Hug, S. Member, S. Kar, R. Baldick, and F. Member, Toward Distributed / Decentralized DC Optimal Power Flow Implementation in Future Electric Power Systems, 3053 (2016), 10.1109/TSG.2016.2614904.

[12] S. Karambelkar, Distributed Optimal Power Flow in a DC Distribution System - MSc Thesis (Delft, 2017).

[13] S. Karambelkar, L. Mackay, S. Chakraborty, L. Ramirez-elizondo, and P. Bauer, Distributed Optimal Power Flow for DC Distribution Grids, (IEEE Power and Energy Society General Meeting, 2017).

[14] J. Mohammadi, S. Kar, and G. Hug, Distributed Approach for DC Optimal Power Flow Calculations, arXiv preprint arXiv:1410.4236 , 1 (2014), arXiv:1410.4236 .

[15] Y. Xu, H. Sun, H. Liu, and Q. Fu, Distributed solution to DC optimal power flow with congestion management, International Journal of Electrical Power and Energy Systems 95, 73 (2018).

[16] D. S. Kirschen and G. Strbac, Wiley (2004) arXiv:arXiv:1011.1669v3 .

[17] G. Hamoud and I. Bradley, Assessment of transmission congestion cost and locational marginal pricing in a competitive electricity market, IEEE Transactions on Power Systems 19, 769 (2004).

[18] S. Boyd, N. Parikh, E. Chu, B. Peleato, and J. Eckstein, Distributed Optimization and Statistical Learning via the Alternating Direction Method of Multipliers, 3, 1 (2011), arXiv:1408.2927 .

[19] M. Kraning, E. Chu, J. Lavaei, and S. Boyd, Dynamic Network Energy Management via Proximal Message Passing Matt, Foundations and Trends in Optimization 1, 70 (2013), arXiv:1204.1106 .

[20] H. Wei, H. Sasaki, J. Kubokawa, and R. Yokoyama, An interior point nonlinear programming for optimal power flow problems with a novel data structure, in Proceedings of the 20th International Conference on Power Industry Computer Applications (1997) pp. 134–141.

[21] W. Lu, M. Liu, S. Lin, and L. Li, Fully decentralized optimal power flow of multi-area interconnected power systems based on distributed interior point method, IEEE Transactions on Power Systems 33, 901 (2018).

[22] Z. Lukszo, Lecture Notes on Engineering Optimization and Integrating Renewables in Electricity Markets, (2016).

[23] J. Mohammadi, G. Hug, and S. Kar, Asynchronous distributed approach for dc optimal power flow, in 2015 IEEE Eindhoven PowerTech (2015) pp. 1–6.

[24] T. Ayken and J. Imura, Asynchronous distributed optimization of smart grid, in 2012 Proceedings of SICE Annual Conference (SICE) (2012) pp. 2098–2102.

[25] M. Zhong and C. G. Cassandras, Asynchronous distributed optimization with event-driven communication, IEEE Transactions on Automatic Control 55, 2735 (2010).

[26] C.-Y. Chang, J. Cortes, and S. Martinez, Scheduled-Asynchronous Distributed Optimization for Optimal Power Flow, IEEE Transactions on Control of Network Systems 5870, 1 (2018).

[27] Stanford University, Lecture Notes on Decomposition Methods, .

[28] D. Asija, P. Choudekar, K. M. Soni, and S. K. Sinha, Power flow study and contingency status of WSCC 9 Bus test system using MATLAB, 2015 International Conference on Recent Developments in Control, Automation and Power Engineering, RDCAPE 2015 , 338 (2015).

[29] Python, socket - Low-level Networking Interface, (2001), accessed: 2018-05-20.